Reconstructing Fire History in Mountain's Complex Environments Using Satellite Time-Series

Fornacca, Davide

UNVERSITÉ DE GENÈVE

Institut des Sciences de l'Environnement

FACULTÉ DES SCIENCES
Prof. Anthony Lehmann

Département de Géographie
et de l'Environnement

FACULTÉ DES SCIENCES DE LA SOCIÉTÉ
Prof. Quoc-Hy Dao

Reconstructing Fire History in Mountain's Complex Environments Using Satellite Time-Series

THÈSE

Présentée à la Faculté des Sciences de l'Université de Genève
pour obtenir le grade de
Docteur ès Sciences, mention Sciences de l'Environnement

par

Davide Fornacca
de
Breganzona (TI)

Thèse N° 5543

GENÈVE
Centre d'Impression de l'Université de Genève
2021

UNIVERSITÉ
DE GENÈVE
FACULTÉ DES SCIENCES

DOCTORAT ÈS SCIENCES, MENTION INTERDISCIPLINAIRE

Thèse de Monsieur Davide FORNACCA

intitulée :

«Reconstructing Fire History in Mountain's Complex Environments Using Satellite Time-Series»

La Faculté des sciences, sur le préavis de Monsieur A. LEHMANN, professeur associé et directeur de thèse (Département F.-A. Forel des sciences de l'environnement et de l'eau), Monsieur Q.-H. DAO, professeur titulaire et codirecteur de thèse (Faculté des sciences de la société, Département de géographie et environnement), Monsieur W. XIAO, professeur (Institut of Eastern-Himalaya Biodiversity Research, Dali University, Dali, China), Madame D. STROPPIANA, docteure (Institute of Electromagnetic Sensing of the Environment, Italian National Research Council, Milan, Italy) et Monsieur Y. YUE, docteur (Beijing Normal University, Beijing, China), autorise l'impression de la présente thèse, sans exprimer d'opinion sur les propositions qui y sont énoncées.

Genève, le 5 février 2021

Thèse - 5543 -

Le Doyen

N.B. - La thèse doit porter la déclaration précédente et remplir les conditions énumérées dans les "Informations relatives aux thèses de doctorat à l'Université de Genève".

Directeurs de thèse

Prof. **Anthony Lehmann**, Institute for Environmental Sciences, University of Geneva, Bd Carl-Vogt 66, 1205 Geneva, Switzerland, Anthony.Lehmann@unige.ch

Prof. **Quoc-Hy Dao**, Department of Geography and the Environment, University of Geneva, Bd Carl-Vogt 66, 1205 Geneva, Switzerland, Hy.Dao@unige.ch

Membres du jury

Prof. **Wen Xiao**, Institute of Eastern-Himalaya Biodiversity Research (IEHBR), Dali University, Hongsheng Rd 2, 671003 Dali, China, xiaow@eastern-himnalaya.cn

Dr. **Daniela Stroppiana**, Institute of Electromagnetic Sensing of the Environment (IREA), Italian National Research Council, Via Bassini 15, 20133 Milan, Italy, stroppiana.d@irea.cnr.it

Dr. **Yaojie Yue**, Beijing Normal University, Xinjiekou Outer St. 19, 100875 Beijing, China, yjyue@bnu.edu.cn

Table of contents

Abstract

Forest fires are major ecological disturbances with both natural and human causes. Ecologists acknowledge wildfires as an important evolutionary force shaping landscapes, ecosystems, and biogeochemical processes, as well as for the ecosystem services they provide, such as creating open spaces, enhancing biodiversity, and pest control. However, they are mostly considered undesirable by the general public because of their potential harm, including loss of life and property, destruction of forest resources, and massive release of aerosols and CO_2 into the atmosphere. Climate, humans, and fire form complex interactions that are still poorly understood by science, often resulting in inefficient fire management practices. A fair part of the problem could be attributed to the chronic lack of primary data needed to sustain analyses. Given the uncertainty in future climatic and socio-economic conditions, predicting how fire regimes could potentially shift from past and current patterns is a difficult task that requires the best available expertise from a wide range of stakeholders. Without long-term, continuous, spatially- and temporally-consistent data, there is no foundation for the knowledge building process. As such, improving data availability is a vital component of informed and effective fire management policies.

The absence or scarcity of data is in particular a problem for less developed regions or in remote areas with limited accessibility, such as isolated mountain environments. Remote sensing technology represents a cost-effective and very powerful solution to reconstruct recent land-surface dynamics. By analyzing time-series of satellite images, it is possible to detect burned areas at different scales in a spatially and temporally consistent manner, and fill in information gaps in these data-poor, remote regions. Although several routines to automatically extract burned areas from satellite images have been developed in the past decades, their application in mountainous environments featuring high habitat heterogeneity (complex landscapes) is limited due to numerous technical and methodological difficulties.

The present doctoral thesis aims at providing basic but spatially-explicit information on historical forest fires in northwest Yunnan, China, an important biodiversity hotspot and representative region characterized by complex landscapes. To broaden the thesis's context, we proposed a fire risk/vulnerability framework that in future work will be fed with the fire data created here.

As a first step, the performance of existing global fire products in mapping burned areas in our study region was evaluated. We showed that the widely adopted datasets developed using the MODIS sensor and a first prototype built on MERIS imagery present very high omission and commission error rates, significantly limiting their usability in this kind of landscape. The results suggest that the contribution of small fires in global fire emission assessments such as GFED4 is probably underestimated and that end-users working in difficult environments require other solutions.

The best available option to detect small fires lies in the longest and most consistent Earth Observation mission, namely the Landsat suite. Our second study presents an in-depth analysis of the burned areas' spectral signal's permanence in several vegetation indices. Burn is a temporary ecological condition that tends to recover relatively quickly according to vegetation type and other factors. The spectral separability of burn scars vs. unburned control samples was evident immediately after fire in all four main vegetation groups of northwest Yunnan but decreased drastically after one growing season due to abundant rains. Grassland and shrub patches recovered even more quickly. The Normalized Burn Ratio and the Normalized Difference Moisture Index were identified as the most suitable spectral indices for long-term burned area mapping, while the Tasseled Cap Brightness and Wetness offered additional discrimination potential.

We then proceeded with the development of a burned area extraction routine tailored to regions characterized by complex landscapes. We first identified the particular remote sensing challenges encountered in these landscapes, and then we proposed solutions for some of them, while for others, we opted for compromise adaptations. Six major difficulties were identified: small fires, rugged terrain casting shadows, long cloud coverage periods, patchy landscapes, fast vegetation recovery, and absence of burned samples to train, test and tune classification models. The selected solutions were integrated into an automated processing routine based on yearly images from the Landsat TM and OLI sensors, which flows through five phases: creation of standardized difference vegetation indices time-series; automatic extraction of multi-class training areas using adaptive z-score thresholds; Random Forests classification; Seeded Region Growing, and spatiotemporal clustering to form coherent burn multi-polygons. A final product of fire events spanning the period 1987-2018 was created and tested for both detection and mapping accuracy. The results are satisfactory, with both omission and commission in the order of 20%, representing a great improvement from the global products assessed previously. This newly created fire database can now be used to derive parameters describing the recent fire regime of northwest Yunnan.

This work represents a step forward toward the inclusion of remote mountainous regions hosting delicate ecosystems in the global assessment of fire impacts. Researchers working in areas with similar difficulties can implement some of the approaches developed in this thesis and finally fill those data gaps that prevent their research advancement.

Resumé

Les incendies de forêt sont des perturbations écologiques majeures qui ont des causes à la fois naturelles et humaines. Les chercheurs en écologie reconnaissent les feux de forêt comme une force évolutive importante qui façonne les paysages, les écosystèmes et les processus biogéochimiques, ainsi que pour les services écosystémiques qu'ils fournissent, tels que la création d'espaces ouverts, la promotion de la biodiversité et la lutte antiparasitaire. Cependant, ils sont généralement considérés comme indésirables par le grand public en raison de leurs impacts négatifs potentiels, notamment la perte de vies humaines et de biens, la destruction des ressources forestières et le rejet massif d'aérosols et de CO_2 dans l'atmosphère. Le climat, les humains et le feu forment des interactions complexes qui sont encore mal comprises par la science, ce qui entraîne souvent des pratiques de gestion des incendies inefficaces. Une bonne partie du problème pourrait être attribuée au manque chronique de données de base nécessaires pour soutenir les analyses. Compte tenu des incertitudes sur les conditions climatiques et socio-économiques futures, prédire la déviation potentielle de l'état historique et actuel des régimes de feu est une tâche difficile qui nécessite l'union d'expertise d'un vaste éventail de partenaires. Sans données de longue date et continues, cohérentes dans l'espace et dans le temps, il n'y a pas de base pour le processus de renforcement des connaissances. C'est pourquoi, l'amélioration de la disponibilité des données est un élément essentiel pour de politiques de gestion des incendies efficaces.

L'absence ou la rareté des données est un problème majeur des régions moins développées ou très reculées avec accessibilité limitée, comme les milieux montagneux isolés. Les technologies de télédétection présentent des solutions avantageuses et très puissantes pour reconstruire les dynamiques récentes de la surface terrestre. Par l'analyse des séries temporelles d'images satellites, il est possible de détecter les surfaces brûlées à différentes échelles et de manière cohérente dans l'espace et le temps, en comblant ainsi les lacunes d'information dans ces régions éloignées et limitées en données. Bien que plusieurs routines d'extraction automatique des zones brûlées à partir d'images satellites aient été développées au cours des dernières décennies, leur application dans des milieux de montagne caractérisés par une grande hétérogénéité des habitats (paysages complexes) est limitée en raison de nombreuses obstacles techniques et méthodologiques.

Cette thèse de doctorat vise à produire des données de base et spatialement explicites sur l'histoire récente des incendies de forêt dans le nord-ouest du Yunnan, en Chine, qui est un haut lieu important pour la biodiversité et une région représentative des paysages complexes. Afin d'élargir l'horizon contextuel de la thèse, nous avons présenté un cadre d'évaluation des risques/vulnérabilités au feu qui, dans nos recherches futures, sera alimenté par les données créées ici.

D'abord, nous avons passé en revue des bases de données globales sur les feux existantes et évalué leurs habilités à cartographier les aires brûlées dans notre région d'étude. Nous avons trouvé que les jeux de données développés avec les capteurs MODIS qui sont largement adoptés par les chercheurs, ainsi que le premier prototype construit à partir d'imagerie MERIS présentent des marges d'erreur d'omission et de commission très élevés, limitant considérablement leur

utilisabilité dans ce type de paysages. Ces résultats suggèrent que la contribution des incendies de petite taille dans les évaluations mondiales des émissions d'incendies telles que GFED4 est probablement sous-estimée et que les utilisateurs travaillant dans des paysages complexes nécessitent doivent se tourner vers d'autres solutions.

La meilleure option disponible pour détecter les feux de forêt de petite taille réside dans la mission d'observation de la Terre la plus longue et cohérente dans le temps, à savoir la suite de produits Landsat. Notre deuxième étude présente une analyse approfondie de la permanence du signal spectral des surfaces brûlées dans plusieurs indices de végétation. L'état brûlé est une condition écologique temporaire qui a tendance à se rétablir assez rapidement selon le type de végétation et d'autres facteurs. La séparabilité spectrale entre des aires-échantillons brûlées vs non-brûlées était évidente immédiatement après l'incendie dans les quatre principaux groupes de végétation du nord-ouest du Yunnan, mais diminuait considérablement après une saison de croissance en raison des pluies abondantes. Les zones de prairies et d'arbustes se sont rétablies encore plus rapidement. Le Normalized Burn Ratio et le Normalized Difference Moisture Index sont identifiés comme les indices spectraux les plus appropriés pour la cartographie des zones brûlées sur le long terme, tandis que le Tasseled Cap Brightness et Wetness offrent un potentiel de discrimination supplémentaire.

Nous avons ensuite procédé au développement d'une routine d'extraction de zones brûlées adaptée aux régions caractérisées par des paysages complexes. Nous avons d'abord identifié les difficultés de télédétection particulières de ces paysages et proposé des solutions ou des modes d'adaptations. Six difficultés majeures ont été identifiées: taille des incendies réduite, relief prononcé projetant des ombres, longues périodes de couverture nuageuse, paysages hétérogènes, rétablissement rapide de la végétation et absence d'échantillons pour entraîner, tester et paramétriser les modèles de classification. Les solutions sélectionnées ont été intégrées dans une routine automatisée basée sur des images Landsat TM et OLI annuelles, composé par cinq phases: création et standardisation de séries temporelles d'indices spectraux différenciés; extraction automatique de zones d'entraînement multi-classes à l'aide de seuils de z-score adaptés; classification par forêts d'arbres décisionnels (Random Forest); segmentation par fusion de régions (Seeded Region Growing) et agrégation spatio-temporelle des pixels pour former des multi-polygones cohérents. Un produit final des événements-incendies couvrant la période 1987-2018 a été créé et sa précision de détection et de cartographie a été testée. Les résultats sont satisfaisants, avec des marges d'erreur d'omission et de commissions de l'ordre de 20%, ce qui représente une amélioration importante par rapport aux produits globaux évalués précédemment. Cette base de données de feux peut maintenant être utilisée pour dériver des paramètres décrivant le régime d'incendies récent dans le nord-ouest du Yunnan.

Ce travail représente un avancement vers l'inclusion des régions montagneuses reculées abritant des écosystèmes délicats dans l'évaluation globale des impacts des incendies. Les chercheurs travaillant dans des domaines présentant des limitations similaires peuvent mettre en œuvre certaines des approches développées dans cette thèse et pourront enfin combler les lacunes de données empêchant la progression de leurs recherches.

Acknowledgments

To understand how the idea of this thesis project came out, we need to go back to the year 2012. At that time, I was years into my bicycle tour adventure, which from my hometown in Switzerland brought me all the way to Thailand. During my volunteering time spent helping and studying the reintroduction of captive gibbons in the rainforest of Phuket, I had the chance to meet a representative of the nature conservation NGO Fauna & Flora International (FFI), who was actively working for the protection of primate species in China. After learning about my passion for research in this field, my educational background in geospatial information technology, and my intention to pursue my travels into the Yunnan province of China, she recommended coming to visit the Institute of Eastern-Himalaya Biodiversity Research (IEHBR) based in Dali University. A few months later, I cycled to Dali and met IEHBR's eccentric director. He welcomed me warmly, and during our conversation, we learned about our common research perspectives and shared vision of nature and the world. After inviting me for lunch in a lovely local restaurant, he proposed some work we could do together, involving monkeys, GIS, and a lot of fun. I've been a full-time team member of IEHBR since late 2014 and began my doctoral program in 2016 on a whole new subject for the Institute and me as well…

First of all, I would like to warmly thank Prof. Wen Xiao, founder and director of IEHBR, who welcomed me to its team, proposed me to pursue an academic career, kept believing in my value, and showed extraordinary patience during difficult years. He provided funding resources and made sure I didn't lack anything. His guiding role in this thesis, continuous support, deep understanding of the Chinese culture, and genuine friendship have been invaluable to me and are continuously fostering our fruitful collaboration.

I am extremely grateful to my thesis co-supervisors at the University of Geneva, Switzerland, Prof. Anthony Lehmann and Prof. Hy Dao, for accepting my proposal and giving me the opportunity to undertake a doctoral research program. Their openness and experience have contributed significantly to the widening of my research horizons. They supported and encouraged me "virtually" while I was working on the terrain in China and integrated me into their research team during my visits to Switzerland by also providing a temporary teaching position within the Geneva international ecosystem.

Due thanks to all my colleagues at IEHBR for their kind support: Xiaoyan Yang, Shuxia Zhang, Guopeng Ren, Yanpeng Li, Shuoran Liu, Zhipang Huang, Depin Li, Rongxing Wang, Rong She, Caicai Zhang, Kun Tan, Xianfu Li, Yuan Mu, Youjing Gong, Chengfa Zhao, Na Li, Yihao Fang, Xiaokang Li, Ying Gao, Haohan Wang, Yujie Jiang, Xu Yang, Yuejun Lu, Ran Duan, Ronglong Yang, Lilei Liu, Junhui Zheng, Kaixing Dai, Ying Yang, and Alexey Reshchikov. Heartful thanks to all our master students who are always ready to help, and the administration of Dali University, in particular Zhong Zuo, for his hard work and commitment to improving the working and living conditions of the resident foreign experts, and for always making my visa renewal smooth and painless.

Big thanks to all my colleagues at the University of Geneva, the enviroSPACE lab, UNEP/GRID--Geneva, and Geneva-Tsinghua Initiative, in particular Charlotte Poussin, Grégory Giuliani, Louise Gallagher, Thomas Maillart, Erika Honeck, Martin Schlaepfer, Pascal Peduzzi, Bernard Debarbieux, and many other wonderful persons I cannot comprehensively list here but that I had the privilege to work and interact with.

Extended thanks to the jury members for their evaluation work and the kind suggestions provided, and to everybody who attended my thesis defense.

A special thank to my good friend and collaborator Riccardo Pansini for all the adventures we shared as researchers in China and for being the older brother who helped me get accustomed to the academic work and lifestyle.

I arrived in Dali in 2012 with a bicycle, a few bags, and some research ideas; now it's 2021, and I have a lovely family, a growing work team, and more research ideas. This work wouldn't have been possible without the inexhaustible enthusiasm and motivational support of my wife Meng Miao and our two smiling angels Elena and Stella. I love you so much. This thesis is also dedicated to my parents and my brother, who kept pushing me, taught me how to follow an ideal and persevere towards its accomplishment. And to the rest of my family and friends in China, Switzerland, and other corners of this wonderful planet: thank you with all my heart.

Remerciements

Afin de comprendre comment l'idée de ce projet de thèse est survenue, il faut revenir à l'année 2012. À cette époque, j'étais au milieu de mon voyage-aventure à vélo qui, parti de mon village natal en Suisse, m'a amené jusqu'en Thaïlande. Pendant ma période de volontariat passé à aider et étudier la réintroduction des gibbons grandis en captivité dans la forêt tropicale de Phuket, j'ai eu le plaisir de rencontrer une déléguée de l'ONG pour la conservation de la nature Fauna & Flora International (FFI), qui était engagée dans la protection des primates en Chine. Après avoir appris de ma passion pour la recherche dans ce domaine, ma formation en technologies de l'information géospatiale et mon intention de poursuivre mes voyages dans la province chinoise du Yunnan, elle me propose de venir visiter le Institute of Eastern-Himalaya Biodiversity Research (IEHBR), basé à l'Université de Dali. Quelques mois plus tard, j'arrive à Dali en pédalant sur mon vélo et je rencontre le directeur excentrique de l'IEHBR. Il m'accueille chaleureusement et, au cours de notre conversation, nous découvrons des points en commun sur les perspectives de recherche et notre vision de la nature et du monde. Après m'avoir invité à déjeuner dans un charmant restaurant local, il me propose de travailler ensemble sur quelques projets impliquant des singes, des SIG et beaucoup de plaisir. Depuis fin 2014, je suis membre à plein temps de l'équipe de l'IEHBR et plus tard en 2016 je commence mon doctorat sur un tout nouveau sujet pour l'Institut et pour moi aussi ...

Tout d'abord, je tiens à remercier chaleureusement le professeur Wen Xiao, fondateur et directeur de l'IEHBR, qui m'a accueilli dans son équipe, m'a proposé de poursuivre une carrière universitaire, a continué à croire en ma valeur et fait preuve d'une patience extraordinaire pendant des années compliquées. Il a fourni les ressources financières et s'est assuré que je ne manquais de rien. Son rôle de directeur sur le terrain dans cette thèse, un soutien moral inépuisable, ainsi que sa profonde compréhension de la culture chinoise m'ont été inestimables, et son amitié est un pilier portant de la durabilité de notre collaboration.

Je suis extrêmement reconnaissant envers mes co-directeurs de thèse à l'Université de Genève, en Suisse, le professeur Anthony Lehmann et le professeur Hy Dao, pour avoir accepté ma proposition de thèse et m'avoir donné l'opportunité d'entreprendre un programme de recherche doctorale. Leur ouverture et leur expérience ont contribué de manière significative à l'élargissement de mes horizons de recherche. Ils m'ont soutenu et encouragé "à distance" pendant que je travaillais sur le terrain en Chine, et m'ont intégré dans leur équipe de recherche lors de mes visites en Suisse en offrant également un poste d'enseignant temporaire au sein de l'écosystème international de Genève.

Merci à tous mes collègues de l'IEHBR pour leur soutien et chaleur humaine : Xiaoyan Yang, Shuxia Zhang, Guopeng Ren, Yanpeng Li, Shuoran Liu, Zhipang Huang, Depin Li, Rongxing Wang, Rong She, Caicai Zhang, Kun Tan, Xianfu Li, Yuan Mu , Youjing Gong, Chengfa Zhao, Na Li, Yihao Fang, Xiaokang Li, Ying Gao, Haohan Wang, Yujie Jiang, Xu Yang, Yuejun Lu, Ran Duan, Ronglong Yang, Lilei Liu, Junhui Zheng, Kaixing Dai, Ying Yang

et Alexey Reshchikov. Un grand merci à tous nos étudiants en master qui sont toujours prêts à aider, et à l'administration de l'Université de Dali, en particulier Zhong Zuo, pour son travail acharné et son engagement à améliorer les conditions de travail et de vie des enseignants étrangers, et pour toujours rendre mon renouvellement de visa une tâche simple et sans douleur.

Un grand merci à tous mes collègues de l'Université de Genève, du laboratoire enviroSPACE, du PNUE / GRID-¬-Genève et de Genève-Tsinghua Initiative, en particulier Charlotte Poussin, Grégory Giuliani, Louise Gallagher, Thomas Maillart, Erika Honeck, Martin Schlaepfer, Pascal Peduzzi, Bernard Debarbieux et bien d'autres personnes formidables que je ne peux pas énumérer ici de manière exhaustive mais avec lesquelles j'ai eu le privilège de travailler et interagir.

Remerciements aux membres du jury pour leur travail d'évaluation et les précieuses suggestions fournies, ainsi qu'à tous ceux qui ont assisté à ma soutenance de thèse.

Un merci spécial à mon ami et collaborateur Riccardo Pansini pour toutes les aventures partagées en tant que chercheurs en Chine et pour être le frère aîné qui m'a aidé dans mon acclimatation au travail et style de vie académique.

Je suis arrivé à Dali en 2012 sur mon vélo, quatre sacoches et quelques idées de recherche ; maintenant, nous sommes 2021 et j'ai une famille superbe, une équipe de travail en pleine croissance et bien plus d'idées de recherche. Ce travail n'aurait pas été possible sans l'enthousiasme inépuisable et le soutien de ma femme Meng Miao et de nos deux anges souriants Elena et Stella. Je vous aime infiniment. Cette thèse est également dédiée à mes parents et mon frère, qui n'ont cessé de me pousser, m'ont appris à poursuivre un idéal et à persévérer vers son accomplissement. Et au reste de ma famille et de mes amis en Chine, en Suisse et dans d'autres coins de cette merveilleuse planète : merci de tout mon cœur.

1. Introduction

1.1. Fire in the Earth System

Since its first appearance soon after plants colonized the bare earth, fire has been an important natural process and evolutionary force, playing a key role in shaping the spatial distribution of ecosystems and their composition (Pyne *et al.* 1996; Bowman *et al.* 2009; Pausas and Keeley 2009). Without fire, our planet's vegetation cover would be very different from its current condition, with almost double the forest cover but less diverse ecosystems (Bond *et al.* 2005). Instead, similarly to giant herbivores, wildfires contributed to the maintenance of several fire-adapted and fire-dependent ecosystems such as open-canopy woodlands, grasslands, and savannas (Bond and Keeley 2005; Staver *et al.* 2011). Several frontline researchers in fire ecology propose a holistic interpretation of the global role of wildfires. They suggest that plant biomass, terrestrial carbon and nutrient cycling, as well as vegetation structure, are regulated by three major recycling pathways interacting and competing at different spatial scales: microbial decomposition, vertebrate herbivory, and wildfires (Pausas and Bond 2020). Wildfires can also be understood and acknowledged for providing various benefits to humans and human societies, being themselves fire-dependent organisms living in a flammable world (Pausas and Keeley 2019). This interpretation goes beyond direct fitness advantages of the domesticated use of fire such as cooking, heating, light source, promotion of social interactions, and protection from predators, for which we have evidence since early hominids (James 1989; Gowlett 2016); or its extensive use as a land management tool adopted from the Paleolithic age for clearing land for human habitat, killing vermin, hunting, etc. Instead, it englobes the overarching contributions of wildfires, meant as vegetation fires ignited by natural sources, to the proper functioning of ecosystems, in a similar manner than other ecosystem services (Bird *et al.* 2008; Pausas and Keeley 2009). For example, they support and stimulate biodiversity, which is itself an important ecosystem service (Costanza *et al.* 1997; Daily *et al.* 1997; Mace *et al.* 2012). When vegetation patches are affected by burn at different degrees of severity, the result is increased habitat heterogeneity offering colonizing opportunities for a wide range of species (Smith 2000; Ketcham and Koprowski 2013). The creation of open habitats is favorable to shade-intolerant plants and animals, in particular a diversity of flowers and pollinators (Brown *et al.* 2017; Carbone *et al.* 2019). However, fire activity is not distributed equally at the global scale, and different ecosystems show diverging relationships with fire. Some of them have evolved with fire, thus becoming dependent on its recurrence, while others show varying degrees of adaptation, from moderate resistance to substantial sensitivity or intolerance where wildfires are extremely rare. It is believed that fire-dependent traits such as the serotinous cones and thick bark of pines represent an adaptive strategy of plants to cope with recurrent fires and other factors in fire-prone environments (Lamont *et al.* 1991; Schwilk and Ackerly 2001; Gómez-González *et al.* 2011; Keeley, Pausas, *et al.* 2011; He *et al.* 2012). In the animal kingdom (but not limited to), responses to fire and smoke may be mostly behavioral, including the use of refugia, exogenous

recolonization, escaping, and other forms of avoidance (Brown and Smith 2000; Smith 2000; Robinson *et al.* 2016; Pausas and Parr 2018; Pausas 2019). The ability for wildlife to survive fires depends on food availability, cover from predators, mobility, behavior, and structural diversity (Smith 2000; Ketcham and Koprowski 2013). Species lacking any response strategy to fire, such as many late successional tree species, are likely to disappear and are in general not found in fire-prone ecosystems.

Ecologists refer to the concept of *fire regime* to describe all the aspects related to the long-term patterns of fire occurrence in different regions. Despite slight variations among authors, components such as spatiotemporal characteristics (frequency, size, seasonality, return interval, etc.), vegetation type, climatic and topographic characteristics, ignition sources, and ecosystem effects are in general included in its definition (Pyne *et al.* 1996; Morgan *et al.* 2001; Westerling *et al.* 2006; Chuvieco, Giglio, *et al.* 2008; Bowman *et al.* 2009; Krawchuk *et al.* 2009; Krebs *et al.* 2010). The global distribution of fire regimes is mostly explained by the interactions of some of these components, identified as main controls of fire: vegetative resources to burn, also referred to as fuel, environmental conditions that promote combustion such as climate/weather and in part topography, and ignitions that originate from natural sources like lightning, volcano eruptions, and even spontaneous combustions, or human-caused, voluntarily or involuntarily. Understanding these interactions and the relative influence of each factor is a research topic of growing interest, especially toward assessing how they have changed through time. A fair amount of supporting evidence points to anthropogenic activities as primary drivers of what are called 'shifts' of fire regimes, referring to a deviation from their historical pattern (Krawchuk *et al.* 2009; Pechony and Shindell 2010; Bowman *et al.* 2011; Hantson *et al.* 2015; Prichard *et al.* 2017). From the moment humans learned how to control fire, they have used it to conquer new spaces and adapt them to suit their needs, affecting landscapes and atmospheric composition beyond their natural variability, which was once mainly dictated by multi-scale climatic factors (Pausas and Keeley 2009; Gowlett 2016; Vannière *et al.* 2016; Blarquez *et al.* 2018; Dietze *et al.* 2019). These alterations became more pronounced with population growth, expansion of agricultural land, livestock grazing, and the beginning of industrialization. However, recent studies show that, with industrialization, fire frequency declined at the global scale, with faster rates after 1950, while population size and density increased (Knorr *et al.* 2016; Andela *et al.* 2017; Forkel *et al.* 2017; Hamilton *et al.* 2018). Effective fire suppression operations attempting to safeguard forest resources and protect people and their property were recognized as the main drivers of this trend. Suppressing fire represents a significant change of perspective of the relationships between fire and humankind driven by a reduced dependence on fire for livelihood and land management, owing to technological progress such as industrial combustion (Pechony and Shindell 2010; Pyne 2016). In a world where resources are limited, wildland fires became unwelcome threats that needed to be minimized. Nowadays, big, intense fires can have catastrophic consequences for both human societies and nature. Fires destroy economically valuable forest resources and create fragmentation, reducing vital habitats for wildlife. They decrease carbon sinks' capacity and release massive amounts of aerosols and CO_2 into the

atmosphere, posing a significant hazard to human health. Moreover, they represent a threat to human life and infrastructure, especially in the wildland-urban interface, i.e., the zone of transition between unoccupied land and human development (Pyne *et al.* 1996; Streets *et al.* 2003; Bowman *et al.* 2009; Turetsky *et al.* 2015).

The complex interactions between climate, landscapes, humans, and fire are still poorly understood by science, often resulting in ineffective and inefficient fire management strategies. Human activities have altered historical fire regimes through their land use practices, starting fires in all sorts of biomes and in any season, including those with very low fire frequency, often turning fire-sensitive habitats into more fire-prone ones. On the other hand, decades of fire suppression have modified the structure of forests, preventing the natural fuel reduction service provided by more frequent, low-intensity fires, and resulting in an increase of devastating high-intensity fires (Keeley 2006; Wang *et al.* 2007; Pechony and Shindell 2010; Bowman *et al.* 2011, 2020; Adams 2013; Pausas and Keeley 2019). Understanding fire regime dynamics is becoming even more critical with climate and socio-economic change. According to climate change scenarios, the risk of fire will probably increase (IPCC 2014a), but this is not necessarily true in every location on the globe. Multivariate models that include anthropogenic factors predict substantial differences between regions owing to different responses to climate factors. Some places would experience an increase in fire activity while other areas would face a decrease in fire activity, therefore suggesting high alterations of the global geographic distribution of fire that could have substantial effects on ecosystems (Krawchuk *et al.* 2009; Pechony and Shindell 2010; Liu *et al.* 2012; Doerr and Santín 2016; Keeley and Syphard 2016; Li, Hughes, *et al.* 2017; Syphard *et al.* 2017; Young *et al.* 2017). According to recent projections based on Shared Socioeconomic Pathways scenarios, the risk and frequency of fires will increase in those areas already more exposed, such as in wildland-urban interface areas (Knorr *et al.* 2016).

The most pressing challenge for human societies is to learn to coexist with fire in a sustainable way (Moritz *et al.* 2014; Schoennagel *et al.* 2017). Fire management frameworks, in which the ecological role of fire is acknowledged and embedded with both nature conservation and the protection of human life and property, are needed.

1.2. Fire in mountains' complex landscapes

Complex landscapes are those characterized by high environmental heterogeneity, including rugged topography, patchy landscapes, and diverse climatic conditions. Mountainous environments are a representative example of complex landscapes with prominent elevational gradient, steep slopes, and limited accessibility. Mountains cover about 25% of the global land area[1] and provide several ecosystem services to human societies, the most essential one being the storing, purification, and provision of freshwater from which half of humanity depends on

[1] According to the broader definition by Kapos *et al.* (2000), which includes high plateaus, intermontane valleys, and hilly forelands.

every day (MA 2005; Grêt-Regamey *et al.* 2012). Mountain forested areas prevent soil erosion on slopes and act as a physical barrier against natural hazards such as avalanches, landslides, and rockfalls. Mountain ecosystems provide goods to local populations, such as crops, timber, fuelwood, medicinal plants, and animal products, as well as monetary benefits through local and nearby lowland markets (Martín-López *et al.* 2019). Topographic and landscape variability results in strong habitat differentiation with multiple, delicate and unique ecosystems supporting rich biodiversity and endemism (Shen 2017). From an ecological perspective, remoteness and isolation acted in favor of a higher rate of speciation and natural intactness, owing to unsuitability for large-scale human settlement and development.

However, mountains are among the most vulnerable regions in the world, particularly sensitive to climatic and anthropogenic influences (Beniston *et al.* 1997; Beniston 2003; Huber *et al.* 2005; Payne *et al.* 2017; Palazzi *et al.* 2019). Dramatic changes have occurred in the past few decades in several mountain ecosystems, affecting their provision of services to local and lowland peoples, as well as tourists (Beniston 2003; Palomo 2017). Melting glaciers and reduced snowpack are modifying water cycles and seriously compromising future freshwater supply (Baker and Moseley 2007; Bahuguna *et al.* 2014; Sommer *et al.* 2020). A combination of biotic and abiotic factors acting at different spatial scales are driving changes in vegetation patterns, which can be observed as a general upward shift of the vegetation belt and the tree line (Tasser *et al.* 2017). Landcover and land use changes are happening at an accelerating rate. On the one hand, several secluded mountainous regions are experiencing land abandonment and emigration towards more convenient locations. Natural reforestation often occurs in these areas with both positive and negative effects, in particular on biodiversity and fire prevention. On the other hand, an intensification of land use is observed in more profitable regions such as valley bottoms, where overexploitation of natural resources is associated with loss of semi-natural elements, soil and water pollution, and further pressure on biodiversity (Zimmermann *et al.* 2010; Haddaway *et al.* 2014; Schirpke *et al.* 2017).

In a dedicated chapter of Agenda 21 (UN 1992), mountains and uplands were acknowledged for the first time at a higher political level as a major component of the global environment, and concerns about the ongoing socio-economic and environmental decline were expressed. Moreover, mountains were explicitly mentioned in the Convention on Biological Diversity (https://www.cbd.int/mountain/). With the declaration of 2002 as the International Year of Mountains (UN 1998), emphasis was put on the specific challenges of sustainable development in mountain areas. It was recognized that, out of general guidelines or top-down centralized policies that failed to consider the specific challenges of mountain development, very little was done to conserve natural resources and empower local people to manage their living environment. Further discussions were held at the Rio+20 conference, and warnings about the vulnerability of fragile mountain ecosystems and marginalized local communities to the adverse impacts of climate change, forest degradation, land use change, and natural disasters were explicitly expressed in the outcome document 'The Future We Want' (UN 2012). Specific targets and indicators for mountains were set with the Aichi Biodiversity Targets and more recently with

the Sustainable Development Goals (SDGs, Agenda 2030, https://sdgs.un.org/goals). The Mountain Research Initiative (https://www.mountainresearchinitiative.org/) considers the SDGs as a suitable framework for assessing sustainable development in mountains because, although only a few targets and indicators refer to these regions directly, several other are pertinent and can be easily scaled down to local realities (Bracher *et al.* 2018). However, these milestones of international cooperation represent non-binding agreements between parties. There is still a pressing need for increased consideration of the challenges for sustainable development in mountainous regions, and more opportunities for interdisciplinary research on the changing mountain environment should be taken (Payne *et al.* 2017; UNEP and GRID-Arendal 2019).

Forest fires in these types of landscapes are not extensively studied such as the more notorious bush fires of Australia (Pyne 1991; Bradstock *et al.* 2012), the boreal forest fires in northeast China, the U.S., Canada, and Russia (Stocks *et al.* 2001; Shu *et al.* 2003; De Groot *et al.* 2013; Guo *et al.* 2014), or the vast savanna fires in the Brazilian cerrado (Coutinho 1990; Miranda *et al.* 2009) and sub-Saharan Africa (Barbosa, Stroppiana, *et al.* 1999; Roberts and Wooster 2008). A distinction should also be made from tropical forest fires such as Amazonia (Morton *et al.* 2008), Southeast Asia and Borneo (Fuller and Murphy 2006; Sloan *et al.* 2017), as well as the Mediterranean-type fires of California (Sugihara *et al.* 2006) or southern Europe (Keeley, Bond, *et al.* 2011). These fires often make the news headlines because of their huge sizes and extended durations, the danger they represent to the population living nearby (wildland-urban interface), or their massive ecological impacts. Instead, fires in mountainous regions are difficult to classify by a major feature such as the dominant vegetation type or a particular climate. Mountains are found at different latitudes, and the elevational gradient results in several life and climatic zones being compressed in relatively small areas. As a result, in the same region, we may find boreal-type forest fires at higher elevations, Mediterranean-style fires in pine forests, savanna-like fires in dry grasslands, and tropical forest fires at lower elevations. However, a representative feature could be put forward: in very heterogeneous landscapes, fires are in general small. Because of this peculiarity, the contribution of small fires to global assessments of fire impacts is often neglected or underestimated, like in the case of agricultural and peat fires (Van der Werf *et al.* 2010; Randerson *et al.* 2012). At the planetary scale, their share in terms of destruction of forest resources, global emissions, and influence on biogeochemical cycles is highly uncertain because of the lack of data preventing proper assessments. Instead, at the local and regional scales, these fires are very important. A small fire burning at high intensity bears the power to heavily affect those fragile ecosystems if their surface area is limited. Wildlife may suffer from excessive fragmentation and the resulting scarcity of foraging sources. Conversely, the abandonment of agricultural and pastoral land acts in favor of forest regrowth, decreasing the natural heterogeneity of mountain landscapes. This results in an increase in the size and the connectivity of flammable surfaces with related changes in fire size, severity, and intensity (Azevedo *et al.* 2011; López-Poma *et al.* 2014; Mantero *et al.* 2020). Moreover, synergies with other natural hazards are exacerbated in complex terrain. For example, trees killed by fire on steep slopes will no longer act as soil stabilizers, accelerating erosion and increasing the

magnitude of avalanches and landslides. With future climate scenarios tending towards warming and perturbations of seasonal patterns (IPCC 2014b), fire and other disturbance regimes will probably experience abnormal shifts, putting at stake the resilience of mountain ecosystems and populations.

The consequences of climate change can often be first observed in mountainous environments, such as melting glaciers, droughts, and more frequent out-of-norm natural hazards, including landscape fires. Owing to their sensitivity to the variations of climate and human activities, mountains are early indicators of what could happen in lowland areas. Continuous and extensive monitoring of the changing mountain environment is essential to support the sustainable management of its delicate ecosystems and ensure a durable provision of their services. The drivers and the impacts of wildfires, as well as their potential evolution, should be understood in the particular context of mountain complex landscapes. Fire risk frameworks should integrate the specific vulnerabilities and resilience characteristics of mountain environments and be based on empirical knowledge. The present thesis proposes a general fire risk framework for data-poor mountainous regions and provides the most essential data needed for any further analysis: a detailed historical fire dataset.

2. Problem statement

2.1. Study region

Northwest Yunnan (NWY) refers to a particular region situated in the Yunnan province of the People's Republic of China, between approximately latitude 24.5°N and 29.5°N, and longitude 98°E and 101.5°E. A clear definition of its geographical boundaries has never been appropriately stated because the term is mainly used by researchers focusing on this particular region (e.g., Xiao *et al.* 2003; Xu and Wilkes 2004; Sherman *et al.* 2007; Ren *et al.* 2009; Yang *et al.* 2014; Li *et al.* 2017). In broad terms, NWY comprises the territories of four prefectures (administrative units equivalent to counties in the U.S.A., provinces in Italy, or districts in Switzerland) of the Yunnan province, namely: Diqing, Nujiang, Lijiang, and Dali. This broader area covers a surface of about 86,700 square km, which represents more than two times the surface of Switzerland. According to a more restrictive definition, the southernmost counties belonging to the prefecture of Dali (Yongping, Yangbi, Weishan, Nanjian, Midu, and Xiangyun) and two counties in the eastern part of Lijiang (Yongsheng and Huaping) are not included in the region. This smaller area, which spans over about 67,000 square km, was also named the 'Yunnan Great Rivers Project (YGRP)' area following a long-term conservation collaboration started in 1999 between the Yunnan provincial government and The Nature Conservancy (https://www.nature.org/), and it is mentioned as such in several scientific articles (e.g., Lassoie *et al.* 2006; Ma *et al.* 2007; Sherman *et al.* 2007). A map of the boundaries of northwest Yunnan is shown in Figure 2-1. NWY lies in a peculiar geological region in the southeasternmost edge of the East Himalayas, at the transition between the Qinghai-Tibet Plateau and the Yunnan-Guizhou Plateau. It is a mountainous region that includes a section of the Hengduan mountains and other smaller complexes, characterized by very rugged terrain. The mountain peaks reach more than 6000 m a.s.l., and the deep valleys are as low as 700 m, carved by four major Asian rivers: the Dulongjiang (a tributary of the Irrawaddy), the Nujiang (upper Salween), the Lancangjiang (upper Mekong) and the Jinshajiang (upper Yangtze). In the northern part of NWY, these rivers flow from North to South in parallel and very close to each other (about 20 km distance in the narrowest point) and are separated by long mountain ranges. These exceptional bio-physical features interact with the seasonal East Asian monsoon, conferring the region a wide variety of climates, landscapes and natural habitats that, compressed within short distances, range from subtropical in the valley bottoms, rising through temperate, boreal, and arctic-alpine life zones to permanent snow on the highest summits (Ma *et al.* 2007). While temperatures are mild during most of the year, even on the vast plateaus situated at 2000 m, precipitation falls mostly between June and August following a longitudinal gradient. Higher annual precipitation amounts are found in the West, reaching 4000 mm in the Dulong valley, and decrease while moving to the East, with minima below 600 mm in the dry valleys of the Yangtze river (Wang *et al.* 2001; Ming and Shi 2007; Tang 2010).

Owing to the extraordinary topographic and environmental gradients, NWY hosts one of the world's most diverse habitats bearing rich biodiversity, a high endemism rate, and rare ecosystems. The region has been recognized as a global biodiversity hotspot and a conservation priority for plant and vertebrate biodiversity (Mackinnon and Carey 1996; Mittermeier *et al.* 1998; Myers *et al.* 2000; CEPF 2002). One of the region's protected areas complex, the Three Parallel Rivers of Yunnan Protected Areas, is inscribed in the UNESCO World Heritage Sites list (http://whc.unesco.org/en/list/1083). Among the most famous flag-species, we can mention the NWY endemic Yunnan Snub-nosed Monkey (*Rhinopithecus bieti*) and the Sclater's Monal (*Lophophorus sclateri*), a pheasant endemic of the east Himalayan region. These mountains are home to the Asian Black Bear (*Ursus thibetanus*), the Red Panda (*Ailurus fulgens*), the Kaulback's Lance-headed Pit Viper (*Protobothrops kaulbacki*), the Gongshan Lazy Toad (*Scutiger gongshanensis*), and offer rest sites for several migratory birds including the Black-necked Crane (*Grus nigricollis*). Yunnan province has the richest flora in China, harboring more than 19.000 species of higher plants, and more than 30% are found in northwest Yunnan (Yang *et al.* 2004; Pu *et al.* 2007; Sherman *et al.* 2008; Qian *et al.* 2020). Major vegetation types include alpine needleleaved forests dominated by *Pinus*, *Picea*, and *Abies* species; subtropical evergreen broadleaved forests composed of *Lithocarpus*, *Castanopsis*, and *Quercus* species; varied shrublands with succulent *Euphorbia royleana* and *Opuntia monacantha* as indicator species but also hosting young *Pinus yunnanensis*, *Rhododendron*, and *Magnolia* species. Moreover, the region hosts alpine meadows, grasslands, and arid savannas in dry valleys (Tang and Ohsawa 2009; Tang 2015). A description of NWY and southwest China's geology, climate, and vegetation can be found in Tang (2015).

The region is also known for its rich cultural heritage. More than 5,5 million people live in the four prefectures of NWY. In addition to the Han, the major ethnic group of China, about 11 ethnic minorities, including Tibetan, Naxi, Bai, Lisu, Dulong, Pumi, etc. inhabit the region and interact with the environment in different ways, varying from shifting cultivation, intensive agriculture, fishing and hunting, gathering of forest products such as medicinal herbs and fungi, and transhuman livestock grazing (Moseley 2006). However, traditional practices of land management, once limited to local subsistence and relatively sustainable, are becoming problematic with increasing population and the transition to the market economy, representing a growing pressure on the environment and, in particular, on biodiversity (Xiao *et al.* 2003; Xu and Wilkes 2004; Buntaine *et al.* 2006; Pu *et al.* 2007). This is exacerbated when considering uncertain future bio-climatic changes and high resource-demanding socioeconomic development, which includes both the agricultural and industrial sectors as well as urban expansion and tourism (CEPF 2002; Willson 2006; Ma *et al.* 2013).

Among traditional land management practices, fire has been used for millennia by local populations, especially by Tibetans in the northern part of NWY, to control vegetation growth in rangelands and farmlands, and it is still used nowadays despite strict regulations (Winkler 2000; Su *et al.* 2015). In fact, following a fire conflagration of unprecedented size and impacts in the Great Xing'an mountains, northeast China, in May 1987, in part attributed to aggressive

fire exclusion policies, the central government implemented reforms aiming to improve fire management and prevention (Shu *et al.* 2003; Chang *et al.* 2007). In NWY, every year during the dry and windy season between November and May, several uncontrolled fires affect wildland areas (Zhao *et al.* 2009), making the region one of the provincial clusters of fire activity, as shown in Figure 2-2. About 99% of forest fires whose ignition sources have been identified are human-caused, mainly related to the use of fire in agriculture or household activities such as heating and cooking, accidental ignitions, burning incense in graveyards, etc. (an example in Figure 2-3). Forest fires are frequent but of relatively small size compared to other areas of China (Shu *et al.* 2003; Xu and Wilkes 2004; Lü *et al.* 2006; Zhao *et al.* 2009; Qin *et al.* 2010; Li, Song, *et al.* 2014; Li, Zhao, *et al.* 2014; Tian *et al.* 2014). Even if small, they may destroy critical patches of forest, create or exacerbate habitat fragmentation, and increase the risk of landslides from steep slopes when heavy rains come. Because of the complexity of topography and the heterogeneous landscapes, the region's natural habitats are already highly fragmented, and ecosystems are confined to small niches, making them highly vulnerable to disturbances (Xiao *et al.* 2003; Pu *et al.* 2007; Sherman *et al.* 2008). The long-term impacts of forest fires in these delicate ecosystems are largely unknown, and no rigorous, spatially-explicit assessment of historical fire activity in the region has been done yet. Little is known about historical fire regimes and their relationship with changing vegetation cover, climatic conditions, socio-economic factors, etc. Without this baseline knowledge, it is not possible to attempt an informed assessment of potential future trends of fire occurrence. Historical and georeferenced fire datasets are the essential variable required if we want to assist land managers in planning the most sustainable fire management practices that can safeguard local ecosystem services without compromising ecosystem resilience (Bowman *et al.* 2011; Su *et al.* 2015; Santín and Doerr 2016).

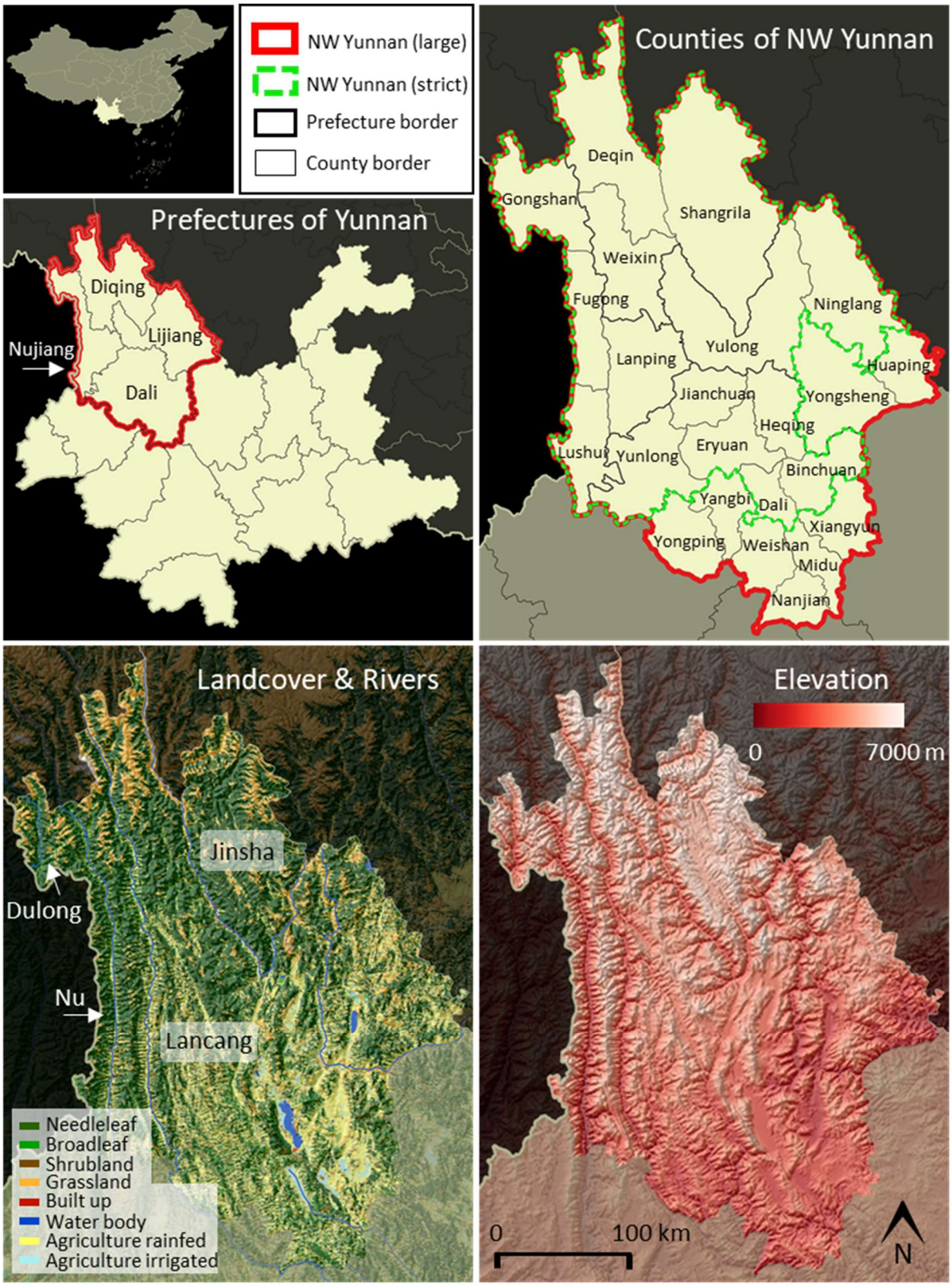

Figure 2-1. Above: maps of Yunnan administrative areas (prefectures and counties). Below: landcover and elevation maps. Data sources: landcover from ESA CCI (https://climate.esa.int/en/projects/land-cover/), elevation from ALOS World 3D – 30m (https://www.eorc.jaxa.jp/ALOS/en/aw3d30/index.htm).

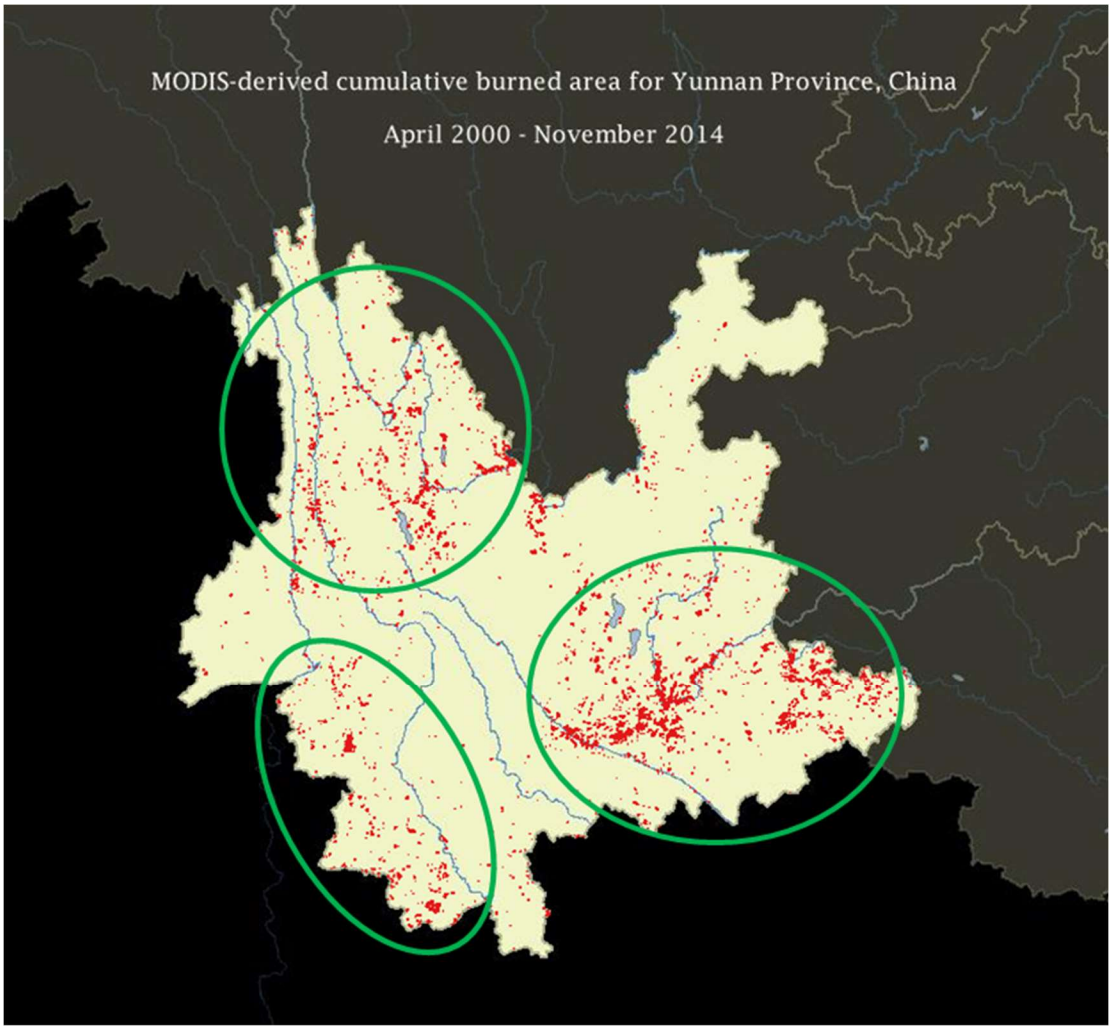

Figure 2-2. Cumulative distribution of burned area detected by the MODIS MCD45A1 product from April 2000 to November 2014 in Yunnan Province, China. Northwest Yunnan (upper left) is one of the three broad spatial clusters of recent fire activity that can be visually discerned.

Figure 2-3. Above: A fire on a mountain near Erhai Lake in Dali, China, in February 2019. Below: Burned area on Cangshan Mountain in Dali, June 2018. Photos by the author.

2.2. Getting fire data

Depending on the temporal range, information on past forest fire events can be obtained from several sources. Sedimentary charcoal records are used to study and reconstruct paleo-fire regimes (mostly from the Last Glacial Maximum but also at the geological period's scale until 420 mya) and match them with major climatic and socio-economic changes (Gavin *et al.* 2007; Power *et al.* 2008; Leys, Carcaillet, *et al.* 2013; Vannière *et al.* 2016; Blarquez *et al.* 2018), while dendrochronology can be used to date fire scars of past centuries, to several millennia (Taylor and Beaty 2005; Amoroso *et al.* 2017; Harley *et al.* 2018). For more recent times, fire records are in general collected by government agencies. Several countries have systematically recorded fire events that occurred on their territory in local, provincial, and national registries, and then organized them in centralized databases. The Canadian National Fire Database (http://cwfis.cfs.nrcan.gc.ca/ha/nfdb) or Switzerland's Swissfire database (http://www.wsl.ch/swissfire/index_EN) are two representative examples. During the last decades, satellite imagery has proven to be a valuable tool for monitoring fire and other Earth dynamics (Pettorelli *et al.* 2014). This technology presents several advantages, such as quasi-global spatial coverage, temporal continuity, and measuring consistency across space and time. They are an excellent tool for collecting data retroactively and filling information gaps, especially in data-poor regions and for low-budget users. For remote regions, satellite observations may represent the only source of information (Khawlie *et al.* 2002). In the field of fire science and management, satellite remote sensing contributions are used for the assessment of fire danger by mapping fuel types and fuel moisture content, the detection of active fires, the evaluation of fire effects on the landscape, and monitoring vegetation recovery (Chuvieco *et al.* 2020). Other remote sensing devices have been successfully employed for land surveys on smaller portions of space, such as aerial imagery (orthophotos) and Unmanned Aerial Vehicles (UAV). Thanks to their low cost and convenience, small UAV are increasingly employed in areas with difficult access such as mountains (Burchfield *et al.* 2020), and for quick and efficient monitoring of active fires (Ambrosia *et al.* 2011).

Official fire inventories are in general owned by government agencies and, unfortunately, not always freely accessible by the public. Moreover, especially for remote and less populated areas, data about historic fire events are often incomplete or inaccurate (Summers *et al.* 2011). This is the case in China (Yang 2014), where the only official and publicly available ground-based data from the government is published in the China Statistical Yearbooks and China Forestry Statistical Yearbooks (partially available at http://www.stats.gov.cn/english/Statisticaldata/AnnualData/). Basic information, such as total burned area, number of fire events, severity rank, and ignition sources are grouped yearly at the provincial level. However, locations are not provided except for a few particularly severe fire events. Unfortunately, the provincial scale of this data is not suitable for regional or local studies. Besides, past research comparing data found in Statistical Yearbooks with data extracted from satellite reported considerable differences in the estimations of burned areas, with a general tendency for underestimation by the Statistical Yearbooks (Yan *et al.* 2006).

Using satellite products to reconstruct recent land surface phenomena, including fire disturbances, in regions lacking baseline data remains the most convenient and effective option. However, the methodologies employed to map a given phenomenon may vary according to several factors such as the spatial and temporal pattern of the disturbance, its spectral characteristics, the aim of the mapping operation (change-detection, impact assessment, time-series analysis, etc.), and the physical properties of the target area. Heterogenous landscapes present several technical and methodological difficulties that make traditional remote sensing routines, particularly image processing and analysis, inadequate and prone to conspicuous errors (Schneiderbauer *et al.* 2007; Ward *et al.* 2011). The main source of errors comes from the extremely rugged terrain and multiple landforms which introduce distortions and shadows in the images complicating their interpretation. This and other challenges are among the subjects that the present thesis tackles and attempts to overcome.

2.3. Aims of the thesis, research questions, and hypotheses

In general, researchers agree that several decades of fire records are needed to understand the recent fire regime of a given region. Historical fire records are also required to assess their relationship with climate/weather, landscape, and socioeconomic factors, in particular their variability in time (Krebs *et al.* 2010; Bowman *et al.* 2011). Understanding fire regimes is an essential prerequisite for sustainable land management and fire safety operations, as well as for planning efficient resilience and adaptation measures towards changing climatic and socio-economic conditions (Chuvieco, Giglio, *et al.* 2008; Bowman *et al.* 2011; Schoennagel *et al.* 2017). The urgent need for good-quality and consistent historical datasets, high-resolution models, and a better geographic representation and coverage of the earth's pyromes, have been repeatedly pointed out by several scientists and reiterated recently (Archibald *et al.* 2013; Bowman 2018; Rogers *et al.* 2020; Bowman *et al.* 2020). In a nutshell, past observed information is necessary to understand the present situation and to predict future trends. While a fair amount of research is addressed to the main flammable biomes of the earth, this thesis acknowledges the global importance of mountains and their specific needs in terms of fire management planning. In particular, we focus on the challenges that several researchers face when trying to obtain basic data in remote and poorly accessible areas.

The main goal of the thesis is:

To develop robust methods for the reconstruction of past fire history which are suitable for heterogeneous mountain environments.

As presented in section 2.1, we take northwest Yunnan as a case study, being an ideal representative region showcasing several technical and methodological challenges in terms of data collection. The methods developed in this thesis are also meaningful to other areas facing similar difficulties.

To achieve this main goal, we organized the overall research in several related objectives listed here together with their related research questions and hypotheses.

1. **To evaluate the quality and the usability of existing global burned area products in the complex landscapes on northwest Yunnan.**

   Question: Are the widely used and freely available global fire products suitable to estimate the past fire activity in mountainous landscapes?

   Hypothesis: The existing fire products highly underestimate the impacts of fire in northwest Yunnan and are therefore unsuitable for more advanced analyses such as the assessment of risks based on past data.

2a. **To assess the spectral permanence of burn scars and their detectability by the Landsat sensors in different vegetation types and at several post-fire time-gaps.**

   Question: For how long can burned areas be successfully detected by the Landsat sensors, given potentially divergent recovery patterns of different vegetation types?

   Hypothesis: Different vegetation types recover at different speeds, and in general, burn scars are difficult to detect after one growing season.

2b. **To identify the most suitable satellite-derived vegetation indices to map burn scars in different vegetation types at different post-fire dates.**

   Question: Which spectral indices show the best separability between burned and unburned vegetation in different vegetation types at different post-fire dates?

   Hypothesis: Vegetation spectral indices perform differently in mapping burned areas at different post-fire dates in different vegetation types.

3. **To identify the different difficulties encountered when mapping burned areas in complex mountain landscapes, develop an automatic solution based on the historical Landsat archive, and evaluate its performance.**

   Question: How can we adapt remote sensing techniques to effectively map burned areas in complex mountainous landscapes without prior spatial information on past fire events?

   Hypothesis: Given the manifold difficulties of remote sensing of fire in heterogeneous landscapes, an automatic mapping routine may include specific solutions and compromise adaptations. Better mapping accuracy than existing global products is achievable.

2.4. Structure of the thesis

The thesis is structured in seven chapters. A general introduction opens on the broad topic of the role of fire in ecosystems and the complex interactions between fire, landscapes, climate, and humans. The focus will then move towards the heterogenous environmental features found in mountainous regions, their delicate ecosystems, the potential hazard represented by changing fire patterns, and the pressing need for specific management plans based on an informed assessment of past impacts of fire.

The second chapter presents the aims, research questions and hypotheses of the thesis, as well as the study region. A short introduction on the core theme of the thesis, namely the need for historical and spatially-explicit data on forest fires, is also included in this chapter.

Chapter 3 presents a conceptual model developed for understanding the patterns of forest fires in mountainous landscapes and predict potential future shifts. From the definition of the concept of *fire regime* and its components, we develop a fire risk framework inspired by the outcome vulnerability model, an approach typically employed in risk assessments of natural hazards. This chapter sets the broad context for long-term research, of which the present thesis represents only the very first and the most challenging step (data collection).

In the fourth chapter, we analyze some of the existing global fire products showing some potential to be adopted as baseline historical fire data for northwest Yunnan. We used a spatial and temporal subsection of the study area and period to obtain a rapid assessment of their mapping capabilities.

With Chapter 5, we start looking at the Landsat satellite capabilities, being the longest satellite mission providing moderate resolution (30 meters) images at regular time intervals. In a time-series perspective, we evaluate the capabilities of 11 spectral indices in detecting burn scars at 1 to 5 years post-fire dates in the four dominant vegetation types found in northwest Yunnan. The best performers are identified and integrated into the development of an automated burned area extraction routine presented in the following chapter.

The major difficulties encountered in remote sensing of fire in data-poor, mountainous complex landscapes are discussed in Chapter 6, and a prototype methodology entirely executable in free GIS software is presented. We produced a dataset of yearly fire polygons from 1987 to 2018 covering our study region, and we tested it for both spatiotemporal fire event detection and burned area mapping accuracy.

The last chapter summarizes the conclusions of each previous chapter with an emphasis on our initial research questions and re-opens with insights on the future work in line with the risk framework proposed in chapter 3.

2.5. Publications and outputs

It is important to note that the publications listed here refer to the author's day-to-day research while in his principal working place in China, under the supervision of Prof. Wen Xiao (included in the thesis jury). The conceptual risk/vulnerability framework is the fruit of the author's work during his Geneva visits in 2016, 2017, and 2018, under the supervision of Prof. Anthony Lehmann and Prof. Hy Dao, co-directors of the thesis, who also oversaw the general course of the research. The fire risk framework's actual implementation represents a second step made possible thanks to the baseline data generated in the present thesis. This step is currently in process but not included here. The related outcomes are planned for the year 2021.

The content of this thesis has been partially published in three peer-reviewed articles and one additional publication is in preparation for a Chinese peer-reviewed journal targeting a specific audience:

- Fornacca D, Wang R, Zhang C, She R, Yang X, Xiao W. Defining recent fire regime in the mountains of Northwest Yunnan using 30 years of fire records derived from Landsat time-series. (in preparation)
- Fornacca D, Ren G, Xiao W (2020) Small fires, frequent clouds, rugged terrain, and no training data: a methodology to reconstruct fire history in complex landscapes. *International Journal of Wildland Fire.* https://doi.org/10.1071/WF20072.
- Fornacca D, Ren G, Xiao W (2018) Evaluating the best spectral indices for the detection of burn scars at several post-fire dates in a mountainous region of Northwest Yunnan, China. *Remote Sensing* **10**, 1196. doi:10.3390/rs10081196.
- Fornacca D, Ren G, Xiao W (2017) Performance of three MODIS fire products (MCD45A1, MCD64A1, MCD14ML), and ESA Fire_CCI in a mountainous area of Northwest Yunnan, China, characterized by frequent small fires. *Remote Sensing* **9**, 1131. doi:10.3390/rs9111131.

A database of georeferenced fire events for the period 1987-2018 including locations, year of burn and area burned was produced and made available on a dedicated GitHub repository: https://github.com/DavideFornacca/Fire

3. A conceptual framework of fire risk in northwest Yunnan

3.1. Describing long-term fire patterns: the concept of *fire regime*

The "traditional" fire triangle concept was first proposed by Clive M. Countryman (1972) and was composed of fuel (flammable biomass), topography, and air mass (weather). In this generalized view, the author attempted to examine what he calls the *fire environment*, focusing mainly on the conditions allowing burning and fire behavior. The model has been widely adopted in fire ecology and evolved significantly toward a better distinction of the interactions and feedbacks between the multiple drivers governing wildland fires across spatial and temporal scales. Figure 3-1 represents a contemporary model proposed by Moritz *et al.* (2005), in which three different triangles correspond to processes happening at three different spatiotemporal scales. Other models exist (e.g., Scott *et al.* 2014; McGranahan and Wonkka 2018), but the underlying concepts are similar.

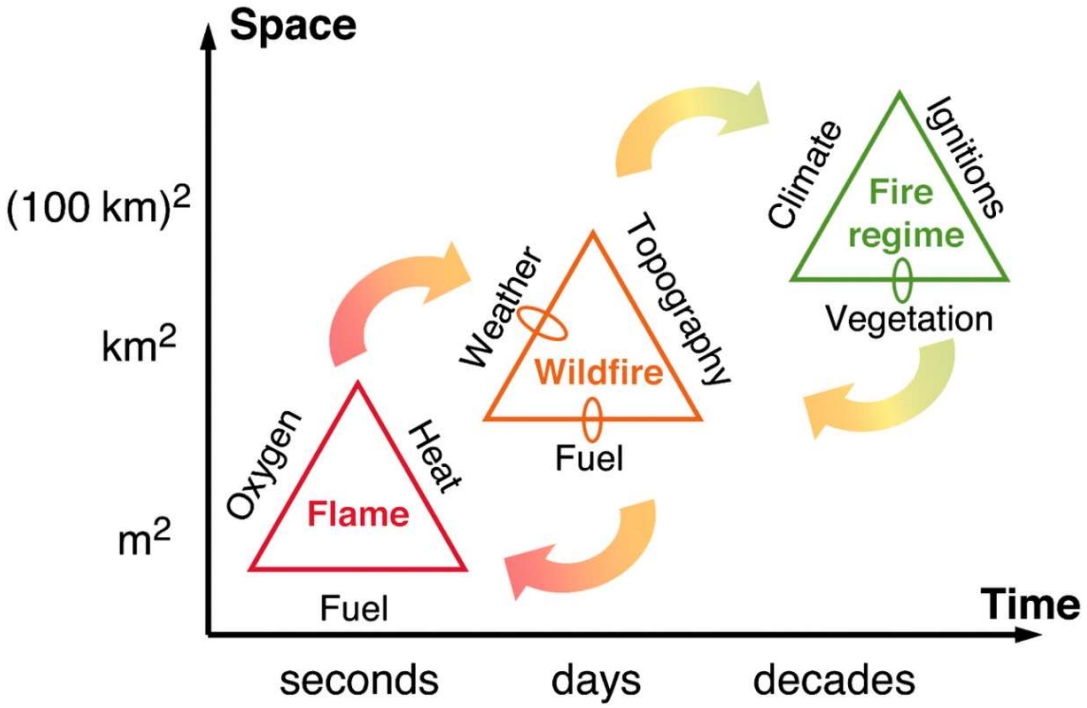

Figure 3-1. Controls on fire at different spatiotemporal scales. Dominant factors that influence fire at the scale of a flame, a single wildfire, and a fire regime. This is an extension of the traditional 'fire triangle' concept (Countryman 1972; Pyne *et al.* 1996), here including broad scales of space and time, the feedbacks that fire has on the controls themselves (small loops), as well as feedbacks between processes at different scales (arrows). Original figure from Moritz *et al.* (2005).

The fundamental elements for a flame to exist are a source of heat (or ignition), fuel, and oxygen. Scaling up to the size and duration of a wildfire, elements determining the condition of fuels and fire behavior (intensity and spread), such as topography and weather, become dominant.

When studying the dynamics of wildland fires over several decades and at the landscape or regional level, we talk about *fire regimes*. Here, fuels are more broadly categorized by vegetation types, while climate patterns are more suitable descriptors of the fire system than short-term weather variables, and ignition sources, whether natural or anthropogenic, are specified. These triangle representations have the advantage of simplifying the fundamental aspects of fire but are not enough to describe all the complex interactions between the different controls. For example, except for the ignition sources, the human dimension influencing vegetation or climate patterns in the case of anthropogenic climate change is not included in this model (McGranahan and Wonkka 2018).

Our main reason for showing Figure 3-1 is to locate the spatiotemporal context of the present research. We aim to set up a framework to better understand the long-term fire occurrence dynamics in northwest Yunnan's mountainous region. For this purpose, the concept of *fire regime* (third triangle) represents a good starting point. As briefly introduced in Section 1.1, this concept has been widely used to classify different fire systems using a set of measurable variables. Fire regimes are regular, multi-decadal burning patterns deeply embedded in different ecosystems at the regional scale. For the sake of clarity, we will follow the conceptual framework proposed by Krebs *et al.* (2010), which is the result of a substantial review of the concept's history and multiple definitions (Figure 3-2). A narrower definition (*sensu stricto*) of fire regime includes only core components related to the spatiotemporal patterns of fire occurrence, that can be grouped in "where" factors (fire locations, distribution, clusters, size, etc.), "when" factors (chronology, seasonality, fire return interval, fire rotation, etc.), and "which" factors (vegetation type and layer, fire behavior and intensity, etc.). In a broader sense (*sensu lato*), the concept includes biotic and abiotic factors controlling the occurrence of fire, including but not limited to those indicated in the fire triangle model. These factors may comprise fuel characteristics (flammability, connectivity, volume, etc.), meteorology and climatic conditions, ignition sources, morphological features of the landscape such as topography, land and fire management policies, and synergisms with other disturbances. Moreover, the immediate effects of fires on landscapes (ecological severity) and human societies may be integrated. Further parameters can be derived from the analysis and combination of the other three groups. The authors clearly state that all parameters are facultative and should be used in a well-defined context according to research and policy goals, as well as data availability. Indeed, the primary information necessary to define most of the model parameters is a dataset of burn events. Some variables such as fire return interval require decades of fire records to be calculated; geographic coordinates are necessary to assess spatial patterns, while only a fine temporal resolution allows the identification of intra-annual variations.

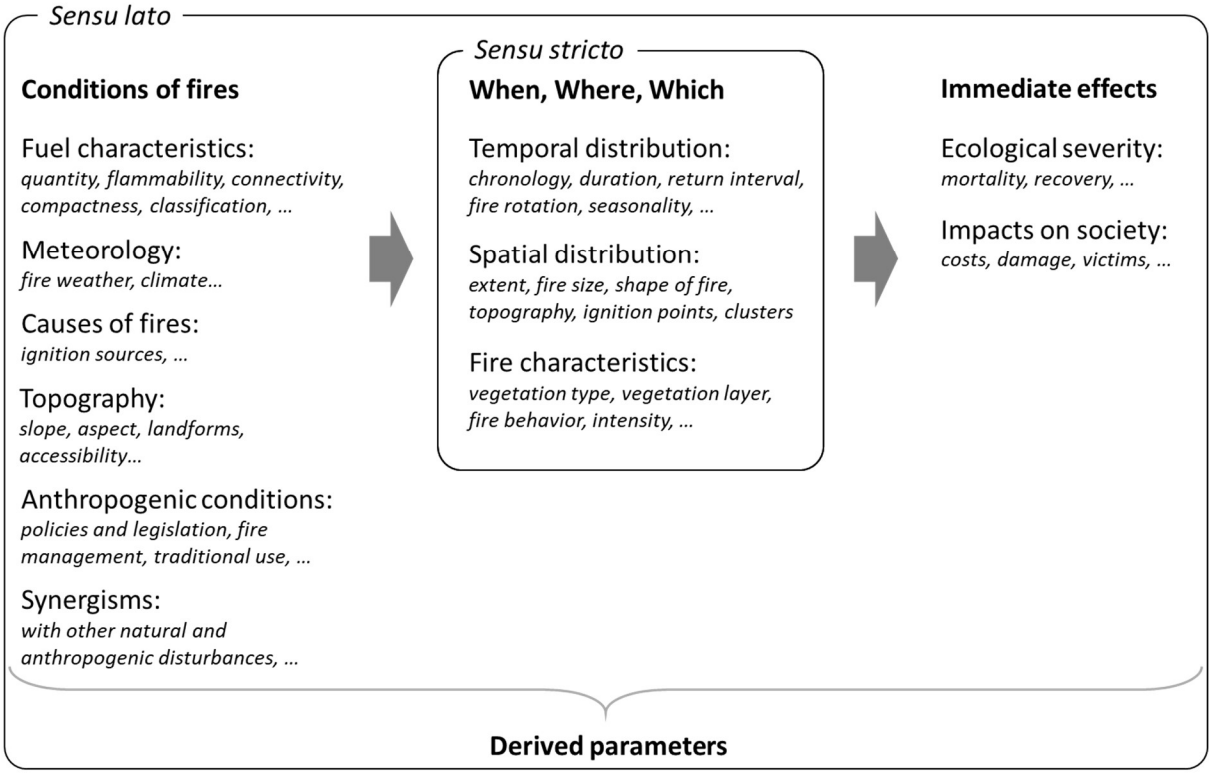

Figure 3-2. Conceptual model of fire regime parameters. Adapted from Krebs *et al.* (2010).

The fire regime framework shown in Figure 3-2 is our modification from the original model by Krebs *et al.* (2010), which can be found in Appendix A for reference. Our adaptation aims to better include the role of topography, which in mountain's complex environments is probably among the most dominant features. Elevation, slope, and aspect interact with climate / weather conditions and sun exposure, influencing vegetation type and the moisture content of soils and fuels. Consequently, fire spread, burn intensity, and severity may be limited or expanded (Deng *et al.* 2007; Linn *et al.* 2007; Flatley *et al.* 2011; Cansler and Mckenzie 2014; Fang *et al.* 2015; Harris and Taylor 2019; Mitsopoulos *et al.* 2019), and post-fire vegetation regeneration and structure may be in turn influenced (Han *et al.* 2015; Ireland and Petropoulos 2015; Bassett *et al.* 2017). Steep slopes affected by fire are more susceptible to subsequent surface erosion and landslides causing changes in soil composition, loss or redistribution of soil, and modification of hydrological systems, also several years after the fire where vegetation recovery is slow (Wondzell and King 2003; Shakesby 2011; Abney *et al.* 2017; Nunes and Lourenço 2017). The relationships between multiscale climatic conditions, including extreme weather events such as prolonged droughts, abnormal temperatures, and storms, with the occurrence, spread, and severity of wildfires have been studied widely and are often considered the dominant determinants of the variation of fire regimes in several biomes (e.g., Jessie 1995; Piñol *et al.* 1998; Taylor and Beaty 2005; Crimmins 2006; Flannigan *et al.* 2009; Zumbrunnen *et al.* 2011; Koutsias *et al.* 2013; Chen *et al.* 2014; Jolly *et al.* 2015; Harvey *et al.* 2016). Another

among the major conditions shaping fire dynamics are anthropogenic interventions. In some ecosystems, such as Mediterranean shrubs and tropical forests, in wildland-urban interfaces, and in those rural and mountainous areas where shifting cultivation is a common practice, humans represent the main fire ignition source. In other biomes such as boreal forests, ignitions by lightning are more common. Long-term land management and fire policies, as well the traditional use of fire have shaped most landscapes and fire regimes to become highly anthropogenic (Pausas and Keeley 2009; Bowman *et al.* 2020), with direct impacts on the number and size of fire events and indirect impacts on the severity and intensity of fires.

The employment of the fire regime model is an essential step to understand the role of fire in a given region. First of all, a range of 'normality' of fire occurrence can be determined and used as a reference for comparison with past and future conditions. Moreover, the multiple factors participating in the system can be identified and included in the model to obtain a better description of the phenomenon. However, these technical specifications of a region's fire activity, if they remain purely descriptive, have limited implications for fire management. Monitoring the spatiotemporal pattern of fire events (i.e., the *sensu stricto* variables) and their immediate impacts is important to detect potential shifts (a deviation from the usual pattern), but the reasons for such shifts are often the result of complex interactions between the different conditions of fire, the fire itself (previous burns), and long-term effects (forest recovery patterns, etc.). To better interpret and understand these complex interactions and the covariation among the different parameters (linear or not), multivariate predictive approaches are often used (Weinstein and Woodbury 2010; Leuenberger *et al.* 2018). These approaches also have the advantage of being able to simulate future fire conditions by modifying certain variables based on projected scenarios. In this context, researchers rely on the concept of risk and probability to support decision making in forest fire policies.

Before extending our discussion on fire risk frameworks, we will have a look at the existing literature (mostly in English) on the fire regimes of China, in particular for the Yunnan province and our study area.

3.2. Fire regimes in China and Yunnan

In China, only a few studies attempted to describe current or historical fire regimes and were in general either encompassing broad regions at relatively coarse spatial resolution or related to specific case studies. The term "fire regime" is rarely used, but publications focusing on one or more controls of fire, patterns of fire occurrence, and impacts of fire are numerous. Therefore, we will mostly focus on those studies related to Yunnan province and northwest Yunnan, but we will also include broader regions if they are themed explicitly on fire regimes.

Chen *et al.* (2017) used MODIS data to extract twelve variables, including fire frequency, intensity, size distribution, and vegetation characteristics. These variables were clustered on a 0.5° grid resulting in six distinct fire regimes in China (Figure 3-3). Most of Yunnan province

was classified as a "low frequency, sporadic, and intense forest fires" region, but a few areas, including the northwest, were "frequent and small fires with a very long fire season duration", which according to observed data is more correct (Shu *et al.* 2003). Using a totally different approach, Krawchuk and Moritz (2009) inferred China's fire regimes by training generalized additive models on climate data and fire regime classes from the United States. Their results showed at least three different kinds of fire regimes in Yunnan due to the high climatic gradient in the province. Their identification of the dominant vegetation and typical ecological effects of fire in NWY were quite correct (Regime R35-200$_{forest}$: return interval of 35-200 years, mixed-wood/evergreen conifer forests with shrub understorey, shrublands. Surface fire in a forest, understorey biomass, including seedlings/saplings, is consumed, non-lethal for mature trees). Other satellite observations showed that anthropogenic fire emissions are mainly owed to crop residue burning in China, even if poorly underestimated by the sensors, and forest fires are concentrated in north and southwest China (Song *et al.* 2009).

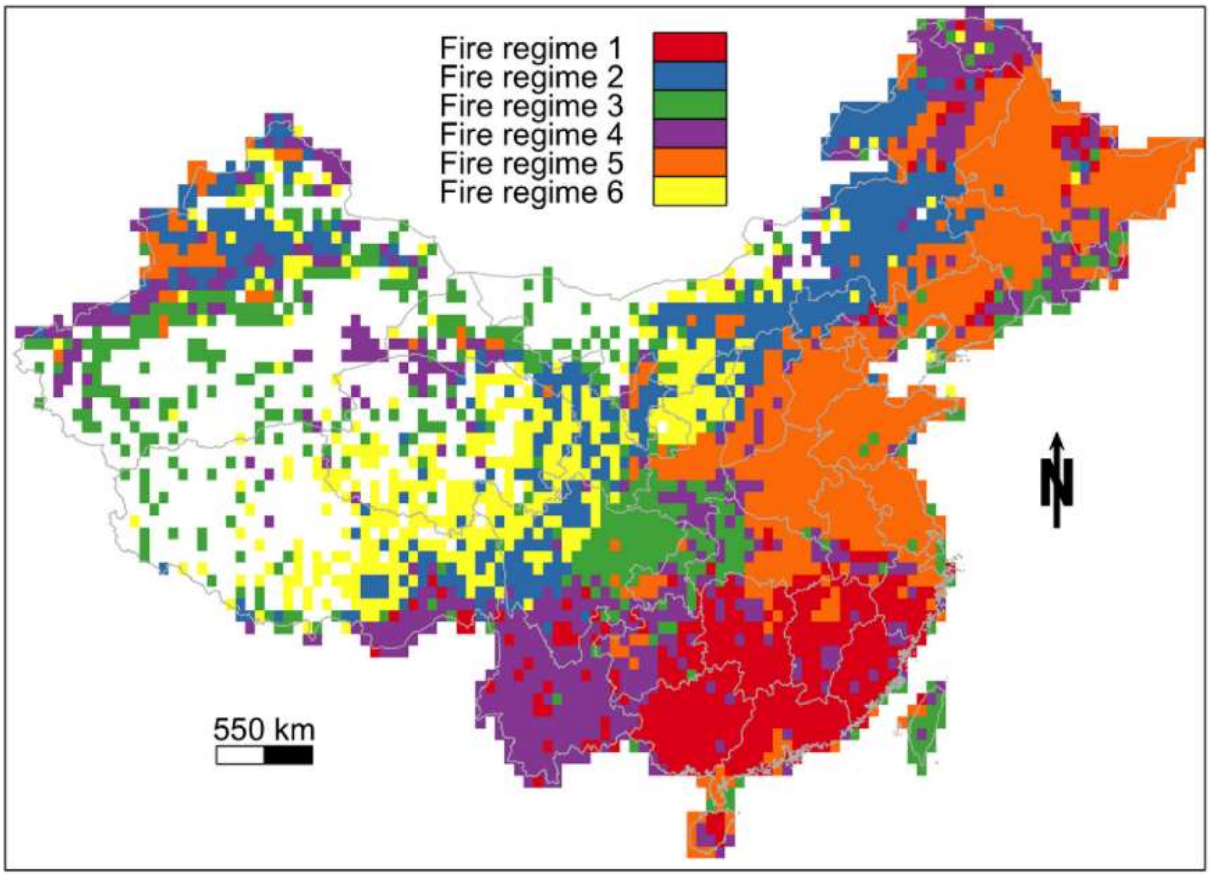

Figure 3-3. The fire regimes of China. Fire regime 1, mainly in southern China: frequent and small fires with a very long fire season duration. Fire regime 2, in inland regions: infrequent, irregular, and high intensity grassland fires. Fire regime 3, mainly in Sichuan basin: infrequent, low intensity and small fires that are not detectable in MCD64A1. Fire regime 4, in northeastern and southwestern China: low frequency, sporadic, and intense forest fires; Fire regime 5, in Northeast and North China plains: frequent, regular, and unevenly sized cropland fires. Fire regime 6, in western China: insignificantly burned grassland fires with low frequency, low intensity and high inter-annual variability. Original figure and caption from the study of Chen *et al.* (2017).

Studies in the boreal forest of northeast China investigated the effects of long-term fire suppression policies on the local fire regime (Chang *et al.* 2007; Wang *et al.* 2007), assessed past decades fire danger and regime (Chang *et al.* 2008; Tian *et al.* 2013), analyzed drivers of fire occurrence (Fang *et al.* 2015) and modeled potential future trends under climate change scenarios (Liu *et al.* 2012). Focusing on the Central Yunnan Plateau, which includes a part of our mountainous study area, Su *et al.* (2015) analyzed how the major vegetation types of the area adapt to fire and determined that the current fire regime is driven by fire-dependent ecosystems. Other studies suggested the particular resilience of Yunnan ecosystems, which are composed of numerous re-sprouting species with high post-fire recovery rates, depending mostly on topographic factors (Han *et al.* 2015, 2016). On a much wider temporal scale, Xiao *et al.* (2017) analyzed macroscopic charcoal records of the region and identified three postglacial periods with high-frequency and high-severity fires. They suggest that, when vegetation and fires were mainly influenced by climate with little human interference (before 4.3 ka), frequent and intense fires played an unfavorable role on plant diversity in the area. Focusing on paleo-fires and recent climatic variables, Li, Hughes, *et al.* (2017) analyzed microscopic charcoals collected in Yunnan sediments to reconstruct past fire dynamics and compared them to a modern fire database. They found that temperatures in the dry periods were the main factor controlling fire frequency for both eras. Another study found that the presence of flammable pine forests and seasonal drought conditions were also present during the late Pliocene (Huang *et al.* 2020). This fire-temperature relationship in the dry season, as well as the influence of other weather variables, were confirmed in other studies focusing on recent fire occurrences in Yunnan (Zhao *et al.* 2009; Chen *et al.* 2012; Zhou *et al.* 2012). A set of multivariate analyses of several landform, meteorological, and vegetation factors but excluding human influences, pointed out the role of the Hengduan mountains in shaping the distribution of seasonal precipitation, thus contributing to higher fire activity in NWY (Cao *et al.* 2017). Surprisingly, we found very little information on human impacts on recent fire patterns. One modeling effort highlighted humans' key role in igniting most wildfires at an intermediate distance from dense activity areas such as countryside villages and farmland (Ye *et al.* 2017), while another study found a higher explanatory power in fire prevention policies (Xiong *et al.* 2020).

3.3. From the fire regime model to a fire risk framework

Fire management is a very complicated task requiring significant amounts of economic resources and, most of all, experience and knowledge. If, after decades of fire management policies dominated by aggressive suppression implemented in several parts of the world, we thought we reached the full domestication and control of the fire element, the growing resurgence of catastrophic wildfires experienced in recent years is proving that mitigation programs need to be reevaluated and that we are still far from understanding the phenomenon (Gill *et al.* 2013; Calkin *et al.* 2014; Bowman *et al.* 2020). Approaches attempting to mitigate fire occurrence (suppression), or the severity, intensity, and spread of fire (thinning, pruning, prescribed burning,

etc.) have shown both successes (Boer *et al.* 2009), mostly in the short term, and failures in the long term. Fuel treatments are sometimes ineffective and require significant and continuous investments to cover large areas while prescribed fire aiming at mimicking pre-industrial fire regimes conflicts with other societal objectives such as reducing emissions and protection of human health (Stubbendieck *et al.* 2007; Pastro *et al.* 2011; Driscoll *et al.* 2015; Buizer and Kurz 2016; Prichard *et al.* 2017). Fire suppression has modified the composition and load of fuels in fire-prone and fire-dependent ecosystems, and together with climate change and excessive human interference on landscapes, is blamed for worsening the impacts of wildfires (Chang *et al.* 2007; Wang *et al.* 2007; Pausas and Keeley 2019).

3.3.1. The Outcome Vulnerability model employed in climate change vulnerability assessments

Fire seems to be the only natural hazard that we stubbornly try to fight, while for other ones such as earthquakes, hurricanes, and floods, we focus more on assessing risks, identifying vulnerabilities, and promote adaptation (Moritz *et al.* 2014). By acknowledging that wildland fires are inevitable, an integrated risk and vulnerability framework as those employed in climate change research and natural hazard assessment may represent a suitable approach to analyze the problem and minimize unwelcome impacts. The very general meaning of *risk* and *vulnerability* is quite common and does not require to be defined here. However, when it comes to their related conceptual frameworks, several definitions and descriptions of components exist, according to different analytical contexts and the research disciplines from where they originate (Nelson *et al.* 2010; Fellmann 2012). When employing them, it is therefore important to clarify their meaning, the research context, the methodological approach, and the targeted spatiotemporal scale. For the purpose of the present thesis, we propose a framework integrating the general risk of fire occurrence and the vulnerability of a particular element at risk (land systems), following the Outcome Vulnerability model used by the IPCC in the climate change context. This model is reproduced in Figure 3-4, modified and adapted from Allen Consulting Group (2005), O'Brien *et al.* (2007), and Fellmann (2012). We chose this earlier model from IPCC because of its simplicity, adaptability to the fire hazard context, and suitability to predictive approaches using future change scenarios. Moreover, there are no apparent nested components, and no excessive relationships are represented. The current IPCC vulnerability model can be found in Appendix B and in IPCC (2014b).

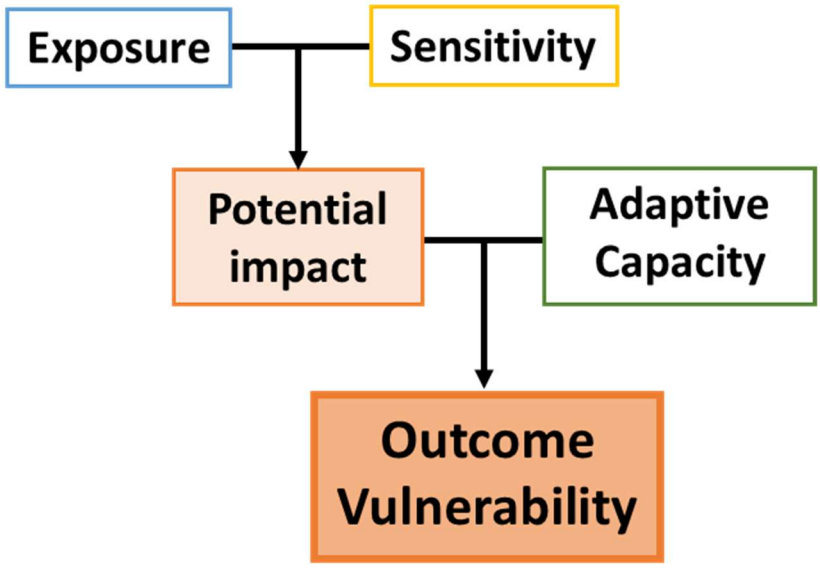

Figure 3-4. Components of an early Outcome Vulnerability model employed by IPCC in the climate change context. Modified and adapted from Allen Consulting Group (2005), O'Brien *et al.* (2007), and Fellmann (2012).

The idea behind the Outcome Vulnerability concept is that the vulnerability of a system (natural habitats, people) to the adverse effects of climate change is a function of three elements. Exposure is the magnitude of climate change likely to be experienced by a system located in a risk area. Sensitivity is the degree of harm inflicted to a system by climate change. Adaptive capacity is the system's potential to tolerate or adapt to climate change effects (O'Brien *et al.* 2007; Dawson *et al.* 2011; Ofori *et al.* 2017). An initial function between exposure and sensitivity defines the potential impact that climate change may have on a system. The system's adaptive capacity, such as existing prevention and mitigation measures or other sources of resilience, may moderate the potential impacts of climate change. The result of this second function is called outcome vulnerability, which can be defined as the propensity of a system to be adversely affected by climate change effects. In this model, the vulnerability is the end-point of a sequence of analyses based on well-defined systems and variables that can be quantified and measured, as well as modified according to projected climatic scenarios from regional and global circulation models (Fellmann 2012). For example, the exposure of living communities to climate change is typically quantified using species distribution models for wildlife or population maps for humans, fitted with climate variables, and then projected onto modeled future climate scenarios (Dawson *et al.* 2011; Ofori *et al.* 2017). Another approach used in the climate change context, typically by social scientists, is the Contextual Vulnerability (or starting-point interpretation), which focuses more on the initial conditions, both biophysical and socio-economic, that determine the vulnerability of a system, i.e., its inability to cope with changing conditions. Because the latter model is more suitable from a human-security perspective (O'Brien *et al.* 2007), we considered it less adaptable to our study.

3.3.2. *The Outcome Vulnerability model adapted to fire hazard*

If, instead of climate change as the object representing hazard, we put wildfire, and as the element at risk, we chose the land systems (as opposed to human property), then the Outcome Vulnerability model could be developed as shown in Figure 3-5. Based on the spatiotemporal scale of the fire regimes (Figure 3-1), the components of our vulnerability framework would be:

- **Exposure:** representing the risk of fire occurrence in a given location, sometimes referred in the literature as fire susceptibility or fire danger. This is determined by the interaction between the various environmental conditions of fire such as those considered in the fire regime model or the classical fire triangle: topography (elevation, slope, aspect, ruggedness, etc.), climate/weather (temperature, precipitation, drought, fire weather indices, etc.), vegetation type (a proxy of fuel flammability, fuel volume, etc.), and human factors (as ignition source, population density, proximity and accessibility to natural land, etc.).

- **Sensitivity:** the response of the element at risk considered when exposed to fire, determining its initial vulnerability. Here we consider the ecosystems' resilience toward to a given fire regime (fire-dependent, fire-intolerant, etc.). We may include species distribution models, protected areas, and provision of ecosystem services as elements representing the sensitivity of different land systems. In heterogeneous mountain environments, forest fragmentation and the size of vegetation patches may be extremely important for assessing the sensitivity to fire. For example, fire-intolerant forests are highly vulnerable to fire, but big patches or well-connected habitats may be more resilient than small, fragmented, and isolated patches.

- **Adaptive Capacity:** the potential of human societies to adapt and control the occurrence of fire. Land management policies, including fire management, laws and regulations, as well as the behavior of people (cultural practices, education, awareness), have an impact on the final vulnerability of land systems. Climate change mitigation efforts may also influence the outcome vulnerability of the system by affecting the climatic control in the exposure element.

The advantage of this structure is that the various components of the model are well separated, making the task of selecting datasets representing each variable, as well as choosing a method for analyzing these variables and compute the model functions relatively easy. However, in the real world, things are much more interconnected. The distinctions between the three elements, especially between sensitivity and adaptive capacity, are sometimes ambiguous, and some degree of nesting pre-exists in the datasets used as proxies in the model (Ofori *et al.* 2017). For example, using distance buffers from villages and roads to represent accessibility by humans to flammable land could refer to fire ignition, but also to extinction potential. The same landcover

dataset may be employed to represent fuel type as an element of exposure and to define the sensitivity of different landscapes.

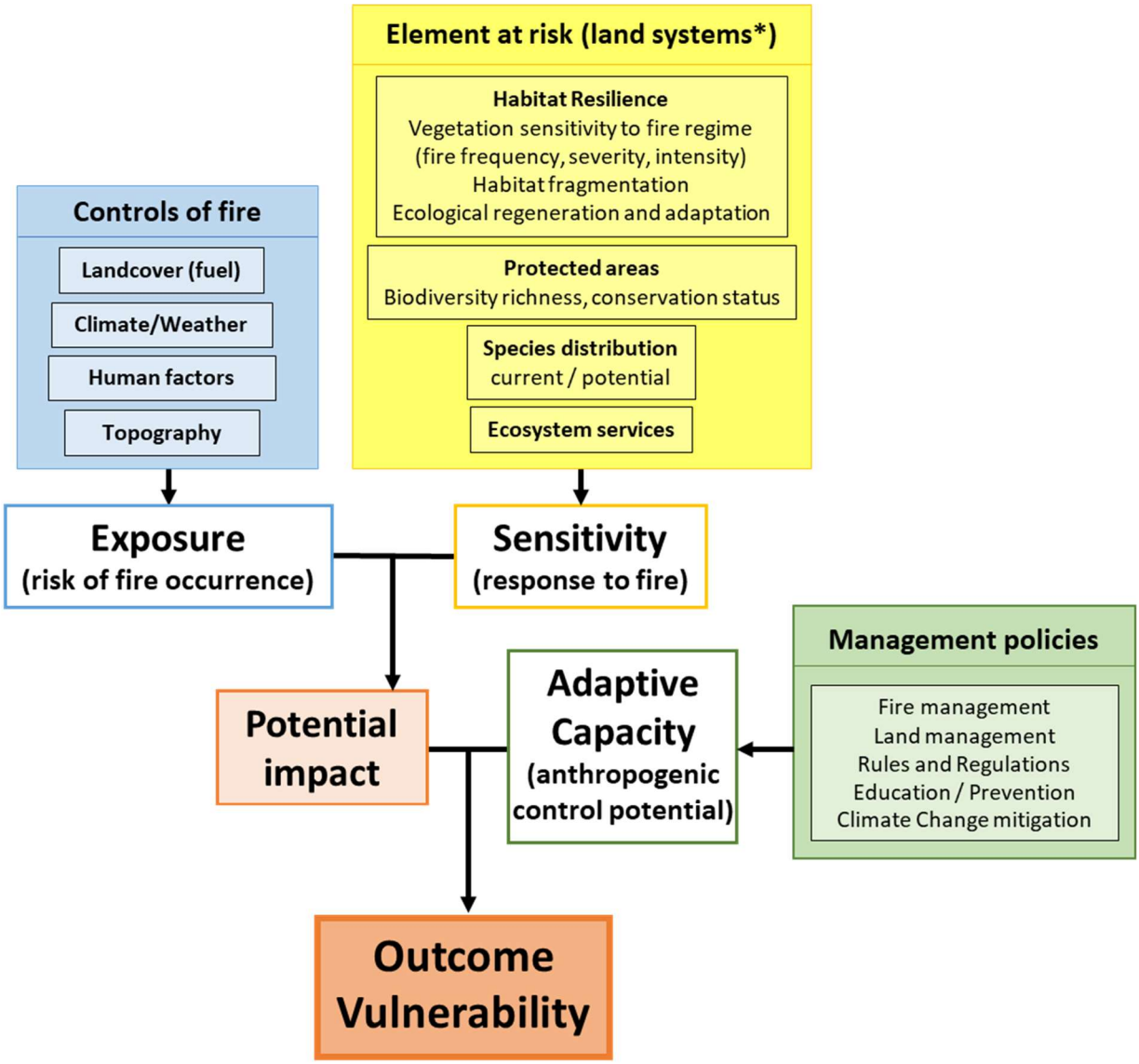

Figure 3-5. Conceptual framework for the vulnerability of land systems to fire developed using an Outcome Vulnerability model. *The components indicated in the yellow box are relevant to the chosen element at risk, which in our case, are the land systems. Other parameters may be more suitable for a different target.

In addition to the voluminous literature on the relationship between fire frequency, size, or severity, with one or more stressors (conditions of fire), authors that proposed quantifications of the present and future risks of wildland fires still focused mainly on exposure. The multi-variate approaches employed and the sources and types of data utilized to define fire risk are numerous (Chuvieco and Congalton 1989; Alonso-Betanzos *et al.* 2002; Ercanoglu *et al.* 2006; Krawchuk *et al.* 2009; Li *et al.* 2012; Chang *et al.* 2013; Li, Zhao, *et al.* 2014; Tian *et al.* 2014; Bui *et al.* 2016; Knorr *et al.* 2016; Valdez *et al.* 2017; Forkel *et al.* 2017; Cao *et al.* 2017; Leuenberger *et al.* 2018; Tehrany *et al.* 2018; Srivastava *et al.* 2019; Jia *et al.* 2019; Kalantar *et al.* 2020). Significantly fewer research effort was put on integrating elements of exposure with vulnerable targets, i.e., the sensitivity of the element at risk (Fennell and Dowling 2003; Chuvieco *et al.* 2010, 2014; Zumbrunnen *et al.* 2011; Soto *et al.* 2013; Semeraro *et al.* 2016; Parente and Pereira 2016; Young *et al.* 2017; Bañales Seguel *et al.* 2018; Dupire *et al.* 2019; Ghorbanzadeh *et al.* 2019), and even less added mitigating factors of adaptive capacity (Gai *et al.* 2011; Connell *et al.* 2019). It is not in the scope of the present thesis to review and describe all these valuable approaches; however, we should note that a first attempt to integrate exposure, sensitivity, and adaptive capacity in the same model specific to fire hazard was proposed by Lavorel *et al.* (2007). For reference, we reproduced this model in Appendix C. Their model shows partially nested elements, several arrows representing causes and effects, and feedback loops. The authors integrated and discussed the different interactions between the dynamics of fire regimes (meso-climate, fire regime, landcover, and land use), the consequences on biophysical and biochemical processes on land and atmosphere, and the consequences for goods, services, and land use (ecosystem functions and services). Such representation gives an idea of the complexity of the human-environment systems involved in fire dynamics, but this complexity can act against the purpose of modeling, that is, simplifying reality.

As a final paragraph for this contextual chapter of the thesis, we propose a potential employment of the proposed conceptual framework. For land management purposes, our integrated risk/vulnerability model aims at identifying and predict the potential impacts of fire on natural habitats (land systems) so that effective adaptive measures and policy adjustments can be implemented in the more sensitive and exposed regions, minimizing the end-point vulnerability of the whole system (Figure 3-6). To fully evaluate the impacts of present and new management policies on the outcome vulnerability, the model should be used iteratively by modifying the different datasets using different scenario narratives and adjusting with new observed results.

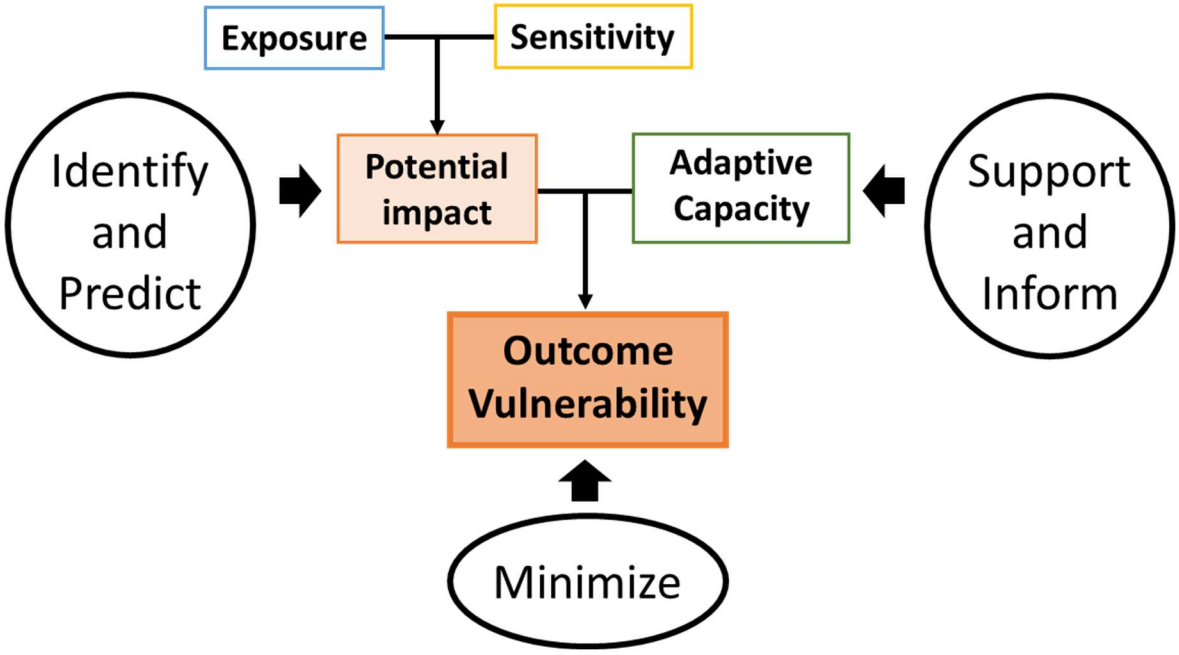

Figure 3-6. Intended use of the integrated risk/vulnerability framework.

Having this framework in mind is an important theoretical step of research. However, to put this model as well as the more descriptive fire regime model into practice, an essential element is needed: historical fire data. The following chapters are all dedicated to making this possible.

4. Evaluation of existing global burned area products

Based on an updated version of:

Fornacca D, Ren G, Xiao W (2017). Performance of three MODIS fire products (MCD45A1, MCD64A1, MCD14ML), and ESA Fire_CCI in a mountainous area of northwest Yunnan, China, characterized by frequent small fires. *Remote Sensing* **9**, 1130.

Abstract: An increasing number of end-users looking for ground data about fire activity in regions where accurate official datasets are not available adopt a free-of-charge global burned area (BA) and active fire (AF) products for applications at the local scale. One of the pressing requirements from the user community is an improved ability to detect small fires (less than 50 ha), whose impact on terrestrial environments is empirically known but poorly quantified, and is often excluded from global earth system models. The newest generation of BA algorithms combines the capabilities of both the BA and AF detection approaches, resulting in a general improvement of detection compared to their predecessors. Accuracy assessments of these products have been done in several ecosystems; but more complex ones, such as regions that are characterized by frequent small fires and steep terrain has never been assessed. This study contributes to the understanding of the performance of global BA and AF products with a first assessment of four selected datasets: MODIS-based MCD45A1; MCD64A1; MCD14ML; and ESA's Fire_CCI, in a mountainous region of northwest Yunnan; P.R China. Owing to the medium to coarse resolution of the tested products and the reduced sizes of fires (often smaller than 50 ha) we used a polygon intersection assessment method where the number and locations of fire events extracted from each dataset were compared against a reference dataset that was compiled using Landsat scenes. The results for the two sample years (2006 and 2009) show that the older, non-hybrid products MCD45A1 and, MCD14ML were the best performers with Sørensen index (F1 score) reaching 0.42 and 0.26 in 2006, and 0.24 and 0.24 in 2009, respectively, while producer's accuracies (PA) were 30% and 43% in 2006, and 16% and 47% in 2009, respectively. All of the four tested products obtained higher probabilities of detection when smaller fires were excluded from the assessment, with PAs for fires bigger than 50 ha being equal to 53% and 61% in 2006, 41% and 66% in 2009 for MCD45A1 and MCD14ML, respectively. Because of the technical limitations of the satellites' sensors, a relatively low performance of the four products was expected. Surprisingly, the new hybrid algorithms produced worse results than the former two. Fires smaller than 50 ha were poorly detected by the products except for the only AF product. These findings are significant for the future design of improved algorithms aiming for increased detection of small fires in a greater diversity of ecosystems.

Keywords: MODIS fire; ESA CCI; burned area detection; mountainous region; Northwest Yunnan; small fires

4.1. Introduction

In recent years, earth observation using sensors on board space-borne satellites has provided useful raw data to detect and monitor active fires and extract burned land patches, not only at national or larger geographic scales but also at the continental and global scales (Tian *et al.* 2005; Zhang *et al.* 2011; Mouillot *et al.* 2014). The availability of free-of-charge, global scale active fire (AF) and burned area (BA) products such as the MODIS derived products (Justice, Giglio, *et al.* 2002) has significantly increased the interest of global community end-users in their adoption for regional to local applications, especially in areas where ground data are lacking or are not publicly available (Mouillot *et al.* 2014). Global AF algorithms use thermal sensors to detect unusual thermal signatures from ongoing fires, and, when this signal is very strong, they are quite reliable. However, detection is only possible during satellite overpasses above the area that is burning, while clouds and dense smoke caused by fires may compromise their detection (Giglio 2007; Roy *et al.* 2008). Examples of global AF detection products include the ATSR Word Fire Atlas product (Arino *et al.* 2012) and MODIS MCD14 (Giglio *et al.* 2003, 2016). Global BA products algorithms are designed to capture abrupt changes between pre- and post-fire reflectance caused by the altering effect of burning on the biomass and the deposit of char and ash on the ground. The resulting burn scars are more persistent in time than the thermal signatures of ongoing fires, but not always easy to detect or distinguish from other disturbances when burn severities are low. Among global BA products, the European Space Agency (ESA) produced GLOBSCAR for the year 2000, using data from the ERS-2 and ATSR-2 sensors (Simon *et al.* 2004). ESA also developed the GBA2000 project (Tansey 2004) and its modified version, the L3JRC project (Tansey *et al.* 2008), based on SPOT-VEGETATION data at 1 km resolution. The algorithms of these two products were combined with the GLOBSCAR algorithm to produce the GlobCarbon BA (Plummer *et al.* 2006, 2007), a multi-sensor approach that covers a longer time period (1998–2007). More recently, under the Fire_cci project, ESA developed the several BA algorithms designed for different sensors, such asFireCCI41 (Alonso-Canas and Chuvieco 2015) based on ENVISAT's MERIS sensor which offers spectral bands in the visible and near infrared spectrum at a spatial resolution of 300 m, and the newest FireCCI51[2] based on MODIS data (Chuvieco *et al.* 2018). Furthermore, NASA's satellites Terra and Aqua are equipped with the MODIS sensors, whose data has been used to produce the MCD45 (Roy, Jin, *et al.* 2005; Roy *et al.* 2008) and MCD64 (Giglio *et al.* 2009) global BA products. The latter was integrated in the Global Fire Emission Database version 4 (GFED4), which is widely used for atmospheric and biogeochemical models (Giglio *et al.* 2010, 2013) and now includes a hybrid version including active fire products (Randerson *et al.* 2017). The MODIS fire products are appreciated by the community of practitioners for their user-friendly access and manipulation, their relatively high spatial resolution (500–1000 m), and their reliability (Mouillot *et al.* 2014; Padilla *et al.* 2015). Several alternative, hybrid, multi-sensor approaches can be found in the

[2] FireCCI41 is the product used in this assessment because it was the latest available at that time (2017). Note that in the present study, we will refer to this product using its original name: Fire_CCI. It is now superseded by FireCCI51.

literature (Van der Werf *et al.* 2006, 2010; Tsela *et al.* 2014), but, for the moment, those methods have not yet delivered a final, ready-to-use product, or are deprecated.

Satellite images are acquired using different types of sensors having different specs in terms of spatial, spectral, and temporal resolution. Consequently, the interpretation of burned vs. unburned pixels can potentially be very different among BA and AF algorithms. Comparative analyses and validation research have shown that, in dissimilar ecosystems, the performance of global AF, and BA products varies considerably (Boschetti, Eva, *et al.* 2004; Schroeder *et al.* 2008; Giglio *et al.* 2010; Núñez Casillas *et al.* 2013; Freeborn *et al.* 2014; Chuvieco *et al.* 2016). All of the above-mentioned global BA and AF products have been widely validated for the main fire-prone biomes, such as boreal forests, Mediterranean scrub and pine forests, tropical forests, woody savannas, and grasslands (Roy, Frost, *et al.* 2005; Csiszar *et al.* 2006; Roy and Boschetti 2009; Urbanski *et al.* 2009; Anaya and Chuvieco 2012; Núñez Casillas *et al.* 2013; Tsela *et al.* 2014; Araújo and Ferreira 2015), but alpine ecosystems have never been assessed.

In this study, we assess the performance of selected global AF and BA products in a portion of our study area situated in the mountainous region of northwest Yunnan (NWY), China. In order to improve the resources management and maintain the ecosystem services in the steep mountainous region of NWY, there is the pressing need to set up a database of historical fire events that will be used as input data for effective risk assessment models. To serve this purpose, we evaluated the potential of global fire products to detect fire events in NWY. We selected those products with the most suitable features in terms of spatial resolution and temporal span[3], and compared them with a reference dataset based on visual interpretation of Landsat TM scenes. The chosen products were MODIS's MCD45A1, MCD64A1, MCD14ML; and ESA's Fire_CCI. A detailed description of each product is provided in the next section. Based on our results, we cross-compared burned areas obtained from the best BA product with those obtained from the only pure AF products (MCD14ML), in order to evaluate the potential use of a merged AF and BA product similar to the ones proposed by Randerson et al. (Randerson *et al.* 2012) or Tsela et al. (Tsela *et al.* 2014). Because of the medium-to-coarse resolution of the selected datasets, a relatively big rate of errors of detection of small fires (<50 ha) is very likely to occur. Small fires may cover only a fraction of the product's pixel and the heterogeneity of burn severities may reduce the spectral signal left by the burn scar, reducing the probability of detection. In the case of the products using AF approaches, small fires' duration may be too short to be detected. Previous studies reported larger errors of omission for small fires (Csiszar *et al.* 2006; Giglio *et al.* 2009; Li, Song, *et al.* 2014; Tsela *et al.* 2014; Araújo and Ferreira 2015). The main aim of this study is to identify which product performs the best and to judge its suitability for applications that require a more accurate and quantified measure of fire activity. The best dataset could be used to generate seeds or as a control data for the accuracy assessment of future regions-specific algorithms.

[3] Note that this selection was performed at the time of the study, which was during the year 2017.

4.2. Data and methodology

4.2.1. Description of study site

This study was done using the broader definition of northwest Yunnan (see Section 2.1). Therefore, a few areas in the southwest portion of the region are included here but not in the following studies. Because of the large amount of time needed to map burned areas from Landsat scenes manually, for this analysis we selected one sample area corresponding to Landsat WRS-2 (Worldwide Reference System) path 131, row 42, and excluded the portions that are outside of the NWY boundary (Figure 4-1). We chose this area because of its high frequency of fires and the availability of cloud-free satellite images for the accuracy assessment. Moreover, the variety of ecosystems that it contains, appropriately represent NWY.

4.2.2. Data processing

In this study, we aim to test the ability of the chosen products in the detection of burn scars, which we consider as objects. We are interested in the number of fires and their location, and not in a subpixel analysis of burned area accuracy (more details in Section 4.2.3). In this perspective, the main processing task consists in the aggregation of raw burned pixels to form consistent objects with unique ID and attributes, called 'fire events'. To guide the aggregation, spatial and temporal rules need to be defined, so that pixels spatially and temporally adjacent belonging to the same fire event are grouped. We chose to produce datasets that are tailored to the spatial and temporal resolution of the sensor from which they were originated. Spatial and temporal accuracies of each product were considered individually. This approach has the advantage to be more flexible to later treatments if fire events need to be further aggregated to satisfy user requirements.

The specifications and processing of the selected AF and BA products and the reference dataset, as well as the spatial and temporal rules for the aggregation of burned pixels are described in detail in the following subsections. Main products' characteristics are summarized in Table 4-1. All data manipulations were performed using geoprocessing techniques within the free GIS software QGIS (http://www.qgis.org).

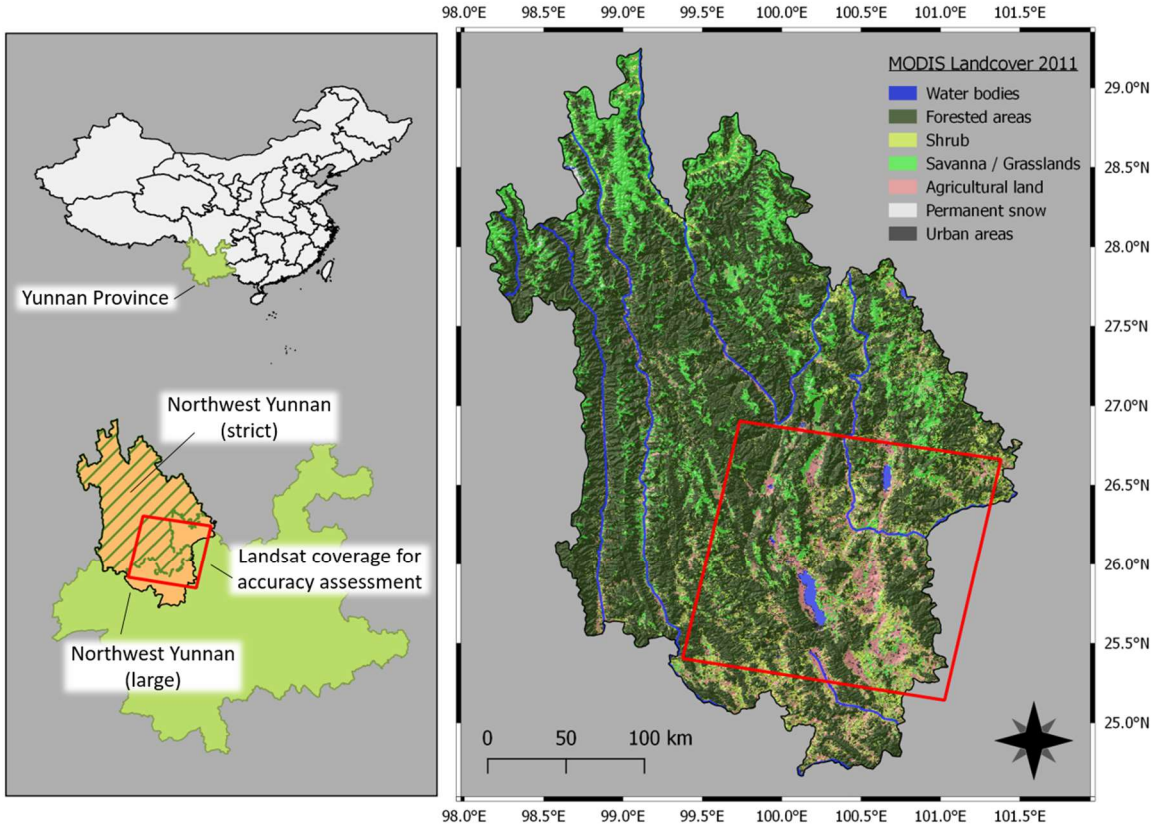

Figure 4-1. Location of the study area. The most restrictive boundaries of northwest Yunnan and a broader definition of the region, as well as the Landsat coverage selected for the accuracy assessment are represented. The large map shows the main landcover classes according to MODIS MCD12Q1 product for 2011 over a shaded relief. Most recent MCD12Q1 version: https://lpdaac.usgs.gov/products/mcd12q1v006/.

4.2.2.1. MODIS Burned Area Collection 5.1 (MCD45A1)

MCD45A1 is one of the MODIS land products suite generated with global MODIS imagery from the Terra and Aqua satellites (Justice, Townshend, *et al.* 2002). The algorithm used to generate this product relies on a bi-directional reflectance model change detection approach to map rapid changes in daily surface reflectance time-series data, at a pixel size of 500 m. Fires occurred in previous seasons or years are excluded and only recent fires are mapped. MCD45A1 information and data access can be found on a dedicated website that is maintained by the University of Maryland (http://modis-fire.umd.edu/). The data are delivered as monthly composites depicting per-pixel approximate Julian day of burning with an eight-days precision interval before and after the date of detection, confidence of detection, surface type, and other information. We selected this product for its relatively high spatial and temporal resolution, and for its good performance (Chang and Song 2009; Anaya and Chuvieco 2012; Moreno Ruiz *et al.* 2013).

We downloaded monthly composites of MCD45A1 from 2001 to 2015, clipped to the extent of NWY (large) and reprojected to the local UTM zone (47N), conserving the 500 m pixel size. To maximize the probability of detection, we kept fire pixels having both high and low confidence of detection levels, but we excluded fire pixels that are mapped over agricultural areas, as recommended in the product's documentation. MCD45A1 retrieves landcover classes from the MODIS MCD12 Land Cover Type Yearly global product (https://lpdaac.usgs.gov/products/mcd12q1v006/). The burned pixels were then aggregated to form consistent fire events using the intersection (logical AND) of the following two rules:

- **Spatial rule:** burned pixels should be directly adjacent to each other or within a maximum distance of 1 pixel. We chose a 1-pixel buffer to minimize inaccuracies related to the coarse spatial resolution of the sensor, such as partially burned pixels that remain undetected.
- **Temporal rule:** pixels should have burning dates within a maximum temporal distance of 16 days. This rule is based on the 8-days precision interval before and after the date of detection proper to the product's algorithm.

The resulting fire events were finally organized in a vector database.

4.2.2.2. MODIS Active Fire Collection 6 (MCD14ML)

The MODIS Active Fire product is produced using a contextual algorithm that applies thresholds to the brightness temperatures from the middle-infrared and thermal infrared channels of the MODIS instrument. Active fires are mapped at 1 km resolution during satellite overpass and, in order to limit false detections, potential burning pixels undergo a series of tests, masking operations, and further rejection tests. MCD14ML is a global monthly fire location product that is delivered as plain ASCII files. It contains the geographic location, date, and some additional information for each fire pixel detected by the sensors. Data download, description, user manuals, and algorithm details can be found on the MODIS Active fire and Burned Area products website (http://modis-fire.umd.edu/). We chose this product for the potential of its different approach and the relatively high resolution. In fact, even if the product's pixel size is 1000 m, under very good observing conditions, a smaller fire of 100 m2 or even 50 m2 can be detected (see the user guide on http://modis-fire.umd.edu/guides.html). Indeed, cloud coverage is the main factor compromising the good detection of active fires and fires may last too shortly to be detected during the next satellite overpass.

Monthly composites of MCD14ML from 2001 to 2015 were downloaded, clipped to the extent of our study region, and reprojected to the local UTM zone (47N). Agriculture fires were masked using MCD12 landcover product. Because MCD14ML hotspots represent fires at 1 km resolution that could be located anywhere within the pixel, the whole pixel was considered as burned. We calculated a 500 m buffer around each point and aggregated the resulting polygons when they were touching or intersecting, and with AF dates differing less than four days, to form

consistent fire events. The temporal distance is reduced when compared to MCD45A1 because the thermal sensor detects fires when they are active, with a high temporal accuracy.

4.2.2.3. MODIS Direct Broadcast Burned Area Collection 6 (MCD64A1)

MCD64 is the latest product of the MODIS Burned Area suite of products. It has been adopted as the standard MODIS burned area product for collection 6, replacing the former MCD45 suite, which will not be generated beyond Collection 5.1. It is based on a hybrid approach that exploits the potential of both MODIS 1 km active fires and 500 m surface reflectance input data. A burn-sensitive vegetation index is calculated from MODIS time series using the short-wave infrared channels, and dynamic thresholds are applied to detect persistent spectral changes. Afterwards, cumulative active fire maps are used to generate regional probability density functions for the classification of burned and unburned training samples that will guide the final determination of burned and unburned pixels. More information and a complete description of the algorithm can be found in Giglio *et al.* (2009). MCD64A1 presents a general improvement in burned area detection over past collections. In particular, a significantly better detection of small fires, and the adaptability to different regional conditions across multiple ecosystems are among the main positive aspects of this product.

In the same manner as the previously introduced MODIS products, we retrieved and processed MCD64A1 GeoTIFF series. The MCD12 landcover mask was applied to exclude burns over agricultural land and fire events were generated using the same spatial and temporal rules used for MCD45A1. Veraverbeke *et al.* (2014) assessed the temporal accuracy of the MCD64A1 product to be more than 4 days before and after the date of detection. We opted for a 16-day temporal window to be consistent with MCD45A1.

4.2.2.4. ESA's Fire_CCI

ESA's Fire_CCI product provides the burned area metric used to quantify the Fire Disturbance variable of the Essential Climate Variables within the ESA's Climate Change Initiative (ESA-CCI). ESA-CCI program details can be found on its webpage (https://climate.esa.int/en/esa-climate/esa-cci/) and in (Hollmann *et al.* 2013). The product was developed in an effort to meet end-users' requirements of a higher resolution BA product. The developing team opted for the capabilities of the Envisat-MERIS 300 m resolution images, which are collected approximately every three days, depending on the latitude. Because the MERIS sensor was mainly designed for ocean color applications and not for land observations, its application to fire disturbance assessment is deemed as scarce (Alonso-Canas and Chuvieco 2015). To overcome these limitations, MERIS data was combined with daily hotspot locations from the MODIS thermal anomalies product (MCD14ML), also contributing to the reduction of commission errors related to the approaches that are entirely based on reflectance changes. The algorithm follows a hybrid two-phase approach: a seed selection phase from MODIS hotspots followed by a Region Growing analysis phase over the MERIS's NIR band and a NIR-derived

spectral index. The resulting product is offered in two forms: a Pixel BA product at 300 m resolution and a Grid BA product at 0.25 degrees resolution.

We downloaded monthly composites of Fire_CCI Pixel BA version 4.1 from https://catalogue.ceda.ac.uk/uuid/bcef9e87740e4cbabc743d295afbe849 [4]. The product time coverage spans from 2005 to 2011. It contains a layer with the date of the first detection, a confidence level layer, and a landcover layer for only the burned pixels, extracted from the CCI Landcover maps (https://climate.esa.int/en/projects/land-cover/). Sub-setting, reprojection, and landcover masking operations were performed, and the same spatial rules as MCD45A1 were applied. Because for regions with high cloud coverage the date of detection may be several days or even weeks after the fire is extinguished (Pettinari *et al.* 2016), the time interval used to aggregate pixels considered as belonging to the same fire event, was increased to 28 days.

Table 4-1. Summary of the selected active fire (AF) and burned areas (BA) products.

Product	Satellite	Spatial Resolution	Temporal Resolution	Time Coverage	Algorithm	Reference
MCD45A1	MODIS Aqua & Terra	500 m	Daily (Terra: day; Aqua: night)	2001–January 2017	Bi-directional reflectance model-based change detection approach	(Roy, Jin, *et al.* 2005)
MCD14ML	MODIS Aqua & Terra	1000 m	Daily (Terra: day; Aqua: night)	2001–present	Contextual algorithm applied on middle and shortwave infrared channels	(Giglio *et al.* 2016)
MCD64A1	MODIS Aqua & Terra	500 m	Daily (Terra: day; Aqua: night)	2001–present	Hybrid algorithm using AF hotspots and dynamic threshold over multi temporal spectral indices changes	(Giglio *et al.* 2009)
Fire_CCI	Envisat-MERIS and MODIS Aqua & Terra	300 m	Daily (MODIS AF); ~3 days (MERIS)	2005–2011	Hybrid algorithm using AF hotspots and multi-temporal changes in reflectance	(Alonso-Canas and Chuvieco 2015)

4.2.2.5. Landsat reference dataset

No suitable official data on fires was available for our study region. Hence, we decided to compare the vector fire events datasets derived from the four selected AF and BA products with a reference dataset that was compiled using 30 m Landsat imagery. Using higher-resolution datasets, such as the Landsat and ASTER archives, is a robust approach that is commonly

[4] This is the current website where the latest and the deprecated datasets can be retrieved.

employed by researchers when assessing the accuracy of BA products of coarser spatial resolution (Barbosa, Grégoire, *et al.* 1999; Roy, Frost, *et al.* 2005; Schroeder *et al.* 2008; Araújo and Ferreira 2015; Padilla *et al.* 2015). Visual interpretation is a time-consuming task because it is performed manually by the analyst who, using empirical knowledge and personal experience, identifies and maps burned patches in the image. Burned areas are clearly visible in Landsat images when integrating the infrared band in the image composite (Figure 4-2, black color), especially when comparing a pre-burn scene with a post-burn scene. Because of time availability constraints, we selected two sample years to be used in the accuracy assessment. The selected years were 2006, from Julian day 25 to 345; and 2009, from Julian day 17 to 52 of the following year (2010). These time frames were chosen for the particularly high fire activity in the study region and the availability of a relatively high number of cloud-free Landsat scenes within the two years. Five Landsat scenes for 2006 (Julian days 25, 57, 137, 217, 345) and six Landsat scenes for 2009 (Julian days 17, 33, 49, 81, 273, and 52 of year 2010) were used to perform visual interpretation, by comparing each scene with the following one in the time line. Additional scenes with only partial visibility over the study region owing to clouds were kept as support in the process. Spectral indices and transformations, such as Tasseled Cap, Normalized Difference Vegetation Index, Normalized Burn Ratio, and image differencing techniques were used to assist the analyst in the extraction of burned areas and the creation of the final reference dataset. Only fires bigger than 12.5 ha (half of a MODIS pixel) were included in the analysis.

4.2.3. Accuracy assessment

Rigorous validation, accuracy assessment protocols, and recommendations have been proposed in the literature (Roy, Frost, *et al.* 2005; Morisette *et al.* 2006; Olofsson *et al.* 2014), but are not suitable for the purpose of our study. The frequent small fires that characterize our study region are difficult to detect with precision using the medium-to-coarse resolution products that we selected to run this task. Specifically, sub-pixel accuracy of burned areas would not give results that are pertinent with what we really want to assess. Therefore, we opted for a more flexible methodology to evaluate their performance against a reference dataset. In this study, the assessment was performed using a polygon intersection approach (Figure 4-2), where the focus is put on the ability of AF and BA products to detect a fire event independently from the size and shape of the burn. Instead of assessing the accuracy of the detection pixel by pixel, we assessed the accuracy of the count and locations of fire events. If a fire event is fully or only partially detected, then the detection is considered as equally successful. To be considered valid, a burned polygon from the tested dataset should at least touch a reference polygon. Commission and omission errors are not related to the area of the fire events that were partially detected, but to those totally omitted or committed. In practice, we selected the tested products' polygons that intersected reference polygons using spatial analysis tools within QGIS, and we compiled an error matrix with the entirety of the reference and tested datasets' fire events. True negative data (non-fire polygons correctly detected) were not artificially created to be included in the error matrix, and they were therefore excluded from the accuracy assessment.

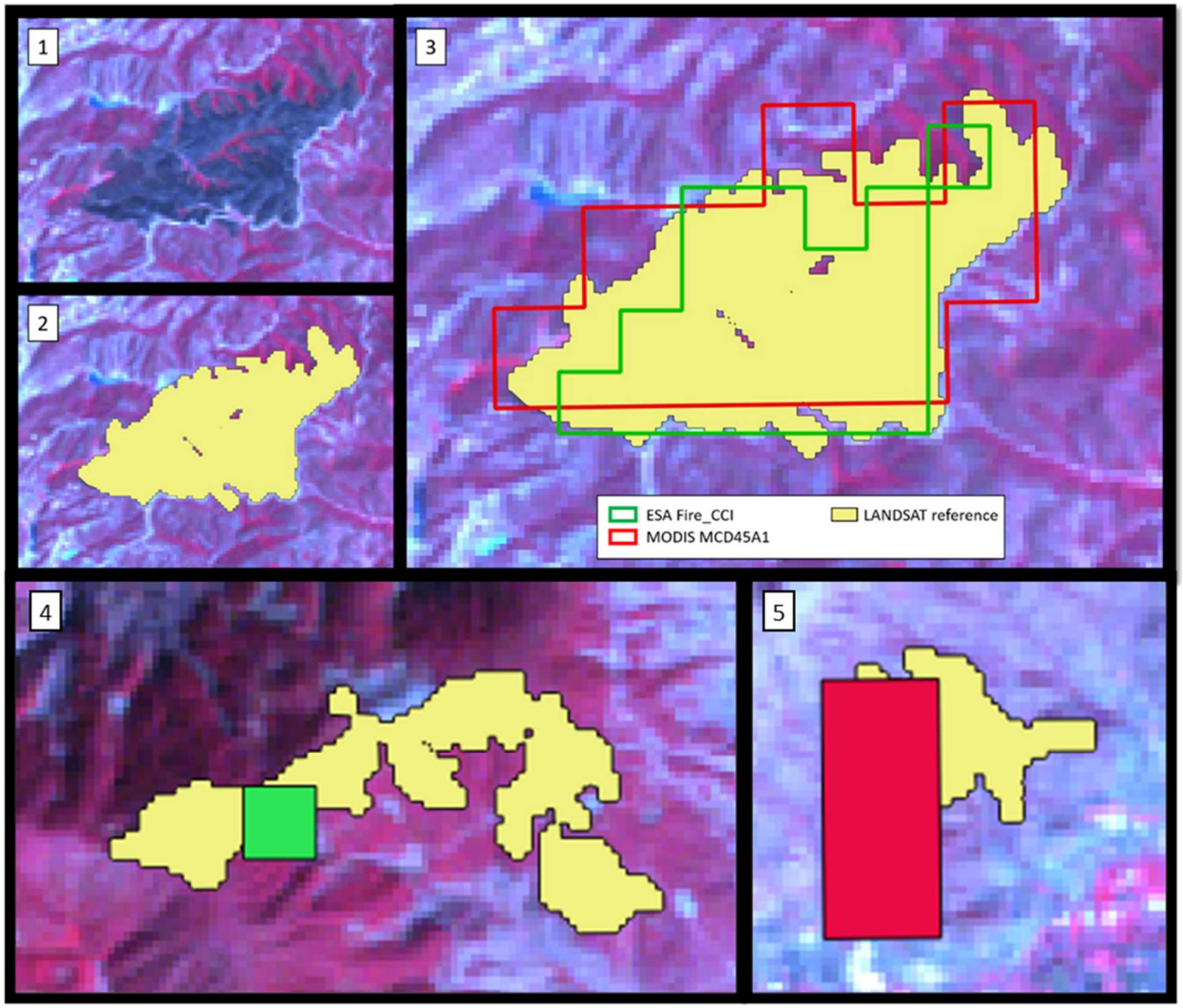

Figure 4-2. Example of polygon intersection assessment: 1. Burn scar visible on Landsat false color infrared composite; 2. Reference dataset manually mapped burn polygon; 3. European Space Agency's (ESA's) Fire_CCI and MCD45A1 products overlay; 4 and 5. Other examples of detection from the two products. Despite both products show different degrees of omission and commission errors at a sub-pixel level, in our accuracy assessment, the two detections of the fire event are considered equally successful.

The usual binary error matrix metrics were extracted to quantify and compare the different products. The metrics were the user's accuracy (UA), which is a measure of the reliability and precision of the product, the producer's accuracy (PA), which denotes the sensitivity, or the probability of detection, and the F1 score [77], also known as Sørensen index or Dice's coefficient, which is the harmonic mean of the two metrics previously mentioned.

Other common metrics relying on true negative data, such as overall accuracy, were not calculated because of their absence in the error matrix. Equations of the three metrics are listed below:

$$\text{F1 Score: F1} = \frac{2\text{TP}}{2\text{TP} + \text{FP} + \text{FN}}$$

$$\text{User's Accuracy: UA} = \frac{\text{TP}}{\text{TP} + \text{FP}} \times 100$$

$$\text{Producer's Accuracy: PA} = \frac{\text{TP}}{\text{TP} + \text{FN}} \times 100$$

where:

- TP = True Positive values, fire events correctly detected by the tested product
- FP = False Positive values, fire events erroneously detected by the tested product (commission)
- FN = False Negative values, fire events not detected by the tested product (omission)

The polygon intersection methodology used in this study could lead to inconsistent results when a tested product heavily overestimates burned areas, because within-polygon commission error is not included in the calculations. However, in general, BA algorithm designers tend to minimize commission errors at the cost of larger omission errors (Roy and Boschetti 2009). Moreover, this more flexible methodology can reduce classification errors raising from image registration inaccuracies. By the mean of these metrics, we compared every tested product towards the reference dataset for the year 2006, 2009, 2006 & 2009 combined, and for three different fire sizes (full dataset: >12.5 ha; more than one MODIS pixel: >25 ha; more than two MODIS pixels: >50 ha) to highlight which product performs better with bigger and smaller fire sizes. Furthermore, we cross-analyzed the best BA performer with the only pure AF product to find out if the two products show divergent abilities in the detection of fires. If the two products detect different fire events - i.e., a low number of correctly detected fires in common between the two products – combining the two products could potentially increase the probability of detection (PA).

4.3. Results

Individual performances of the four tested global products are summarized in Table-4-2. Overall, the capabilities of all the products in the detection of small burned areas in this mountainous study region are relatively low. For both years 2006 and 2009, and consequently 2006 and 2009 combined, the best performer was MCD45A1, displaying the highest F1 scores (0.42, 0.24, 0.31, respectively) and the highest UA (lower errors of commission). The best PA was obtained by the only pure active fire product (MCD14ML), which reached 47% in 2009, but this result was to the detriment of UA, which was among the lowest, and had a negative impact on the F1 score. The other two products, MCD64A1 and Fire_CCI, showed lower performances

in the detection of fire events. In 2006, the probability of detection of all the products increased when excluding smaller fire events from the analysis, exceeding 25% for fire sizes bigger than 50 ha (two MODIS pixels), except for Fire_CCI, who only scored 17%. In 2009, PAs improved with an increasing fire size, but for MCD45A1 and MCD64A1 the values were lower than in 2006, while for MCD14ML and Fire_CCI, PA values were higher (66% and 18% for fires bigger than 50 ha).

Details about PAs per fire event size are shown in Table 4-3. According to the reference dataset, there were 70 fire events in total in 2006: 15 fire events with a BA size between 12.5 to 25 ha, 19 fire events between 25 to 50 ha, and 36 fire events bigger than 50 ha. In 2009, a total of 144 fire events occurred with number (n) per size of 55, 45, and 44, respectively. In both years, most of the fire events that were correctly detected by the products were bigger than 50 ha. Only MCD14ML was able to detect smaller fires conspicuously, especially in 2009. The other products scored very low, with detected events smaller than 50 ha virtually null.

A more detailed analysis of the user's accuracy is illustrated in Table 4-4. We classified each committed fire event by its size in pixels. We can clearly observe that most of the committed fire events are of very small size (mostly 1 pixel) for the three MODIS products, while Fire_CCI shows more weighty errors in both 2006 and 2009. The very low UA of MCD14ML shown in Table 4-3 appears less serious when adding fire size information.

The results of the cross-comparison of MCD45A1 and MCD14ML are shown in Table 4-5. For the two assessed years, the number of fire events correctly detected by both products was very small when compared to the sum of corrected detections when merging the two products. In total (2006 & 2009 combined), only 22 out of 120 correctly detected fires were in common between MCD45A1 and MCD14ML. If these two datasets were combined to form a unique merged dataset, the producer's accuracy would clearly increase. PAs of the merged products, including all fire sizes, would be 59%, 55%, 56%, while MCD45A1 alone has 30%, 16%, 21%, and, MCD14ML alone has 43%, 47%, and 46% for the years 2006, 2009, and 2006 and 2009, respectively. Consequently, UA would also be smoothed down, with a negative impact on the F1 scores. Still, F1 scores for the merged product would be better than any single product in 2009 and the second best in 2006.

Table 4-2. Performances of MCD45A1, MCD64A1, MCD14ML, and Fire_CCI products in a control site in northwest Yunnan for the year 2006, 2009, and 2006 & 2009 combined. F1 score and user's accuracy (UA) are shown for burned areas (BA) > 12.5 ha (full dataset) only, while producer's accuracy (PA) is shown for BA > 12.5 ha, > 25 ha, and > 50 ha.

	2006					2009					2006 & 2009				
	F1 score	UA (%)	PA (%) BA>12.5ha	PA (%) BA>25ha	PA (%) BA>50ha	F1 score	UA (%)	PA (%) BA>12.5ha	PA (%) BA>25ha	PA (%) BA>50ha	F1 score	UA (%)	PA (%) BA>12.5ha	PA (%) BA>25ha	PA (%) BA>50ha
MCD45A1	0.42	70	30	36	53	0.24	52	16	24	41	0.31	59	21	28	46
MCD64A1	0.22	69	13	16	25	0.08	30	5	6	9	0.13	44	7	10	16
MCD14ML	0.26	19	43	51	61	0.24	16	47	57	66	0.25	17	46	55	64
Fire_CCI	0.16	37	10	13	17	0.1	11	10	13	18	0.12	15	10	13	18

Table 4-3. Number of fire events correctly detected (det) and producer's accuracy (PA) of MCD45A1, MCD64A1, MCD14ML, and Fire_CCI products in a control site in northwest Yunnan for the year 2006, 2009, and 2006, and 2009 combined. Three different BA sizes are shown: 12.5 to 25 ha, 25 to 50 ha, and >50 ha.

	2006						2009						2006 & 2009					
	BA 12.5-25ha (n=15)		BA 25-50ha (n=19)		BA > 50ha (n=36)		BA 12.5-25ha (n=55)		BA 25-50ha (n=45)		BA > 50ha (n=44)		BA 12.5-25ha (n=70)		BA 25-50ha (n=64)		BA > 50ha (n=80)	
	det	PA	det	PA	det	PA	det	PA	det	PA	det	PA	det	PA	det	PA	det	PA
MCD45A1	1	6.7%	1	5.3%	19	52.8%	2	3.6%	3	6.7%	18	40.9%	3	4.3%	4	6.3%	37	46.3%
MCD64A1	0	0.0%	0	0.0%	13	36.1%	2	3.6%	1	2.2%	4	9.1%	2	2.9%	1	1.6%	17	21.3%
MCD14ML	2	13.3%	6	31.6%	22	61.1%	17	30.9%	22	48.9%	29	65.9%	19	27.1%	28	43.8%	51	63.8%
Fire_CCI	0	0.0%	1	5.3%	6	16.7%	2	3.6%	4	8.9%	8	18.2%	2	2.9%	5	7.8%	14	17.5%

Table 4-4. Number of committed fire events organized by their size in pixels. Pixel size is relative to individual fire products.

	N° of fire events / commission pixels											
	2006						2009					
	1px	2px	3px	4-7px	8-20px	>20px	1 px	2 px	3px	4-7px	8-20px	>20px
MCD45A1	7	2	.	.	.	.	9	2	3	4	4	1
MCD64A1	2	2	.	.	.	.	5	9	.	.	2	.
MCD14ML	100	20	7	.	.	.	239	69	15	21	3	.
Fire_CCI	3	.	2	3	2	2	55	19	7	13	13	7

Table 4-5. Cross-comparison of reference fires detected and not detected by MODIS MCD14ML (active fire) and MCD45A1 (burned area). The tables emphasize fires detected by both products, fires detected by only one of the two products, and fire not detected by both products. This cross-comparison is useful to evaluate if the two products are sensitive to the same fire events or detect different fire events. Producer's accuracy is calculated using the detection rate of a possible merged product (merged detection).

2006 fires > 12.5 ha				
		MCD14ML		Tot.
		det	not det	MCD45A1
MCD 45A1	detected	10	11	21
	not detected	20	29	
	Tot. MCD14ML	30		
	Ref. Landsat fires		70	
	Merged fires		177	
	Merged detection		41	
	Omitted		29	
	Committed		136	
	Producer's Acc		**58.6%**	
	User's Acc		**23.2%**	
	F1 score		**0.33**	

2009 fires > 12.5 ha				
		MCD14ML		Tot.
		det	not det	MCD45A1
MCD 45A1	detected	12	11	23
	not detected	56	65	
	Tot. MCD14ML	68		
	Ref. Landsat fires		144	
	Merged fires		438	
	Merged detection		79	
	Omitted		65	
	Committed		359	
	Producer's Acc		**54.9%**	
	User's Acc		**18.0%**	
	F1 score		**0.27**	

2006 & 2009 fires > 12.5 ha				
		MCD14ML		Tot.
		det	not det	MCD45A1
MCD 45A1	detected	22	22	44
	not detected	76	94	
	Tot. MCD14ML	98		
	Ref. Landsat fires		214	
	Merged fires		615	
	Merged detection		120	
	Omitted		94	
	Committed		495	
	Producer's Acc		**56.1%**	
	User's Acc		**19.5%**	
	F1 score		**0.29**	

4.4. Discussion

Four different freely available global BA and AF datasets were compared towards a higher resolution reference dataset to assess their ability in the detection of fire events in a mountainous region characterized by frequent fires of small size. Because the accuracy assessment methodology chosen in this study differs substantially from the ones used for studies in other regions, a direct comparison of the results with those studies cannot be done. However, our findings need to be critically interpreted and discussed in the peculiar context of detection and quantification of small fire events. As expected, owing to the landscape and topographic characteristics of the target region, and the technical specifications of the tested global datasets, the performance of the products was relatively low. The F1 score, which is the harmonic mean of precision and recall (i.e., producer's accuracy and user's accuracy), was comprised between 0.08 and 0.42 in the two analyzed years, which are very low values A closer look at the omission and commission errors allows for the identification of the error type with the highest impact on the results. The choice of a given tradeoff between the two error types determines the results. For example, using less conservative rules (e.g., lower thresholds) to separate burned from unburned pixels will result in improved probabilities of detection at the cost of greater commission errors. As stated before, BA algorithm designers often opt for the opposite approach, containing commission errors at the cost of larger omission errors (Roy and Boschetti 2009), and our results confirm this statement. Almost all of the analyzed models are more accurate (lower commission) than sensitive (higher omission). Only MCD14ML, the only pure AF-based product, displayed higher probabilities of detection (PA), but also showed the lowest UAs, leading to a relatively reduced F1 score. It is worth mentioning that the low PA may be overstated in our approach. In fact, active fires detected by the MCD14ML product may be correct, but the resulting burned area may be smaller than the minimum size that is considered in this analysis (12.5 ha), or may have left a very light burn scar that escaped the analyst's interpretation when manually mapping fire perimeters for the reference dataset.

The influence of fire event size on the probability of detection can be highlighted when analyzing PAs for different fire sizes: every product obtained improved PAs for larger fires. Table 4-3 clearly illustrates the very poor detection of fires that are smaller than 50 ha by the tested products, except for MCD14ML, who reached PAs between 13% and 49%. Comparable results were found in other studies (Hantson *et al.* 2013). 50 ha correspond to two MODIS pixels. Sub-pixel analysis of burned patches performed in past studies (Boschetti, Flasse, *et al.* 2004; Giglio *et al.* 2009; Tsela *et al.* 2014) reported that a 50% of BA proportion in a MODIS pixel can be considered as an appropriate threshold for medium resolution burned area detection, while a threshold of 75% highly increased the sensitivity of the MODIS products. In our study, this was only true for the MCD14ML, while the other products had very low sensitivity for such small burned areas. A possible explanation for this difference could be the shape and location of small fires in this mountainous region that is characterized by narrow valleys with steep mountain flanks. The area of a small fire could span over two or more MODIS pixels, covering only small fractions of each pixel, consequently resulting in a failure of the detection of that fire event in any of the

affected pixels. Moreover, several fires occur in herbaceous vegetation that burns very fast but also recovers very fast without leaving heavily marked and clearly spectrally-discernable scars. These conditions are not favorable to BA algorithms, which are based on abrupt and permanent changes in spectral reflectances (Hall *et al.* 2016).

One of the main differences between the four datasets is their algorithm approach. MCD45A1 is a pure BA-based dataset, MCD14ML is a pure AF-based dataset, while MCD64A1 and Fire_CCI use hybrid approaches. This difference was expected to cause dissimilar results. The fact that AF-based algorithms are more sensitive to small fires and in general show higher probabilities of detection, but also many false detections (errors of commission), was already highlighted in previous studies. More recent algorithms were designed using hybrid approaches in order to take advantage of both AF and BA methods, while trying to minimize the errors of commission. The latest MODIS product, MCD64A1, showed great potential and an improved detection of smaller fires in other cases, but its performance in our study region was not as good as its predecessor's. Likewise, Tsela et al. (Tsela *et al.* 2014) found that MCD45A1 detects smaller burned areas (50% of a MODIS pixel) better than MCD64A1, and when presenting the new hybrid algorithm, Giglio et al. (Giglio *et al.* 2009) stated that the minimum burn size for reliable detection is in the order of 120 ha. ESA's Fire_CCI product performed poorly as well. A possible reason for the failure of detection lies in the hybrid algorithms strategies: both hybrid approaches rely heavily on a probabilistic selection of candidate burned pixels based on MCD14ML. Hotspots are used as starting seeds for the Fire_CCI product, while the MCD64A1 product employs them as training samples for a classification over previously created maps of persistent changes in a vegetation index. Although in general very low, omission error from the AF product is entirely absorbed by the hybrid algorithm. Those fires not detected by the AF product will be excluded from further processing. This approach is very efficient to overcome excessive commission errors but may be too restrictive for the detection of small burned patches in mountainous regions. Moreover, without a proper topographic adjustment of the raw satellite images, the real surface area of a pixel in a rugged terrain and on steep slopes is bigger than on a flat regular terrain, making the detection of small fires more difficult.

Because of the higher spatial resolution of the Fire_CCI product (300 m), a better detection of smaller fires was expected, but our results proved the opposite. For both of the assessed years, Fire_CCI performed similarly to MCD64A1, and worse than the other two products. Pixel size analysis showed a tendency for big commission errors on account of the confusion between burned land and other disturbances. Among the four tested products, Fire_CCI is the newest and its validation is still at its beginning stage. Preliminary comparisons showed good agreements with other global products, but greater omission and commission errors (Padilla *et al.* 2015; Pettinari *et al.* 2016; Chuvieco *et al.* 2016). Further validation is in progress.

4.5. Chapter conclusion

The impact of small size disturbances on terrestrial and atmospheric environments is very important, not only at local and regional scales, but also at the planetary and continental scales. Modeling of the Earth System should include those small fires in order to acquire a better understanding of fire disturbance as a global driving force of ecosystem change. Mountainous ecosystems are home to rich and rare biological species and are very sensitive to pressures induced by human activities and climate change. The study presented in this chapter contributes to this understanding by delivering a first assessment of the strengths and shortcomings of the existing, free-of-charge, global BA and AF products, in a representative region that has never been assessed before. The four global products tested in this study were selected because of their relatively high temporal and spatial resolution. The outcomes of the accuracy assessment allowed for the identification of the best product and a preliminary insight into fire activity in this region. Our main conclusions are as follows:

1. The analyzed global AF and BA products shows poorer results in our mountainous area than in other ecosystems, mainly because of the smaller size of fires. For burned areas bigger than 50 ha, the best product could detect more than 60% of the fire events. Detection decreases drastically for smaller burned areas.
2. The two former MODIS fire products, first MCD45A1 then MCD14ML, were the best performers in our study area, followed by MCD64A1 and Fire_CCI. These results did not align with our expectations. The newest algorithms are designed using hybrid approaches that combine the capabilities of both AF and BA methods. Therefore, among other improvements, they should have performed better in the detection of small fires. On the contrary, they obtained lower scores and higher commission and omission errors than their predecessors. This has important implications for the design of future algorithms. MCD45A1 being the best performer suggests that the bi-directional reflectance algorithm is still valid and deserves more consideration, for example, by being integrated in a hybrid approach. Unfortunately, MCD45A1 has been discontinued since January 2017 and replaced by the hybrid MCD64A1, which produced worse results.
3. At present, the usefulness of the existing global BA and AF products for the quantification of small fires is still marginal. These products were mainly designed for global or vast regions assessments and the spatial resolution of the sensors that are used to generate these datasets represents a physical limit that cannot be passed. Yet, taking into account the high rate of omission and commission, MCD45A1 and MCD14ML's data can be used to obtain preliminary insights on the fire activity of regions that are characterized by relatively small fires or to partially assess the accuracy of other burned area extraction methods.

Hence, based on the results of the present study, we recommend a re-evaluation of the new hybrid algorithms so that they can account for small fires occurring in ecosystems that feature complex landscape and topographic traits. Improved algorithms would not only benefit global and

continental scale applications, but also serve the increasing number of users that are working in smaller regions where no other reliable data about fire activity is available. Our study suggests that, despite the sensors' resolution limitations, there is room for improvements in algorithm design. Adopting sensors with higher spatial resolution like the MERIS sensor used in the Fire_CCI product is undoubtedly the right direction to follow to improve the burned area mapping phase. Still, the first selection of seeds based on MODIS thermal bands needs to be rethought.

We believe that a more accurate quantification of small fires, as well as other disturbance phenomena at global scale will be soon achievable, also thanks to the onset of big data technology. Existing alternatives could lie on higher resolution AF products like the 375 m VIIRS AF sensor aboard the Suomi National Polar-orbiting Partnership satellite (Schroeder *et al.* 2014), which collects images about every 12 h. However, its archive is very recent, beginning from the year 2012. Active fire data for previous years need to rely on the MODIS or other AF products. In addition, the Landsat archive offers four decades of 30 m resolution imagery, which has been widely used for all sorts of fire-related applications. In this perspective, recently, a lot of effort is put in the reconstruction of fire history using Landsat-based algorithms, such as the Burned Area Essential Climate Variable (BAECV) algorithm, which has been applied to the conterminous United States (Hawbaker *et al.* 2017). This algorithm maps burned areas with a minimum size of 4.05 ha, which is an ideal minimum size for mountainous areas. A first assessment performed by Vanderhoof et al. (Vanderhoof *et al.* 2017) found that, in a mountainous ecoregion of the western United States, BAECV detected 33% and 76% of fires with sizes 4.05 to 10 ha and 10 to 25 ha, respectively. These are very positive and encouraging results, which are calling for the application and validation of BAECV and other Landsat-based fire extraction algorithms over other regions of the world.

5. Evaluating fire scars permanence in fire spectral indices

The content of this chapter is based on the following publication. However, a few adaptations and updates have been added.

Fornacca D, Ren G, Xiao W (2018) Evaluating the best spectral indices for the detection of burn scars at several post-fire dates in a mountainous region of northwest Yunnan, China. *Remote Sensing* **10**, 1196.

Abstract: Remote mountainous regions are among the Earth's last remaining wild spots, hosting rare ecosystems and rich biodiversity. Because of access difficulties and low population density, baseline information about natural and human-induced disturbances in these regions is often limited or nonexistent. Landsat time series offer invaluable opportunities to reconstruct past land cover changes. However, the applicability of this approach strongly depends on the availability of good quality, cloud-free images, acquired at a regular time interval, which in mountainous regions are often difficult to find. The present study analyzed burn scar detection capabilities of 11 widely used spectral indices (SI) at 1 to 5 years after fire events in four dominant vegetation groups in a mountainous region of northwest Yunnan, China. To evaluate their performances, we used *M*-statistic as a burned-unburned class separability index, and we adapted an existing metric to quantify the SI residual burn signal at post-fire dates compared to the maximum severity recorded soon after the fire. Our results show that Normalized Burn Ratio (NBR) and Normalized Difference Moisture Index (NDMI) are always among the three best performers for the detection of burn scars starting 1 year after fire but not for the immediate post-fire assessment, where the Mid Infrared Burn Index, Burn Area Index, and Tasseled Cap Greenness were superior. Brightness and Wetness peculiar patterns revealed long-term effects of fire in vegetated land, suggesting their potential integration to assist other SI in burned area detection several years after the fire event. However, in general, class separability of most of the SI was poor after one growing season, owing to the seasonal rains and the relatively fast regrowth rate of shrubs and grasses, confirming the difficulty of assessment in mountainous ecosystems. Our findings are meaningful for the selection of a suitable SI to integrate in burned area detection workflows, according to vegetation type and time lag between image acquisitions.

Keywords: spectral indices; mountain fire; residual severity; disturbance and recovery; time series; burned area detection

5.1. Introduction

With the opening of the Landsat archive in 2008, nearly four decades of moderate resolution images of the Earth have been made available to the global public. Scientists from a vast range of fields are using these data for research purposes and to develop all sort of applications at local to global scales. In recent years, thanks to increasing storage capabilities, local computing power, and cloud computing technology, the analysis of dense time series has become accessible to ordinary users at reduced costs, catalyzing the development of algorithms to systematically process the data and extract targeted information (Wulder *et al.* 2012; Gómez *et al.* 2016). In order to monitor specific land surface dynamics such as natural or human-induced disturbances, land use/land cover change, or urban expansion, a common approach involves the processing and transformation of the raw spectral information contained in remotely sensed images, resulting in the enhancement of the target phenomena. For this purpose, spectral indices (SI) based on the most sensitive spectral bands while minimizing noise have been designed and integrated in change detection workflows to highlight particular land change events and evaluate their temporal trends (Jackson and Huete 1991; Bannari *et al.* 1995; Yang *et al.* 2007; Xue and Su 2017). In the case of fire disturbance, several SI initially intended to monitor vegetation productivity, such as the Normalized Difference Vegetation Index or the Enhanced Vegetation Index, as well as specially tailored SI such as the Normalized Burn Ratio and the Burn Area Index, have been employed to detect burned areas and assess the degree of impact of the disturbance using different satellite sensors (a few examples: Chen et al., 2016; Escuin et al., 2008; Kavzoglu et al., 2016; Martin Pilar & Chuvieco, 1998). More recently, these SI have been incorporated in time series analysis in order to systematically detect burned areas and monitor long-term vegetation recovery (Huang *et al.* 2010; Kennedy *et al.* 2010; Bastarrika, Chuvieco, and Martín 2011; Bastarrika *et al.* 2014; de Carvalho Júnior *et al.* 2015; Hawbaker *et al.* 2017; White *et al.* 2017).

To help researchers in the selection of the most suitable SI for a given situation, several authors performed comparative studies in different ecosystems and using different satellite sensors. In Mediterranean-like ecosystems characterized by chaparral, shrubs, and pine vegetation, several SI were tested on multitemporal sets of Landsat Thematic Mapper (TM), Enhanced Thematic Mapper (ETM+), NOAA Advanced Very High Resolution Radiometer (AVHRR), Moderate Resolution Imaging Spectroradiometer / Advanced Spaceborne Thermal Emission and Reflection Radiometer Airborne Simulator (MODIS/ASTER), and the Chinese Huanjing (HJ) (Chuvieco *et al.* 2002; Escuin *et al.* 2008; Veraverbeke *et al.* 2010, 2011; Harris *et al.* 2011; Liu *et al.* 2016), while in boreal forests, grasslands, and tundra, comparative assessments have been done mainly using Landsat (Epting *et al.* 2005; Loboda *et al.* 2013; Lu *et al.* 2016) and Sentinel-2 (Huang *et al.* 2016). The latter study included other vegetation types, such as tropical and subtropical woody savannas, which have also been assessed using TM (Melchiori *et al.* 2015). A particular study from Schepers et al. (Schepers *et al.* 2014) tested SI capabilities in the heathland shrubs of Belgium using Airborne Imaging Spectroscopy. All the referenced studies evaluated SI capabilities for the discrimination of burned areas and for mapping burn severity short time after the fires occurred.

With a focus on post-fire vegetation recovery patterns, other authors compared different SI responses at multiple post-fire dates using time-series approaches (Chen *et al.* 2011; Lozano *et al.* 2012; Pickell *et al.* 2016; Hislop *et al.* 2018). Summarizing the results of this comprehensive volume of literature, performance divergences were found in different ecosystems and in the time lag between date of the burn and the post-fire image used for the assessment. However, certain patterns have been observed and interpretations suggested. For example, the SI that integrate the shortwave infrared domain of the electromagnetic spectrum, corresponding roughly to wavelengths between 1100 and 3000 nanometers, tended to be more suitable for long-term vegetation recovery than for immediate burn-scar mapping, thanks to their sensitivity to forest structure and moisture content. On the contrary, SI relying on visible and near infrared light could accurately map burned patches if employed immediately after the fire event, when the magnitude of change in vegetation's chlorophyll content was the highest (Lozano *et al.* 2012; Pickell *et al.* 2016; Hislop *et al.* 2018). In general, even if the famous Normalized Burn Ratio (Key and Benson 2006) was often considered the best SI, our literature review founds that there is no single SI that constantly excels and overperforms the others in every ecosystem, scale and time lag conditions, both for burned area mapping and severity assessments, as well as for vegetation recovery characterization.

Of the tested vegetation types, Mediterranean pine/shrubs, semi-dry savannas, and boreal forests are among the most fire prone ecosystems on Earth, explaining the higher amount of published research targeting these regions. Much less can be found about impacts of fire in mountain environments, although they are extremely important for their ecological value while being highly vulnerable to climate change and natural disasters (http://www.fao.org/mountain-partnership). Remoteness, contrasting topography and patchy landscapes that characterize alpine regions dictate harsh living conditions and access difficulties, limiting field research opportunities and presenting particular challenges for the monitoring of disturbances using remote sensing approaches (Weiss and Walsh 2009). Medium to high resolution imagery is required to assess changes in such complex ecosystems and frequent cloud cover fairly affects the quality of the images. Topographic effects are known to introduce distortions and artifacts that need to be corrected during the preprocessing stage of image analysis, together with routine radiometric and atmospheric corrections. Moreover, rugged terrain and sun angle create shades that obscure some portions of the image, highly affecting reflectance values. Several topographic correction methods have been developed and tested, and it is in general suggested to include them in preprocessing operations (Gitas and Devereux 2006; Ediriweera *et al.* 2013), as well as using spectral band ratios which are less affected by topographic effects (Weiss and Walsh 2009). However, in very rugged terrain and low sun elevation conditions, the performance of these correction methods decreases drastically (Tan *et al.* 2013; Sola *et al.* 2016).

In this chapter, we focus on the mountainous region of northwest Yunnan, China, where wildland fires occur frequently during the dry and windy season, between December and May (Qin *et al.* 2010; Su *et al.* 2015). According to official statistics, more than 99% of forest fires in southwest China including Yunnan are caused by anthropogenic ignitions, often related to the widespread use of fire in agriculture (Li, Song, *et al.* 2014). The main peculiarity of forest fires in

this region is their relatively small size, in general 100 to 300 hectares and rarely above 1000 hectares, which heavily impact the performance of the existing burned area products commonly used in regional and global assessments of fire impacts, such as MODIS MCD64A1 and ESA Fire_CCI (Fornacca *et al.* 2017). Therefore, efficient burned area extraction algorithms require image data of a finer resolution, such as 30 m Landsat imagery, and the use of suitable SI. However, cloud-free images are not always available in this region to a point that dense time series are impossible to construct. Time lag between acceptable scene acquisitions can reach several months or even years, further complicating burn scar detection. In this context, our study aims to address the common difficulties encountered by analysts working in mountainous areas who need to deal with low image frequencies and several vegetation types coexisting in the same region. We selected eleven among the most popular SI widely used for burned area and burn severity assessments and analyzed the spectral trajectories of burned and unburned pixels over time in northwest Yunnan's four major vegetation types. The permanence of the spectral signal that characterize burned land was assessed following a 1-year temporal sampling design and the SI that better highlight the signal were identified at each post-fire year. Our approach can be associated with vegetation recovery evaluations because the detectability of the residual signal of burned areas is strictly related to vegetation regrowth. The next section explains in detail how we adapted existing conceptual frameworks and tailored the metrics to better serve our research question.

5.2. Data and methods

5.2.1. Selection of burn / reference plots and sampling methodology

As mention in section 2.1 of this thesis, official and accurate data about forest fires such as location and date are unfortunately not available for our study region. Consequently, the burned plots were manually drawn within natural or anthropogenic burned areas (no experimental burns) by the means of visual interpretation of Landsat TM scenes and MODIS fire products (MCD45A1 and MCD64A1) at various dates (http://modis-fire.umd.edu/). Burned plots followed the burned area perimeter using particular care in avoiding peripheral pixels to keep the core of the burned area. Consequently, shape and size were different among plots. In a first stage, a total of 50 fires were identified from Landsat images (path/row 131/042 and 132/041), 25 of which were confirmed by the MODIS products. A second round of selection was performed in order to obtain 12 burn plots equally representing four dominant land cover classes (3 plots per class). The land cover classes were extracted and aggregated from the European Space Agency Climate Change Initiative (ESA CCI) Landcover product (https://climate.esa.int/en/projects/land-cover/), and were: needleleaved forests, broadleaved forests, shrublands, and grasslands. The basic requirements for the 12 final burn plots consisted in having a relatively narrow time lag between the pre-fire and the immediate post-fire image dates, and having good quality, 1-year temporal interval Landsat scenes in all of the five years following the burn. Images affected by clouds were also considered as long as they did not cover the selected burned plots. The final dataset was composed of a 7-images time series for each burn plot. The frequent presence of clouds in the study region was the main problem

in both selection phases and reduced drastically the number of acceptable burn plots. All Landsat scenes were retrieved from the United States Geological Survey EarthExplorer repository (https://earthexplorer.usgs.gov/). The scenes were already preprocessed by the provider according to Level-2 surface reflectance standards using the Landsat Ecosystem Disturbance Adaptive Processing System (LEDAPS) radiometric calibration and atmospheric correction algorithms (Vermote *et al.* 1997). Level-2 images account for most of the artifacts introduced by rugged terrain but topographic shades persist in the images. Our tests of existing topographic correction methods gave poor results because of the excessive steepness of most of the slopes in the study region. We therefore chose to rely on the slight normalizing effect of band ratios, which is used by most of the SI, and on the selection of yearly Landsat scenes at same periods of the year, where sun elevation, sun azimuth and vegetation phenology are similar. Average fire severity for each burn plot was estimated using Delta NBR (dNBR) between the pre-fire and post-fire images. According to the burn severity assessment protocol used by the USDA Forest Service (FireMon documentation: https://www.fs.fed.us/rm/pubs/rmrs_gtr164/rmrs_gtr164_13_land_assess.pdf), five plots were high severity burns, three plots were moderate-high severity burns, two plots were moderate-low severity burns, and two plots were low severity burns. A map of the region and location of the 12 burn plots is shown in Figure 5-1 and additional details are described in Table 5-1.

Thirty random points (samples) were created inside each burn plot and thirty control points of similar land cover classes and similar slope/aspect were created in the near proximity of each burn plot, to be used as unburned reference samples. Slope/aspect similarity was considered in order to further minimize the bias introduced by topography. Control points were within 4 km except for burn plot number 5 for whom, owing to the presence of snow and clouds, suitable sample points could be found only 35 km away. In summary, every plot was characterized by a dominant land cover class, was composed of 30 burn samples and 30 external unburned samples, and each sample was assigned its own land cover class. In total, 720 sample points were used in our analysis.

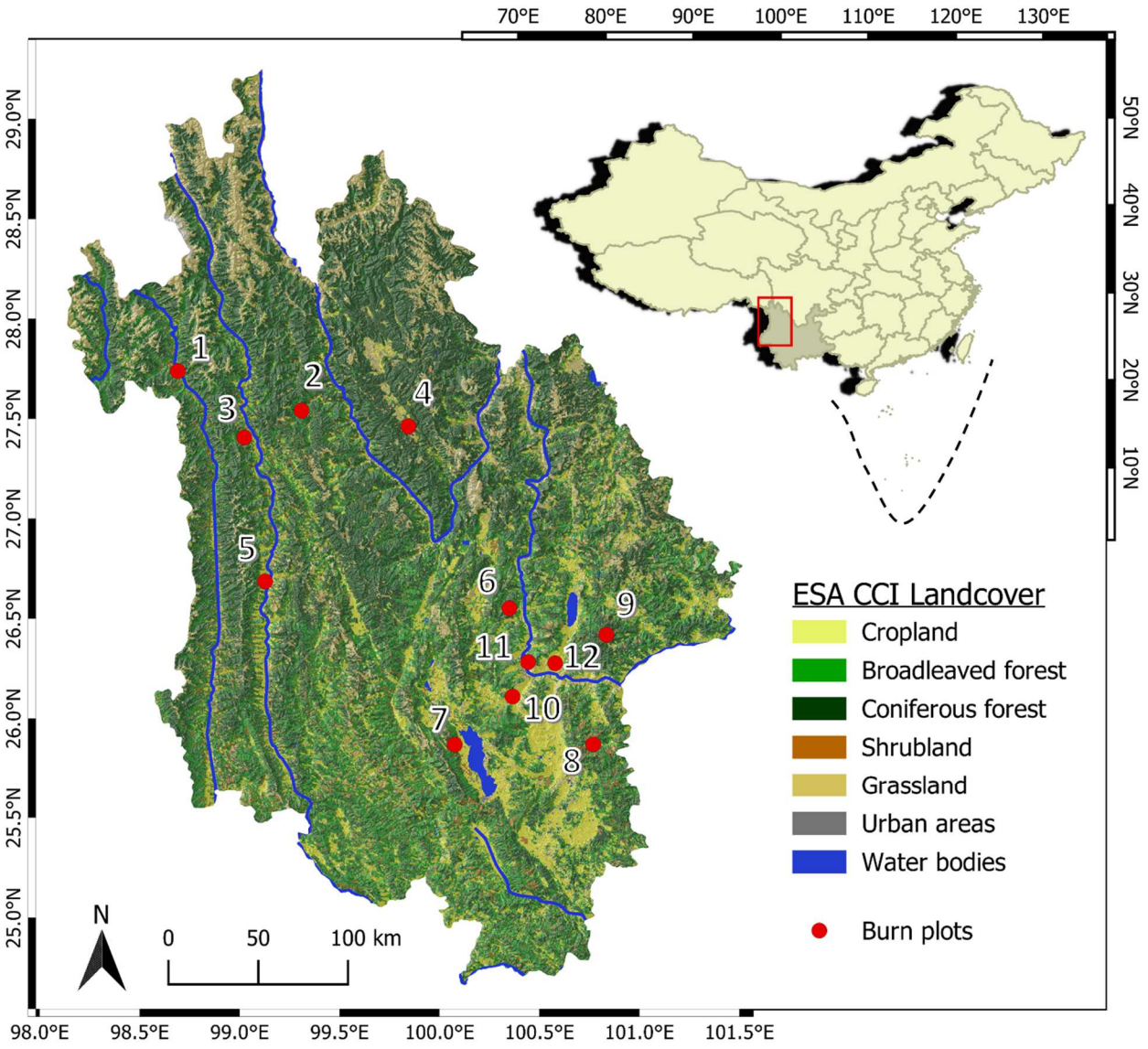

Figure 5-1. Map of northwest Yunnan and location of burn plots. The land cover classes in this map of northwest Yunnan have been aggregated from the European Space Agency Climate Change Initiative (ESA CCI) Landcover product (reference in the core text, section 5.2.1.), and are represented over a shaded relief layer. Detailed information of the 12 burn plots is given in Table 5-1.

Table 5-1. Landsat TM time series for the 12 selected burn plots. Locations of the burn plots are indicated with the geographic coordinates of their center, WGS84, decimal degrees. ESA LC: land cover class extracted from the European Space Agency Landcover product; DOY: day of year (Julian day); LS_pre, LS_post, LS_1, …: Landsat scene date in yyyymmdd format at pre-burn, post-burn, 1,2, … years after burn, respectively.

Plot ID	Lat	Long	ESA LC	Size Sq. km	MODIS Year_DOY	LS_pre	LS_post	LS_1	LS_2	LS_3	LS_4	LS_5
Plot_01	27.74	98.69	broad	2.15	2006_007	20051028	20060201	20070220	20080310	20090209	20100212	20110303
Plot_02	27.54	99.31	broad	1.26		19990214	19990302	20000217	20010118	20020105	20030108	20040111
Plot_03	27.41	99.02	shrub	0.7	2006_005	20051028	20060201	20070103	20080310	20090209	20100212	20110303
Plot_04	27.46	99.85	needle	0.74	2005_334	20051113	20060201	20070103	20080310	20090209	20100212	20110303
Plot_05	26.69	99.12	shrub	7.25	2006_011	20051028	20060201	20070103	20080310	20090209	20100212	20110303
Plot_06	26.55	100.35	broad	1.1		19980204	19980409	19990223	20000414	20010212	20020303	20030306
Plot_07	25.87	100.08	shrub	2.08	2003_065	20030218	20030306	20040221	20050207	20060226	20070301	20080216
Plot_08	25.87	100.77	needle	0.33		20030306	20030509	20040425	20050428	20060517	20070301	20080404
Plot_09	26.42	100.84	needle	3.43		19950212	19950316	19960302	19970201	19980204	19990223	20000210
Plot_10	26.11	100.37	grass	2.28		20021029	20030101	20040104	20050106	20060125	20061227	20080216
Plot_11	26.28	100.44	grass	1.67		20030306	20030322	20040221	20050207	20060226	20070301	20080216
Plot_12	26.28	100.58	grass	1.44		20030101	20030218	20040104	20050106	20060125	20061227	20080216

5.2.2. Description of Spectral Indices and processing

Among the wide range of existing spectral indices and image transformation techniques described in the literature, we selected 11 different approaches developed for the Landsat sensors and commonly used for the assessment of burn severity and the extraction of burned areas. SI equations were applied to each Landsat scene in the time series (see Table 5-1). Finally, SI values from the newly created layers were extracted at the location of each of the 720 sample points. All operations were performed using the ENVI software from Harris Geospatial (https://www.harris.com/solution/envi/) and QGIS (http://www.qgis.org/).

SI equations, literature references and all abbreviations used in this section are listed in Table 5-2 and in its caption. The following sections describe the selected indices, divided in four groups according to the spectral bands used for their design.

5.2.2.1. SI using visible and near-infrared domains of the electromagnetic spectrum

One of the most known and widely used spectral indices, NDVI takes advantage of green vegetation's strong absorption of visible red light, in contrast with its high reflection of near-infrared light. The damage to vegetation caused by fire results in a significant decrease of the NDVI. Because of its applicability to a wide range of sensors, including those lacking SWIR bands, its simplicity and relatively good performance, NDVI has been used extensively to map burned areas, assess burn severity and monitor vegetation recovery (Hudak *et al.* 2007; Escuin *et al.* 2008; Kennedy *et al.* 2010; Vogelmann *et al.* 2012; Schmidt *et al.* 2015). Similar to NDVI, GEMI uses the visible red and near infrared domains but was designed following a non-linear approach in an attempt to reduce undesired atmospheric effects. Although its application to burn scar detection was mainly done with MODIS and SPOT sensors (Stroppiana *et al.* 2002; Lasaponara 2006; Cao *et al.* 2009), we decided to include it in our Landsat TM study and evaluate its potential. BAI was initially designed for NOAA-AVHRR images in Mediterranean environments but has also been tested with Landsat TM (Chuvieco *et al.* 2002). It focuses on the specific spectral signal of charcoal in areas affected by fire and is computed from the spectral distance from each pixel to a reference spectral point, where recently burned areas tend to converge. Reference reflectance values of the convergence point, set to 0.1 for red and 0.06 for NIR, were defined based on literature and several sets of satellite sensor images analyzed by the authors (Martin Pilar and Chuvieco 1998).

5.2.2.2. SI using near-infrared and shortwave infrared domains of the electromagnetic spectrum

Initially designed for burned area extraction, NBR is the most popular spectral index used for burn severity assessments with different sensors in several ecosystems around the world. In numerous comparative analyses, NBR proved to be one of the most efficient SI (Epting *et al.* 2005; Kennedy *et al.* 2010; Veraverbeke *et al.* 2010; Harris *et al.* 2011; Schepers *et al.* 2014). In time series analyses, NBR showed good correlations with field-based composite burn index

scores several years after a fire, thus representing an efficient tool for vegetation recovery monitoring (Chen *et al.* 2011; Hislop *et al.* 2018). Unlike the three previously described SI, NBR uses the band pair SWIR and NIR instead of the visible red, which has shown to be sensitive to reflectance changes caused by fire. NDMI is very similar to NBR but uses the shorter SWIR band instead of the longer one, which has revealed to be equally sensitive to wet/dry content of soils and vegetation. However, it has been rarely tested for burned area discrimination (Bastarrika, Chuvieco, and Martín 2011; Mazher 2013; Melchiori *et al.* 2015). BAIML and BAIMs are a modified version of the BAI tailored for the MODIS sensors which offer SWIR channels, but they are also used with Landsat images (Bastarrika, Chuvieco, and Martín 2011; Mazher 2013; Melchiori *et al.* 2015). Following the same logic as the one defined for BAI, convergence point values for NIR and SWIR bands were chosen by their creators based on the analysis of MODIS time series, and were set to 0.05 for NIR and 0.2 for SWIR. These values were kept unchanged for the long and short versions of the SWIR used by the Landsat TM instrument.

5.2.2.3. SI using different shortwave infrared domains of the electromagnetic spectrum

Designed for arid savannah and shrub ecosystems, MIRBI combines the two SWIR bands because of their better separability in burned areas. Several authors working in these vegetation types have reported its good performance, often superior to the widely used NBR and other SI (Schepers *et al.* 2014; Lu *et al.* 2016).

5.2.2.4. Image transformation techniques using multiple bands

The Tasseled Cap Transformation (TassCap) is a conversion of the original image data to a new coordinate system with a new set of orthogonal axes by applying different weights to the bands. Studies have shown how using TassCap in replacement or in addition to other indices can improve the accuracy of the results when detecting fire scars and fire severity (Rogan and Yool 2001; Mbow *et al.* 2004; Kennedy *et al.* 2010; Hislop *et al.* 2018). The added value of integrating TassCap derived indices Brightness, Greenness, and Wetness lies in their integration of a larger range of spectral information instead of limited band ratios. The band coefficients for surface reflectance of Landsat TM are given by Crist (Crist 1985).

Table 5-2. List of spectral indices and image transformation techniques. Blue = visible blue Landsat Thematic Mapper (TM) band 1; Green = visible green Landsat TM band 2; Red = visible red Landsat TM band 3; NIR = near infrared Landsat TM band 4; sSWIR = shorter shortwave infrared Landsat TM band 5; lSWIR = longer shortwave infrared Landsat TM band 7.

SI full name	Abbr.	Equation	Reference
Normalized Difference Vegetation Index	**NDVI**	$\frac{Red - NIR}{Red + NIR}$	(Rouse *et al.* 1973)
Global Environmental Monitoring Index	**GEMI**	$\gamma(1 - 0.25 * \gamma) - \frac{Red - 0.125}{1 - Red}$ where $\gamma = \frac{2(NIR^2 - Red^2) + 1.5 * NIR + 0.5 * Red}{NIR + Red + 0.5}$	(Pinty and Verstraete 1992)
Burn Area Index	**BAI**	$\frac{1}{(0.1 - Red)^2 + (0.06 - NIR)^2}$	(Martin Pilar and Chuvieco 1998)
Normalized Burn Ratio	**NBR**	$\frac{NIR - lSWIR}{NIR + lSWIR}$	(López García and Caselles 1991; Koutsias and Karteris 2000; Key and Benson 2006)
Normalized Difference Moisture Index	**NDMI**	$\frac{NIR - sSWIR}{NIR + sSWIR}$	(Wilson and Sader 2002)
Burned Area Index Modified - LSWIR -	**BAIML**	$\frac{1}{(NIR - 0.05 * NIR)^2 + (lSWIR - 0.2 * lSWIR)^2}$	(Martín *et al.* 2006)
Burned Area Index Modified - sSWIR -	**BAIMs**	$\frac{1}{(NIR - 0.05 * NIR)^2 + (sSWIR - 0.2 * sSWIR)^2}$	
Mid Infrared Burn Index	**MIRBI**	$10 * lSWIR - 9.8 * sSWIR + 2$	(Trigg and Flasse 2001)
TassCap Brightness	**BRI**	$0.2043 * Blue + 0.4158 * Green + 0.5524 * Red + 0.5741 * NIR + 0.3124 * sSWIR + 0.2303 * lSWIR$	(Crist and Cicone 1984; Crist 1985)
TassCap Greenness	**GRE**	$-0.1603 * Blue - 0.2819 * Green - 0.4934 * Red + 0.794 * NIR - 0.0002 * sSWIR - 0.1446 * lSWIR$	
TassCap Wetness	**WET**	$0.0315 * Blue + 0.2021 * Green + 0.3102 * Red + 0.1594 * NIR - 0.6806 * sSWIR - 0.6109 * lSWIR$	

5.2.3. Analysis and metrics

Figure 5-2 illustrates a conceptual model of the different temporal trajectories of burned and unburned samples. The proposed model has been adapted from previous models developed initially by Key (Key 2006) and then modified by Chompuchan & Lin (Chompuchan and Lin 2017). We assume that the ecological condition of vegetation, which could be measured by a given spectral index, follows a regular pattern through time. In addition to natural seasonal fluctuations, the trajectory is also subject to a certain degree of interannual variability driven by to multiple factors such as different interannual climate/weather conditions, differences in phenological timing, or residual radiometric inaccuracies. Our analysis follows a temporal resolution scheme of 1 year, but cloud-free Landsat scenes are rarely available at the same date for several consecutive years. For this reason, instead of analyzing the single trajectory of burned samples, we decided to compare it with the trajectory of reference unburned pixels of same vegetation type. Considering the spectral fluctuations of vegetation not affected by fire gives a more realistic picture on the ecological condition of the disturbed vegetation and presents some interesting advantages. For example, a simple comparison of solely burned samples at two different dates, such as between pre-fire and post-fire, does not account for potential variations of vegetation phenology and unusual weather events which may affect the overall vegetation. Consequently, an undefined bias in the quantification of change is introduced. According to specific purposes, this bias may need to be quantified, especially when working with long-term time series (Key 2006; de Carvalho Júnior *et al.* 2015). Another advantage of this approach lies on the possibility to analyze differences in the pre-fire condition of burned and unburned vegetation, illustrated in Figure 5-2 as the distance $t^0_{burn} - t^0_{ref}$. However, this is not the focus of the present study.

According to the conceptual model (Figure 5-2), the physical effect of burning on vegetation will result in an abrupt deviation from the regular trajectory, reaching the maximum distance short time after the fire or, if a delayed vegetation mortality effect exists, several months or years after the fire (Key 2006; Chompuchan and Lin 2017). This distance corresponds to the magnitude of maximum severity and is quantified as $t^m_{burn} - t^m_{ref}$. At any time after the point of maximum severity, residual severity can be calculated using the distance $t^a_{burn} - t^a_{ref}$.

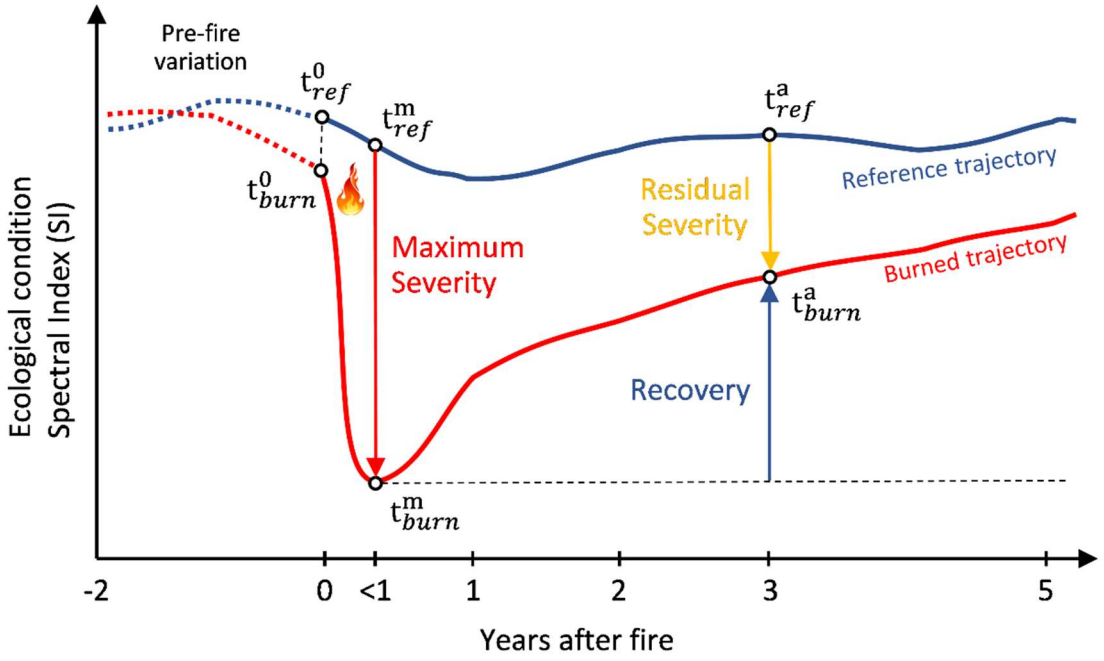

Figure 5-2. Temporal trajectories of burned and unburned vegetation. This conceptual model represents the effect of fire on vegetation as well as severity and recovery patterns. Spectral Indices serve as proxies to represent the ecological condition of the vegetation. Modified and adapted from Key (2006) and Chompuchan and Lin (2017).

In this chapter of the thesis, the capabilities of the previously described SI to detect burned areas at several dates after the fire events were evaluated and compared using the following three approaches:

- **Visual analysis of temporal plots of the SI**
  Using Figure 5-2 as a model, temporal trajectories of each SI were plotted to visually analyze the spectral response of vegetation after a fire event, compared to unburned reference samples. This kind of graphic representation allows for a quick preliminary assessment of SI behavior and fire disturbance patterns. Specifically, the trajectories of burned and unburned samples show the effect of fire and the natural temporal fluctuation of unburned vegetation. Maximum severity and the existence of a delayed mortality effect can be identified. Moreover, recovery and residual severity dynamics can be followed along the timeline.

- **Analysis of burned-unburned separability capabilities of SI, the *M*-statistic**
  The ability of each SI to separate burned from unburned pixels can be compared using statistical metrics that quantify the spectral distance between two distributions. The *M*-statistic is a measure of class separability defined by Kaufman and Remer (Kaufman and Remer 1994) as the difference between the means (μ) of two classes normalized by the sum of their standard deviations (σ). It can be interpreted as a signal-to noise-ratio, where the distance of the means represents the signal while the sum of the standard deviations

represents the noise. This metric has been previously used in several studies related to burned area discrimination (Lasaponara 2006; Smith *et al.* 2007; Libonati *et al.* 2011; Melchiori *et al.* 2015). The *M*-statistic is expressed as:

$$M = \frac{(\mu_1 - \mu_2)}{(\sigma_1 + \sigma_2)}$$

A value of $M > 1.0$ indicates good separation between the burned and the unburned classes, while $M < 1$ indicates poorer separation, given by closer means and/or larger standard deviations. Figure 5-3 shows a graphic representation of a burned area and the *M* value a pre-fire and several post-fire dates.

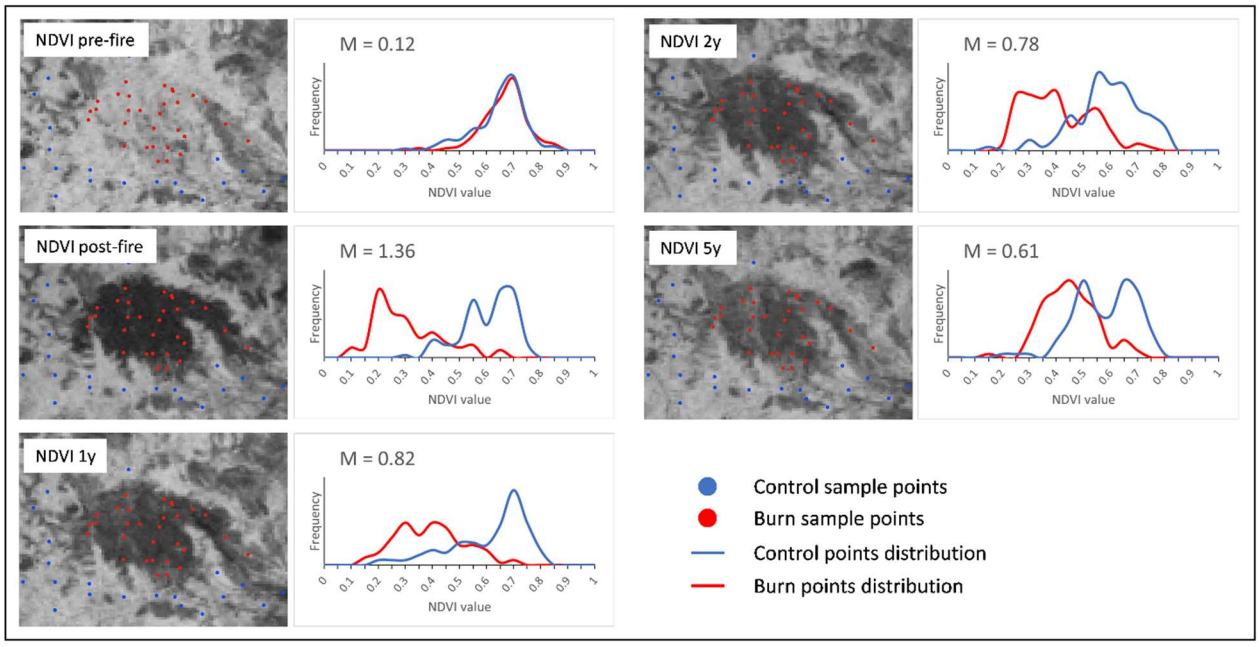

Figure 5-3. Burned vs. unburned class distributions for the NDVI at pre-fire, post-fire, and 1, 2, 5 years after fire. An example of burn scar with corresponding burn and control sample points, as well as the *M*-statistic results are illustrated.

- **SI enhancement of residual severity**

Recovery and residual severity can be quantified by dividing their magnitudes at a given post-fire date with the magnitude of the disturbance at the time of maximum severity. This concept has been used by Lin *et al.* (2004) to assess vegetation recovery after a landslide. The authors defined the Vegetation Recovery Rate which uses NDVI as input. The same structure was adopted by Chompuchan and Lin (2017) to assess recovery after fire disturbances, but NDVI was replaced with NBR. We adapted this methodology to compare the capabilities of each selected SI to enhance residual severity at several post-fire dates. Our adjustments consist in the quantification of the residual severity instead of the recovery (see Figure 5-2), and the use of SI values of unburned plots as a reference for healthy vegetation instead of pre-fire values of burned

samples. We name this metric Residual Severity Ratio (*RSR*), and using the terminology presented in Figure 5-2, we define it as the ratio between Residual Severity and Maximum Severity. *RSR* is expressed with the following equation:

$$RSR_{SI} = \frac{SI(t^{a}_{burn}) - SI(t^{a}_{ref})}{SI(t^{m}_{burn}) - SI(t^{m}_{ref})}$$

RSR values close to 1, indicate low recovery from the stage of maximum severity and may indicate that an SI shows good capabilities to enhance residual severity. However, when interpreting this metric, particular attention should be given to the pattern of the SI trajectories of the burned and the unburned classes displayed on the graphic plots and to the separation capabilities of the SI at the time of maximum severity.

Following the three approaches mentioned above, the analysis was initially performed on the overall dataset, using the mean of all samples of all fires. To investigate possible differences in SI responses between the four dominant ecosystems in northwest Yunnan, sample points were aggregated according to their vegetation class, and the same analysis was performed.

5.3. Results and discussion

5.3.1. Spectral indices' general response to fire in northwest Yunnan

A comprehensive representation of the temporal trajectories of the 11 SI is illustrated in Figure 5-4. Most of the SI present similar response patterns following fire, with a pronounced deviation right after the fire (point of maximum severity), a relatively fast recovery during the first year after the fire, and a slow recovery during the following years. Visually, all SI except the TassCap Wetness show a well-marked response at the immediate post-fire assessment which confirms their wide employment for burn severity evaluation. However, a less sharp recovery slope following the maximum severity point suggests that NDMI and NBR could better enhance residual severity than the other SI several years after the fire, while MIRBI appears to be the least performant. The observation of the graphic plots also reveals singular behaviors of Brightness and Wetness. The former has a similar response than the other indices right after fire: the effect of burning on the biomass and the deposit of ash and charcoal significantly decrease the values of Brightness. Though, this effect seems to last very shortly. In fact, one year after the fire, the index's values increase drastically, becoming higher than those of unburned vegetation (reference and burned lines crossed). This is probably an effect of the rainy season washing away dark deposits of ash and charcoal and exposing bare soil, while new green matter (leaves, grass, etc.) has not had the time to recover properly. The Wetness index follows a different pattern. The immediate effect of burn seems to have only a slight decreasing effect on Wetness values, but the magnitude of this effect grows in the following years, showing a clear difference from the unburned vegetation. This suggests that the long-term effects of fire on vegetation include a decrease of moisture content in the affected site in favor of more arid conditions, which, together

with post-fire climate conditions, may affect vegetation regrowth dynamics several years after the fire (Meng *et al.* 2015).

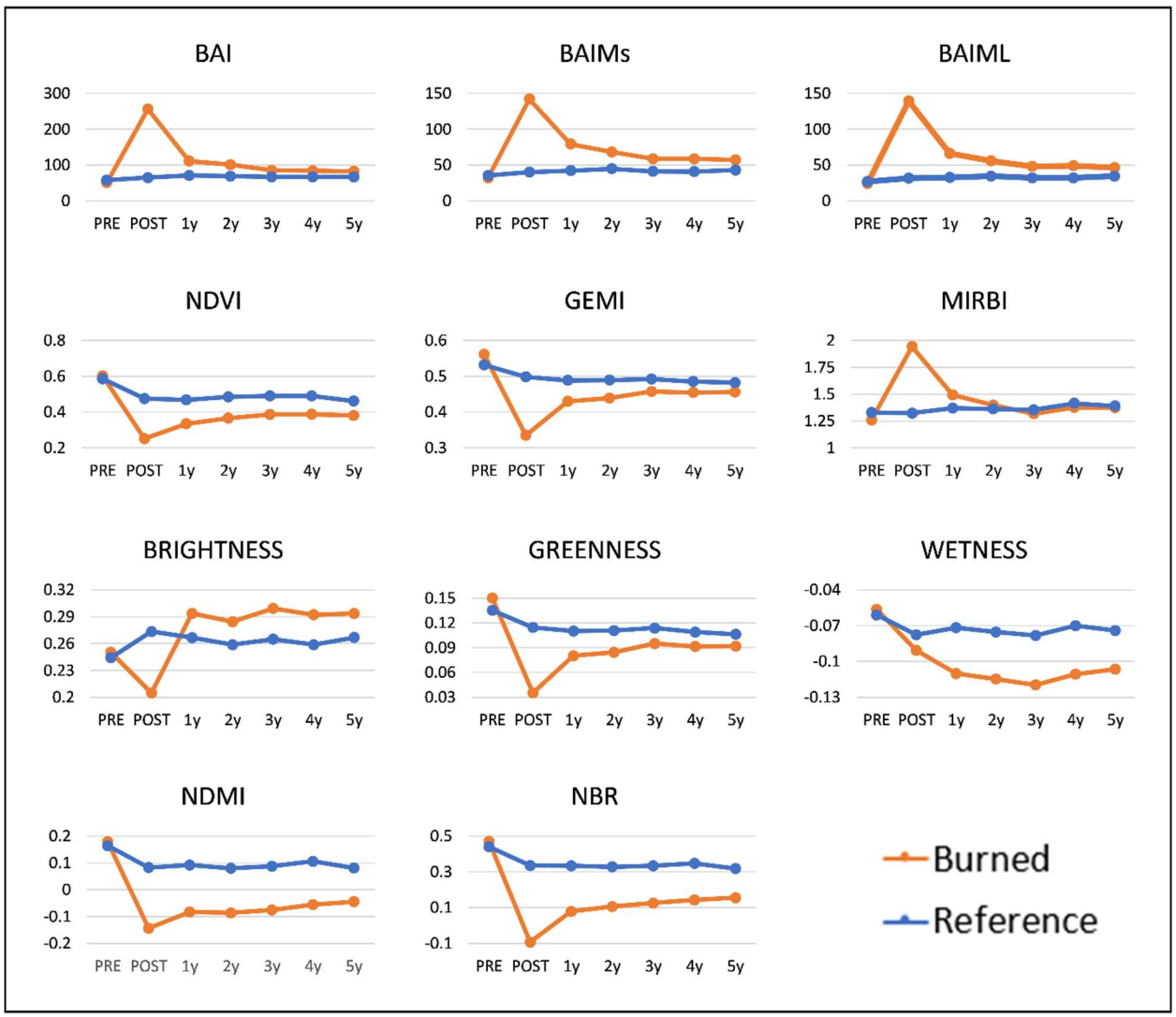

Figure 5-4. Spectral Indices' trajectories over time: pre- and post-fire, and 1, 2, 3, 4, and 5 years following the fire. The plots represent the SI mean values for the burned and the reference samples of the whole dataset.

The results of separability and residual severity assessments are shown in Table 5-3. According to the ideal value of $M > 1$, the separability values are in general not very optimal. At the first post-fire assessment, only MIRBI, Greenness, BAI, and GEMI obtained *M* values higher than 1. However, if we compare post-fire *M* values with the pre-fire ones, NBR and NDVI still show a significant difference (pre-fire *M*: 0.07 and 0.05, post-fire *M*: 0.88 and 0.82, respectively). Brightness and Wetness appear to be the less suitable for burned area mapping shortly after fire. These results do not necessarily mean that the indices cannot detect burned areas, but that relying on a static threshold to separate burned from unburned patches may be subject to a higher rate of error. It must be noted that these results are based on the average values of all burn plots which,

taken individually, have different time lags between pre-fire and immediate post-fire images and include different vegetation types (see Table 5-1). The influence of time lag and vegetation type on the quality of post-fire assessments by the SI has been pointed out in numerous research results (Loboda *et al.* 2007; Picotte and Robertson 2011; Parker *et al.* 2015). Although several comparative studies mentioned in the introduction recognize NBR as the best SI for immediate post-fire assessment, our results found that MIRBI has the greatest separability capabilities, as confirmed by Lu et al. (Lu *et al.* 2016). However, starting from 1 year after the fire, separability radically decreases for the four best performers mentioned before, while NBR, NDMI, NDVI, BAIML, and BAIMs proved to be more resistant. Among them, NBR, NDMI, and BAIML are the three best performers in all five post-fire years. In terms of *RSR* and as shown in the graphic plots, NDMI is the most suitable SI to enhance the residual severity several years after fire, even if its separability potential decreases. NDVI shows good *RSR* at 1 and 2 years after fire, while Brightness takes over at 3, 4, and 5 years after fire. Nevertheless, the separability capability of Brightness at these time frames remains poor. The case of Wetness needs further clarification. Maximum severity and best separability of Wetness, albeit rather poor, is reached at the 3rd post-fire year. The trajectory of the burned samples, as showed in the graphic plot, indicates that the biggest shift from unburned samples appears at the 1 year post-fire assessment. Afterwards, *RSR* remains relatively stable, which explains the resulting high values. The meaning of this pattern is that the perturbations in Wetness caused by fire persists for a few years before the recovery phase begins. The graphic plots and *RSR* also indicate that, except for the Wetness index whose trajectory reveals persisting moisture stress, no delayed mortality effect seem to exist regarding fire disturbance in northwest Yunnan. Maximum severity appears always at the immediate post-fire assessment (MS value in Table 5-3).

Table 5-3. Separability index (*M*-statistic) and Residual Severity Ratio (*RSR*) for the 11 SI. Highlighted cells indicate the three best performers at the given post-fire time in the following rank/color order: 1st, 2nd, 3rd. Pre-fire *M*-statistic values are shown as reference. MS = maximum severity from which *RSR* is calculated. Negative values of *RSR* indicate that the trajectory of the burned class crossed the trajectory of the unburned control class.

	***M*-statistic - All fire plots (mean)**							**RSR - All fire plots (mean)**					
	pre	**post**	**1y**	**2y**	**3y**	**4y**	**5y**	**post**	**1y**	**2y**	**3y**	**4y**	**5y**
BAI	0.08	1.12	0.28	0.28	0.16	0.17	0.15	**MS**	0.21	0.17	0.10	0.09	0.08
GEMI	0.12	1.08	0.35	0.30	0.20	0.18	0.16	**MS**	0.36	0.31	0.21	0.19	0.16
NBR	0.07	0.88	0.60	0.55	0.53	0.48	0.39	**MS**	0.59	0.52	0.49	0.48	0.38
NDVI	0.05	0.82	0.49	0.43	0.37	0.34	0.28	**MS**	0.60	0.53	0.46	0.46	0.36
BRI	0.03	0.39	0.13	0.14	0.16	0.16	0.14	**MS**	-0.39	-0.37	-0.50	-0.49	-0.39
GRE	0.12	1.24	0.36	0.34	0.23	0.23	0.20	**MS**	0.38	0.33	0.24	0.22	0.18
WET	0.05	0.11	0.31	0.36	0.37	0.36	0.29	0.32	0.93	0.95	**MS**	0.98	0.78
BAIML	0.13	0.74	0.50	0.47	0.40	0.43	0.32	**MS**	0.31	0.20	0.15	0.16	0.11
BAIMs	0.09	0.75	0.41	0.34	0.27	0.31	0.23	**MS**	0.36	0.23	0.17	0.18	0.14
MIRBI	0.12	1.29	0.20	0.07	0.06	0.07	0.03	**MS**	0.20	0.06	-0.06	-0.06	-0.03
NDMI	0.04	0.64	0.55	0.54	0.54	0.51	0.38	**MS**	0.77	0.73	0.72	0.71	0.55

5.3.2. Spectral indices' response to fire by vegetation type

The four main vegetation types of northwest Yunnan react differently to fire and show dissimilar recovery patterns. These patterns can be observed in the SI trajectories and can be quantified by comparing the values of *M*-statistic and *RSR* between vegetation types. The temporal trajectories of burned and unburned samples for the four major vegetation classes in NWY are represented in Figure 5-5. Among them, we can notice that needleleaved and broadleaved forests tend to recover slower than shrublands and grasslands. This pattern is found in all the SI. Grasslands samples are characterized by burned and unburned trajectories that quickly converge after 1 year. Recovery of shrublands seems to be a little slower than grasslands, with some residual severity visible at 1 year post-fire in NDMI, NBR, NDVI, Brightness and Wetness. A particular behavior is observed in the shrublands graphic plots. At the 1 year post-fire assessment, the trajectory of unburned pixels shows an important shift similar but not as severe as the burned samples (GEMI, NBR, NDVI, Greenness, Wetness, NDMI). A valid explanation lies in the dates of burn of the shrub burn plots. As shown in Table 5-1, two of the three plots were burned during the dry season between 2005 and 2006, which is described as one of the most severe droughts in Yunnan and other regions of China in the last 50 years (Cheng and Xie 2008). This extreme climate conditions had a significant impact on vegetation and soils, such as pronounced decreases in moisture content and primary productivity, which are visible in the SI. The trajectories show that the unburned vegetation remains under stress for several years after the drought event, while the burned trajectory joins the unburned one after a few years. This suggests that the shrubs have recovered quickly from the fire, but they are still under stress from the general drought condition, showing similar absolute values of SI. Another isolated behavior

is found in BAIMs which is the only SI to detect a delayed mortality effect at the 1 year post-fire assessment in needleleaved vegetation. The peculiarity of BAIMs is its combined use of the near infrared and the shorter shortwave infrared bands of the Landsat TM sensor, an approach also adopted by the NDMI. The latter, although not showing a delayed mortality effect in needle leaved forest, tends to remain stable between the post-fire and the 1 year assessment compared to the other SI. Such a pattern may reveal higher sensitivity of BAIMs and NDMI for the detection of delayed mortality. Finally, the Wetness index draws an unusual trajectory in grassland vegetation. Instead of decreasing constantly after the fire like in other vegetation classes, it increases slightly at the immediate post-fire assessment and rapidly rejoins the same conditions as the unburned grass. A possible explanation for this distinct behavior could be that fire boosts recovery of grassland by eliminating dead plant material, competing weeds and small shrubs. Furthermore, with adequate soil moisture conditions, the darkening effect of fire increases soil surface temperature, stimulating earlier growth (Stubbendieck *et al.* 2007). In support to this hypothesis, the values of Brightness in grasslands fall drastically in this time frame compared to other vegetation types.

More precise information is given by the *M*-statistic and *RSR* results shown in Table 5-4. At the immediate post-fire assessment, MIRBI, GEMI, Greenness and BAI have very good separability ($M > 1$) in all vegetation types. NBR follows with good separability in three vegetation types (M lower than 1 in broadleaved forest only) and NDVI in two vegetation types (*M* lower than 1 in shrubland and grassland). Brightness proves good separability in grassland ($M = 1.18$) but very poor separability in other vegetation types. Overall, the best separability is found in needleleaved forest, with all SI having *M* values above 1 at the immediate post-fire assessment, except for BAIML, BAIMs, Brightness, and Wetness. The last one tends to respond to fire later than other indices, as a result of decreased biomass and gradual loss of moisture content in soils some years after a fire event (Rogan and Yool 2001). The colored highlights in Table 5-4 clearly tell us that, in all vegetation types and in most of the post-fire dates, NBR and NDMI score among the three best performers in both separability and enhancement of residual severity capabilities. Slightly lower scores are observed in grassland and shrubs ecosystems, where at some dates other SI such as MIRBI and Wetness performed similarly or better. Moreover, NDVI, which is normally used as an indicator of general vegetation condition, obtained separability and *RSR* scores comparable to the best index in broadleaved and needleleaved forests. *RSR* values are in general higher in needleleaved and broadleaved forests than it is in shrublands and grasslands, indicating slower recovery and longer persistence of fire scars. Except for NDMI that quantifies *RSR* at 63% (0.63) with the highest separability ($M = 0.40$) 1 year after the burn, all other indices perform significantly worse in grass-dominated landscapes, and from 2 years after the burn, scars are almost undistinguishable by any SI. A similar tendency though less pronounced is observable in shrubland ecosystems.

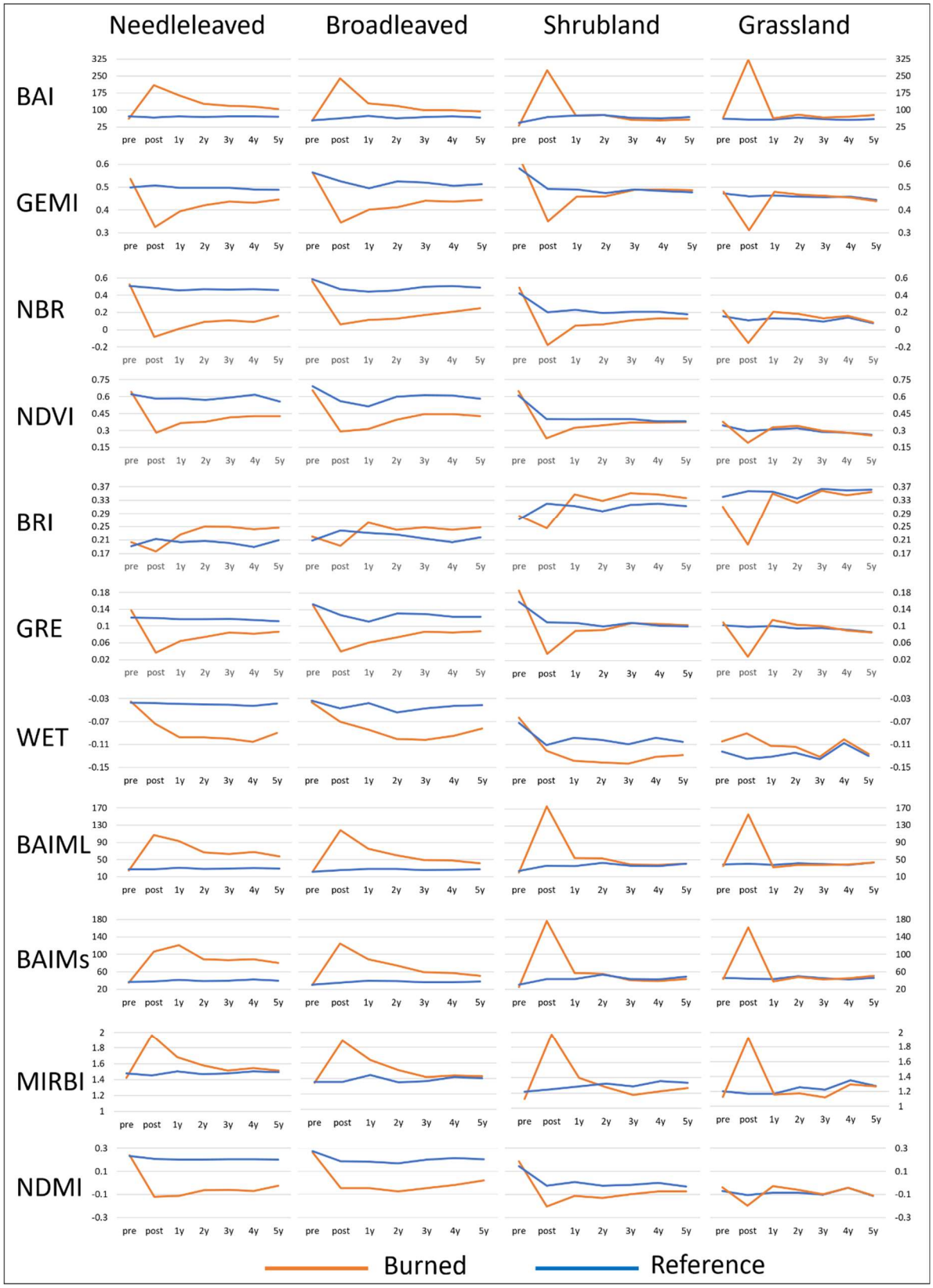

Figure 5-5. Temporal trajectories for 11 spectral indices in four major vegetation types in northwest Yunnan.

Table 5-4. Separability index (*M*-statistic) and Residual Severity Ratio (*RSR*) for the 11 SI in the four major vegetation types of northwest Yunnan. Highlighted cells indicate the three best performers at the given post-fire time in the following rank/color order: 1st, 2nd, 3rd. Pre-fire *M*-statistic values are shown as reference. MS = maximum severity from which *RSR* is calculated. Negative values of *RSR* indicate that the trajectory of the burned class crossed the trajectory of the unburned control class.

		***M*-Statistic**						**Residual Burn Ratio**					
		Post	**1y**	**2y**	**3y**	**4y**	**5y**	**Post**	**1y**	**2y**	**3y**	**4y**	**5y**
Coniferous Needleleaved Forest	**BAI**	1.13	0.70	0.55	0.38	0.43	0.33	MS	0.65	0.41	0.32	0.29	0.24
	GEMI	1.11	0.56	0.42	0.30	0.31	0.24	MS	0.57	0.41	0.33	0.31	0.24
	NBR	1.32	1.12	1.13	1.05	0.97	0.81	MS	0.79	0.67	0.63	0.67	0.53
	NDVI	1.36	0.82	0.78	0.88	0.87	0.61	MS	0.72	0.64	0.58	0.63	0.43
	BRI	0.26	0.16	0.29	0.30	0.36	0.25	−0.69	0.44	0.81	0.91	MS	0.70
	GRE	1.27	0.63	0.54	0.36	0.41	0.34	MS	0.63	0.50	0.39	0.39	0.30
	WET	0.48	0.71	0.70	0.74	0.75	0.70	0.58	0.94	0.92	0.95	MS	0.82
	BAIML	0.75	0.85	0.98	0.77	0.85	0.70	MS	0.78	0.47	0.43	0.46	0.35
	BAIMs	0.75	0.82	0.87	0.66	0.74	0.60	0.87	MS	0.63	0.59	0.59	0.51
	MIRBI	1.31	0.39	0.26	0.06	0.09	0.04	MS	0.35	0.22	0.06	0.08	0.03
	NDMI	1.09	1.10	0.98	0.99	0.92	0.78	MS	0.96	0.81	0.80	0.84	0.68
Broadleaved Forest	**BAI**	1.09	0.46	0.53	0.29	0.27	0.26	MS	0.32	0.31	0.17	0.15	0.15
	GEMI	1.13	0.59	0.60	0.39	0.34	0.35	MS	0.52	0.63	0.45	0.39	0.37
	NBR	0.81	0.81	0.76	0.88	0.69	0.60	MS	0.81	0.81	0.81	0.74	0.59
	NDVI	1.13	0.77	0.81	0.78	0.74	0.71	MS	0.75	0.76	0.64	0.61	0.57
	BRI	0.30	0.21	0.09	0.17	0.20	0.17	MS	−0.69	−0.32	−0.72	−0.79	−0.63
	GRE	1.27	0.68	0.71	0.47	0.43	0.43	MS	0.58	0.66	0.49	0.43	0.41
	WET	0.21	0.39	0.44	0.50	0.45	0.38	0.41	0.84	0.84	MS	0.94	0.74
	BAIML	0.75	0.73	0.72	0.77	0.73	0.59	MS	0.51	0.35	0.25	0.23	0.15
	BAIMs	0.77	0.64	0.56	0.50	0.52	0.34	MS	0.54	0.40	0.25	0.23	0.15
	MIRBI	1.07	0.41	0.34	0.09	0.03	0.06	MS	0.37	0.30	0.10	0.03	0.05
	NDMI	0.64	0.73	0.77	0.81	0.69	0.55	0.94	0.93	0.99	MS	0.94	0.74
Shrubland	**BAI**	1.02	0.00	0.00	0.09	0.11	0.11	MS	0.00	0.00	−0.04	−0.05	−0.05
	GEMI	1.00	0.23	0.11	0.01	0.05	0.07	MS	0.23	0.10	0.01	−0.05	−0.06
	NBR	1.02	0.49	0.38	0.29	0.22	0.15	MS	0.48	0.34	0.26	0.20	0.13
	NDVI	0.71	0.32	0.22	0.14	0.05	0.03	MS	0.45	0.32	0.20	0.07	0.05
	BRI	0.44	0.20	0.20	0.20	0.17	0.17	MS	−0.47	−0.41	−0.46	−0.37	−0.34
	GRE	1.15	0.25	0.12	0.02	0.05	0.05	MS	0.25	0.11	0.02	−0.04	−0.05
	WET	0.08	0.34	0.42	0.32	0.30	0.23	0.24	MS	0.98	0.84	0.82	0.57
	BAIML	0.77	0.32	0.24	0.10	0.09	0.01	MS	0.14	0.08	0.02	0.02	0.00
	BAIMs	0.78	0.17	0.03	0.05	0.06	0.09	MS	0.10	0.01	−0.02	−0.02	−0.04
	MIRBI	1.42	0.21	0.11	0.24	0.30	0.18	MS	0.16	−0.06	−0.15	−0.18	−0.09
	NDMI	0.69	0.43	0.42	0.34	0.29	0.17	MS	0.65	0.58	0.46	0.42	0.24
Grassland	**BAI**	1.90	0.05	0.11	0.08	0.15	0.17	MS	0.02	0.05	0.03	0.05	0.06
	GEMI	1.54	0.13	0.07	0.04	0.04	0.07	MS	−0.10	−0.06	−0.03	0.03	0.04
	NBR	1.12	0.37	0.32	0.21	0.07	0.04	MS	−0.28	−0.23	−0.14	−0.07	−0.03
	NDVI	0.72	0.12	0.13	0.06	0.00	0.05	MS	−0.17	−0.19	−0.08	0.00	0.05
	BRI	1.18	0.03	0.07	0.03	0.09	0.05	MS	0.04	0.08	0.04	0.09	0.04
	GRE	1.69	0.22	0.15	0.09	0.05	0.01	MS	−0.21	−0.12	−0.07	0.04	0.01
	WET	0.47	0.16	0.10	0.04	0.06	0.04	MS	0.43	0.24	0.10	0.14	0.09
	BAIML	0.87	0.17	0.12	0.09	0.05	0.01	MS	−0.05	−0.04	−0.02	0.01	0.00
	BAIMs	0.91	0.11	0.03	0.05	0.06	0.07	MS	−0.05	−0.01	−0.02	0.02	0.03
	MIRBI	1.94	0.02	0.15	0.20	0.11	0.01	MS	−0.01	−0.11	−0.14	−0.07	−0.01
	NDMI	0.57	0.40	0.19	0.04	0.01	0.01	MS	−0.63	−0.29	−0.05	0.02	−0.01

The interpretation of the performance of Brightness, especially regarding *RSR* values which are often higher than other SI, is prone to confusion. First, it is important to note that its separability abilities are quite low in all land cover types and at any post-fire date, except for a noticeable $M = 1.10$ in grassland at the immediate post-fire assessment. Second, abrupt shifts of the burn trajectory versus the unburned reference trajectory as indicated by *RSR* negative values call for particular caution and require further clarification. At the 1 year post-fire assessment, the trajectory of burned samples shifts to values higher than the unburned trajectory in most of the vegetation classes. In the following years, the two trajectories progress almost in parallel with small variations of both reference and burned samples. These variations coupled with the smaller spectral distance at the immediate post-burn assessment (initial maximum severity point) explain the inflated *RSR* values. In other words, the *RSR* of Brightness could highlight a persistent disturbed status of the vegetation, however, the *M*-statistic values being relatively low indicate high overlap between burned and unburned pixels. These results advise against the employment of Brightness for burned area mapping without other supporting tools.

5.3.3. Summary of results: which spectral indices should we chose?

Our results in a mountainous region characterized by frequent small fires and a fast-recovering vegetation promoted by abundant summer rains shows that all spectral indices are valid tools to separate burned from unburned vegetation at the immediate post-fire assessment, except for Wetness and Brightness that follow different patterns. Among them, MIRBI, BAI, and Greenness are the best when averaging all vegetation types, while NDVI and NBR get better scores in isolated vegetation types. Other studies obtained similar results, e.g., better discrimination capabilities of BAI (Chuvieco *et al.* 2002; Schepers *et al.* 2014; Liu *et al.* 2016), Greenness (Rogan and Yool 2001; Loboda *et al.* 2013), or MIRBI in shrub-savannah ecosystems (Trigg and Flasse 2001; Melchiori *et al.* 2015; Lu *et al.* 2016). Although NBR is often considered the best SI for burned area mapping short time after fire and therefore widely used for burn severity assessments (Epting *et al.* 2005; Escuin *et al.* 2008; Veraverbeke *et al.* 2010; Harris *et al.* 2011; Schepers *et al.* 2014; Melchiori *et al.* 2015; Hislop *et al.* 2018), our results demonstrated that in certain vegetation types other SI would offer a better option. The limitations of NBR for immediate post-fire assessment were already pointed out by Roy et al. (Roy *et al.* 2006).

From one year after the fire events, burned areas in shrublands and grasslands are very difficult to discriminate. Despite low discrimination capabilities, NDMI and NBR are the best choice, while Wetness could offer a valuable support in shrublands starting from two years after the fires. In more vegetated areas such as broadleaved and needleleaved forests, fire scars are more persistent and NBR has often shown to perform better than in sparsely vegetated land (French *et al.* 2008; Veraverbeke *et al.* 2011). From one to five years after the fire, the best SI are NBR and NDMI, followed by NDVI in broadleaved vegetation and BAIML in needle leaved vegetation. Brightness and Wetness have lower separability capabilities but can be useful to analyze residual severity and recovery. The other SI analyzed in this study performed

consistently worse and proved to be less suitable for long term monitoring of fire disturbance. The spectral response of BAI strongly depends on the persistence of charcoal deposits (Chuvieco *et al.* 2002). Both of its modified versions, which were initially designed for the MODIS sensor, could not reach the same performance as the best SI, as also found by (Melchiori *et al.* 2015), and therefore represent a second choice for long term monitoring of post-fire vegetation recovery. The spectral behavior of GEMI is similar to Greenness but results of metrics are almost always worse. Finally, MIRBI resulted very unsuitable for long term burned area detection.

Our results are in line with recent studies on SI capabilities for mapping vegetation recovery, which found that the SI that integrated the shortwave infrared domain of the electromagnetic spectrum such as NBR, NDMI, and Wetness are more suitable for long term vegetation recovery, while indices relying on visible and near-infrared domains were more suitable for immediate post-fire assessment (Chen *et al.* 2011; Lozano *et al.* 2012; Pickell *et al.* 2016; Hislop *et al.* 2018). Our graphic plots show that this is particularly true in less vegetated ecosystems (shrubs, grass). However, we also found that NDVI is as robust as NBR and NDMI in broadleaved forest several years after fire.

Finally, it is important to note that *M*-statistic and *RSR* only quantify separability between burned and unburned samples and residual severity magnitude. These metrics do not quantify the quality of burned area mapping. Further analysis of the mapping capabilities of SI should include change detection and classification methodologies with detailed accuracy assessments quantifying omission and commission errors. Moreover, to improve our knowledge of fire in mountainous regions, additional research on burned area detectability by SI in different slope/aspect and hill shading conditions as well as their capabilities to discriminate fire disturbances from other types of change is highly suggested.

5.4. Chapter conclusions

The wide-ranging amount of literature on Landsat spectral indices performance for the detection of burned areas suggests that there is no unique model that over performs the others in any spatiotemporal circumstances. Instead, different vegetation types and different time lags between image acquisition dates greatly influence the spectral indices behavior. In this study, the spectral trajectories of eleven among the most common spectral indices widely employed in burned area extraction have been analyzed in four major vegetation types in a mountainous area of northwest Yunnan, China. As previous literature suggested, two main performance variability patterns can be highlighted. First, a temporal pattern: significant performance differences were observed between immediate post-fire assessment and from one to several years after fire. Second, a vegetation type pattern: a clear difference between more vegetated (needleleaved and broadleaved forest) versus less vegetated landscapes (shrublands and grasslands) exists. Therefore, in order to optimize accuracy of burned area detection algorithms, the best spectral indices should be selected accordingly. In general, when time lag is short (< 1 year), MIRBI and the Tasseled Cap Greenness are the most suitable indices, followed by the BAI. When time lag

is longer (>1 year), NBR and NDMI are the most suitable to detect residual severity and more realistically track vegetation recovery. However, fire scars in grassland ecosystems are almost undetectable by any spectral index after one growing season. The Tasseled Cap Wetness revealed to be very useful for monitoring long-term residual severity starting from 2 years after a fire.

Delicate mountain ecosystems are particularly sensitive to climate variations which, together with patchy land cover, frequent clouds, and relatively fast vegetation regeneration, make it challenging to systematically extract burned areas and assess impacts and recovery. To better isolate fire disturbance from the overall variation of the vegetation's ecological condition, we designed a conceptual model that relativizes the spectral response of burned pixels by integrating the spectral response of unburned pixels. The metrics used to quantify class separability (*M*-statistic) and magnitude of residual severity (*RSR*), were adapted to this model. The high inter-annual variability of unburned vegetation observed in the resulting graphic plots confirms the validity of this approach. Therefore, relying solely on the pre-fire condition of the burned vegetation to assess recovery, may introduce bias coming from other disturbances. Instead, keeping track of general vegetation conditions over time allows for the identification of other environmental factors influencing recovery, such as general drought. Thus, this approach is particularly suitable to assess vegetation vulnerability to fire under changing climate and weather conditions.

6. Building a fire extraction routine for mountain's complex landscapes

The content of this chapter is based on the following publication. However, a few adaptations and updates have been added.

Fornacca D, Ren G, Xiao W (2020) Small fires, frequent clouds, rugged terrain, and no training data: a methodology to reconstruct fire history in complex landscapes. *International Journal of Wildland Fire*. https://doi.org/10.1071/WF20072.

Abstract: To understand current regional fire regimes, we need accurate statistics of historical fire events spanning over several decades, including at least the number of fires, their location, and area burned. Satellite images from the Landsat missions offer a unique opportunity to reconstruct land surface dynamics in almost any region of the world, especially where this knowledge is missing, such as in remote mountainous areas. The task of extracting burned scars in these regions in a systematic and automated way presents several difficulties. Using the mountainous region of northwest Yunnan in China as a test area, we developed an automated burned area extraction routine based on the Landsat archive which attempts to overcome these issues, in particular the inexistence of burned samples to use for training and testing, the rugged relief, and the constant presence of clouds during the rainy season which highly affects the availability of usable scenes within a year. The algorithm flows through five phases: creation of standardized difference vegetation indices time-series; automatic extraction of multi-class training areas using adaptive z-score thresholds; Random Forests classification; Seeded Region Growing, and spatiotemporal clustering to form coherent burn multi-polygons. A final product of fire events spanning the period 1987-2018 is created. Accuracy assessment of location and number of fire polygons using a stratified random sampling design shows satisfying results with reduced omission (20%) and commission (22%) errors compared to global fire products in the same region. Pixel-level accuracy of single fire events showed a minimization of commission (13%) at the expense of higher omission (27%). This routine represents a step forward for the integration of small fires in multi-scale assessments of their environmental impacts.

Keywords: Landsat, adaptive thresholds, time-series normalization, fire events, mountainous area, training data

6.1. Introduction

As mentioned several times in the present document, the poor or restricted availability of accurate environmental and socio-economic data for knowledge-building processes is a common barrier encountered by researchers, especially those focusing on remote, mountainous, and less populated areas of the world (Schneiderbauer *et al.* 2007; Mouillot *et al.* 2014). Earth Observations provide repeated synoptic views of our planet and can partially fill spatiotemporal information gaps in a very efficient way. In particular, the availability of long-term time-series images from the Landsat satellite missions offers great opportunities for the development of all sorts of Earth Observation applications. Thanks to its continuous, near-global coverage from the mid-1970s to the present date, it is now possible to reconstruct the recent history of land surface dynamics in locations where this knowledge has been out of reach, because limited by physical and environmental constraints or not available to the public (Wulder *et al.* 2012, 2019; He *et al.* 2018; Zhu *et al.* 2019). Mountainous landscapes are among these regions of difficult access that can significantly benefit from remote sensing technology. However, mainly owing to the rugged topography and heterogeneous landscape, the extraction of information from satellite images in these regions presents specific challenges requiring particular attention from the analyst, who will need to adapt ordinary processing routines and develop new ones (Mulders 2001; Heinimann *et al.* 2003; Schneiderbauer *et al.* 2007; Yang *et al.* 2007; Ren *et al.* 2009; Weiss and Walsh 2009; Ward *et al.* 2011; Zhang *et al.* 2014).

Several time-series land change detection methodologies have been applied to burned area mapping, such as the Burned Area Mapping Software (BAMS) (Bastarrika *et al.* 2014), the Composite2Change (C2C) (Hermosilla *et al.* 2015), the Landsat-based detection of Trends and Recovery (LandTrendr) (Kennedy *et al.* 2010), or the Vegetation Change Tracker (VCT) (Huang *et al.* 2010). A review of these approaches and many others can be found in (Gómez *et al.* 2016; Meng and Zhao 2017; Zhu 2017; Chuvieco *et al.* 2019). However, when considering the application of these existing solutions for mountainous regions, several complications arose. Among major shortcomings we found that models based on dense time-series (i.e. more than one Landsat scene per year) or gap-fill approaches such as Best Available Pixel (BAP) are not applicable in NWY because of the heavy presence of clouds in most of the scenes within a year. On the other hand, methodologies based on too large time-lag in the time-series (more than 1 year) are also not suitable because of fast post-fire vegetation recovery. Other approaches have been designed for satellite sensors not relevant to this region, and most of them rely on existing ground data to train and tune the algorithms, which in several regions of the world are not available.

To improve the regional discrimination of burned land, some authors proposed ecosystem specific algorithms adapted to medium to coarse resolution sensors. For example, Bastarrika, Chuvieco, and Martin (2011) developed a new automatic burned area mapping algorithm based on MODIS time series for the Mediterranean ecosystem, obtaining higher accuracy (kappa = 0.846) and a lower omission error (17.1%) than the standard MCD45 product (kappa = 0.704,

omission error = 38.6%). Chuvieco, Englefield, *et al.* (2008) produced a 23-years long time series of burned land using 10-day composites of NOAA-AVHRR data in boreal forests; Merino-de-Miguel *et al*. (2010) used MODIS products in Galicia; while other studies employed MODIS products in western United States, Latin America, and northeast China (Fraser *et al.* 2000; Chuvieco, Opazo, *et al.* 2008; Urbanski *et al.* 2009; Yang *et al.* 2013).

Learning from the reviewed approaches, we describe here a methodology for the systematic reconstruction of burn history (a database of fire events including location and time) and extraction of burned areas (area of each fire event), which addresses the issues and requirements of remote, mountainous areas. The specific challenges and the line of action chosen to tackle them are described in the next section. Afterwards, the different components of the proposed solution are explained, while the results section provides accuracy metrics for two different assessment methods that are then extensively discussed. The conclusion section summarizes the findings and drafts future development plans. Although the resulting solution is tested in northwest Yunnan, researchers working in areas with similar difficulties can implement some of the approaches and finally fill those data gaps that prevent the advancement of their research.

6.2. Challenges and potential solutions for burned area extraction in the complex landscapes of northwest Yunnan

In this section, we review the particular issues of remote sensing in the case of the systematic extraction of past burn scars in regions characterized by complex landscapes. For each of them, we propose a potential solution or at least a way to adapt to each of these obstacles. A summary of the problems and solutions is shown in Figure 6-1.

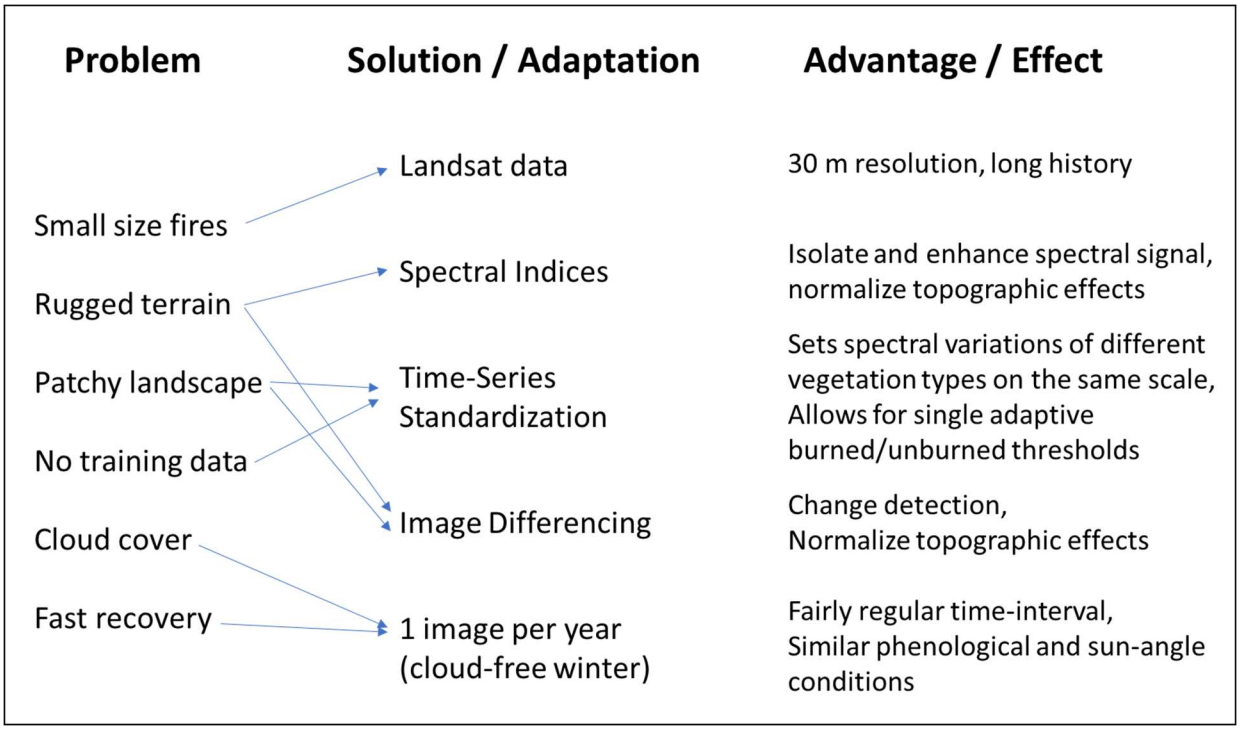

Figure 6-1. Summary of remote sensing of burned areas difficulties encountered in regions characterized by complex landscapes and no training data, and proposed solutions / adaptations.

6.2.1. Rugged topography

When modeling mountainous environments on 2-dimensional surfaces, important distortions are inevitably introduced. For example, linear distances on slopes are different than on flat land, affecting density maps, area calculations, and cost-distance analysis. Sun angle and relief affect illumination patterns, creating shadows that greatly reduce the intensity of spectral signals (Itten and Meyer 1993; Schneiderbauer *et al.* 2007). Shady areas can be easily confused with burned areas (Mitri and Gitas 2004; Chuvieco *et al.* 2019). Several authors have attempted to solve or at least minimize this problem by identifying and classifying shady pixel separately, often using illumination models based on sun angle at the date of the satellite image acquisition and Digital Elevation Models (DEM), or by developing topographic correction techniques that are now highly recommended as an integral step in image preprocessing (McDonald *et al.* 2000; Riaño *et al.* 2003; Gitas and Devereux 2006; Cheng *et al.* 2008; Gao and Zhang 2009; Hantson and Chuvieco 2011; Ediriweera *et al.* 2013; Fan *et al.* 2018). However, some studies found divergent results varying from insignificant improvements, improvement in shady areas at the cost of deterioration in well-illuminated areas, and introduction of additional distortions when relief is too rugged and slopes too steep (Richter *et al.* 2009; Hantson and Chuvieco 2011; Tan *et al.* 2013; Chance *et al.* 2016; Sola *et al.* 2016; Pimple *et al.* 2017).

Our tests of various topographic correction techniques gave unacceptable results. Therefore, we found a partial solution in the use of band-ratios, on which several vegetation

indices are built, and image differencing, which have proven to be able to minimize these unwelcomed effects (Holben and Justice 1981; Matsushita *et al.* 2007; Weiss and Walsh 2009; Piper and Yeo 2011). Because topographic shadows affect all spectral bands in a similar manner, computing a ratio between two bands will have a normalizing effect. Image differencing will have a similar effect, provided that the images used to compute change detection have similar sun angle illumination.

6.2.2. Patchy landscapes with different vegetation types

Habitat heterogeneity and fragmented vegetation are typical features of mountainous regions with extreme altitudinal gradients. Researchers developing mapping routines for this kind of landscape have often reported these difficulties (Khawlie *et al.* 2002; Heinimann *et al.* 2003; Cayuela *et al.* 2006; Ren *et al.* 2009; Mohammed *et al.* 2020; Zhao *et al.* 2020). Owing to the particular geographical situation (both altitudinal and latitudinal) of northwest Yunnan, different vegetation types coexist with pronounced human interference on the mountain slopes, mostly in the form of agriculture and tree plantations (Figure 6-2). Agricultural land changes very quickly and in a different manner according to the crop type and the farmers' practices (including slash-and-burn). Moreover, during the dry season, sparsely vegetated surfaces look similar to burned areas, especially when the lag between the fire event data and the data of the post-fire image used for the mapping is large, in the order of several months. Difficulties arise when choosing the ideal thresholds to separate burned and unburned pixels that may be quite different according to vegetation types within a given image. In a time-series perspective, thresholds for one image may not be suitable for other images because of spectral inconsistencies introduced by differences in sun elevation, atmospheric conditions, phenology, etc.

Also in this case, image differencing can minimize these issues but not entirely remove them. Thresholds adapted to each image should be preferred over a single fixed threshold for the whole time-series. This can be achieved by normalizing the time-series which has shown to equalize the magnitude of change in different vegetation types (de Carvalho Júnior *et al.* 2015). Among the different normalization techniques, z-score standardization was selected (more details in Section 6.3.2.1).

Figure 6-2. Patchy landscape in the mountains around Yunlong Natural Taiji Eight-Diagram on the Bijiang river, Yunlong county. Photo by the author.

6.2.3. Disturbances of limited size compared to other regions

With patchy landscapes come forest fires of smaller size compared to those in vast forests such as boreal areas or extensive woodlands. Burned area detection by satellite becomes more difficult if sensors have coarse spatial resolution capabilities. The existing satellite-based global fire products such as the MODIS suite (Justice, Giglio, *et al.* 2002) and ESA_cci (Chuvieco *et al.* 2016) are relatively recent, tracking burned areas back to the year 2000 the earliest. Also, these products are not suitable for estimating burned area and fire counts in patchy landscapes, because of their coarse spatial resolution omitting more than 50% of the fire events (Fornacca *et al.* 2017).

As may be evident at this stage of this thesis, we reiterate that the best option for reconstructing the fire history of mountainous regions lies in the Landsat long archive and moderate (30 m) spatial resolution.

6.2.4. Constant or partial (seasonal) cloud coverage

Unfavorable atmospheric conditions represent another widespread limitation for optical remote sensing. Haze alters the radiance recorded by the sensors and reduces visibility, requiring calibration processes to obtain 'clean' reflectance values comparable with other scene acquisitions (Fang and Yang 2014; Zhu 2017; Ahmad *et al.* 2019). Several dehazing techniques and atmospheric corrections algorithms have been developed, and some of them are integrated in deliverable satellite products such as the LEDAPS algorithm for Landsat TM sensors (Masek *et al.* 2013) and the LaSRC for the Landsat OLI sensor (Vermote *et al.* 2016). Although hazy scenes can be at least partially recovered, clouds block the illumination of a good portion of the electromagnetic spectrum used by passive sensors such as visible and infrared light. Moreover, depending on their elevation, they cast shadows on other areas that cannot be corrected with topographic normalization methods. Consequently, the information of the land surface covered by clouds in that scene is lost. According to the analysis's aim, clouds and their shades can be removed by masking operations (Zhu and Woodcock 2012, 2014; Goodwin *et al.* 2013), and the affected pixels can be potentially replaced with cloud-free pixels extracted from other images. This gap-fill operation is performed using a Best-Available-Pixel (BAP) approach, which consists of searching for suitable pixels in images temporally close to the target image (White *et al.* 2014; Hermosilla *et al.* 2015). Alternatively, active microwave remote sensing solutions such as radar could be considered for their ability to penetrate clouds. However, for burned area mapping purposes, radar images are difficult to interpret, and performance results vary significantly among the studies which tested them; some considering them promising (Huang and Siegert 2004; Polychronaki *et al.* 2013; Belenguer-Plomer *et al.* 2019), while other finding significant limitations or suggesting a complementary adoption with optical images (Siegert and Ruecker 2000; Stroppiana *et al.* 2015; Tanase *et al.* 2020).

The seasonal monsoon-type climate of northwest Yunnan results in long periods of cloudy conditions (Figure 6-3). The acquisition frequency of Landsat 4-5 images is relatively low (16 days) compared to other satellites such as MODIS, which fairly limits the selection of candidate scenes for time-series in areas with high cloud cover (Hawbaker *et al.* 2017). This represents a major problem when detecting non-permanent effects of natural or human-induced disturbances such as wildland fires (Melchiorre and Boschetti 2018; Fornacca *et al.* 2018). The time interval between candidate scenes could vary substantially each year, resulting in very irregular time-series challenging to analyze because of pronounced differences in vegetation phenology, sun angle, and climatic conditions (Key 2006; Verbyla *et al.* 2008). Consequently, an approach based on regular time-interval data is preferred. For our study region, a time-series using single yearly winter images was built.

Figure 6-3. An example of query results for Landsat TM scenes in a portion of northwest Yunnan (WRS path 131, row 42) in 2011, from the USGS's EarthExplorer provider (www.earthexplorer.usgs.gov). The thumbnails illustrate how cloud-free images are very limited.

6.2.5. Fast vegetation recovery owing to abundant rains

A condition that goes along with high cloud coverage, abundant seasonal rains are typical of tropical regions. Regular precipitation and a warm weather boost vegetation regrowth, quickly hiding light fire scars. This is particularly pronounced in grassland/savannah-like ecosystems but also in pine forests, which are in general composed of fire-adapted species with rapid resprouting. As a consequence, the time window to detected burned areas is restricted, and several fire events will remain undetected, as shown in Figure 6-4 (see also Figure 5-4 and Figure 5-5 in Chapter 5 and in Fornacca *et al.* 2018).

As highlighted in the previous point, adding one or more candidate scenes within a year is not a suitable approach because of the frequent and extensive presence of clouds. A regular, 1-year interval time-series remains the best choice.

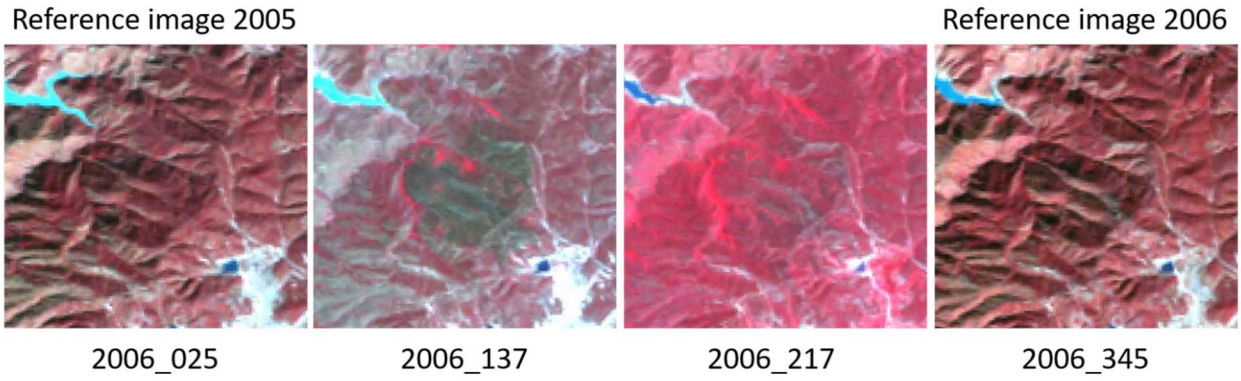

Figure 6-4. Example of fast vegetation recovery after burn. Dates are in Year_DayOfYear format. The first and last Landsat false-color composites are the reference scenes used in the time-series, while the second and third scenes have been added for analysis. The fire occurred and recovered in between the two reference dates, leaving almost no spectrally detectable trace.

6.2.6. No prior knowledge on fire occurrence available

Many algorithms and existing burned area extraction routines rely on existing data for training, testing, and parameter tuning. In the case of NWY and several other regions of the World, this information is missing. Moreover, burned area samples or hotspots derived from other products may not reliably represent burn in these complex regions, providing low quality or erroneous training data, as highlighted in Chapter 4 (Fornacca *et al.* 2017). Therefore, the ideal burn scar mapping algorithm should not rely on pre-existing data to train and test the models, for tuning the parameters or determining thresholds.

For this purpose, we looked into methodologies to automatically extract burn evidence based on the images composing the time-series. A few automatic threshold determination techniques for change detection based on the images' density distributions have been explored (Bruzzone and Fernandez Prieto 2000; D'Addabbo *et al.* 2004; Vázquez-Jiménez *et al.* 2017). Recently, Woźniak & Aleksandrowicz (Woźniak and Aleksandrowicz 2019) proposed a self-adjusting thresholding methodology applied to burned area detection that can be automatically applied to any vegetation type while maintaining satisfactory mapping accuracy. In our case, we used standardized time-series and determined different probabilities of burn based on standards deviations from the mean (details in section 6.3.2.2).

6.3. Materials and methods

6.3.1. Study region and data

The NWY region could be covered by 7 Landsat tiles, namely WRS-2 path/row 131/041, 131/042, 132/040, 132/041, 132/042, 133/040, and 133/041 (Figure 6-5). The time frame of the selected images was from the year 1987 to 2018, corresponding to consistently available Landsat

TM and OLI Collection 1 images for the region, retrieved from a United States Geological Survey (USGS) data provider (https://earthexplorer.usgs.gov/). No scenes from the ETM+ sensor were used because of its mechanical failure, consequently creating a 2-year gap in the time-series (2011 and 2012). All images were geometrically and radiometrically corrected, as well as calibrated to surface reflectance values by the provider using the LEDAPS (Masek *et al.* 2013) and the LaSRC (Vermote *et al.* 2016) algorithms, for TM and OLI scenes respectively, according to the Level-2 standards. Candidate images were selected on a yearly basis during the dry season (winter) because of the favorable atmospheric conditions with low cloud cover. Figure 6-6 shows the time-series dates for each path/row tile, while the precise dates in tabular format can be found in Appendix D. Overall, image dates were comprised between 10th October and 20th April (range: 193 days), with an average around 24th December and a standard deviation of 33 days. The largest interannual date shift was of 131 days in tiles 131/042 and 132/042, but the average shift was 35 days with a standard deviation of 26 days.

Three additional datasets were used as input in the burned area extraction workflow. Administrative boundaries for the delimitation of NWY were provided by the GADM project version 3.6 (https://gadm.org/). Two landcover datasets of circa year 2000 and year 2010 mapped at 30 m resolution were produced by the GlobeLand30 project (http://www.globallandcover.com/). Furthermore, active fire points from the MODIS MCD14ML product (http://modis-fire.umd.edu/) were used for the sampling design in the validation part.

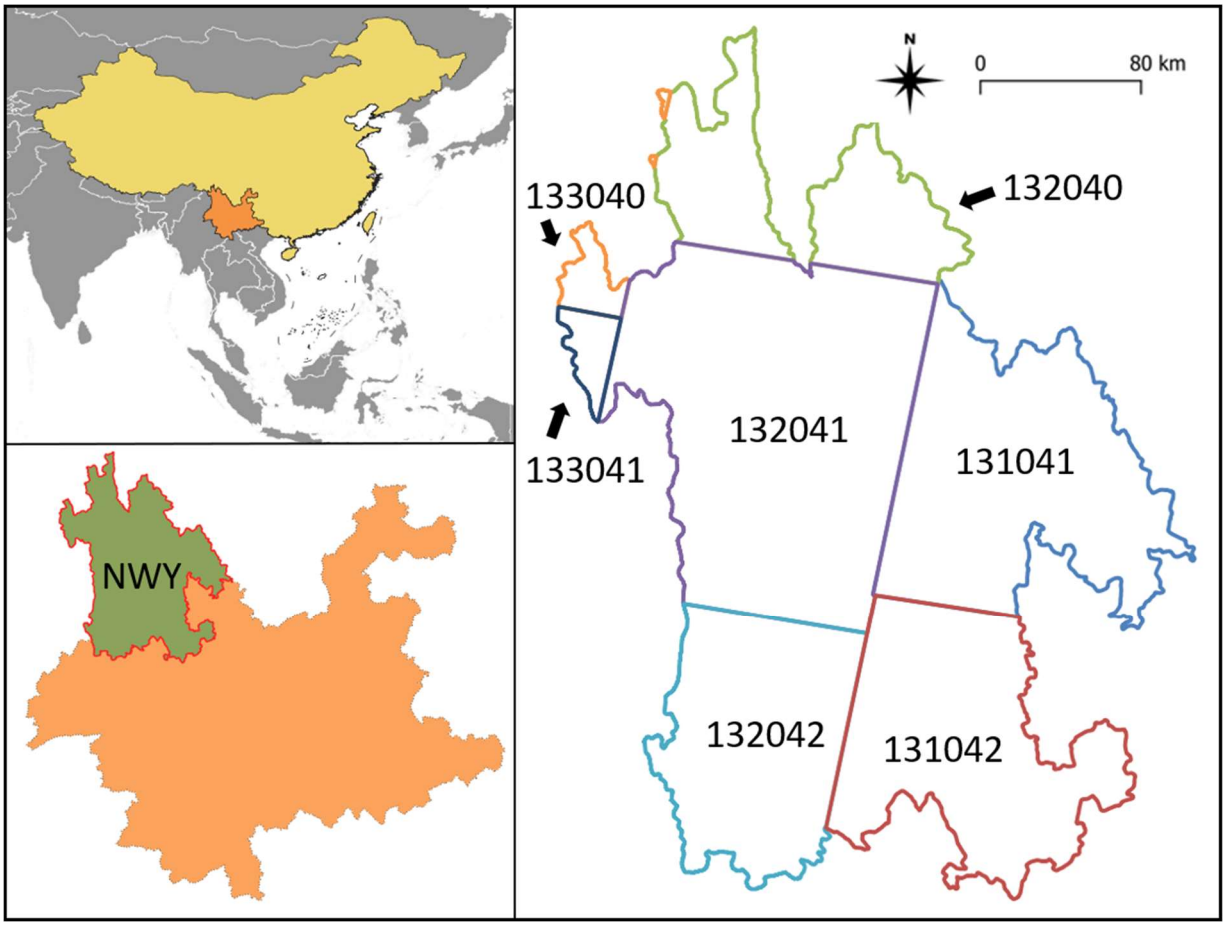

Figure 6-5. Location of the study area, northwest Yunnan (NWY). Landsat WRS-2 path/row coverages clipped to the boundary of the study region are shown in different colors (also used in Figure 6-6).

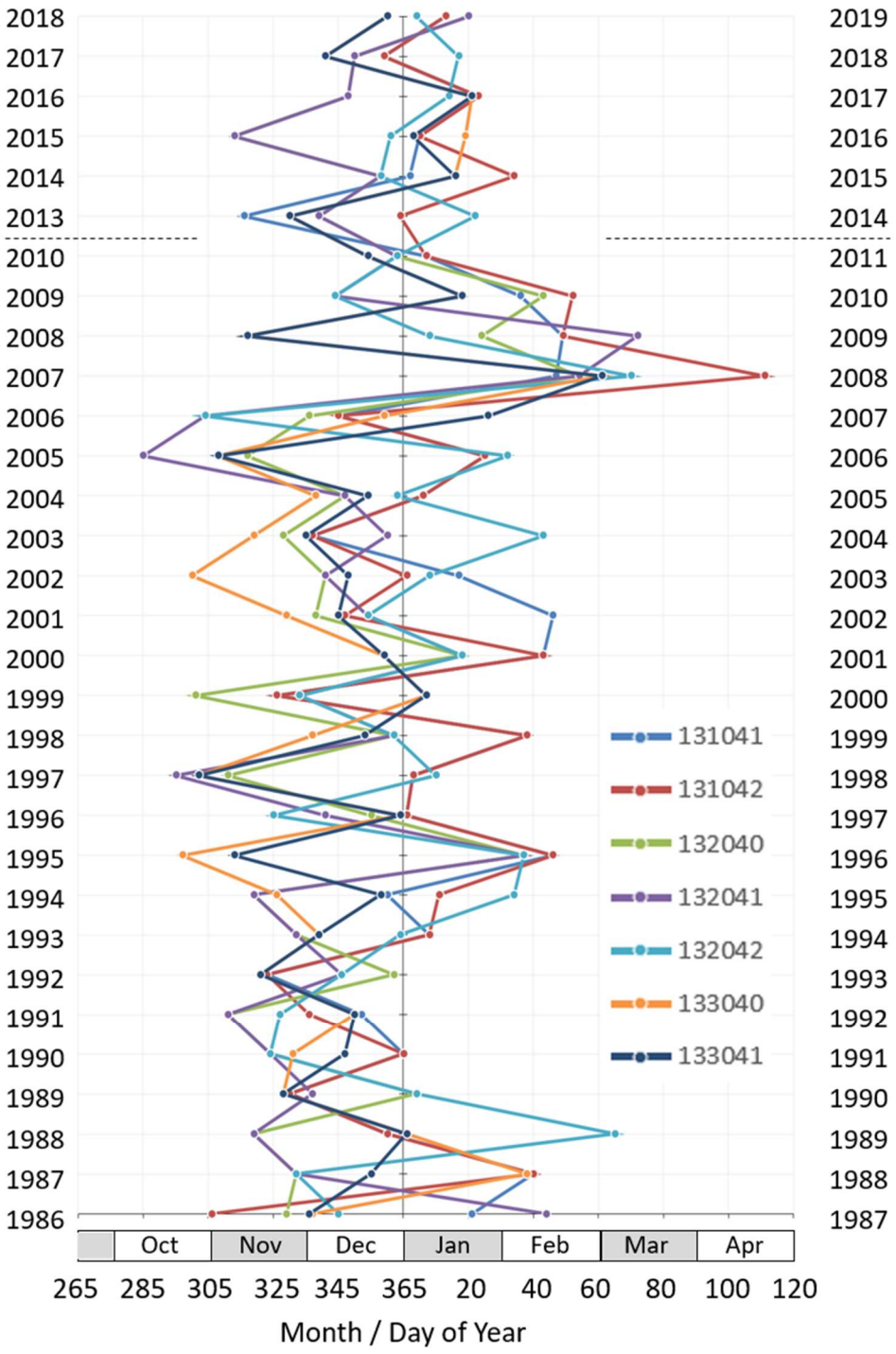

Figure 6-6. Variation of image dates in each WRS-2 path/row time-series. Because images were selected during the winter months, dates vary between the current and the following year, resulting in a "double y-axis". The raw data in tabula format can be found in Appendix D.

6.3.2. Burned area extraction workflow

One of the aims of the authors was to create an automated burned area and fire event extraction routine that can be easily reproduced by any researcher with basic GIS and remote sensing knowledge, without advanced programming skills. The resulting burned area extraction workflow is composed of five main phases. The first phase consists mainly of preprocessing steps to organize the time-series while the last step is the cleaning and reorganization of the results to form a fire event geodatabase. The second, third, and fourth steps are the core part of the process that, similarly to other previously developed fire extraction routines (Stroppiana *et al.* 2012; Roteta *et al.* 2019), consist in the creation of seeds or training areas to input a classification model followed by a pixel aggregation operation. These steps are described here, and a semantic processing workflow is presented in Figure 6-7.

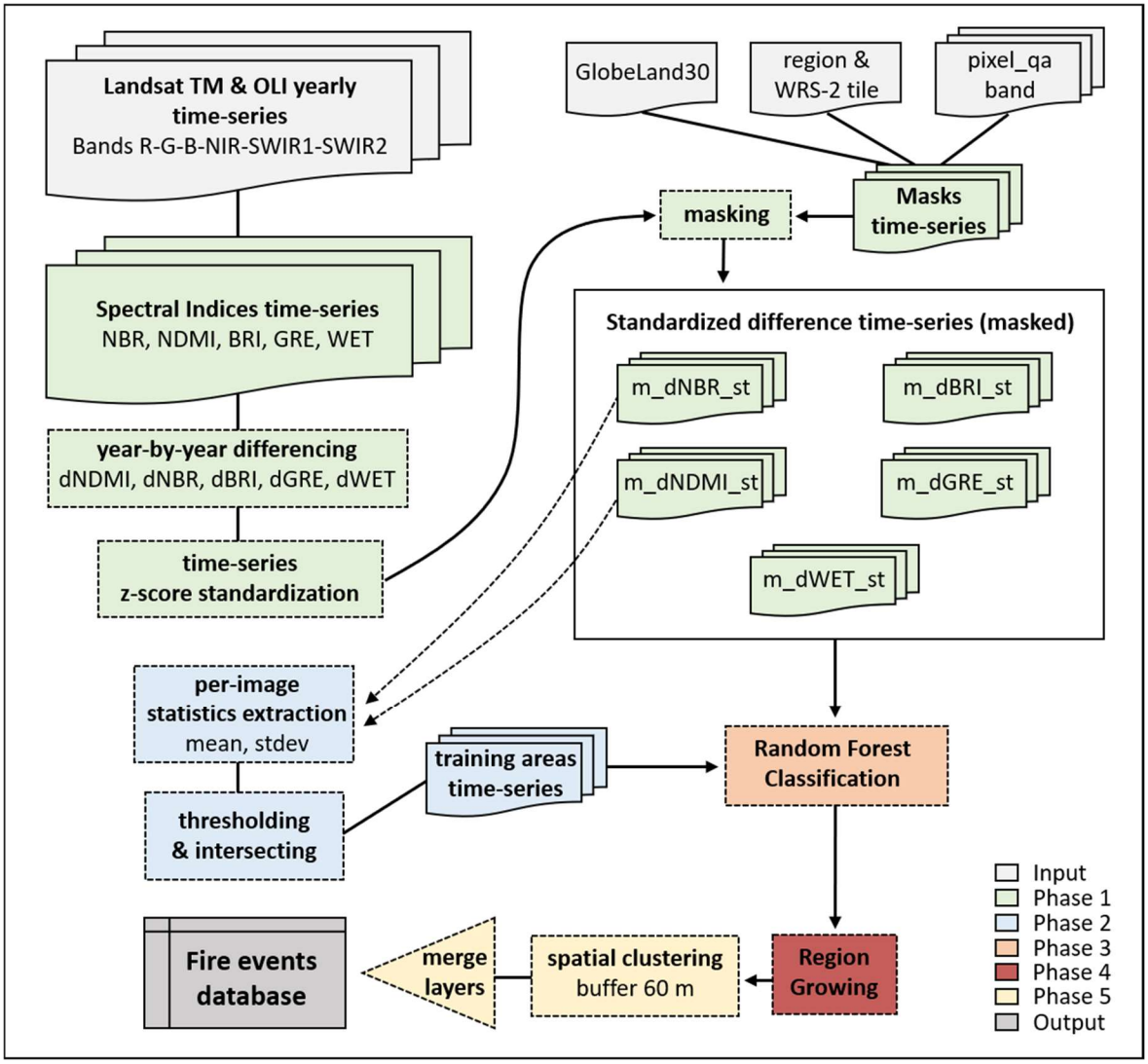

Figure 6-7. Processing workflow. The five phases of the burning area and fire events database creation are represented with colors. Light and dark grey elements represent the initial input data and the final output, respectively.

6.3.2.1. Phase 1 - Construction of the standardized time-series

As suggested in the requirements list, the use of fire-related spectral indices is highly suggested. Those that perform the best for detecting burned areas at time lags of about one year in our study region are the Normalized Burn Ratio (NBR) (López García and Caselles 1991; Koutsias and Karteris 2000; Key and Benson 2006) and the Normalized Difference Moisture Index (NDMI) (Wilson and Sader 2002). Additionally, The Tasseled Cap (Crist and Cicone 1984; Crist 1985; Baig *et al.* 2014) Brightness (BRI), Greenness (GRE), and Wetness (WET) can add complementary information of residual burn scars (Fornacca *et al.* 2018). After extracting these five indices for every image of the time-series, a sequential image differencing process where each year is subtracted by the following year's values (resulting in dNBR, dNDMI, dBRI, dGRE, and dWET) is executed. Bi-temporal image differencing is a common change detection approach, widely used in burned area and burn severity assessments (Lu *et al.* 2004; Key and Benson 2006), which can also be successfully applied to image pairs from different sensors provided that their spectral characteristics are similar, such as between Landsat TM, ETM+, and OLI, and proper calibration is performed (Oguro *et al.* 2003; Steven *et al.* 2003; Li *et al.* 2013; Flood 2014; She *et al.* 2015; Roy *et al.* 2016; Mancino *et al.* 2020). No calibration coefficients were applied but a normalized version of the difference images using z-score standardization was produced. De Carvalho Júnior et al. (de Carvalho Júnior *et al.* 2015) used this technique with NBR time-series from the MODIS sensor. The authors demonstrated how the temporal trajectories of different vegetation types showing different spectral behaviors can be harmonized using standardization, allowing for the discrimination of burned areas using a single threshold. Moreover, the negative effects of seasonal lag as shown in Figure 6-6 can also be mitigated with this approach. A visual example of the effect of standardization on difference images of our time-series is illustrated in Figure 6-8 and Appendix E reports a figure from de Carvalho Júnior *et al*. (2015) showing NBR temporal trajectories of two vegetation types before and after standardization. The formula to calculate the z-score of the temporal curve of each pixel is:

$$z = \frac{x - \mu}{\sigma}$$

where μ is the mean and σ is the standard deviation of the time-series at a given pixel location. The last step of this first phase is the masking of unwanted pixels. The images were clipped to the study region boundary while clouds, cloud shadows, and snow were masked using the *pixel_qa* band provided with the Landsat Level-2 surface reflectance product. Undesired landcover classes (urban, snow, agriculture) were derived from GlobeLand30 and removed.

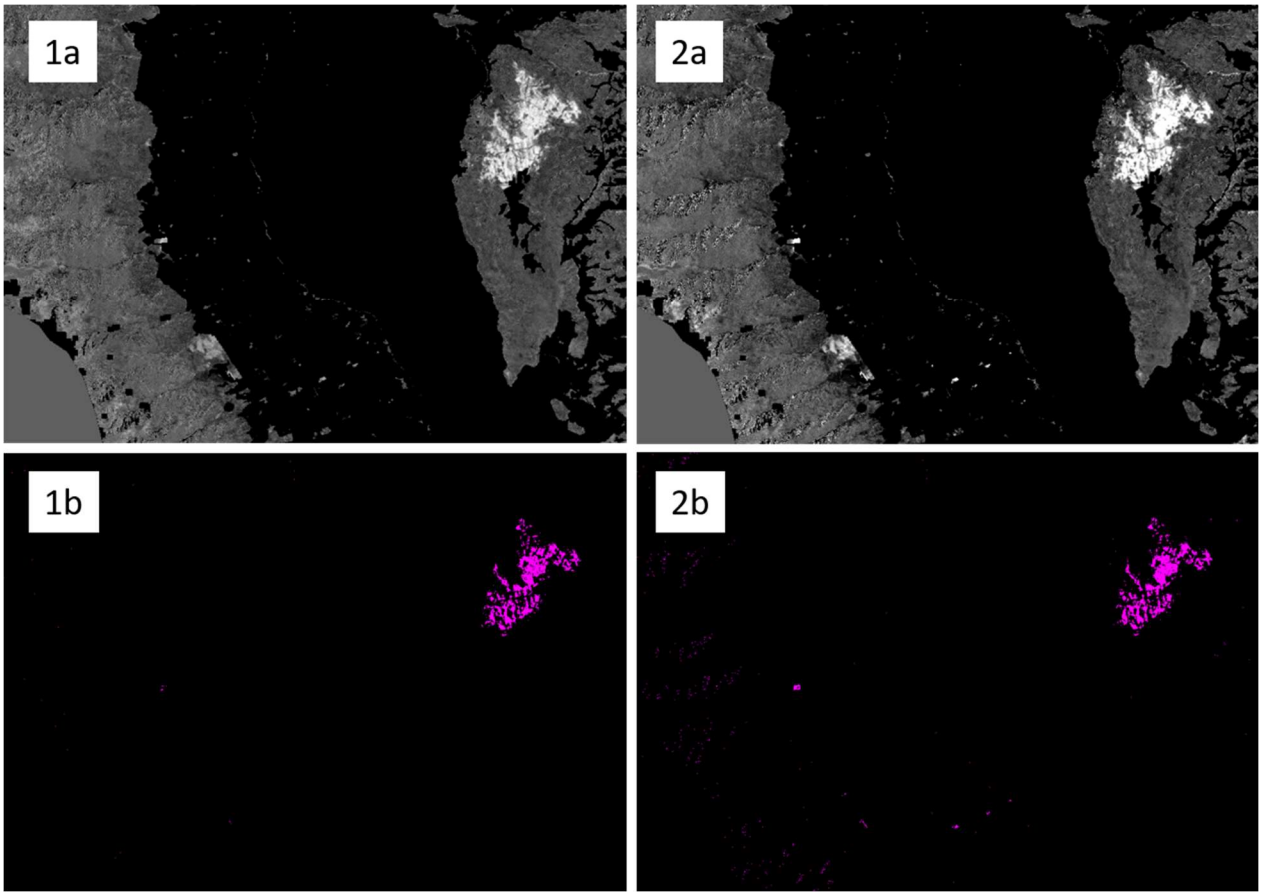

Figure 6-8. Effect of time-series standardization over a difference Normalized Burn Ratio (dNBR) image of the year 2006. A big fire can be observed in the upper right corner of the images. (**1a**) standardized dNBR; (**2a**) dNBR; (**1b**) binary standardized dNBR with the threshold set at 3 standard deviations from the mean; (**2b**) binary dNBR with the threshold set to match the detected fire shape of quadrant 1b. This figure shows how standardization produces less noisy images allowing for a better definition of the threshold separating burned from unburned pixels. In the image 2b, several noisy pixels can be seen at the bottom and left sides of the image.

6.3.2.2. Phase 2 – Adaptive thresholding and training data extraction

The second phase consists in the automatic extraction of ad-hoc training areas for every image. As shown in the introduction section of the present chapter and highlighted as a basic requirement for this burned area extraction routine, locations of historical fires are unknown and the possibility to use polygons retrieved from other burned area products has been rejected because of their insufficient accuracy in NWY. If these data were available, optimum thresholds to separate burned to unburned areas based on differenced spectral indices could be defined using accuracy measures such as the Cohen's Kappa coefficient (Cohen 1960) or by analyzing AUC-ROC curves. As a solution to overcome this problem, we use basic statistical metrics to define several classes that will be fed into a classification model. In standardized series, a value (z-score) of 0 represents the series mean, while other values represent the degree of deviation from the mean. Using *n* standard deviations from the mean is a common statistical method to define

thresholds of continuous images representing change (Fung and Ledrew 1988; Sahoo *et al.* 1988; Vázquez-Jiménez *et al.* 2018), and a conservative threshold set as n=3 is used for detecting outliers in a normal distribution, where about 0.27% of the data represents this class (Grafarend 2006; Leys, Ley, *et al.* 2013). Our choice for this method lies in the idea that a burned area can be considered as a sudden and temporary anomaly (noise) over the rest of the landscape that in general changes slightly and slowly (signal). Because the radical change caused by burn represents only a very small portion of the difference image, their pixel values will be found over the tails of the distribution while the unchanged pixels will be concentrated around the mean.

Mean and standard deviation were extracted from each standardized dNBR and dNDMI time-series and five classes were calculated based on different standard deviation distances from the mean. The equivalent classes from the two spectral indices were intersected and a sieving process was performed to remove small areas (< 5 pixels). Every class corresponds to a different degree and likelihood of change; however, we consider reliable change attributed to burning when the number of standard deviations from the mean is above 3 (conservative thresholds for anomaly detection).

6.3.2.3. Phase 3 – Random Forests classification (RF)

The resulting year-specific training areas are used as input into a Random Forests classifier (Breiman 2001), a state-of-the-art machine learning model widely used in remote sensing (Belgiu and Drăgu 2016). The Random Forests (RF) algorithm is an ensemble learning method that builds multiple decision trees using random selections of the training data. It has shown excellent results in classification problems related to burn scar detection and severity mapping with Landsat images (Collins *et al.* 2018; Long *et al.* 2019; Mitsopoulos *et al.* 2019; Vetrita and Cochrane 2019). The role of RF in our routine is to improve the classification accuracy that would result from a simple threshold cut from Phase 1. Experimental trials using a subset of our study region showed significant improvements in the results, especially in minimizing commission errors (Figure 6-9).

RF training and classification were performed iteratively on every year and path/row of the time-series, using the five standardized difference spectral indices (referred to as m_dNBR_st, m_dWET_st, etc. in Figure 6-7) as inputs. RF parameters were tuned over an experimental subset of the dataset. With only five variables as input, we were able to set a relatively high number of trees in the forest (*max_num_of_trees_in_the_forest* = 1000) ensuring high performance and reasonable processing speed. The maximum depth of the tree parameter (*max_depth*) was set to 5, representing the best compromise between under- and overfitting. At the end of the classification process, binaries burned/unburned images were produced by grouping the classes and separating them according to our conservative threshold principle (z-score=3).

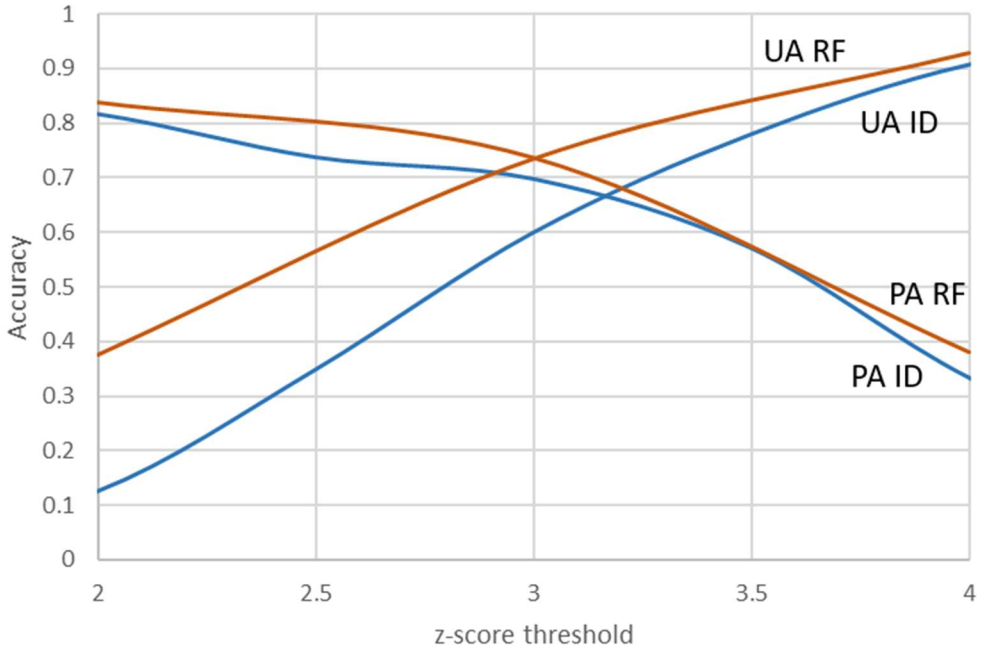

Figure 6-9. Producer's Accuracy (PA) and User's Accuracy (UA) of the detection of fire events at different burned/unburned threshold cuts. Blu lines represent accuracy when setting thresholds after image differencing in Phase 2 (PA ID and UA ID). Orange lines represent accuracy when setting thresholds (grouping classes) after Random Forests classification in Phase 3 (PA RF and UA RF). RF classification allows a significant accuracy improvement over a simple image difference thresholding, especially in terms of User's Accuracy (reduction of commission error).

6.3.2.4. Phase 4 – Seeded Region Growing (SRG)

To improve the mapping accuracy of the core burns detected in the previous phases, a Seeded Region Growing process (Adams and Bischof 1994) was added to the routine. SRG has two functions: it minimizes omission errors by including neighboring pixels excluded from the previous conservative cut, and it merges fragmented burn patches belonging to the same fire event. This ensures better burn mapping precision and compactness of burn perimeters. The main sensitive parameter that needs to be tuned for RG is the *Similarity Threshold* which determines whether a candidate neighboring pixel should be included in the growing region or not. To set this parameter we refer one more time to the probability distribution of the change images (m_dNBR_st and m_dNDMI_st). Because in the previous phase we adopted a conservative threshold (z-score=3) to determine core burned areas, here we allow them to include pixels with a lower magnitude of change. All pixels with a z-score between 2 and 3 were selected and their similarity values were averaged to obtain the *Similarity Threshold* parameter for SRG.

6.3.2.5. Phase 5 - Spatiotemporal clustering of fire events

The last phase consists of reorganizing the results of the RF classification and SRG into coherent burn events, defined as single fires that occurred in a certain place at a certain time. This is a necessary step if we want our product to be able to inform beyond localized yearly

burned pixels and become a database of single fire events. For this purpose, the pixels in the resulting binary images need to be further clustered to form distinct objects, following criteria of space and time. The temporal dimension pre-exists from the initial input images (yearly) and cannot be detailed any further, except for potential fires occurring at the moment of the satellite image acquisition which would be detected in two consecutive years. Thus, only spatial clustering can be performed. The burn pixels of a given year were merged using a distance radius of 60 meters. Resulting polygons smaller than 62,500 square meters (250 x 250 m) were removed because of their high likelihood to represent noise and errors and to set a minimum burn size form small but important forest fires in terms of ecological impact. Finally, all layers from all years and tiles were merged into the final fire events database. Every fire event (polygon) conserves its original information: path and row of the Landsat tile where it was extracted and the dates of Landsat pre and post images used in the bi-temporal differencing. Additionally, a new field containing the area of the polygons was added.

6.3.2.6. Software and processing tools

All processing was performed within the QGIS software (https://qgis.org/), which offers processing tools from partner projects such as SAGA GIS (http://www.saga-gis.org), GRASS GIS (https://grass.osgeo.org/) and Orfeo Toolbox (https://www.orfeo-toolbox.org/), as well as scripting capabilities with the Python programming language (PyQGIS). The implementation of Seeded Region Growing in SAGA was developed by Bechtel et al. (Bechtel *et al.* 2008) and the Random Forests within the Orfeo Toolbox is based on OpenCV libraries (https://docs.opencv.org/). All tools are freely available to the community and open-source.

6.3.3. Accuracy assessment

The final product is a database of fire events represented by multi-polygon geometries. A rigorous evaluation of the accuracy of such a product should include an overall assessment of its abilities to detect fire events and their location through the years, as well as quantifying burned area at the single fire level. The following sub-sections describe these two validation approaches.

6.3.3.1. Spatiotemporal polygon intersection approach

To extensively assess a dataset's accuracy in space and time, particular care should be given to the sampling strategy. Burned area is a temporary phenomenon that in general affects a small portion of a region, unevenly distributed both in space and time. Selective sampling of a few test sites may be useful to obtain local accuracy measures at a given time and location but can hardly be inferred over larger regions and timeframes in a statistically meaningful manner (Chuvieco *et al.* 2019). Recent approaches to test burned area datasets adopt several levels of stratification of the sampling units to assure a fair and meaningful assessment of the accuracy of both burned and unburned land (Padilla *et al.* 2014, 2015, 2017; Boschetti *et al.* 2016; Roteta *et al.* 2019). Following this approach, we created a grid of 10 x 10 km units covering the entire

study area. Peripheric squares that partially fell outside of the border were removed as well as those where non-valid LULC (water bodies, agriculture, urban, snow) occupied most of the square. A total of 147 square samples, distributed over 15 years, were randomly selected for manual delineation of burned patches. In the absence of any sort of reference data, this manual operation was performed using all available Landsat and Sentinel-2 (from the year 2016 to 2018) images within the assessed year. The strata were defined according to fire activity rates derived from yearly active fire spots as detected by the MODIS MCD14ML product using the following scheme:

- **Temporal stratification**: historical MODIS active fire counts were used to calculate the proportional fire frequency of each assessed year (Table 6-1, first and second rows). The 147 sample squares were distributed among the assessed years according to the resulting ratios. This approach increases the probability of selecting squares containing fires;
- **Spatial stratification**: For each assessed year, every sample unit was tagged as high or low fire frequency according to the number of MODIS active fire spots falling within its boundary. To assure a fair representation of both burned and unburned accuracy, we assigned an equal number of samples to both classes (high/low fire frequency), preferring high fire activity when the number of samples to be assigned was odd (Table 6-1, greyed area).

As a consequence of the MODIS product being available from April 2000 only, the accuracy assessment was based on the period 2001-2018. However, the years 2011, 2012, and 2013 were excluded from the assessment because of the gap between the decommissioning of Landsat 5 and the beginning of operations the Landsat 8 mission. Although several vegetation types are found in the study region, the dominant vegetation type in all 10x10 km sample units was the same (pine forests). Therefore, no stratification according to vegetation type was performed. Owing to the difficulty when interpreting burned patches visually, only fire events bigger than 62,500 square meters (250x250 m) were considered for this accuracy assessment. The sampling design and assignation results are shown in Figure 6-10 and Table 6-1, respectively.

The accuracy assessment was performed using a polygon intersection approach: fire events (polygons) were considered successfully detected if they overlapped the reference polygon, without setting any minimal rate of area overlapping. More details on this approach can be found in Fornacca et al. (Fornacca *et al.* 2017). We used the common metrics derived from the error matrix of modeled versus reference fires: User's Accuracy (UA), which measures the precision of the model (opposite of commission error); Producer's Accuracy (PA), which measures the probability of detection of the model (opposite of omission error); Sørensen–Dice coefficient or F1 score (Dice 1945; Sørensen 1948), which calculates the harmonic mean of UA and PA; and Overall Accuracy (see section 4.2.3 for the equations).

Additionally, we used the entire sampling grid to measure the spatiotemporal correlation of the MODIS MCD14ML points with those of the resulting modeled fires centroids. Because

the total distribution of MCD14ML in the 10x10 km grid units was not normal (Skewness = 2.68, Kurtosis = 9.56), we used non-parametric Spearman's rho (ρ) to run the tests (Spearman 1904).

6.3.3.2. Pixel-based burned area assessment of single fire events

The second accuracy assessment focuses on the product capabilities to quantify the burned area of single fire events. We selected 30 fire events distributed among five burn size classes defined using a Natural Breaks scheme. The reason for such a classification was to assure the inclusion of bigger fires which are rarer than smaller ones. By the mean of visual interpretation, burned perimeters were digitized and used as references. Bounding boxes wrapping up both reference and modeled fire events were drawn to delineate the assessment area for each fire (Figure 6-10). Quantification of accuracy was performed using the same metrics adopted in the polygon intersection approach, as well as Cohen's Kappa coefficient (Cohen 1960). This assessment was performed at the original 30 m image resolution.

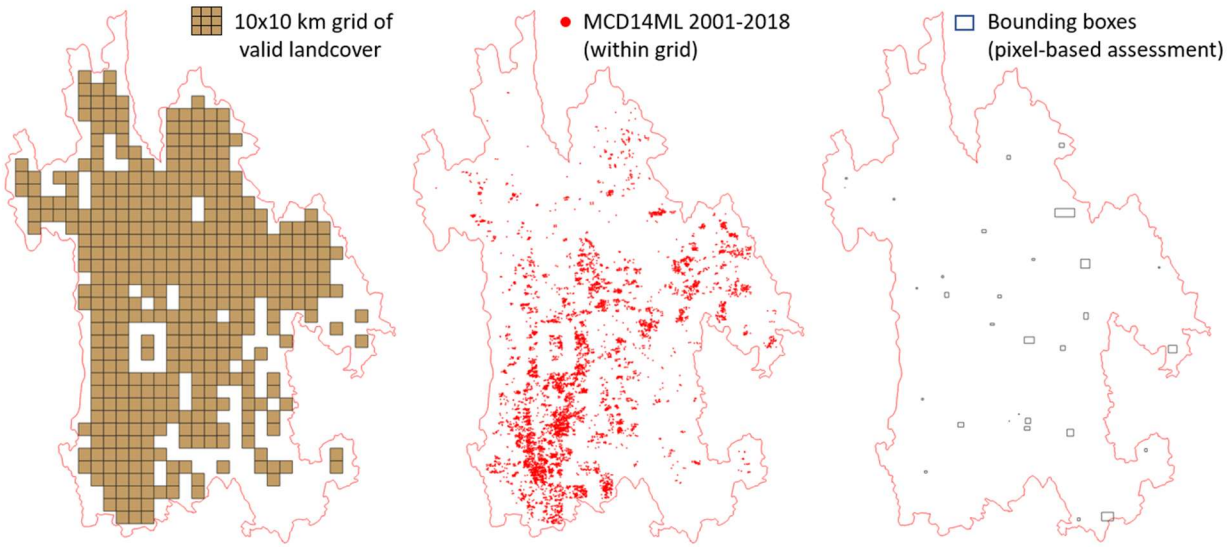

Figure 6-10. Accuracy assessment design. The left map shows the valid 10x10 km samples used for the stratified random selection; the center map shows the cumulated distribution of MODIS Active Fire spots (MCD14ML) falling within the validation grid which determine high and low AF frequency for each sample; the right map shows the bounding boxes of selected fires used for the pixel-based burned area assessment.

Table 6-1. Stratified random sampling scheme for accuracy assessment of fire polygons. The temporal stratification assigns the number of samples to be assessed each year according to the ratio of MODIS MCD14ML Active Fires (AF), for a total of 147 samples. Every year's samples are then randomly selected among high and low AF frequency samples separately and in equal number, with priority for high AF frequency samples if the total is odd (grey highlights).

		2001-2018	2001	2002	2003	2004	2005	2006	2007	2008	2009	2010	2014	2015	2016	2017	2018
Temporal stratification	**AF points totals**	5384	83	41	170	281	184	767	589	189	748	1241	554	288	48	164	37
	Ratio (%)	100	1.5	0.8	3.2	5.2	3.4	14.2	10.9	3.5	13.9	23	10.3	5.3	0.9	3	0.7
	Sample distribution per year	147	2	1	5	7	5	21	16	5	21	34	15	8	1	5	1
Spatial stratification	**Assign to low AF frequency**	68	**1**	**0**	**2**	**3**	**2**	**10**	**8**	**2**	**10**	**17**	**7**	**4**	**0**	**2**	**0**
	Assign to high AF frequency	79	**1**	**1**	**3**	**4**	**3**	**11**	**8**	**3**	**11**	**17**	**8**	**4**	**1**	**3**	**1**

6.4. Results

The resulting dataset contained 10,549 polygons representing fire events in NWY for the period 1987-2018, 5033 of which from 2001. A total area of about 3156 square kilometers burned during the overall period, the equivalent of about 4.7% of NWY area. Fire polygons for the overall period and the 2001-2018 centroids falling inside the validation grid are represented in Figure 6-11. Visually, we can notice that the produced dataset shows similar distributions of fire points to MCD14ML, with higher concentrations in the southern and eastern parts of the study region. The Spearman's rank correlation coefficient between the overall distribution of MCD14ML points and the resulting dataset was $\rho = 0.39$ (P-value < 0.001), indicating a moderate and significant spatial agreement. This correlation was significant for every year during the analyzed period (2001-2018 without 2011, 2012, and 2013), with the weakest magnitude in 2008 ($\rho = 0.12$, P-value $= 0.011$) and the highest in 2010 ($\rho = 0.66$, P-value < 0.001). Details of Spearman correlation can be found in Table 6-2.

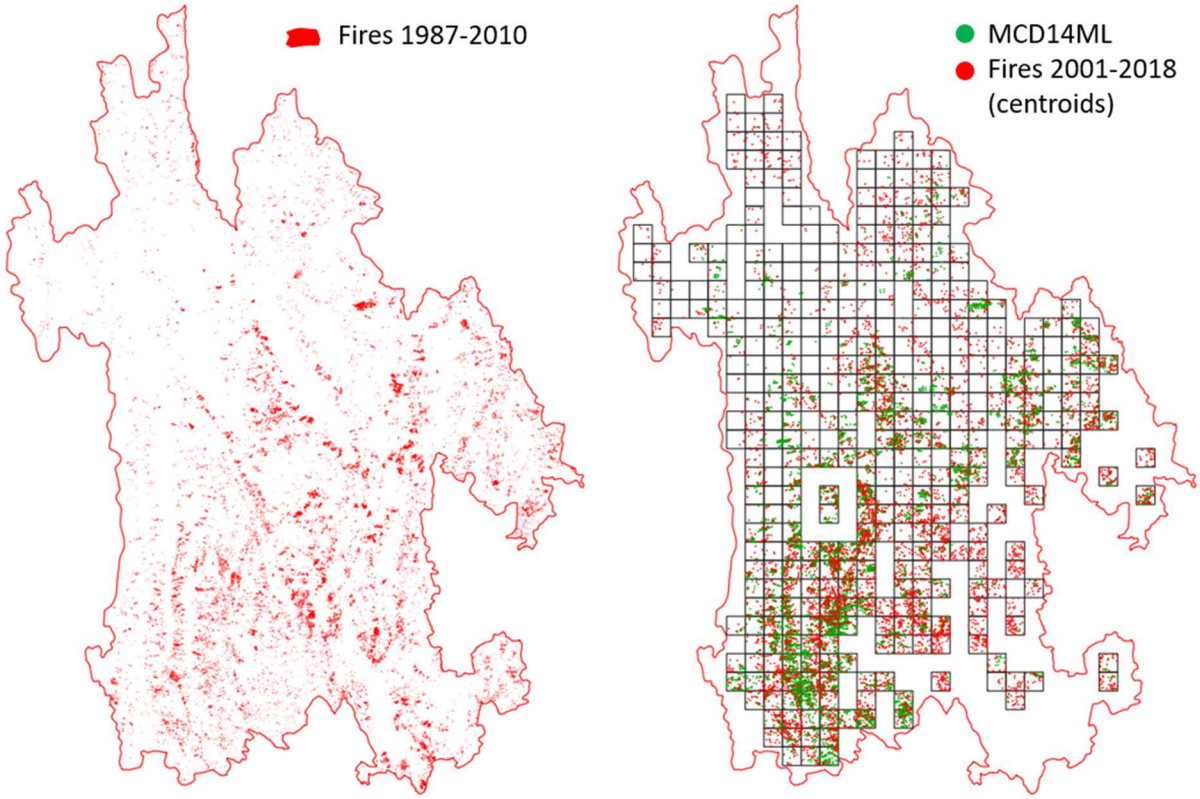

Figure 6-11. The left map shows the resulting fire polygons (1987-2018) in overall northwest Yunnan. The right map shows the distribution of fire centroids and MODIS MCD14ML points within the validation grid only, from 2001 to 2018.

Table 6-2. Spatiotemporal Spearman correlation between MCD14ML Active Fire hotspots and the present study's resulting dataset (centroids). The correlation is based on a 10x10 km validation grid drawn within the study region.

	df (n-2)	rho	p-value
2001	428	0.21	**< 0.001**
2002	428	0.16	**0.001**
2003	428	0.48	**< 0.001**
2004	428	0.33	**< 0.001**
2005	428	0.27	**< 0.001**
2006	428	0.38	**< 0.001**
2007	428	0.54	**< 0.001**
2008	428	0.12	**0.011**
2009	428	0.30	**< 0.001**
2010	428	0.66	**< 0.001**
2014	428	0.43	**< 0.001**
2015	428	0.48	**< 0.001**
2016	428	0.24	**< 0.001**
2017	428	0.33	**< 0.001**
2018	428	0.15	**0.002**
Total	428	0.39	**< 0.001**

Table 6-3 shows the results of the polygon intersection assessment of the 147 samples, aggregated by year. The overall accuracy of the samples (1: when in a sample all fires are detected and no commission errors; 0: when a sample contains omission or commission errors) was 0.69, resulting from 101 fully correct samples (all fires detected and no errors of commission) and 46 containing at least one mistake (n = 147). A total of 198 fires were visually identified, 159 of which were correctly detected, and 39 were omitted, while 45 fires were erroneously detected by our model. These numbers translate into a Dice's coefficient of 0.79, a Producer's Accuracy equal to 0.80, and User's Accuracy equal to 0.78, for the overall assessed period. In general, the results for the fires detected with Landsat 5 (2001 to 2010) were superior to those obtained with Landsat 8 (2014 to 2018), except for their UA.

Moreover, the stratified sampling design was expected to return a relatively balanced number of samples containing fires and samples not containing any fire. In the reference dataset, the fires were distributed in 80 sampling units, while in the remaining 67 no fire was observed. Similarly, our product detected fires in 81 samples.

Table 6-3. Accuracy assessment of the polygon intersection approach. The results of the 147 10x10 km samples have been aggregated by year, from 2001 to 2010 for Landsat 5 (LS5) and from 2014 to 2018 for Landsat 8 (LS8).

Year	No. of samples	Correct samples	Reference fires	Detected correctly	Omitted	Committed
2001	2	2	1	1	0	0
2002	1	1	3	3	0	0
2003	5	2	12	8	4	2
2004	7	5	4	2	2	0
2005	5	5	16	16	0	0
2006	21	15	22	13	9	1
2007	16	9	39	39	0	18
2008	5	4	5	5	0	1
2009	21	11	24	18	6	10
2010	34	24	51	41	10	11
2014	15	10	8	5	3	2
2015	8	7	6	4	2	0
2016	1	1	1	1	0	0
2017	5	4	6	3	3	0
2018	1	1	0	0	0	0
Total	**147**	**101**	**198**	**159**	**39**	**45**

Producer's Accuracy:	**0.80** (LS5: 0.82, LS8: 0.62)
User's Accuracy:	**0.78** (LS5: 0.77, LS8: 0.87)
Dice's Coefficient (F1 score):	**0.79** (LS5: 0.80, LS8: 0.72)
Overall sample accuracy:	**0.69** (LS5: 0.67, LS8: 0.77)

Results of the pixel-based burned area accuracy are summarized in Table 6-4. User's Accuracy is often higher than Producer's Accuracy, the latter showing values below 0.50 in four out of thirty samples. In comparison, UA was always above 0.50, the lowest value found in sample s02 (UA = 0.61). Globally, the product underestimates burned areas in the order of 27% (PA = 0.73) but minimizes false detections with only a 13% error margin (UA = 0.87). Summary metrics showed an overall accuracy stabilizing at 93%, with F1 at 0.79 and Kappa at 0.69.

Table 6-4. Pixel-based accuracy assessment of the burned area perimeters of 30 fire events. PA: Producer's Accuracy, UA: User's Accuracy.

Sample	Correct burned	Correct unburned	Omitted pixels	Committed pixels	PA	UA	Kappa	F1	Overall Accuracy
s01	356	870	264	30	0.57	0.92	0.57	0.71	0.81
s02	82	86	1	52	0.99	0.61	0.54	0.76	0.76
s03	170	152	23	47	0.88	0.78	0.64	0.83	0.82
s04	272	981	262	25	0.51	0.92	0.54	0.65	0.81
s05	269	989	704	10	0.28	0.96	0.27	0.43	0.64
s06	72	43	23	5	0.76	0.94	0.60	0.84	0.80
s07	933	2595	1295	137	0.42	0.87	0.39	0.57	0.71
s08	599	843	839	19	0.42	0.97	0.33	0.58	0.63
s09	1198	1195	404	153	0.75	0.89	0.63	0.81	0.81
s10	1184	2968	690	342	0.63	0.78	0.55	0.70	0.80
s11	855	884	410	105	0.68	0.89	0.55	0.77	0.77
s12	1269	1966	551	100	0.70	0.93	0.66	0.80	0.83
s13	1864	2122	849	490	0.69	0.79	0.50	0.74	0.75
s14	3430	4596	1154	332	0.75	0.91	0.67	0.82	0.84
s15	2211	5670	820	419	0.73	0.84	0.68	0.78	0.86
s16	1454	1972	100	350	0.94	0.81	0.76	0.87	0.88
s17	1618	4463	802	147	0.67	0.92	0.68	0.77	0.87
s18	2236	11212	4969	109	0.31	0.95	0.34	0.47	0.73
s19	6508	10117	1620	907	0.80	0.88	0.73	0.84	0.87
s20	5959	7744	1175	616	0.84	0.91	0.77	0.87	0.88
s21	5281	6087	1072	1288	0.83	0.80	0.66	0.82	0.83
s22	4454	8030	1842	280	0.71	0.94	0.69	0.81	0.85
s23	4799	8617	524	339	0.90	0.93	0.87	0.92	0.94
s24	9888	27193	7578	315	0.57	0.97	0.60	0.71	0.82
s25	27349	74712	6019	8248	0.82	0.77	0.71	0.79	0.88
s26	14584	36404	4500	1388	0.76	0.91	0.76	0.83	0.90
s27	13135	50623	2715	4578	0.83	0.74	0.72	0.78	0.90
s28	12515	17226	1094	1190	0.92	0.91	0.85	0.92	0.93
s29	9809	7282	1320	495	0.88	0.95	0.80	0.92	0.90
s30	12449	20930	10448	357	0.54	0.97	0.52	0.70	0.76
Total	**146802**	**318572**	**54067**	**22873**	**0.73**	**0.87**	**0.69**	**0.79**	**0.93**

6.5. Discussion

We proposed a prototype methodology to extract burned areas and build historical fire inventories from Landsat TM and OLI images in regions that present particular challenges to remote sensing approaches, such as the complex landscapes of mountainous remote areas. The main difficulties we attempted to overcome were the lack of ground data for model training and testing, the limited availability of cloud-free satellite images, and land morphology effects such as shades created by rugged relief and mosaic landscapes. A good balance between omission and commission errors in terms of spatiotemporal fire events detection was found, with both error types stabilizing around 20%, while errors of commission in mapping burned areas were minimized to about 13%, often at the cost of higher omission which reached 27%. In terms of accuracy, our prototype represents an improvement compared to the performance of existing products in the same region, i.e., MODIS fire products and ESA Fire_CCI (Fornacca *et al.* 2017). Among the salient findings, we demonstrated how it is possible to automatically extract image-specific training data and set thresholds from standardized change images using conservative thresholds such as in outlier detection techniques. This approach is extremely valuable when no other sources of information are available. Methodologies to extract training samples from the input images have been proposed before, like for example, the algorithm from Stroppiana *et al.* (2012), which uses a soft aggregation of partial burn/unburn evidence from a flexible number of spectral indices, or advanced statistical methods as proposed by Woźniak and Aleksandrowicz (2019). Our solution opts for a more conservative approach in this initial selection and adds time-series normalization of difference images to minimize potential sources of noise (Figure 6-8).

We identified the sources of commission errors as coming from inaccuracies in cloud and cloud shade masks, noise caused by very low illumination in steep slopes, and limitations of the LULC mask employed, which in several cases erroneously assigned forest pixels to other classes such as agroforestry and agriculture. The low commission found in burned perimeter mapping is a very encouraging result given the fact that this error type is a common problem of systematic burned area extraction over large areas and long periods of time (Roy and Boschetti 2009; Bastarrika, Chuvieco, and Martín 2011; Stroppiana *et al.* 2012). The reasons for the omission errors are multiple. The main one is the fast recovery of burned vegetation, especially in less forested ecosystems such as grasslands and shrublands (Fornacca *et al.* 2018). During the production phase of the reference dataset used for the accuracy assessment, it was reported that several fires occurred and recovered within a year, making them completely or partially undetectable in the image used in the time-series (Figure 6-4). Moreover, one of the fundamentals from which the methodology was build was the use of multiple thresholds based on time-series z-scores to extract training samples, followed by a classification step and a conservative cut to separate burned from unburned classes. Softening the threshold would likely reduce omission errors but increase commission. Another important aspect to understand the performance of the product is the sampling design used for the accuracy assessment. The stratified random sampling scheme adopted in our study assured a fair distribution of samples between burned and unburned classes by means of an independent fire frequency dataset

(MCD14ML). The re-evaluation of several burned area products using stratified random sampling often reported much higher omission and commission errors than previously assessed using test sites, namely in the order of 42% and 68%, respectively (Padilla *et al.* 2015; Chuvieco *et al.* 2019). However, a recently developed burned area algorithm with higher spatial resolution images from Sentinel-2 (Roteta *et al.* 2019) showed great improvements in the African continent, with omission and commission around 26.5% and 19.3%, respectively. In this context and despite the particular environmental challenges of the study region, our product performs relatively well. In particular, the very low commission error presents a unique advantage for the quantification of fire activity: the product is able to reliably estimate a minimum in terms of burned area while the consideration of the omission rate can give hints on a more realistic magnitude of the disturbance.

The spatiotemporal correlation found with the MODIS14ML confirms the pertinence of our results, even if the latter has been found to produce relatively high errors of commission in this region (Fornacca *et al.* 2017). Unfortunately, we do not have quantitative information about forest fire counts and burned area specifically for NWY; however, we can compare our results with the statistics at the provincial level, as reported in the official website of the Chinese National Bureau of Statistics (https://www.stats.gov.cn/tjsj/). The official statistics reported a total of 5822 fire events and a burned area of 153,974 hectares in overall Yunnan, while our product detected 4861 fires and 167,700 burned hectares in NWY, during the period 2003 to 2018. Another source available in Chinese only (Wu *et al.* 2009) states that from 1951 to 1998, the annual average number of fires in Yunnan was 2725 and the annual average burned area was 138,259 hectares, values much higher than those reported by the National Bureau but over different periods. In an attempt to estimate biomass burning in mainland China, Yan et al. (Yan *et al.* 2006) found that satellite sensors detected a 13 times wider burned area than what was shown in national statistics for the year 2000. NWY is certainly one of the hotspots of fire activity in Yunnan province; however, these results highlight significant discrepancies between satellite observations and other sources that require further investigation. A multitude of small fires caused by routine human activities, especially in grassland-shrubs and mixed wild vegetation with tree plantations or fields on the flank of the mountains, occur every year. These fires are probably not taken into account in the national reports, which focus more on forest fires requiring the mobilization of significant suppression resources. In addition, the particular remoteness of the areas may represent a limitation to the continuous surveillance of wildland fires. On the other side, a source of inaccuracy in fire counts may be related to the high fragmentation of the resulting fire polygons. Even after the spatiotemporal aggregation of the polygons performed in Phase 5, single fire events may still be composed of several separate polygons which will inflate the fire counts. However, this does not explain the high burned area. Another hypothesis may be the difficulty in discriminating burn from other disturbances, as suggested by the presence of commission errors (UA).

The major limitation to the significance of our results comes from the methodology used to build the reference dataset for the accuracy assessment, which is based on data derived from

the same source as the assessed product, except for the last two years where Sentinel-2 images were included. This approach is not ideal but still valid when no other options are available (Vanderhoof *et al.* 2017; Chuvieco *et al.* 2019). However, we should consider the potential bias represented by the correlation between the model and the reference datasets. Another limitation is what is commonly referred to as "business decision". Despite the routine developed is mostly automated and an automatic threshold extraction method has been proposed, a few parameters need to be set by the analyst, according to its project goals and requirements, such as whether to maximize omission or commission errors. In particular, the final z-score threshold to separate burned from unburned classes, the similarity threshold to set the Seeded Region Growing algorithm, and the distance buffer to merge the resulting polygons can be adapted to potentially obtain better results.

Finally, a caveat when using this methodology or the derived product needs to be stated. The lack of usable images from the Landsat 7 mission (ETM+ sensor) created a gap between the years 2010 and 2013. Consequently, the fire polygons included in the year 2013 are extracted from the comparison between images from end 2010 (or beginning 2011) and end 2013 (or beginning 2014). These fire events are likely to have occurred during the year 2013 but may include burns from 2011 and 2012 but with substantial omission rates. Therefore, the accuracy of the year 2013 could not be assessed with the data available. Furthermore, the compared scenes have been acquired using different sensors (TM and OLI), which potentially introduce bias when comparing spectral indices, even after time-series standardization. Calibration coefficients for single bands (Roy *et al.* 2016) and for several spectral indices (Steven *et al.* 2003; Mancino *et al.* 2020) based on linear relationships between the values derived from different sensors have been proposed. However, among the different spectral indices analyzed, the most recent work on this topic (Mancino *et al.* 2020) showed that NBR mean values between the ETM+ and OLI sensors are the least affected and their relationship is not linear, limiting their calibration potential. For the present version of the algorithm, we decided to not apply calibration coefficients. It is therefore advised to consider 2011 and 2012 as missing years and pay particular attention when using fire data of the year 2013.

We believe this algorithm can be easily scaled up and tested in other regions with similar difficulties as NWY. Further automation can be achieved, for example by using Python scripting for standalone or QGIS software applications. With the advent of datacube architecture technology such as the Google Earth Engine (https://earthengine.google.com), big data manipulation does not represent a barrier anymore, allowing researchers to use their algorithms over large areas and temporal ranges (Gorelick *et al.* 2017). Our methodology could be integrated into a datacube and optimized to allow users to set their preferred parameters at each phase, e.g. the choice of the vegetation indices most appropriate for a given study region and adapt the z-score thresholds for training data generation.

6.6. Chapter conclusions

The historical Landsat archive is probably the most convenient way to overcome past underestimations of the ecological impacts of small fires and gain insights into recent fire dynamics in regions where this phenomenon is poorly understood. The burn scar and fire event extraction methodology presented here addressed some of the common challenges of these regions characterized by complex landscapes, including frequent clouds, rugged terrain, and absence of training data. The methodology proved to be very useful to estimate fire numbers and locations, with both errors of omission and commission in the order of 20%, while the accuracy of burned perimeters maximized commission over omission. These results represent a great improvement compared to existing products, allowing for the reliable estimation of minimum rates of fire activity. While commission could be easily reduced by tightening a threshold parameter, omission errors related to fast vegetation recovery after fire remain a hard challenge to be improved, but would certainly be a lesser issue in regions where vegetation recovery is slower.

A dataset of fire events for northwest Yunnan spanning over the period 1987-2018 has been created (see Appendix F) and can now be used for future analysis of recent fire dynamics in the region.

7. Wrap-up and conclusions

7.1. General conclusions and recommendations

Being an integral component of land surface dynamics providing vital ecosystem services, wildland fires are inevitable. We live in a world where virtually all landscapes have been subject to different degrees of anthropogenic influence. This makes it clear that the occurrence of fires does not only depend on weather and vegetation conditions but also on several human factors, and all these variables are governed by complex interactions and feedback loops that we still poorly understand. Fire and land management policies' effectiveness could improve substantially from a better comprehension of the spatiotemporal patterns of fire occurrence and the identification of risks and vulnerabilities. For example, fire suppression resources, which represent a conspicuous budget on the shoulders of public administrations (therefore taxpayers), should be allocated in the most vulnerable areas where the harm caused by fire is unbearable. Conversely, in fire-dependent areas, wildfires can be tolerated or even promoted by management practices focusing more on ensuring regular burns distributed heterogeneously over the landscape as well as other particular management practices.

In this work, we highlighted the ecological importance of mountain environments and their particular sensitivity to climatic and anthropogenic changes. Their typical fragmented landscapes are particularly vulnerable to natural hazards to the point that minimal alterations, such as land abandonment or extended dry periods, could highly impact the long-term functioning of ecosystems, including the role of fire regimes. We recognized that improving the management effectiveness of mountains is paramount not only at the local scale but for ecosystems and people globally. Therefore, we referred to the concept of *fire regime* as an initial framework to understand the recent and current patterns of fire occurrence in a given region. Core variables such as fire frequency, area burned, return interval, etc., as well as more broad information on the conditions of fire and its immediate effects on the environment and society, may be included in the framework. Yet quantitative, the fire regime concept remains purely descriptive. A more analytical framework aiming at identifying areas where fire management should be prioritized was then proposed. We integrated the concepts of risk and vulnerability following a scheme widely used in the assessment of the impacts of climate change. The advantage of this outcome vulnerability model lies in its modularity (fire risk is separated from habitat vulnerability and adaptive capacity) and its simplicity in integrating and analyzing geospatial datasets using probabilistic approaches. The parameters of the model can be easily manipulated to predict and identify future vulnerable regions according to changes in climate, land use - landcover, and human factors. This framework has not yet been tested, but we expect it to run with minimal data and provide a first assessment of vulnerability to fire at a broad scale.

We pointed out that, among the main difficulties encountered when analyzing mountains, there is a chronic lack of baseline data for research. In our case, without spatially- and temporally-explicit information on past fire occurrence, fire regimes cannot be defined, the

risk/vulnerability framework cannot be implemented, nor could any sort of evidence-based knowledge be established, and informed decisions be taken. This is the reason why, after proposing this contextual framework, we set the main aim of the thesis as:

To develop robust methods for the reconstruction of past fire history which are suitable for heterogeneous mountain environments.

As a representative study case, we focused on northwest Yunnan, China, a mountainous region characterized by an extreme environmental heterogeneity, including climate, topography, and landscapes. No data on fire is publicly available for this region.

To achieve this main goal, we organized our research in several objectives with related research questions that guided the several steps of our work. We report them here together with our findings, conclusions, and recommendations.

1. **To evaluate the quality and the usability of existing global burned area products in the complex landscapes on northwest Yunnan.**

   Question: Are the widely used and freely available global fire products suitable to estimate the past fire activity in mountainous landscapes?

   Given the fact that official data about fire locations and dates are not publicly available in China, we opted for existing satellite solutions. We analyzed the fire products produced with the MODIS and MERIS sensors from NASA and ESA satellite missions. As hypothesized, mainly due to the coarse resolution of the sensors (500 m for MODIS, 300 m for MERIS), these products highly underestimate the impacts of fire in northwest Yunnan, as well as potentially any region presenting similar landscape features and affected by fires of relatively small size. We conclude that fire occurrences cannot be quantified reliably and consequently fire regimes cannot be defined, also because of their too short temporal coverage.

   Furthermore, the extremely high errors of omission shown in our mountainous area suggest unsuitability for purposes of validation or training algorithms for burned area extraction.

   One of the MODIS product (MCD64A1) is used in the Global Fire Emission Database v.4. Our findings inform on the fact that the contribution of small fires is underestimated at the global level and that many regions of the world are not represented in the model.

   Since the date of our analysis (2017), a new version of the ESA product and other projects have been published. We suggest performing a new test with these newly available products and keep reporting on the importance of the inclusion of mountainous regions in wildland fire talks.

2a. To assess the spectral permanence of burn scars and their detectability by the Landsat sensors in different vegetation types and at several post-fire time-gaps.

Question: For how long can burned areas be successfully detected by the Landsat sensors, given potentially divergent recovery patterns of different vegetation types?

We moved our attention toward the Landsat mission because it became evident that for the purpose of our thesis this was the best option. Because of the relatively poor temporal resolution and the high cloud coverage during the summers, we had to evaluate potential time ranges to compose a time-series for burned area extraction. We used spectral vegetation indices and image transformation techniques pertinent to burned area detection to isolate the signal and calculate a separability index between burned and unburned samples. We found that different vegetation types recover at different speeds, with broadleaved forests being the slowest (sufficient separability several years after fire), followed by coniferous forests (still detectable after 1 year). Shrubs and grasslands recovered very quickly and were often hardly detectable after 1 year post-fire.

We conclude that a regular 1-year interval time series could potentially include the majority of burned areas, but omission errors would be present mostly for grasslands and shrublands areas.

2b. To identify the most suitable satellite-derived vegetation indices to map burn scars in different vegetation types at different post-fire dates.

Question: Which spectral indices show the best separability between burned and unburned vegetation in different vegetation types at different post-fire dates?

Indeed, spectral indices showed different detectability patterns in terms of separability between burned and unburned samples, according to vegetation and time after burn. Some spectral indices such as MIRBI, Tasseled Cap GREENNESS, and NDVI are ideal for immediate post-fire mapping, but in the long term, other spectral indices such as NBR and NDMI perform better. Needleleaved and broadleaved forests showed similar and consistent separability patterns among the different spectral indices, while the two other vegetation types had less clear patterns. However, NBR and NDVI appeared in general superior, especially starting from 1 year post-fire.

We conclude that, in the mountains of northwest Yunnan, due to persistent cloud coverage during a good portion of the year, a time-series of 1-year interval Landsat images is suggested for burned area detection and that NBR, NDMI, as well as the three tasseled cap indices, should be used in the methodology.

3. **To identify the different difficulties encountered when mapping burned areas in complex mountain landscapes, develop an automatic solution based on the historical Landsat archive, and evaluate its performance.**

Question: How can we adapt remote sensing techniques to effectively map burned areas in complex mountainous landscapes without prior spatial information on past fire events?

This was the final objective of the present thesis, where all the difficulties of remote sensing applications had to be expressed and faced. We identified six major challenges and proposed a solution or a compromise adaptation to each of them. The challenges were: small size of fires, rugged terrain creating shades in the images, patchy landscapes, frequent cloud cover, fast recovery of vegetation, and no prior information on fires to use as training data. It should be noted that every one of these difficulties represents an entire research topic and that it was not our intention to propose an in-depth analysis and extensively tested solutions to each challenge. Our aim was to develop an automatic burned area extraction routine that could minimize these sources of error. Several common techniques used in the field of change detection from remotely sensed images were employed in our solution, including the use of spectral indices, image differencing, classification with powerful machine learning models, and an object-based approach. The hardest challenge was to select training data for classification and set the thresholds separating the burned and the unburned classes in an automatic way without reference information to tune the algorithm. This routine needed to be applicable to every image in the time-series and be efficient for burns in different vegetation types. We found a solution in normalization operations performed over time-series and other concepts related to normal distributions such as outlier detection.

The resulting fire dataset was tested for accuracy thoroughly, obtaining satisfying results. Estimations of commission and omission errors were in the order of 20% both, while pixel-based mapping accuracy minimized commission at the cost of higher omission.

We conclude that good automatic mapping results can be achieved efficiently over vast areas presenting multiple remote sensing obstacles. The Landsat archive represents the best option to reconstruct fire history and potentially other land surface dynamics, tracing them back to circa the mid-1980s, if we exclude the earlier coarser resolution images from the MSS sensor.

7.2. A product and a methodology

In the most synthetic way, we can say that the main outcomes of the present thesis are a final usable product and an automated burned area mapping methodology that can be transferred, adapted, and scaled up.

The final product consists of a dataset of polygons representing burned areas that occurred between the years 1987 and 2018. The attribute table includes the area of each polygon, the year

of burn, and the WRS-2 tile of the originating Landsat scene. The file is available on a dedicated GitHub repository (https://github.com/DavideFornacca/Fire) and can be freely accessed by anybody in need. The different shortcomings, limitations, and caveats are clearly stated in the corresponding publication and need to be understood before using the data.

One of the most salient findings of this product is its quantification of fire counts and area burned in contrast with those reported in official government statistics (at the provincial level). This further confirms earth observations' massive potential in creating raw data about land surface repeatedly and globally. After proper treatment and analysis, the raw data becomes valuable information supporting decision making. This process is more effective and rapid when data is of high quality and openly made available to the scientific community through end-point spatial data infrastructures. Moreover, datacube architectures are solving the common end-users limitations of storage space and processing power, enabling them to harness some of the capabilities of big spatiotemporal data.

Although automatic (no need to manually select training data), our burned area extraction routine requires some parameters to be set by the analyst according to his/her specific requirements. The methodology has been developed using freely available satellite images and freely available software packages so that anybody having access to a computer and an internet connection can implement it and adapt it. The modular architecture of the routine can potentially be translated into scripts for datacubes such as JavaScript for the Google Earth Engine to increase automatization and, as mentioned previously, removing storage and processing power barriers.

We hope that other researchers working in complex environments will find inspiration in the methods demonstrated in this thesis. The lack of data and other technical difficulties should not be source of refrain from tackling the challenges of complex environments. This thesis is a proof that these information gaps can be finally filled. Local high-resolution data is as important as global data. Research in these regions is fundamental and should not be neglected, but valorized and integrated with global assessments. Local effects of climate, socio-economic, and land dynamics changes represent an early warning of what could happen at the regional to the global scale, and the analysis of past phenomena is critical to predict what could happen in the future.

7.3. Future work

This thesis represents the very first step of a long-term research program. With the dataset produced here, we can finally put it to work, opening up to a wide range of research opportunities. Future research plans, some of which are currently ongoing, are listed here:

- Definition of recent fire regime: with fire records spanning over the past 30 years, it is possible to depict several parameters describing the current regional fire regime and even identify existing trends. However, some parameters such as fire return interval may require information over a much longer period, while seasonality requires information at

a higher spatial resolution than the 1-year dataset created here. This analysis will help to quantify the current pattern of fire occurrence that can be compared with past and future patterns.

- Implement the risk / vulnerability model: the conceptual framework proposed in this thesis can be fed with this historical fire dataset coupled with available covariates. Prediction of future vulnerable areas using climate and socio-economic change scenarios will add an extra layer of information for land managers, assisting them in defining policies and the allocating of fire prevention resources.
- Research focus on the relationship between land use and wildfire: in particular land fragmentation caused by fire and, inversely, habitat merging (previously separated patches being connected again) caused by agriculture and pasture abandonment in the mountain environment.
- As a continuation of the work presented in Chapter 5, an in-depth assessment of vegetation recovery patterns in targeted areas would be a logical step. We hypothesize that the vegetation of northwest Yunnan is turning into more flammable ecosystems, with pine species colonizing other areas, also due to extensive tree planting policies.
- Test, adapt, and improve the present fire extraction methodology in other regions.

References

Abney RB, Sanderman J, Johnson D, Fogel ML, Berhe AA (2017) Post-wildfire Erosion in mountainous terrain leads to rapid and major redistribution of soil organic carbon. *Frontiers in Earth Science* **5**, 1–16. doi:10.3389/feart.2017.00099.

Adams MA (2013) Mega-fires, tipping points and ecosystem services: Managing forests and woodlands in an uncertain future. *Forest Ecology and Management* **294**, 250–261. doi:10.1016/j.foreco.2012.11.039.

Adams R, Bischof L (1994) Seeded Region Growing. *IEEE Transactions on Pattern Analysis and Machine Intelligence* **16**, 641–647. doi:10.1109/34.295913.

Ahmad A, Abdullah MM, Sufahani SF, Queguan S, Sakidin H (2019) Haze effects on satellite remote sensing imagery and their corrections. *International Journal of Advanced Computer Science and Applications* **10**, 69–76.

Allen Consulting Group (2005) Climate change: Risk and vulnerability. Promoting an efficient adaptation response in Australia. (Canberra) https://www.nintione.com.au/?p=5211.

Alonso-Betanzos A, Fontenla-Romero O, Guijarro-Berdiñas B, Hernández-Pereira E, Canda J, Jimenez E, Luis Legido J, Niz SM, Paz-Andrade C, Inmaculada Paz-Andrade M (2002) A Neural Network Approach for Forestal Fire Risk Estimation. In '15th Eur. Conf. Artif. Intell.', 643–647

Alonso-Canas I, Chuvieco E (2015) Global burned area mapping from ENVISAT-MERIS and MODIS active fire data. *Remote Sensing of Environment* **163**, 140–152. doi:10.1016/j.rse.2015.03.011.

Ambrosia VG, Wegener S, Zajkowski T, Sullivan D V., Buechel S, Enomoto F, Lobitz B, Johan S, Brass J, Hinkley E (2011) The Ikhana unmanned airborne system (UAS) western states fire imaging missions: from concept to reality (2006-2010). *Geocarto International* **26**, 85–101. doi:10.1080/10106049.2010.539302.

Amoroso MM, Daniels L, Baker PJ, Camarero JJ (Eds) (2017) 'Dendroecology. Tree-Ring Analyses Applied to Ecological Studies.' (Springer, Cham) doi:https://doi.org/10.1007/978-3-319-61669-8.

Anaya JA, Chuvieco E (2012) Accuracy assessment of burned area products in the Orinoco basin. *Photogrammetric Engineering & Remote Sensing* **78**, 53–60.

Andela N, Morton DC, Giglio L, Chen Y, Van der Werf GR, Kasibhatla PS, DeFries RS, Collatz GJ, Hantson S, Kloster S, Bachelet D, Forrest M, Lasslop G, Li F, Mangeon S, Melton JR, Yue C, Randerson JT (2017) A human-driven decline in global burned area. *Science* **356**, 1356–1362. doi:10.1126/science.aal4108.

Araújo FM De, Ferreira LG (2015) Satellite-based automated burned area detection: A performance assessment of the MODIS MCD45A1 in the Brazilian savanna. *International Journal of Applied Earth Observation and Geoinformation* **36**, 94–102. doi:10.1016/j.jag.2014.10.009.

Archibald S, Lehmann CER, Gómez-dans JL, Bradstock RA (2013) Defining pyromes and global syndromes of fire regimes. *Proceedings of the National Academy of Sciences* **110**, 6442–6447. doi:10.1073/pnas.1211466110/-/DCSupplemental.www.pnas.org/cgi/doi/10.1073/pnas.1211466110.

Arino O, Casadio S, Serpe D (2012) Global night-time fire season timing and fire count trends using the ATSR instrument series. *Remote Sensing of Environment* **116**, 226–238. doi:10.1016/j.rse.2011.05.025.

Azevedo JC, Moreira C, Castro JP, Loureiro C (2011) Agriculture Abandonment, Land-use Change and Fire Hazard in Mountain Landscapes in Northeastern Portugal. 'Landsc. Ecol. For. Manag. Conserv.' (Eds C Li, R Lafortezza, J Chen) pp. 329–351. (Higher Education Press, Beijing and Springer-Verlag Berlin Heidelberg) doi:10.1007/978-3-642-12754-0_14.

Bahuguna IM, Rathore BP, Brahmbhatt R, Sharma M, Dhar S, Randhawa SS, Kumar K, Romshoo S, Shah RD, Ganjoo RK, Ajai (2014) Are the Himalayan glaciers retreating? *Current Science* **106**, 1008–1013. https://www.jstor.org/stable/24102387.

Baig MHA, Zhang L, Shuai T, Tong Q (2014) Derivation of a tasseled cap transformation based on Landsat 8 at-satellite reflectance. *Remote Sensing Letters* **5**, 423–431. doi:10.1080/2150704x.2014.915434.

Baker BB, Moseley RK (2007) Advancing Treeline and Retreating Glaciers: Implications for Conservation in Yunnan, P.R. China. *Arctic, Antarctic, and Alpine Research* **39**, 200–209. doi:10.1657/1523-0430(2007)39[200:ATARGI]2.0.CO;2.

Bañales Seguel C, De la Barrera F, Burrows AS (2018) An analysis of wildfire risk and historical occurrence for a Mediterranean biosphere reserve, central Chile. *Journal of Environmental Engineering and Landscape Management*.

Bannari A, Morin D, Bonn F, Huete AR (1995) A review of vegetation indices. *Remote Sensing Reviews* **13**, 95–120. doi:10.1080/02757259509532298.

Barbosa PM, Grégoire J-M, Pereira JMC (1999) An Algorithm for Extracting Burned Areas from Time Series of AVHRR GAC Data Applied at a Continental Scale. *Remote Sensing of Environment* **69**, 253–263.

Barbosa PM, Stroppiana D, Grégoire JM, Pereira JMC (1999) An assessment of vegetation fire in Africa (1981-1991): Burned areas, burned biomass, and atmospheric emissions. *Global Biogeochemical Cycles* **13**, 933–950. doi:10.1029/1999GB900042.

Bassett M, Leonard SWJ, Chia EK, Clarke MF, Bennett AF (2017) Interacting effects of fire severity, time since fire and topography on vegetation structure after wildfire. *Forest Ecology and Management* **396**, 26–34. doi:10.1016/j.foreco.2017.04.006.

Bastarrika A, Alvarado M, Artano K, Martinez M, Mesanza A, Torre L, Ramo R, Chuvieco E (2014) BAMS: A Tool for Supervised Burned Area Mapping Using Landsat Data. *Remote Sensing* **6**, 12360–12380. doi:10.3390/rs61212360.

Bastarrika A, Chuvieco E, Martin MP (2011) Automatic burned land mapping from MODIS time series images: Assessment in Mediterranean ecosystems. *IEEE Transactions on Geoscience and Remote Sensing* **49**, 3401–3413. doi:10.1109/TGRS.2011.2128327.

Bastarrika A, Chuvieco E, Martín MP (2011) Mapping burned areas from Landsat TM/ETM+ data with a two-phase algorithm: Balancing omission and commission errors. *Remote Sensing of Environment* **115**, 1003–1012. doi:10.1016/j.rse.2010.12.005.

Bechtel B, Ringeler A, Böhner J (2008) Segmentation for Object Extraction of Treed Using MATLAB and SAGA. *Hamburger Beiträge zur Physischen Geographie und Landschaftsökologie* **19**, 1–12.

Belenguer-Plomer MA, Tanase MA, Fernandez-Carrillo A, Chuvieco E (2019) Burned area detection and mapping using Sentinel-1 backscatter coefficient and thermal anomalies. *Remote Sensing of Environment* **233**, 111345. doi:10.1016/j.rse.2019.111345.

Belgiu M, Drăgu L (2016) Random forest in remote sensing: A review of applications and future directions. *ISPRS Journal of Photogrammetry and Remote Sensing* **114**, 24–31. doi:10.1016/j.isprsjprs.2016.01.011.

Beniston M (2003) Climatic change in mountain regions: a review of possible impacts. *Climatic Change* **59**, 5–31. doi:10.1007/978-94-015-1252-7_2.

Beniston M, Diaz HF, Bradley RS (1997) Climatic change at high elevation sites: an overview. *Climatic Change* **36**, 233–251.

Bird RB, Bird DW, Codding BF, Parker CH, Jones JH (2008) The '"fire stick farming"' hypothesis: Australian Aboriginal foraging strategies, biodiversity, and anthropogenic fire mosaics. *Proceedings of the National Academy of Sciences* **105**, 14796–14801.

Blarquez O, Talbot J, Paillard J, Lapointe-Elmrabti L, Pelletier N, Gates St-Pierre C (2018) Late Holocene influence of societies on the fire regime in southern Québec temperate forests. *Quaternary Science Reviews* **180**, 63–74. doi:10.1016/j.quascirev.2017.11.022.

Boer MM, Sadler RJ, Wittkuhn RS, McCaw L, Grierson PF (2009) Long-term impacts of prescribed burning on regional extent and incidence of wildfires-Evidence from 50 years of active fire management in SW Australian forests. *Forest Ecology and Management* **259**, 132–142. doi:10.1016/j.foreco.2009.10.005.

Bond WJ, Keeley JE (2005) Fire as a global 'herbivore': The ecology and evolution of flammable ecosystems. *Trends in Ecology and Evolution* **20**, 387–394. doi:10.1016/j.tree.2005.04.025.

Bond WJ, Woodward FI, Midgley GF (2005) The Global Distribution of Ecosystems in a world without Fire. *New Phytologist* **165**, 525–538. doi:10.1111/j.1469-8137.2004.01252.x.

Boschetti L, Eva HD, Brivio PA, Grégoire J-M (2004) Lessons to be learned from the comparison of three satellite-derived biomass burning products. *Geophysical Research Letters* **31**, 2–5. doi:10.1029/2004GL021229.

Boschetti L, Flasse SP, Brivio PA (2004) Analysis of the conflict between omission and commission in low spatial resolution dichotomic thematic products: The Pareto Boundary. *Remote Sensing of Environment* **91**, 280–292. doi:10.1016/j.rse.2004.02.015.

Boschetti L, Stehman S V., Roy DP (2016) A stratified random sampling design in space and time for regional to global scale burned area product validation. *Remote Sensing of Environment* **186**, 465–478. doi:10.1016/j.rse.2016.09.016.

Bowman DMJS (2018) Wildfire science is at a loss for comprehensive data. *Nature* **560**, 7. doi:10.1038/d41586-018-05840-4.

Bowman DMJS, Balch JK, Artaxo P, Bond WJ, Carlson JM, Cochrane MA, D'Antonio CM, DeFries RS, Doyle JC, Harrison SP, Johnston FH, Keeley JE, Krawchuk MA, Kull CA, Marston JB, Moritz MA, Prentice IC, Roos CI, Scott AC, Swetnam TW, Van der Werf GR, Pyne SJ (2009) Fire in the earth system. *Science* **324**, 481–484. doi:10.1126/science.1163886.

Bowman DMJS, Balch JK, Artaxo P, Bond WJ, Cochrane MA, D'Antonio CM, Defries RS, Johnston FH, Keeley JE, Krawchuk MA, Kull CA, Mack M, Moritz MA, Pyne S, Roos CI, Scott AC, Sodhi NS, Swetnam TW (2011) The human dimension of fire regimes on Earth. *Journal of Biogeography* **38**, 2223–2236. doi:10.1111/j.1365-2699.2011.02595.x.

Bowman DMJS, Kolden CA, Abatzoglou JT, Johnston FH, van der Werf GR, Flannigan M (2020) Vegetation fires in the Anthropocene. *Nature Reviews Earth & Environment* **1**, 500–515. doi:10.1038/s43017-020-0085-3.

Bracher C, Wymann von Dach S, Adler C (2018) Challenges and Opportunities in Assessing Sustainable Mountain Development Using the UN Sustainable Development Goals. A Report Compiled by the Mountain Research Initiative (MRI), in collaboration with the Centre for Development and Environment (CDE). CDE Working Paper 3. (Bern, Switzerland)

Bradstock RA, Gill AM, Williams RJ (Eds) (2012) 'Flammable Australia: fire regimes, biodiversity and ecosystems in a changing world.' (CSIRO Publishing: Collingwood VIC)

Breiman L (2001) Random Forests. *Machine Learning* **45**, 5–32.

Brown JK, Smith JK (Eds) (2000) 'Wildland fire in ecosystems: effects of fire on flora.' (Ogden, UT)

Brown J, York A, Christie F, McCarthy M (2017) Effects of fire on pollinators and pollination. *Journal of Applied Ecology* **54**, 313–322. doi:10.1111/1365-2664.12670.

Bruzzone L, Fernandez Prieto D (2000) Automatic analysis of the difference image for unsupervised change detection. *IEEE Transactions on Geoscience and Remote Sensing* **38**, 1171–1182.

Bui DT, Le KT, Nguyen VC, Le HD, Revhaug I (2016) Tropical forest fire susceptibility mapping at the Cat Ba National Park Area, Hai Phong City, Vietnam, *Remote Sensing* **8**, 347. doi:10.3390/rs8040347.

Buizer M, Kurz T (2016) Too hot to handle: Depoliticisation and the discourse of ecological modernisation in fire management debates. *Geoforum* **68**, 48–56. doi:10.1016/j.geoforum.2015.11.011.

Buntaine MT, Mullen RB, Lassoie JP (2006) Human use and conservation planning in alpine areas on northwestern Yunnan, China. *Environment, Development and Sustainability*. doi:10.1007/s10668-006-9025-8.

Burchfield DR, Petersen SL, Kitchen SG, Jensen RR (2020) sUAS-Based Remote Sensing in Mountainous Areas : Benefits, Challenges, and Best Practices. *Papers in Applied Geography* **6**, 72–83. doi:10.1080/23754931.2020.1716385.

Calkin DE, Cohen JD, Finney MA, Thompson MP (2014) How risk management can prevent future wildfire disasters in the wildland-urban interface. *Proceedings of the National Academy of Sciences* **111**, 746–751. doi:10.1073/pnas.1315088111.

Cansler CA, Mckenzie D (2014) Climate, fire size, and biophysical setting control fire severity and spatial pattern in the northern Cascade Range, USA. *Ecological Applications* **24**, 1037–1056.

Cao X, Chen J, Matsushita B, Imura H, Wang L (2009) An automatic method for burn scar mapping using support vector machines. *International Journal of Remote Sensing* **30**, 577–594. doi:10.1080/01431160802220219.

Cao Y, Wang M, Liu K (2017) Wildfire susceptibility assessment in southern China: A comparison of multiple methods. *International Journal of Disaster Risk Science* **8**, 164–181. doi:10.1007/s13753-017-0129-6.

Carbone LM, Tavella J, Pausas JG, Aguilar R (2019) A global synthesis of fire effects on pollinators (M Mayfield, Ed.). *Global Ecology and Biogeography* **28**, 1487–1498. doi:10.1111/geb.12939.

de Carvalho Júnior OA, Guimarães RF, Silva CR, Gomes RAT (2015) Standardized time-series and interannual phenological deviation: New techniques for burned-area detection using long-term MODIS-NBR dataset. *Remote Sensing* **7**, 6950–6985. doi:10.3390/rs70606950.

Cayuela L, Golicher JD, Salas Rey J, Rey Benayas JM (2006) Classification of a complex landscape using Dempster-Shafer theory of evidence. *International Journal of Remote Sensing* **27**, 1951–1971. doi:10.1080/01431160500181788.

CEPF (2002) Ecosystem profile: Mountains of Southwest China Hotspot. https://www.cepf.net/our-work/biodiversity-hotspots/mountains-southwest-china.

Chance CM, Hermosilla T, Coops NC, Wulder MA, White JC (2016) Effect of topographic correction on forest change detection using spectral trend analysis of Landsat pixel-based composites. *International Journal of Applied Earth Observation and Geoinformation* **44**, 186–194. doi:10.1016/j.jag.2015.09.003.

Chang Y, He HS, Bishop I, Hu YM, Bu RC, Xu CG, Li XZ (2007) Long-term forest landscape responses to fire exclusion in the Great Xing'an Mountains, China. *International Journal of Wildland Fire* **16**, 34–44. doi:10.1071/WF05093.

Chang Y, He HS, Hu Y, Bu R, Li X (2008) Historic and current fire regimes in the Great Xing'an Mountains, northeastern China: Implications for long-term forest management. *Forest Ecology and Management* **254**, 445–453. doi:10.1016/j.foreco.2007.04.050.

Chang D, Song Y (2009) Comparison of L3JRC and MODIS global burned area products from 2000 to 2007. *Journal of Geophysical Research* **114**, 1–20. doi:10.1029/2008JD011361.

Chang Y, Zhu Z, Bu R, Chen H, Feng Y, Yuehui L, Hu Y, Wang Z (2013) Predicting fire occurrence patterns with logistic regression in Heilongjiang Province, China. *Landscape Ecology* **28**, 1989–2004. doi:10.1007/s10980-013-9935-4.

Chen F, Lin X, Niu S, Wang S, Li D (2012) Influence of climate change on forest fire in Yunnan Province, southwestern China. *Journal of Beijing Forestry University* **34**, 7–15. doi:10.13332/j.1000-1522.2012.06.010.

Chen W, Moriya K, Sakai T, Koyama L, Cao CX (2016) Mapping a burned forest area from Landsat TM data by multiple methods. *Geomatics, Natural Hazards and Risk* **7**, 384–402. doi:10.1080/19475705.2014.925982.

Chen F, Niu S, Tong X, Zhao J, Sun Y, He T (2014) The Impact of Precipitation Regimes on Forest Fires in Yunnan Province, Southwest China. *The Scientific World Journal* **2014**, 1–9. doi:10.1155/2014/326782.

Chen D, Pereira JMC, Masiero A, Pirotti F (2017) Mapping fire regimes in China using MODIS active fire and burned area data. *Applied Geography* **85**, 14–26. doi:10.1016/j.apgeog.2017.05.013.

Chen X, Vogelmann JE, Rollins M, Ohlen D, Key CH, Yang L, Huang C, Shi H (2011) Detecting post-fire burn severity and vegetation recovery using multitemporal remote sensing spectral indices and field-collected composite burn index data in a ponderosa pine forest. *International Journal of Remote Sensing* **32**, 7905–7927. doi:10.1080/01431161.2010.524678.

Cheng W, Tian Q, Wang L (2008) A model of topographic correction and reflectance retrieval for optical satellite data in forested areas. *The International Archives of the Photogrammetry, Remote Sensing and Spatial Information Sciences* **37**, 243–248.

Cheng J, Xie M (2008) The analysis of regional climate change features over Yunnan in recent 50 years. *Progress in Geography* **27**, 19–26.

Chompuchan C, Lin CY (2017) Assessment of forest recovery at Wu-Ling fire scars in Taiwan using multi-temporal Landsat imagery. *Ecological Indicators* **79**, 196–206. doi:10.1016/j.ecolind.2017.04.038.

Chuvieco E, Aguado I, Jurdao S, Pettinari ML, Yebra M, Salas J, Hantson S, De La Riva J, Ibarra P, Rodrigues M, Echeverría M, Azqueta D, Román M V., Bastarrika A, Martínez S, Recondo C, Zapico E, Martínez-Vega FJ (2014) Integrating geospatial information into fire risk assessment. *International Journal of Wildland Fire* **23**, 606–619. doi:10.1071/WF12052.

Chuvieco E, Aguado I, Salas J, García M, Yebra M, Oliva P (2020) Satellite remote sensing contributions to wildland fire science and management. *Current Forestry Reports* **6**, 81–96. doi:10.1007/s40725-020-00116-5.

Chuvieco E, Aguado I, Yebra M, Nieto H, Salas J, Martín MP, Vilar L, Martínez J, Martín S, Ibarra P, de la Riva J, Baeza J, Rodríguez F, Molina JR, Herrera MA, Zamora R (2010) Development of a framework for fire risk assessment using remote sensing and geographic information system technologies. *Ecological Modelling* **221**, 46–58. doi:10.1016/j.ecolmodel.2008.11.017.

Chuvieco E, Congalton RG (1989) Application of Remote Sensing and Geographic Information Systems to forest fire hazard mapping. *Remote Sensing of Environment* **29**, 147–159.

Chuvieco E, Englefield P, Trishchenko AP, Luo Y (2008) Generation of long time series of burn area maps of the boreal forest from NOAA-AVHRR composite data. *Remote Sensing of Environment* **112**, 2381–2396. doi:10.1016/j.rse.2007.11.007.

Chuvieco E, Giglio L, Justice CO (2008) Global characterization of fire activity: Toward defining fire regimes from Earth observation data. *Global Change Biology* **14**, 1488–1502. doi:10.1111/j.1365-2486.2008.01585.x.

Chuvieco E, Martin MP, Palacios A (2002) Assessment of different spectral indices in the red–near-infrared spectral domain for burned land discrimination. *International Journal of Remote Sensing* **23**, 5103–5110. doi:10.1080/01431160210153129.

Chuvieco E, Mouillot F, van der Werf GR, San Miguel J, Tanasse M, Koutsias N, García M, Yebra M, Padilla M, Gitas I, Heil A, Hawbaker TJ, Giglio L (2019) Historical background and current developments for mapping burned area from satellite Earth observation. *Remote Sensing of Environment* **225**, 45–64. doi:10.1016/J.RSE.2019.02.013.

Chuvieco E, Opazo S, Sione W, del Valle H, Anaya JA, di Bella C, Cruz I, Manzo L, López G, Mari N, González-Alonso F, Morelli F, Setzer A, Csiszar IA, Kanpandegi JA, Bastarrika A, Libonati R (2008) Global Burned-Land Estimation in Latin America Using Modis Composite Data. *Ecological Applications* **18**, 64–79.

Chuvieco E, Pettinari ML, Lizundia-Loiola J, Storm T, Padilla Parellada M (2018) ESA Fire Climate Change Initiative (Fire_cci): MODIS Fire_cci Burned Area Pixel product, version 5.1. doi:10.5285/58f00d8814064b79a0c49662ad3af537.

Chuvieco E, Yue C, Heil A, Mouillot F, Alonso-Canas I, Padilla M, Pereira JMC, Oom D, Tansey K (2016) A new global burned area product for climate assessment of fire impacts. *Global Ecology and Biogeography* **25**, 619–629. doi:10.1111/geb.12440.

Cohen J (1960) A coefficient of agreement for nominal scales. *Educational and Psychological Measurement* **20**, 37–46. http://epm.sagepub.com.

Collins L, Newell G, Mellor A (2018) The utility of Random Forests for wildfire severity mapping. *Remote Sensing of Environment* **216**, 374–384. doi:10.1016/j.rse.2018.07.005.

Connell J, Watson SJ, Taylor RS, Avitabile SC, Schedvin N, Schneider K, Clarke MF (2019) Future fire scenarios: Predicting the effect of fire management strategies on the trajectory of high-quality habitat for

threatened species. *Biological Conservation* **232**, 131–141. doi:10.1016/j.biocon.2019.02.004.

Costanza R, D'Arge R, de Groot R, Farber S, Grasso M, Hannon B, Limburg K, Naeem S, O'Neill R V., Paruelo J, Raskin RG, Sutton P, van den Belt M (1997) The value of the world's ecosystem services and natural capital. *Nature* **387**, 253–260.

Countryman CM (1972) 'The Fire Environment Concept.' (Forest Service, U.S. Department of Agriculture: Berkeley, California)

Coutinho LM (1990) Fire in the ecology of the Brazilian cerrado. 'Fire Trop. Biota. Ecol. Stud. (Analysis Synth.' (Ed JG Goldammer) pp. 82–105. (Springer: Berlin, Heidelberg) doi:10.1007/978-3-642-75395-4_6.

Crimmins MA (2006) Synoptic climatology of extreme fire-weather conditions across the southwest United States. *International Journal of Climatology* **26**, 1001–1016. doi:10.1002/joc.1300.

Crist EP (1985) A TM Tasseled Cap equivalent transformation for reflectance factor data. *Remote Sensing of Environment* **17**, 301–306. doi:10.1016/0034-4257(85)90102-6.

Crist EP, Cicone RC (1984) A physically-based transformation of Thematic Mapper data - The TM Tasseled Cap. *IEEE Transactions on Geoscience and Remote Sensing* **GE-22**, 256–263.

Csiszar IA, Morisette JT, Giglio L (2006) Validation of active fire detection from moderate-resolution satellite sensors: The MODIS example in Northern Eurasia. *IEEE Transactions on Geoscience and Remote Sensing* **44**, 1757–1764. doi:10.1109/TGRS.2006.875941.

D'Addabbo A, Satalino G, Pasquariello G, Blonda P (2004) Three different unsupervised methods for change detection : an application. In 'Int. Geosci. Remote Sens. Symp.', Anchorage, AK, USA. 1980–1983. (IEEE: Anchorage, AK, USA) doi:10.1109/ IGARSS.2004.1370735.

Daily GC, Alexander S, Ehrlich LG, Lubchenco J, Matson PA, Mooney HA, Postel S, Schneider SH, Tilman D, Woodwell GM (1997) Ecosystem Services: Benefits supplied to human societies by natural ecosystems. *Issues in Ecology* **2**,

Dawson TP, Jackson ST, House JI, Prentice IC, Mace GM (2011) Beyond predictions: Biodiversity conservation in a changing climate. *Science* **332**, 53–58. doi:10.1126/science.332.6030.664-b.

Deng Y, Chen X, Chuvieco E, Warner T, Wilson JP (2007) Multi-scale linkages between topographic attributes and vegetation indices in a mountainous landscape. *Remote Sensing of Environment* **111**, 122–134. doi:10.1016/j.rse.2007.03.016.

Dice LR (1945) Measures of the amount of ecologic association between species. *Ecology* **26**, 297–302.

Dietze E, Brykała D, Schreuder LT, Jażdżewski K, Blarquez O, Brauer A, Dietze M, Obremska M, Ott F, Pieńczewska A, Schouten S, Hopmans EC, Słowiński M (2019) Human-induced fire regime shifts during 19th century industrialization: A robust fire regime reconstruction using northern Polish lake sediments. *PLoS ONE* **14**, 1–20. doi:10.1371/journal.pone.0222011.

Doerr SH, Santín C (2016) Global trends in wildfire and its impacts: Perceptions versus realities in a changing world. *Philosophical Transactions of the Royal Society B: Biological Sciences* **371**, doi:10.1098/rstb.2015.0345.

Driscoll DA, Bode M, Bradstock RA, Keith DA, Penman TD, Price OF (2015) Resolving future fire management conflicts using multicriteria decision making. **30**, 196–205. doi:10.1111/cobi.12580.

Dupire S, Curt T, Bigot S, Fréjaville T (2019) Vulnerability of forest ecosystems to fire in the French Alps. *European Journal of Forest Research* **138**, 813–830. doi:10.1007/s10342-019-01206-1.

Ediriweera S, Pathirana S, Danaher T, Nichols D, Moffiet T (2013) Evaluation of different topographic corrections for Landsat TM data by prediction of foliage projective cover (FPC) in topographically complex landscapes. *Remote Sensing* **5**, 6767–6789. doi:10.3390/rs5126767.

Epting J, Verbyla DL, Sorbel B (2005) Evaluation of remotely sensed indices for assessing burn severity in interior Alaska using Landsat TM and ETM+. *Remote Sensing of Environment* **96**, 328–339. doi:10.1016/j.rse.2005.03.002.

Ercanoglu M, Weber KT, Langille J, Neves R (2006) Modeling wildland fire susceptibility Using fuzzy systems. *GIScience & Remote Sensing* **43**, 268–282. doi:10.2747/1548-1603.43.3.268.

Escuin S, Navarro R, Fernández P (2008) Fire severity assessment by using NBR (Normalized Burn Ratio) and NDVI (Normalized Difference Vegetation Index) derived from LANDSAT TM/ETM images. *International Journal of Remote Sensing* **29**, 1053–1073. doi:10.1080/01431160701281072.

Fan W, Li J, Liu Q, Zhang Q, Yin G, Li A, Zeng Y, Xu B, Xu X, Zhou G, Du H (2018) Topographic correction of forest image data based on the canopy reflectance model for sloping terrains in multiple forward mode. *Remote Sensing* **10**, 717. doi:10.3390/rs10050717.

Fang L, Yang J (2014) Atmospheric effects on the performance and threshold extrapolation of multi-temporal Landsat derived dNBR for burn severity assessment. *International Journal of Applied Earth Observation and Geoinformation* **33**, 10–20. doi:10.1016/j.jag.2014.04.017.

Fang L, Yang J, Zu J, Li G, Zhang J (2015) Quantifying influences and relative importance of fire weather, topography, and vegetation on fire size and fire severity in a Chinese boreal forest landscape. *Forest Ecology and Management* 1–11. doi:10.1016/j.foreco.2015.01.011.

Fellmann T (2012) The assessment of climate change-related vulnerability in the agricultural sector: reviewing conceptual frameworks. InMeybeck A, Lankoski J, Redfern S, Azzu N, Gitz V (eds) 'Build. Resil. Adapt. to Clim. Chang. Agric. Sect.', Rome, Italy. 37–61. (Food and Agriculture Organization of the United Nations Organisation for Economic Co-operation and Development: Rome, Italy)

Fennell DA, Dowling RK (Eds) (2003) 'Ecotourism policy and planning.' (CAB International: Wallingford, UK)

Flannigan MD, Krawchuk MA, De Groot WJ, Wotton BM, Gowman LM (2009) Implications of changing climate for global wildland fire. *International Journal of Wildland Fire* **18**, 483–507. doi:10.1071/WF08187.

Flatley WT, Lafon CW, Grissino-Mayer HD (2011) Climatic and topographic controls on patterns of fire in the southern and central Appalachian Mountains, USA. *Landscape Ecology* **26**, 195–209. doi:10.1007/s10980-010-9553-3.

Flood N (2014) Continuity of reflectance data between Landsat-7 ETM+ and Landsat-8 OLI, for both top-of-atmosphere and surface reflectance: A study in the Australian landscape. *Remote Sensing* **6**, 7952–7970. doi:10.3390/rs6097952.

Forkel M, Dorigo W, Lasslop G, Teubner I, Chuvieco E, Thonicke K (2017) A data-driven approach to identify controls on global fire activity from satellite and climate observations (SOFIA V1). *Geoscientific Model Development* **10**, 4443–4476. doi:10.5194/gmd-10-4443-2017.

Fornacca D, Ren G, Xiao W (2017) Performance of Three MODIS Fire Products (MCD45A1, MCD64A1, MCD14ML), and ESA Fire_CCI in a Mountainous Area of Northwest Yunnan, China, Characterized by Frequent Small Fires. *Remote Sensing* **9**, 1131. doi:10.3390/rs9111131.

Fornacca D, Ren G, Xiao W (2018) Evaluating the Best Spectral Indices for the Detection of Burn Scars at Several Post-Fire Dates in a Mountainous Region of Northwest Yunnan, China. *Remote Sensing* **10**, 1196. doi:10.3390/rs10081196.

Fornacca D, Ren G, Xiao W (2020) Small fires, frequent clouds, rugged terrain and no training data: A methodology to reconstruct fire history in complex landscapes. *International Journal of Wildland Fire*. doi:10.1071/WF20072.

Fraser RH, Li Z, Cihlar J (2000) Hotspot and NDVI Differencing Synergy (HANDS)-A new technique for burned area mapping over boreal forest. *Remote Sensing of Environment* **74**, 362–376.

Freeborn PH, Cochrane MA, Wooster MJ (2014) A Decade Long, Multi-Scale Map Comparison of Fire Regime Parameters Derived from Three Publically Available Satellite-Based Fire Products: A Case Study in the Central African Republic. *Remote Sensing* **6**, 4061–4089. doi:10.3390/rs6054061.

French NHF, Kasischke ES, Hall RJ, Murphy KA, Verbyla DL, Hoy EE, Allen JL (2008) Using Landsat data to assess fire and burn severity in the North American boreal forest region - An overview and summary of results. *International Journal of Wildland Fire* **17**, 443–462.

Fuller DO, Murphy K (2006) The ENSO-fire dynamic in insular Southeast Asia. *Climatic Change* **74**, 435–455. doi:10.1007/s10584-006-0432-5.

Fung T, Ledrew E (1988) The determination of optimal threshold levels for change detection using various accuracy indices. *Photogrammetric Engineering & Remote Sensing* **54**, 1449–1454. https://www.asprs.org/wp-content/uploads/pers/1988journal/oct/1988_oct_1449-1454.pdf.

Gai C, Weng W, Yuan H (2011) GIS-Based Forest Fire Risk Assessment and Mapping. In '2011 Fourth Int. Jt. Conf. Comput. Sci. Optim.', 1240–1244. (IEEE) doi:10.1109/CSO.2011.140.

Gao Y, Zhang W (2009) A simple empirical topographic correction method for ETM + imagery. *International Journal of Remote Sensing* **30**, 2259–2275. doi:10.1080/01431160802549336.

Gavin DG, Hallett DJ, Feng SH, Lertzman KP, Prichard SJ, Brown KJ, Lynch JA, Bartlein P, Peterson DL (2007) Forest fire and climate change in western North America: Insights from sediment charcoal records. *Frontiers in Ecology and the Environment* **5**, 499–506. doi:10.1890/060161.

Ghorbanzadeh O, Blaschke T, Gholamnia K, Aryal J (2019) Forest fire susceptibility and risk mapping using social/infrastructural vulnerability and environmental variables. *Fire* **2**,

Giglio L (2007) Characterization of the tropical diurnal fire cycle using VIRS and MODIS observations. *Remote Sensing of Environment* **108**, 407–421. doi:10.1016/j.rse.2006.11.018.

Giglio L, Descloitres J, Justice CO, Kaufman YJ (2003) An enhanced contextual fire detection algorithm for MODIS. *Remote Sensing of Environment* **87**, 273–282. doi:10.1016/S0034-4257(03)00184-6.

Giglio L, Loboda T V., Roy DP, Quayle B, Justice CO (2009) An active-fire based burned area mapping algorithm for the MODIS sensor. *Remote Sensing of Environment* **113**, 408–420. doi:10.1016/j.rse.2008.10.006.

Giglio L, Randerson JT, van der Werf GR (2013) Analysis of daily, monthly, and annual burned area using the fourth-generation global fire emissions database (GFED4). *Journal of Geophysical Research: Biogeosciences* **118**, 317–328. doi:10.1002/jgrg.20042.

Giglio L, Randerson JT, van der Werf GR, Kasibhatla PS, Collatz GJ, Morton DC, DeFries RS (2010) Assessing variability and long-term trends in burned area by merging multiple satellite fire products. *Biogeosciences* **7**, 1171–1186. doi:10.5194/bg-7-1171-2010.

Giglio L, Schroeder W, Justice CO (2016) The collection 6 MODIS active fire detection algorithm and fire products. *Remote Sensing of Environment* **178**, 31–41. doi:10.1016/j.rse.2016.02.054.

Gill MA, Stephens SL, Cary GJ (2013) The worldwide '"wildfire"' problem. *Ecological Applications* **23**, 438–454.

Gitas IZ, Devereux BJ (2006) The role of topographic correction in mapping recently burned Mediterranean forest areas from LANDSAT TM images. *International Journal of Remote Sensing* **27**, 41–54. doi:10.1080/01431160500182992.

Gómez-González S, Torres-Díaz C, Bustos-Schindler C, Gianoli E (2011) Anthropogenic fire drives the evolution of seed traits. *Proceedings of the National Academy of Sciences* **108**, 18743–18747. doi:10.1073/pnas.1108863108.

Gómez C, White JC, Wulder MA (2016) Optical remotely sensed time series data for land cover classification: A review. *ISPRS Journal of Photogrammetry and Remote Sensing* **116**, 55–72. doi:10.1016/j.isprsjprs.2016.03.008.

Goodwin NR, Collett LJ, Denham RJ, Flood N, Tindall D (2013) Cloud and cloud shadow screening across Queensland, Australia: An automated method for Landsat TM/ETM+ time series. *Remote Sensing of Environment* **134**, 50–65. doi:10.1016/j.rse.2013.02.019.

Gorelick N, Hancher M, Dixon M, Ilyushchenko S, Thau D, Moore R (2017) Google Earth Engine: Planetary-scale geospatial analysis for everyone. *Remote Sensing of Environment* **202**, 18–27. doi:10.1016/j.rse.2017.06.031.

Gowlett JAJ (2016) The discovery of fire by humans : a long and convoluted process. *Philosophical Transactions of the Royal Society B* **371**, doi:http://dx.doi.org/10.1098/rstb.2015.0164.

Grafarend EW (2006) 'Linear and Nonlinear Models: Fixed Effects, Random Effects, and Mixed Models.' (Walter de Gruyter: Berlin)

Grêt-Regamey A, Brunner SH, Kienast F (2012) Mountain Ecosystem Services: Who Cares? *Mountain Research and Development* **32**, S23–S34. doi:10.1659/MRD-JOURNAL-D-10-00115.S1.

De Groot WJ, Cantin AS, Flannigan MD, Soja AJ, Gowman LM, Newbery A (2013) A comparison of Canadian and Russian boreal forest fire regimes. *Forest Ecology and Management* **294**, 23–34. doi:10.1016/j.foreco.2012.07.033.

Guo F, Innes JL, Wang G, Ma X, Sun L, Hu H, Su Z (2014) Historic distribution and driving factors of human-caused fires in the Chinese boreal forest between 1972 and 2005. *Journal of Plant Ecology* **8**, 480–490. doi:10.1093/jpe/rtu041.

Haddaway NR, Styles D, Pullin AS (2014) Evidence on the environmental impacts of farm land abandonment in high altitude/mountain regions: A systematic map. *Environmental Evidence* **3**, 1–7. doi:10.1186/2047-2382-3-17.

Hall J V., Loboda T V., Giglio L, McCarty GW (2016) A MODIS-based burned area assessment for Russian croplands: Mapping requirements and challenges. *Remote Sensing of Environment* **184**, 506–521. doi:10.1016/j.rse.2016.07.022.

Hamilton DS, Hantson S, Scott CE, Kaplan JO, Pringle KJ, Nieradzik LP, Rap A, Folberth GA, Spracklen D V., Carslaw KS (2018) Reassessment of pre-industrial fire emissions strongly affects anthropogenic aerosol forcing. *Nature Communications* **9**, doi:10.1038/s41467-018-05592-9.

Han J, Shen Z, Ying L, Li G, Chen A (2015) Early post-fire regeneration of a fire-prone subtropical mixed Yunnan pine forest in Southwest China: Effects of pre-fire vegetation, fire severity and topographic factors. *Forest Ecology and Management* **356**, 31–40. doi:10.1016/j.foreco.2015.06.016.

Han J, Ying L, Li G, Shen Z (2016) Spatial patterns of species diversity in the herb layer of early post-fire regeneration in mixed Pinus yunnanensis forests. *Chinese Journal of Plant Ecology* **40**, 200–211. doi:10.17521/cjpe.2015.0161.

Hantson S, Chuvieco E (2011) Evaluation of different topographic correction methods for Landsat imagery. *International Journal of Applied Earth Observation and Geoinformation* **13**, 691–700. doi:10.1016/j.jag.2011.05.001.

Hantson S, Padilla M, Corti D, Chuvieco E (2013) Strengths and weaknesses of MODIS hotspots to characterize global fire occurrence. *Remote Sensing of Environment* **131**, 152–159. doi:10.1016/j.rse.2012.12.004.

Hantson S, Pueyo S, Chuvieco E (2015) Global fire size distribution is driven by human impact and climate. *Global Ecology and Biogeography* **24**, 77–86. doi:10.1111/geb.12246.

Harley GL, Baisan CH, Brown PM, Falk DA, Flatley WT, Id HDG, Hessl A, Heyerdahl EK, Kaye MW, Id CWL, Id EQM, Maxwell RS (2018) Advancing dendrochronological studies of fire in the United States. *Fire* **1**, 4–9. doi:10.3390/fire1010011.

Harris L, Taylor AH (2019) Previous burns and topography limit and reinforce fire severity in a large wildfire. *Ecosphere* **8**, doi:10.1002/ecs2.2019.

Harris S, Veraverbeke S, Hook SJ (2011) Evaluating Spectral Indices for Assessing Fire Severity in Chaparral Ecosystems (Southern California) Using MODIS/ASTER (MASTER) Airborne Simulator Data. *Remote Sensing* **3**, 2403–2419. doi:10.3390/rs3112403.

Harvey BJ, Donato DC, Turner MG (2016) Drivers and trends in landscape patterns of stand-replacing fire in forests of the US Northern Rocky Mountains (1984–2010). *Landscape Ecology* **31**, 2367–2383. doi:10.1007/s10980-016-0408-4.

Hawbaker TJ, Vanderhoof MK, Beal YJG, Takacs JD, Schmidt GL, Falgout JT, Williams B, Fairaux NM, Caldwell MK, Picotte JJ, Howard SM, Stitt S, Dwyer JL (2017) Mapping burned areas using dense time-

series of Landsat data. *Remote Sensing of Environment* **198**, 504–522. doi:10.1016/j.rse.2017.06.027.

He T, Pausas JG, Belcher CM, Schwilk DW, Lamont BB (2012) Fire-adapted traits of Pinus arose in the fiery Cretaceous. *New Phytologist* **194**, 751–759. doi:10.1111/j.1469-8137.2012.04079.x.

He G, Zhang Z, Jiao W, Long T, Peng Y, Wang G, Yin R, Wang W, Zhang X, Liu H, Cheng B, Xiang B (2018) Generation of ready to use (RTU) products over China based on Landsat series data. *Big Earth Data* **2**, 56–64. doi:10.1080/20964471.2018.1433370.

Heinimann A, Breu T, Kohler T (2003) The challenge of applying Geographic Information Systems to sustainable mountain development. *Mountain Research and Development* **23**, 312–319. doi:10.1659/0276-4741(2003)023[0312:Tcoagi]2.0.Co;2.

Hermosilla T, Wulder MA, White JC, Coops NC, Hobart GW (2015) An integrated Landsat time series protocol for change detection and generation of annual gap-free surface reflectance composites. *Remote Sensing of Environment* **158**, 220–234. doi:10.1016/j.rse.2014.11.005.

Hislop S, Jones S, Soto-Berelov M, Skidmore AK, Haywood A, Nguyen T (2018) Using Landsat Spectral Indices in Time-Series to Assess Wildfire Disturbance and Recovery. *Remote Sensing* **10**, 460. doi:10.3390/rs10030460.

Holben B, Justice C (1981) An examination of spectral band ratioing to reduce the topographic effect on remotely sensed data. *International Journal of Remote Sensing* **2**, 115–133. doi:10.1080/01431168108948349.

Hollmann R, Merchant CJ, Saunders R, Downy C, Buchwitz M, Cazenave A, Chuvieco E, Defourny P, de Leeuw G, Forsberg R, Holzer-Popp T, Paul F, Sandven S, Sathyendranath S, van Roozendael M, Wagner W (2013) The ESA Climate Change Initiative: Satellite Data Records for Essential Climate Variables. *Bulletin of the American Meteorological Society* **94**, 1541–1552. doi:10.1175/BAMS-D-11-00254.1.

Huang C, Goward SN, Masek JG, Thomas N, Zhu Z, Vogelmann JE (2010) An automated approach for reconstructing recent forest disturbance history using dense Landsat time series stacks. *Remote Sensing of Environment* **114**, 183–198. doi:10.1016/j.rse.2009.08.017.

Huang H, Roy DP, Boschetti L, Zhang HK, Yan L, Kumar SS, Gomez-Dans J, Li J (2016) Separability analysis of Sentinel-2A Multi-Spectral Instrument (MSI) data for burned area discrimination. *Remote Sensing* **8**, doi:10.3390/rs8100873.

Huang Y-J, Shen H, Jia L-B, Li S-F, Su T, Nam G-S, Zhu H, Zhou Z-K (2020) Macroscopic fossil charcoals as proxy of a local fire linked to conifer-rich forest from the late Pliocene of northwestern Yunnan, Southwest China. *Palaeoworld*. doi:10.1016/j.palwor.2020.07.005.

Huang S, Siegert F (2004) ENVISAT multisensor data for fire monitoring and impact assessment. *International Journal of Remote Sensing* **25**, 4411–4416. doi:10.1080/01431160412331269670.

Huber UM, Bugmann HKM, Reasoner MA (Eds) (2005) 'Global Change and Mountain Regions: An Overview of Current Knowledge.' (Springer Netherlands) doi:10.1007/978-1-4020-3508-1.

Hudak AT, Morgan P, Bobbitt MJ, Smith AMS, Lewis SA, Lentile LB, Robichaud PR, Clark JT, McKinley RA (2007) The relationship of multispectral satellite imagery to immediate fire effects. *Fire Ecology Special Issue* **3**, 64–90.

IPCC (2014a) 'Climate Change 2014: Impacts, Adaptation, and Vulnerability. Part B: Regional Aspects. Contribution of Working Group II to the Fifth Assessment Report of the Intergovernmental Panel on Climate Change.' (VR Barros, CB Field, DJ Dokken, KJ Mach, MD Mastrandrea, TE Bilir, M Chatterjee, KL Ebi, YO Estrada, RC Genova, B Girma, ES Kissel, AN Levy, S MacCracken, PR Mastrandrea, and LL White, Eds.). (Cambridge University Press: Cambridge, United Kingdom and New York, NY, USA) https://academic.oup.com/qje/article-lookup/doi/10.2307/1881805.

IPCC (2014b) 'Climate Change 2014: Impacts, Adaptation, and Vulnerability. Part A: Global and Sectoral Aspects. Contribution of Working Group II to the Fifth Assessment Report of the Intergovernmental Panel on Climate Change.' (CB Field, VR Barros, DJ Dokken, KJ Mach, MD Mastrandrea, TE Bilir, M Chatterjee, KL Ebi, YO Estrada, RC Genova, B Girma, ES Kissel, AN Levy, S MacCracken, PR Mastrandrea, and LL White, Eds.). (Cambridge University Press: Cambridge, United Kingdom and New

York, NY, USA) papers2://publication/uuid/B8BF5043-C873-4AFD-97F9-A630782E590D.

Ireland G, Petropoulos GP (2015) Exploring the relationships between post- fi re vegetation regeneration dynamics, topography and burn severity: A case study from the Montane Cordillera Ecozones of Western Canada. *Applied Geography* **56**, 232–248. doi:10.1016/j.apgeog.2014.11.016.

Itten KI, Meyer P (1993) Geometric and radiometric correction of TM data of mountainous forested areas. *IEEE Transactions on Geoscience and Remote Sensing* **31**, 764–770. doi:10.1109/36.239898.

Jackson RD, Huete AR (1991) Interpreting vegetation indices. *Preventive Veterinary Medicine* **11**, 185–200.

James SR (1989) Hominid use of fire in the lower and middle Pleistocene. *Current Anthropology* **30**, 1–26.

Jessie E (1995) Relative importance of fuels and weather on fire behavior in subalpine forests. *Ecology* **76**, 747–762.

Jia X, Gao Y, Wei B, Wang S, Tang G, Zhao Z (2019) Risk assessment and regionalization of fire disaster based on analytic hierarchy process and MODIS Data: A case study of Inner Mongolia, China. *Sustainability* **11**, 6263. doi:10.3390/su11226263.

Jolly WM, Cochrane MA, Freeborn PH, Holden ZA, Brown TJ, Williamson GJ, Bowman DMJS (2015) Climate-induced variations in global wildfire danger from 1979 to 2013. *Nature Communications* **6**, 1–11. doi:10.1038/ncomms8537.

Justice CO, Giglio L, Korontzi S, Owens J, Morisette JT, Roy DP, Descloitres J, Alleaume S, Petitcolin F, Kaufman Y (2002) The MODIS fire products. *Remote Sensing of Environment* **83**, 244–262. doi:10.1016/S0034-4257(02)00076-7.

Justice CO, Townshend JRG, Vermote EF, Masuoka E, Wolfe RE, Saleous N, Roy DP, Morisette JT (2002) An overview of MODIS Land data processing and product status. *Remote Sensing of Environment* **83**, 3–15. doi:10.1016/S0034-4257(02)00084-6.

Kalantar B, Ueda N, Idrees MO, Janizadeh S, Ahmadi K, Shabani F (2020) Forest fire susceptibility prediction based on machine learning models with resampling algorithms on remote sensing data. *Remote Sensing* **12**, 3682.

Kapos V, Rhind J, Edwards M, Price MF, Ravilious C (2000) Developing a map of the world's mountain forests. 'For. Sustain. Mt. Dev. a state Knowl. Rep. 2000'. (Eds MF Price, N Butt) pp. 4–9. (CAB International Publishing: Wallingford, UK) doi:10.1007/1-4020-3508-X_52.

Kaufman YJ, Remer LA (1994) Detection of Forests Using Mid-IR Reflectance: An Application for Aerosol Studies. *IEEE Transactions on Geoscience and Remote Sensing* **32**, 672–683. doi:10.1109/36.297984.

Kavzoglu T, Erdemir MY, Tonbul H (2016) Evaluating performances of spectral indices for burned area mapping using object-based image analysis. In Bailly J-S, Griffith D, Josselin D (eds) 'Proc. Spat. Accuracy', Montpellier, France. 162–168. (international Spatial Accuracy Research Association: Montpellier, France) http://www.spatial-accuracy.org.

Keeley JE (2006) Fire management impacts on invasive plants in the western United States. *Conservation Biology* **20**, 375–384. doi:10.1111/j.1523-1739.2006.00339.x.

Keeley JE, Bond WJ, Bradstock RA, Pausas JG, Rundel PW (2011) 'Fire in Mediterranean ecosystems: ecology, evolution and management.' (Cambridge University Press)

Keeley JE, Pausas JG, Rundel PW, Bond WJ, Bradstock RA (2011) Fire as an evolutionary pressure shaping plant traits. *Trends in Plant Science* **16**, 406–411. doi:10.1016/j.tplants.2011.04.002.

Keeley JE, Syphard AD (2016) Climate change and future fire regimes: Examples from California. *Geosciences* **6**. doi:10.3390/geosciences6030037.

Kennedy RE, Yang Z, Cohen WB (2010) Detecting trends in forest disturbance and recovery using yearly Landsat time series: 1. LandTrendr - Temporal segmentation algorithms. *Remote Sensing of Environment* **114**, 2897–2910. doi:10.1016/j.rse.2010.07.008.

Ketcham SL, Koprowski JL (2013) Impacts of wildfire on wildlife in Arizona: A synthesis. In Gottfried GJ, F. FP,

Gebow BS, Eskew LG, Collins LC (eds) 'USDA For. Serv. Proc. RMRS-P-67', Tucson, AZ. 345–350. (U.S. Department of Agriculture, Forest Service, Rocky Mountain Research Station: Tucson, AZ) http://cals.arizona.edu/research/redsquirrel/res_pdf/Ketcham%26Koprowski_ImpactsWidlfire_on_Wildlife_AZ_rmrs_p067_345_350.pdf.

Key CH (2006) Ecological and Sampling Constraints on Defining Landscape Fire Severity. *Fire Ecology* **2**, 34–59. doi:10.4996/fireecology.0202034.

Key CH, Benson NC (2006) Landscape Assessment: Ground measure of severity, the Composite Burn Index; and Remote sensing of severity, the Normalized Burn Ratio. (Ogden, UT) https://pubs.er.usgs.gov/publication/2002085.

Khawlie M, Awad M, Shaban A, Kheir RB, Abdallah C (2002) Remote sensing for environmental protection of the eastern Mediterranean rugged mountainous areas, Lebanon. *ISPRS Journal of Photogrammetry and Remote Sensing* **57**, 13–23. doi:10.1016/S0924-2716(02)00115-6.

Knorr W, Arneth A, Jiang L (2016) Demographic controls of future global fire risk. *Nature Climate Change* **6**, 781–785. doi:10.1038/nclimate2999.

Koutsias N, Karteris M (2000) Burned area mapping using logistic regression modeling of a single post-fire Landsat-5 Thematic Mapper image. *International Journal of Remote Sensing* **21**, 673–687. doi:10.1080/014311600210506.

Koutsias N, Xanthopoulos G, Founda D, Xystrakis F, Nioti F, Pleniou M, Mallinis G, Arianoutsou M (2013) On the relationships between forest fires and weather conditions in Greece from long-term national observations (1894-2010). *International Journal of Wildland Fire* **22**, 493–507. doi:10.1071/WF12003.

Krawchuk MA, Moritz MA (2009) Fire regimes of China: Inference from statistical comparison with the United States. *Global Ecology and Biogeography* **18**, 626–639. doi:10.1111/j.1466-8238.2009.00472.x.

Krawchuk MA, Moritz MA, Parisien M-A, Van Dorn J, Hayhoe K (2009) Global pyrogeography: The current and future distribution of wildfire. *PLoS ONE* **4**. doi:10.1371/journal.pone.0005102.

Krebs P, Pezzatti GB, Mazzoleni S, Talbot LM, Conedera M (2010) Fire regime: History and definition of a key concept in disturbance ecology. *Theory in Biosciences* **129**, 53–69. doi:10.1007/s12064-010-0082-z.

Lamont BB, Le Maitre DC, Cowling RM, Enright NJ (1991) Canopy seed storage in woody plants. *The Botanical Review* **57**, 277–317.

Lasaponara R (2006) Estimating spectral separability of satellite-derived parameters for burned areas mapping in the Calabria region by using SPOT-Vegetation data. *Ecological Modelling* **196**, 265–270. doi:10.1016/j.ecolmodel.2006.02.025.

Lassoie JP, Goldman KE, Moseley RK (2006) Ground-based photomonitoring of ecoregional ecological changes in Northwestern Yunnan, China. In 'USDA For. Serv. Proc. RMRS-P-42CD', 140–151

Lavorel S, Flannigan MD, Lambin EF, Scholes MC (2007) Vulnerability of land systems to fire: Interactions among humans, climate, the atmosphere, and ecosystems. *Mitigation and Adaptation Strategies for Global Change* **12**, 33–53. doi:10.1007/s11027-006-9046-5.

Leuenberger M, Parente J, Tonini M, Pereira MG, Kanevski M (2018) Wildfire susceptibility mapping: Deterministic vs. stochastic approaches. *Environmental Modelling and Software* **101**, 194–203. doi:10.1016/j.envsoft.2017.12.019.

Leys B, Carcaillet C, Dezileau L, Ali AA, Bradshaw RHW (2013) A comparison of charcoal measurements for reconstruction of Mediterranean paleo-fire frequency in the mountains of Corsica. *Quaternary Research (United States)* **79**, 337–349. doi:10.1016/j.yqres.2013.01.003.

Leys C, Ley C, Klein O, Bernard P, Licata L (2013) Detecting outliers: Do not use standard deviation around the mean, use absolute deviation around the median. *Journal of Experimental Social Psychology* **49**, 764–766. doi:10.1016/j.jesp.2013.03.013.

Li W, Clauzel C, Dai Y, Wu G, Giraudoux P, Li L (2017) Improving landscape connectivity for the Yunnan snub-nosed monkey through cropland reforestation using graph theory. *Journal for Nature Conservation* **38**, 46–

55. doi:10.1016/j.jnc.2017.06.002.

Li X, Fu G, Zeppel MJB, Yu X, Zhao G, Eamus D, Yu Q (2012) Probability Models of Fire Risk Based on Forest Fire Indices in Contrasting Climates over China. *Journal of Resources and Ecology* **3**, 105–117. doi:10.5814/j.issn.1674-764x.2012.02.002.

Li S, Hughes AC, Su T, Lebreton J, Oskolski AA, Sun M, Ferguson DK, Zhou Z (2017) Fire dynamics under monsoonal climate in Yunnan, SW China : past, present and future. *Palaeogeography, Palaeoclimatology, Palaeoecology* **465**, 168–176. doi:10.1016/j.palaeo.2016.10.028.

Li P, Jiang L, Feng Z (2013) Cross-Comparison of Vegetation Indices Derived from Landsat-7 Enhanced Thematic Mapper Plus (ETM+) and Landsat-8 Operational Land Imager (OLI) Sensors. *Remote Sensing* **6**, 310–329. doi:10.3390/rs6010310.

Li J, Song Y, Huang X, Li M (2014) Comparison of forest burned areas in mainland China derived from MCD45A1 and data recorded in yearbooks from 2001 to 2011. *International Journal of Wildland Fire* **24**, 103–113. http://dx.doi.org/10.1071/WF14031.

Li X, Zhao G, Yu X, Yu Q (2014) A comparison of forest fire indices for predicting fire risk in contrasting climates in China. *Natural Hazards* **70**, 1339–1356. doi:10.1007/s11069-013-0877-6.

Libonati R, DaCamara CC, Pereira JMC, Peres LF (2011) On a new coordinate system for improved discrimination of vegetation and burned areas using MIR/NIR information. *Remote Sensing of Environment* **115**, 1464–1477. doi:10.1016/j.rse.2011.02.006.

Lin CY, Lo HM, Chou WC, Lin WT (2004) Vegetation recovery assessment at the Jou-Jou Mountain landslide area caused by the 921 Earthquake in Central Taiwan. *Ecological Modelling* **176**, 75–81. doi:10.1016/j.ecolmodel.2003.12.037.

Linn R, Winterkamp J, Edminster C, Colman JJ, Smith WS (2007) Coupled influences of topography and wind on wildland fire behaviour. In 'Int. J. Wildl. Fire', 183–195 doi:10.1071/WF06078.

Liu W, Wang L, Zhou Y, Wang S, Zhu J, Wang F (2016) A comparison of forest fire burned area indices based on HJ satellite data. *Natural Hazards* **81**, 971–980. doi:10.1007/s11069-015-2115-x.

Liu Z, Yang J, Chang Y, Weisberg PJ, He HS (2012) Spatial patterns and drivers of fire occurrence and its future trend under climate change in a boreal forest of Northeast China. *Global Change Biology* **18**, 2041–2056. doi:10.1111/j.1365-2486.2012.02649.x.

Loboda T V., French NHF, Hight-Harf C, Jenkins L, Miller ME (2013) Mapping fire extent and burn severity in Alaskan tussock tundra: An analysis of the spectral response of tundra vegetation to wildland fire. *Remote Sensing of Environment* **134**, 194–209. doi:10.1016/j.rse.2013.03.003.

Loboda T V., O'Neal KJ, Csiszar I (2007) Regionally adaptable dNBR-based algorithm for burned area mapping from MODIS data. *Remote Sensing of Environment* **109**, 429–442. doi:10.1016/j.rse.2007.01.017.

Long T, Zhang Z, He G, Jiao W, Tang C (2019) 30 m Resolution global annual burned area mapping based on Landsat images and Google Earth Engine. *Remote Sensing* **11**, 489. doi:10.3390/rs11050489.

López-Poma R, Orr BJ, Bautista S (2014) Successional stage after land abandonment modulates fire severity and post-fire recovery in a Mediterranean mountain landscape. *International Journal of Wildland Fire* **23**, 1005–1015. doi:10.1071/WF13150.

López García MJ, Caselles V (1991) Mapping burns and natural reforestation using thematic mapper data. *Geocarto International* **6**, 31–37. doi:10.1080/10106049109354290.

Lozano FJ, Suárez-Seoane S, de Luis-Calabuig E (2012) Does fire regime affect both temporal patterns and drivers of vegetation recovery in a resilient Mediterranean landscape? A remote sensing approach at two observation levels. *International Journal of Wildland Fire* **21**, 666. doi:10.1071/WF10072.

Lu B, He Y, Tong A (2016) Evaluation of spectral indices for estimating burn severity in semiarid grasslands. *International Journal of Wildland Fire* **25**, 147–157. doi:10.1071/WF15098.

Lu D, Mausel P, Brondizio E, Moran EF (2004) Change detection techniques. *International Journal of Remote*

Sensing **25**, 2365–2407. doi:10.1080/0143116031000139863.

Lü A, Tian H, Liu M, Liu J, Melillo JM (2006) Spatial and temporal patterns of carbon emissions from forest fires in China from 1950 to 2000. *Journal of Geophysical Research* **111**, 1–12. doi:10.1029/2005JD006198.

Ma Z, Liu J, Yang S (2013) Climate Change in Southwest China during 1961–2010: Impacts and Adaptation. *Advances in Climate Change Research* **4**, 223–229. doi:10.3724/SP.J.1248.2013.223.

Ma C, Moseley RK, Chen W, Zhou Z (2007) Plant diversity and priority conservation areas of Northwestern Yunnan, China. *Biodiversity and Conservation* **16**, 757–774. doi:10.1007/s10531-005-6199-6.

Mace GM, Norris K, Fitter AH (2012) Biodiversity and ecosystem services: a multilayered relationship. *Trends in Ecology and Evolution* **27**, 19–26. doi:10.1016/j.tree.2011.08.006.

Mackinnon JR, Carey G (1996) 'A Biodiversity review of China.' (World Wide Fund for Nature (WWF) International, WWF China Programme: Beijing, China) https://books.google.com/books?id=IV7wAAAAMAAJ.

Mancino G, Ferrara A, Padula A, Nolè A (2020) Cross-Comparison between Landsat 8 (OLI) and Landsat 7 (ETM+) Derived Vegetation Indices in a Mediterranean Environment. *Remote Sensing* **12**, 291. doi:10.3390/rs12020291.

Mantero G, Morresi D, Marzano R, Motta R, Mladenoff DJ, Garbarino M (2020) The influence of land abandonment on forest disturbance regimes: a global review. *Landscape Ecology* **35**, 2723–2744. doi:10.1007/s10980-020-01147-w.

Martín-López B, Leister I, Cruz PL, Palomo I, Grêt-Regamey A, Harrison PA, Lavorel S, Locatelli B, Luque S, Walz A (2019) Nature's contributions to people in mountains: A review. *PLoS ONE* **14**, 1–24. doi:10.1371/journal.pone.0217847.

Martín MP, Gómez I, Chuvieco E (2006) Burnt Area Index (BAIM) for burned area discrimination at regional scale using MODIS data. *Forest Ecology and Management* **234**, S221. doi:10.1016/j.foreco.2006.08.248.

Martin Pilar M, Chuvieco E (1998) Cartografía De Grandes Incendios Forestales En La Península Ibérica a Partir De Imágenes Noaa-Avhrr. *Serie Geografica* **7**, 109–128.

Masek JG, Vermote EF, Saleous N, Wolfe R, Hall FG, Huemmrich F, Gao F, Kutler J, Lim TK (2013) LEDAPS Calibration, Reflectance, Atmospheric Correction Preprocessing Code, Version 2. Model product. doi:https://doi.org/10.3334/ORNLDAAC/1146.

Matsushita B, Yang W, Chen J, Onda Y, Qiu G (2007) Sensitivity of the Enhanced Vegetation Index (EVI) and Normalized Difference Vegetation Index (NDVI) to Topographic Effects: A Case Study in High-Density Cypress Forest. *Sensors* **7**, 2636–2651.

Mazher A (2013) Comparative analysis of mapping burned areas from Landsat TM images. *Journal of Physics: Conference Series* **439**. doi:10.1088/1742-6596/439/1/012038.

Mbow C, Goïta K, Bénié GB (2004) Spectral indices and fire behavior simulation for fire risk assessment in savanna ecosystems. *Remote Sensing of Environment* **91**, 1–13. doi:10.1016/j.rse.2003.10.019.

McDonald ER, Wu X, Caccetta P, Campbell N (2000) Illumination correction of Landsat TM data in south east NSW. In 'Proc. Tenth Australas. Remote Sens. Conf.',

McGranahan DA, Wonkka CL (2018) Wildland Fire Science Literacy : Education, Creation, and Application. *Fire* **1**. doi:10.3390/fire1030052.

Melchiori AE, Cândido P, Libonati R, Morelli F, Setzer A, de Jesus SC, Garcia Fonseca LM, Körting TS (2015) Spectral indices and multi-temporal change image detection algorithms for burned area extraction in the Brazilian Cerrado. InINPE (ed) 'An. XVII Simpósio Bras. Sensoriamento Remoto - SBSR', João Pessoa-PB, Brasil. 643–650. (João Pessoa-PB, Brasil)

Melchiorre A, Boschetti L (2018) Global Analysis of Burned Area Persistence Time with MODIS Data. *Remote Sensing* **10**, 750. doi:10.3390/rs10050750.

Meng R, Dennison PE, Huang C, Moritz MA, D'Antonio CM (2015) Effects of fire severity and post-fire climate

on short-term vegetation recovery of mixed-conifer and red fir forests in the Sierra Nevada Mountains of California. *Remote Sensing of Environment* **171**, 311–325. doi:10.1016/j.rse.2015.10.024.

Meng R, Zhao F (2017) Remote sensing of fire effects: A review for recent advances in burned area and burn severity mapping. 'Remote Sens. Hydrometeorol. hazards'. (Eds GP Petropoulos, T Islam) pp. 261–283. (CRC Press, Taylor & Francis Group) https://www.crcpress.com/Remote-Sensing-of-Hydrometeorological-Hazards/Petropoulos-Islam/p/book/9781498777582.

Merino-de-Miguel S, Huesca M, González-Alonso F (2010) Modis reflectance and active fire data for burn mapping and assessment at regional level. *Ecological Modelling* **221**, 67–74. doi:10.1016/j.ecolmodel.2009.09.015.

Ming Q, Shi Z (2007) New discussion on dry valley formation in the Three Parallel Rivers region. *Journal of Desert Research* **27**, 99–104.

Miranda HS, Sato MN, Neto WN, Aires FS (2009) Fires in the cerrado, the Brazilian savanna. 'Trop. Fire Ecol.' pp. 427–450. (Springer: Berlin, Heidelberg) doi:10.1007/978-3-540-77381-8_15.

Mitri GH, Gitas IZ (2004) A semi-automated object-oriented model for burned area mapping in the Mediterranean region using Landsat-TM imagery. *International Journal of Wildland Fire* **13**, 367–376. doi:10.1071/WF03079.

Mitsopoulos I, Chrysafi I, Bountis D, Mallinis G (2019) Assessment of factors driving high fire severity potential and classification in a Mediterranean pine ecosystem. *Journal of Environmental Management* **235**, 266–275. doi:10.1016/j.jenvman.2019.01.056.

Mittermeier RA, Myers N, Thomsen JB, da Fonseca GAB, Olivieri S (1998) Biodiversity Hotspots and Major Tropical Wilderness Areas: Approaches to Setting Conservation Priorities. *Conservation Biology* **12**, 516–520. doi:10.1046/j.1523-1739.1998.012003516.x.

Mohammed I, Marshall M, de Bie K, Estes L, Nelson A (2020) A blended census and multiscale remote sensing approach to probabilistic cropland mapping in complex landscapes. *ISPRS Journal of Photogrammetry and Remote Sensing* **161**, 233–245. doi:10.1016/j.isprsjprs.2020.01.024.

Moreno Ruiz JA, García Lázaro JR, Del Águila Cano I, Leal PH (2013) Burned area mapping in the North American boreal forest using terra-MODIS LTDR (2001-2011): A comparison with the MCD45A1, MCD64A1 and BA GEOLAND-2 products. *Remote Sensing* **6**, 815–840. doi:10.3390/rs6010815.

Morgan P, Hardy CC, Swetnam TW, Rollins MG, Long DG (2001) Mapping fire regimes across time and space: Understanding coarse and fine-scale fire patterns. *International Journal of Wildland Fire* **10**, 329–342. doi:10.1071/wf01032.

Morisette JT, Baret F, Liang S (2006) Special issue on global land product validation. *IEEE Transactions on Geoscience and Remote Sensing* **44**, 1695–1697.

Moritz MA, Batllori E, Bradstock RA, Gill AM, Handmer J, Hessburg PF, Leonard J, McCaffrey S, Odion DC, Schoennagel T, Syphard AD (2014) Learning to coexist with wildfire. *Nature* **515**, 58–66. doi:10.1038/nature13946.

Moritz MA, Morais ME, Summerell LA, Carlson JM, Doyle JC (2005) Wildfires, complexity, and highly optimized tolerance. *Proceedings of the National Academy of Sciences* **102**, 17912–17917. doi:10.1073/pnas.0508985102.

Morton DC, Defries RS, Randerson JT, Giglio L, Schroeder W, van der Werf GR (2008) Agricultural intensification increases deforestation fire activity in Amazonia. *Global Change Biology* **14**, 2262–2275. doi:10.1111/j.1365-2486.2008.01652.x.

Moseley RK (2006) Historical Landscape Change in Northwestern Yunnan, China. *Mountain Research and Development* **26**, 214–219. doi:10.1659/0276-4741(2006)26.

Mouillot F, Schultz MG, Yue C, Cadule P, Tansey K, Ciais P, Chuvieco E (2014) Ten years of global burned area products from spaceborne remote sensing-A review: Analysis of user needs and recommendations for future developments. *International Journal of Applied Earth Observation and Geoinformation* **26**, 64–79. doi:10.1016/j.jag.2013.05.014.

Mulders MA (2001) Advances in the application of remote sensing and GIS for surveying mountainous land. *International Journal of Applied Earth Observation and Geoinformation* **3**, 3–10. doi:10.1016/S0303-2434(01)85015-7.

Myers N, Mittermeier RA, Mittermeier CC, da Fonseca GAB, Kent J (2000) Biodiversity hotspots for conservation priorities. *Nature* **403**, 853–858.

Nelson R, Kokic P, Crimp S, Meinke H, Howden SM (2010) The vulnerability of Australian rural communities to climate variability and change : Part I - Conceptualising and measuring vulnerability. *Environmental Science & Policy* **13**, 8–17. doi:10.1016/j.envsci.2009.09.006.

Nunes AN, Lourenço L (2017) Increased vulnerability to wildfires and post fire hydro-geomorphic processes in Portuguese mountain regions: what has changed? *Open Agriculture* **2**, 70–82. doi:10.1515/opag-2017-0008.

Núñez Casillas L, García Lázaro JR, Moreno Ruiz JA, Arbelo M (2013) A Comparative Analysis of Burned Area Datasets in Canadian Boreal Forest in 2000. *The Scientific World Journal* **2013**, 1–13. doi:10.1155/2013/289056.

O'Brien K, Eriksen S, Nygaard LP, Schjolden A (2007) Why different interpretations of vulnerability matter in climate change discourses. *Climate Policy* **7**, 73–88. doi:10.1080/14693062.2007.9685639.

Ofori BY, Stow AJ, Baumgartner JB, Beaumont LJ (2017) Influence of adaptive capacity on the outcome of climate change vulnerability assessment. *Scientific Reports* **7**, 1–12. doi:10.1038/s41598-017-13245-y.

Oguro Y, Suga Y, Takeuchi S, Ogawa H, Tsuchiya K (2003) Monitoring of a rice field using Landsat-5 TM and Landsat-7 ETM+ data. *Advance in Space Research* **32**, 2223–2228. doi:lO.l016/SO273-1177(03)00697-5.

Olofsson P, Foody GM, Herold M, Stehman S V., Woodcock CE, Wulder MA (2014) Good practices for estimating area and assessing accuracy of land change. *Remote Sensing of Environment* **148**, 42–57. doi:10.1016/j.rse.2014.02.015.

Padilla M, Olofsson P, Stehman S V., Tansey K, Chuvieco E (2017) Stratification and sample allocation for reference burned area data. *Remote Sensing of Environment* **203**, 240–255. doi:10.1016/j.rse.2017.06.041.

Padilla M, Stehman S V., Chuvieco E (2014) Validation of the 2008 MODIS-MCD45 global burned area product using stratified random sampling. *Remote Sensing of Environment* **144**, 187–196. doi:10.1016/j.rse.2014.01.008.

Padilla M, Stehman S V., Ramo R, Corti D, Hantson S, Oliva P, Alonso-Canas I, Bradley A V., Tansey K, Mota B, Pereira JMC, Chuvieco E (2015) Comparing the accuracies of remote sensing global burned area products using stratified random sampling and estimation. *Remote Sensing of Environment* **160**, 114–121. doi:10.1016/j.rse.2015.01.005.

Palazzi E, Mortarini L, Terzago S, von Hardenberg J (2019) Elevation-dependent warming in global climate model simulations at high spatial resolution. *Climate Dynamics* **52**, 2685–2702. doi:10.1007/s00382-018-4287-z.

Palomo I (2017) Climate Change Impacts on Ecosystem Services in High Mountain Areas: A Literature Review. *Mountain Research and Development* **37**, 179–187. doi:10.1659/MRD-JOURNAL-D-16-00110.1.

Parente J, Pereira MG (2016) Structural fire risk: The case of Portugal. *Science of The Total Environment* **573**, 883–893. doi:10.1016/j.scitotenv.2016.08.164.

Parker BM, Lewis T, Srivastava SK (2015) Estimation and evaluation of multi-decadal fire severity patterns using Landsat sensors. *Remote Sensing of Environment* **170**, 340–349. doi:10.1016/j.rse.2015.09.014.

Pastro LA, Dickman CR, Letnic M (2011) Burning for biodiversity or burning biodiversity? Prescribed burn vs. wildfire impacts on plants, lizards, and mammals. *Ecological Applications* **21**, 3238–3253. doi:10.1890/10-2351.1.

Pausas JG (2019) Generalized fire response strategies in plants and animals. *Oikos* **128**, 147–153. doi:10.1111/oik.05907.

Pausas JG, Bond WJ (2020) On the three major recycling pathways in terrestrial ecosystems. *Trends in Ecology*

and Evolution **35**, 767–775. doi:10.1016/j.tree.2020.04.004.

Pausas JG, Keeley JE (2009) A burning story: The role of fire in the history of life. *BioScience* **59**, 593–601. doi:10.1525/bio.2009.59.7.10.

Pausas JG, Keeley JE (2019) Wildfires as an ecosystem service. *Frontiers in Ecology and the Environment* **17**, 289–295. doi:10.1002/fee.2044.

Pausas JG, Parr CL (2018) Towards an understanding of the evolutionary role of fire in animals. *Evolutionary Ecology* **32**, 113–125. doi:10.1007/s10682-018-9927-6.

Payne D, Spehn EM, Snethlage M, Fischer M (2017) Opportunities for research on mountain biodiversity under global change. *Current Opinion in Environmental Sustainability* **29**, 40–47. doi:10.1016/j.cosust.2017.11.001.

Pechony O, Shindell DT (2010) Driving forces of global wildfires over the past millennium and the forthcoming century. *Proceedings of the National Academy of Sciences* **107**, 19167–19170. doi:10.1073/pnas.1003669107.

Pettinari ML, Chuvieco E, Alonso-canas I, Padilla Parellada M (2016) ESA CCI ECV Fire Disturbance: Product user guide, version 2.1.

Pettorelli N, Laurance WF, Brien TGO, Wegmann M, Nagendra H, Turner W (2014) Satellite remote sensing for applied ecologists: opportunities and challenges. *Journal of Applied Ecology* **51**, 839–848. doi:10.1111/1365-2664.12261.

Pickell PD, Hermosilla T, Frazier RJ, Coops NC, Wulder MA (2016) Forest recovery trends derived from Landsat time series for North American boreal forests. *International Journal of Remote Sensing* **37**, 138–149. doi:10.1080/2150704X.2015.1126375.

Picotte JJ, Robertson K (2011) Timing constraints on remote sensing of wildland fire burned area in the southeastern US. *Remote Sensing* **3**, 1680–1690. doi:10.3390/rs3081680.

Pimple U, Sitthi A, Simonetti D, Pungkul S, Leadprathom K, Chidthaisong A (2017) Topographic correction of Landsat TM-5 and Landsat OLI-8 imagery to improve the performance of forest classification in the mountainous terrain of Northeast Thailand. *Sustainability* **9**, 1–26. doi:10.3390/su9020258.

Piñol J, Terradas J, Lloret F (1998) Climate warming, wildfire hazard, and wildfire occurrence in coastal eastern Spain. *Climatic Change* **38**, 345–357. doi:10.1023/A:100531663.

Pinty B, Verstraete MM (1992) GEMI: a non-linear index to monitor global vegetation from satellites. *Vegetatio* **101**, 15–20. doi:10.1007/BF00031911.

Piper LA, Yeo M (2011) Ecolabels, Ecocertification and Ecotourism. InPerić J (ed) 'Sustain. Tour. Socio-Cultural, Environ. Econ. Impact', Rijeka. 279–294. (University of Rijeka, Faculty of Tourism and Hospitality Management: Rijeka)

Plummer S, Arino O, Ranera F, Tansey K, Chen J, Dedieu G, Eva HD, Piccolini I, Leigh R, Borstlap G, Beusen B, Fierens F, Heyns W, Benedetti R, Lacaze R, Garrigues S, Quaife T, De Kauwe M, Quegan S, Raupach M, Briggs P, Poulter B, Bondeau A, Rayner P, Schultz M, McCallum I (2007) An update on the Globcarbon initiative: Multi-sensor estimation of global biophysical products for global terrestrial carbon studies. In 'Eur. Sp. Agency, (Special Publ. ESA SP',

Plummer S, Arino O, Simon M, Steffen W (2006) Establishing an earth observation product service for the terrestrial carbon community: The Globcarbon initiative. *Mitigation and Adaptation Strategies for Global Change* **11**, 97–111. doi:10.1007/s11027-006-1012-8.

Polychronaki A, Gitas IZ, Veraverbeke S, Debien A (2013) Evaluation of ALOS PALSAR imagery for burned area mapping in Greece using object-based classification. *Remote Sensing* **5**, 5680–5701. doi:10.3390/rs5115680.

Power MJ, Marlon J, Ortiz N, Bartlein PJ, Harrison SP, Mayle FE, Ballouche A, Bradshaw RHW, Carcaillet C, Cordova C, Mooney S, Moreno PI, Prentice IC, Thonicke K, Tinner W, Whitlock C, Zhang Y, Zhao Y, Ali AA, Anderson RS, Beer R, Behling H, Briles C, Brown KJ, Brunelle A, Bush M, Camill P, Chu GQ, Clark

J, Colombaroli D, Connor S, Daniau AL, Daniels M, Dodson J, Doughty E, Edwards ME, Finsinger W, Foster D, Frechette J, Gaillard MJ, Gavin DG, Gobet E, Haberle S, Hallett DJ, Higuera P, Hope G, Horn S, Inoue J, Kaltenrieder P, Kennedy L, Kong ZC, Larsen C, Long CJ, Lynch J, Lynch EA, McGlone M, Meeks S, Mensing S, Meyer G, Minckley T, Mohr J, Nelson DM, New J, Newnham R, Noti R, Oswald W, Pierce J, Richard PJH, Rowe C, Sanchez Goñi MF, Shuman BN, Takahara H, Toney J, Turney C, Urrego-Sanchez DH, Umbanhowar C, Vandergoes M, Vanniere B, Vescovi E, Walsh M, Wang X, Williams N, Wilmshurst J, Zhang JH (2008) Changes in fire regimes since the last glacial maximum: An assessment based on a global synthesis and analysis of charcoal data. *Climate Dynamics* **30**, 887–907. doi:10.1007/s00382-007-0334-x.

Prichard SJ, Stevens-Rumann CS, Hessburg PF (2017) Tamm Review: Shifting global fire regimes: Lessons from reburns and research needs. *Forest Ecology and Management* **396**, 217–233. doi:10.1016/j.foreco.2017.03.035.

Pu Y, Zhang Z, Pu L, Hui C (2007) Biodiversity and its fragility in Yunnan, China. *Journal of Forestry Research* **18**, 39–47. doi:10.1007/s11676-007-0008-x.

Pyne SJ (1991) 'Burning bush: a fire history of Australia.' (University of Washington Press)

Pyne SJ (2016) Fire in the mind: Changing understandings of fire in western civilization. *Philosophical Transactions of the Royal Society B* **371**. doi:10.1098/rstb.2015.0166.

Pyne SJ, Andrews PL, Laven RD (1996) 'Introduction to wildland fire.' (John Wiley & Sons, Ed.). (New York, USA)

Qian L, Chen J, Deng T, Sun H (2020) Plant diversity in Yunnan : Current status and future directions. *Plant Diversity* **42**, 281–291. doi:10.1016/j.pld.2020.07.006.

Qin X, Li Z, Zhang Z (2010) Distribution Pattern of Fires in China Based on Satellite Data. In '2010 Second lITA Int. Conf. Geosci. Remote Sens.', Qingdao, China. 503–506. (Qingdao, China)

Randerson JT, Chen Y, Van der Werf GR, Rogers BM, Morton DC (2012) Global burned area and biomass burning emissions from small fires. *Journal of Geophysical Research: Biogeosciences* **117**, 1–23. doi:10.1029/2012JG002128.

Randerson JT, Van der Werf GR, Giglio L, Collatz GJ, Kasibhatla PS (2017) Global Fire Emissions Database, Version 4.1 (GFEDv4). doi:10.3334/ORNLDAAC/1293.

Ren GP, Zhu AX, Wang W, Xiao W, Huang Y, Li GQ, Li DP, Zhu JG (2009) A hierarchical approach coupled with coarse DEM information for improving the efficiency and accuracy of forest mapping over very rugged terrains. *Forest Ecology and Management* **258**, 26–34. doi:10.1016/j.foreco.2009.03.043.

Riaño D, Chuvieco E, Salas J, Aguado I (2003) Assessment of different topographic corrections in Landsat-TM data for mapping vegetation types. *IEEE Transactions on Geoscience and Remote Sensing* **41**, 1056–1061. doi:10.1109/TGRS.2003.811693.

Richter R, Kellenberger T, Kaufmann H (2009) Comparison of topographic correction methods. *Remote Sensing* **1**, 184–196. doi:10.3390/rs1030184.

Roberts GJ, Wooster MJ (2008) Fire detection and fire characterization over Africa using meteosat SEVIRI. *IEEE Transactions on Geoscience and Remote Sensing* **46**, 1200–1218. doi:10.1109/TGRS.2008.915751.

Robinson NM, Leonard SWJ, Bennett AF, Clarke MF (2016) Are forest gullies refuges for birds when burnt? The value of topographical heterogeneity to avian diversity in a fire-prone landscape. *Biological Conservation* **200**, 1–7. doi:10.1016/j.biocon.2016.05.010.

Rogan J, Yool SR (2001) Mapping fire-induced vegetation depletion in the Peloncillo Mountains, Arizona and New Mexico. *Remote Sensing* **22**, 3101–3121.

Rogers BM, Balch JK, Goetz SJ, Lehmann CER, Turetsky M (2020) Focus on changing fire regimes: interactions with climate, ecosystems, and society. *Environmental Research Letters* **15**.

Roteta E, Bastarrika A, Padilla M, Storm T, Chuvieco E (2019) Development of a Sentinel-2 burned area algorithm: Generation of a small fire database for sub-Saharan Africa. *Remote Sensing of Environment* **222**,

1–17. doi:10.1016/j.rse.2018.12.011.

Rouse JW, Haas RH, Schell JA, Deering DW (1973) Monitoring vegetation systems in the Great Plains with ERTS.pdf. In 'Third ERTS Symp. NASA', Washington DC. 309–317. (NASA: Washington DC)

Roy DP, Boschetti L (2009) Southern Africa validation of the MODIS, L3JRC, and GlobCarbon burned-area products. *IEEE Transactions on Geoscience and Remote Sensing* **47**, 1032–1044. doi:10.1109/TGRS.2008.2009000.

Roy DP, Boschetti L, Justice CO, Ju J (2008) The collection 5 MODIS burned area product — Global evaluation by comparison with the MODIS active fire product. *Remote Sensing of Environment* **112**, 3690–3707. doi:10.1016/j.rse.2008.05.013.

Roy DP, Boschetti L, Trigg SN (2006) Remote sensing of fire severity: Assessing the performance of the normalized burn ratio. *IEEE Geoscience and Remote Sensing Letters* **3**, 112–116. doi:10.1109/LGRS.2005.858485.

Roy DP, Frost PGH, Justice CO, Landmann T, Le Roux JL, Gumbo K, Makungwa S, Dunham K, Du Toit R, Mhwandagara K, Zacarias A, Tacheba B, Dube OP, Pereira JMC, Mushove P, Morisette JT, Santhana Vannan SK, Davies ID (2005) The Southern Africa Fire Network (SAFNet) regional burned-area product-validation protocol. *International Journal of Remote Sensing* **26**, 4265–4292. doi:10.1080/01431160500113096.

Roy DP, Jin Y, Lewis PE, Justice CO (2005) Prototyping a global algorithm for systematic fire-affected area mapping using MODIS time series data. *Remote Sensing of Environment* **97**, 137–162. doi:10.1016/j.rse.2005.04.007.

Roy DP, Kovalskyy V, Zhang HK, Vermote EF, Yan L, Kumar SS, Egorov A (2016) Characterization of Landsat-7 to Landsat-8 reflective wavelength and normalized difference vegetation index continuity. *Remote Sensing of Environment* **185**, 57–70. doi:10.1016/j.rse.2015.12.024.

Sahoo PK, Soltani S, Wong AKC (1988) A survey of thresholding techniques. *Computer Vision, Graphics, and Image Processing* **41**, 233–260.

Santín C, Doerr SH (2016) Fire effects on soils : the human dimension. *Philosophical Transactions of the Royal Society B* **371**, 28–34.

Schepers L, Haest B, Veraverbeke S, Spanhove T, Borre J Vanden, Goossens R (2014) Burned area detection and burn severity assessment of a heathland fire in Belgium using airborne imaging spectroscopy (APEX). *Remote Sensing* **6**, 1803–1826. doi:10.3390/rs6031803.

Schirpke U, Kohler M, Leitinger G, Fontana V, Tasser E, Tappeiner U (2017) Future impacts of changing land-use and climate on ecosystem services of mountain grassland and their resilience. *Ecosystem Services* **26**, 79–94. doi:10.1016/j.ecoser.2017.06.008.

Schmidt M, Lucas R, Bunting P, Verbesselt J, Armston J (2015) Multi-resolution time series imagery for forest disturbance and regrowth monitoring in Queensland, Australia. *Remote Sensing of Environment* **158**, 156–168. doi:10.1016/j.rse.2014.11.015.

Schneiderbauer S, Zebisch M, Steurer C (2007) Applied Remote Sensing in Mountain Regions: A Workshop Organized by EURAC in the Core of the Alps. *Mountain Research and Development* **27**, 286–287. doi:10.1659/mrd.0928.

Schoennagel T, Balch JK, Brenkert-Smith H, Dennison PE, Harvey BJ, Krawchuk MA, Mietkiewicz N, Morgan P, Moritz MA, Rasker R, Turner MG, Whitlock C (2017) Adapt to more wildfire in western North American forests as climate changes. *Proceedings of the National Academy of Sciences* **114**, 4582–4590. doi:10.1073/pnas.1617464114.

Schroeder W, Oliva P, Giglio L, Csiszar IA (2014) The New VIIRS 375m active fire detection data product: Algorithm description and initial assessment. *Remote Sensing of Environment* **143**, 85–96. doi:10.1016/j.rse.2013.12.008.

Schroeder W, Prins E, Giglio L, Csiszar IA, Schmidt C, Morisette JT, Morton DC (2008) Validation of GOES and MODIS active fire detection products using ASTER and ETM+ data. *Remote Sensing of Environment* **112**,

2711–2726. doi:10.1016/j.rse.2008.01.005.

Schwilk DW, Ackerly DD (2001) Flammability and serotiny as strategies : correlated evolution in pines. *Oikos* **94**, 326–336. https://www.jstor.org/stable/3547577.

Scott AC, Bowman DMJS, Bond WJ, Pyne SJ, Alexander ME (2014) 'Fire on Earth: An Introduction.' (John Wiley & Sons, Ltd.: Chichester, UK) https://www.wiley.com/en-us/Fire+on+Earth%3A+An+Introduction-p-9781119953579.

Semeraro T, Mastroleo G, Aretano R, Facchinetti G, Zurlini G, Petrosillo I (2016) GIS Fuzzy Expert System for the assessment of ecosystems vulnerability to fire in managing Mediterranean natural protected areas. *Journal of Environmental Management* **168**, 94–103. doi:10.1016/j.jenvman.2015.11.053.

Shakesby RA (2011) Post-wildfire soil erosion in the Mediterranean: Review and future research directions. *Earth-Science Reviews* **105**, 71–100. doi:10.1016/j.earscirev.2011.01.001.

She X, Zhang L, Cen Y, Wu T, Huang C, Baig MHA (2015) Comparison of the continuity of vegetation indices derived from Landsat 8 OLI and Landsat 7 ETM+ data among different vegetation types. *Remote Sensing* **7**, 13485–13506. doi:10.3390/rs71013485.

Shen Z (2017) Mountain Biogeography. 'Int. Encycl. Geogr. People, Earth, Environ. Technol.' (Eds D Richardson, N Castree, MM Goodchild, A Kobayashi, W Liu, RA Marston) pp. 1–7. (John Wiley & Sons, Ltd.) doi:10.1002/9781118786352.wbieg0369.

Sherman R, Mullen RB, Li H, Fang Z, Wang Y (2007) Alpine ecosystems of northwest Yunnan, China: An initial assessment for conservation. *Journal of Mountain Science* **4**, 181–192. doi:10.1007/s11629-007-0181-6.

Sherman R, Mullen RB, Li H, Fang Z, Wang Y (2008) Spatial patterns of plant diversity and communities in Alpine ecosystems of the Hengduan Mountains, northwest Yunnan, China. *Journal of Plant Ecology* **1**, 117–136. doi:10.1093/jpe/rtn012.

Shu L, Tian X, Wang M (2003) A Study on Forest Fire Occurrence in China. In 'XII World For. Congr.', Quebec City, Canada. (Quebec City, Canada) http://www.fao.org/docrep/ARTICLE/WFC/XII/0278-B1.HTM.

Siegert F, Ruecker G (2000) Use of multitemporal ERS-2 SAR images for identification of burned scars in south-east Asian tropical rainforest. *International Journal of Remote Sensing* **21**, 831–837. doi:10.1080/014311600210632.

Simon M, Plummer S, Fierens F, Hoelzemann JJ, Arino O (2004) Burnt area detection at global scale using ATSR-2: The GLOBSCAR products and their qualification. *Journal of Geophysical Research D: Atmospheres* **109**, 1–16. doi:10.1029/2003JD003622.

Sloan S, Locatelli B, Wooster MJ, Gaveau DLA (2017) Fire activity in Borneo driven by industrial land conversion and drought during El Niño periods, 1982–2010. *Global Environmental Change* **47**, 95–109. doi:10.1016/j.gloenvcha.2017.10.001.

Smith JK (Ed) (2000) 'Wildland fire in ecosystems: effects of fire on fauna.' (Ogden, UT)

Smith AMS, Drake NA, Wooster MJ, Hudak AT, Holden ZA, Gibbons CJ (2007) Production of Landsat ETM+ reference imagery of burned areas within Southern African savannahs: Comparison of methods and application to MODIS. *International Journal of Remote Sensing* **28**, 2753–2775. doi:10.1080/01431160600954704.

Sola I, González-Audícana M, Álvarez-Mozos J (2016) Multi-criteria evaluation of topographic correction methods. *Remote Sensing of Environment* **184**, 247–262. doi:10.1016/j.rse.2016.07.002.

Sommer C, Malz P, Seehaus TC, Lippl S, Zemp M, Braun MH (2020) Rapid glacier retreat and downwasting throughout the European Alps in the early 21st century. *Nature Communications* **11**. doi:10.1038/s41467-020-16818-0.

Song Y, Liu B, Miao W, Chang D, Zhang Y (2009) Spatiotemporal variation in nonagricultural open fire emissions in China from 2000 to 2007. *Global Biogeochemical Cycles* **23**. doi:10.1029/2008GB003344.

Sørensen T (1948) A method of establishing groups of equal amplitude in plant sociology based on similarity of

species content and its application to analyses of the vegetation on Danish commons. *Det Kongelige Danske Videnskabernes Selskab Biologiske Skrifter* **V**, 42. http://www.tandfonline.com/doi/full/10.3109/00016924809131205.

Soto MEC, Molina-Martínez JR, Rodríguez y Silva F, Alvear GHJ (2013) A territorial fire vulnerability model for Mediterranean ecosystems in South America. *Ecological Informatics* **13**, 106–113. doi:10.1016/j.ecoinf.2012.06.004.

Spearman C (1904) The proof and measurement of association between two things. *The American journal of psychology* **15**, 72–101. doi:10.1037/h0065390.

Srivastava PK, Petropoulos GP, Gupta M, Singh SK, Islam T, Loka D (2019) Deriving forest fire probability maps from the fusion of visible/infrared satellite data and geospatial data mining. *Modeling Earth Systems and Environment* **5**, 627–643. doi:10.1007/s40808-018-0555-5.

Staver AC, Archibald S, Levin SA (2011) The global extent and determinants of savanna and forest as alternative biome states. *Science* **334**, 230–232. doi:10.1126/science.1210465.

Steven MD, Malthus TJ, Baret F, Xu H, Chopping MJ (2003) Intercalibration of vegetation indices from different sensor systems. *Remote Sensing of Environment* **88**, 412–422. doi:10.1016/j.rse.2003.08.010.

Stocks BJ, Wotton BM, Flannigan MD, Fosberg MA, Cahoon DR, Goldammer JG (2001) Boreal Forest Fire Regimes And Climate Change. 'Remote Sens. Clim. Model. Synerg. Limitations. Adv. Glob. Chang. Res.' (Eds M Beniston, MM Verstraete) pp. 233–246. (Springer, Dordrecht) doi:10.1007/0-306-48149-9_10.

Streets DG, Yarber KF, Woo J-H, Carmichael GR (2003) Biomass burning in Asia: Annual and seasonal estimates and atmospheric emissions. *Global Biogeochemical Cycles* **17**, n/a-n/a. doi:10.1029/2003GB002040.

Stroppiana D, Azar R, Calò F, Pepe A, Imperatore P, Boschetti M, Silva JMN, Brivio PA, Lanari R (2015) Integration of optical and SAR data for burned area mapping in Mediterranean regions. *Remote sensing* **7**, 1320–1345. doi:10.3390/rs70201320.

Stroppiana D, Bordogna G, Carrara P, Boschetti M, Boschetti L, Brivio PA (2012) A method for extracting burned areas from Landsat TM/ETM+ images by soft aggregation of multiple Spectral Indices and a region growing algorithm. *ISPRS Journal of Photogrammetry and Remote Sensing* **69**, 88–102. doi:10.1016/j.isprsjprs.2012.03.001.

Stroppiana D, Pinnock S, Pereira JMC, Grégoire J-M (2002) Radiometric analysis of SPOT-VEGETATION images for burnt area detection in Northern Australia. *Remote Sensing of Environment* **82**, 21–37. doi:10.1016/S0034-4257(02)00021-4.

Stubbendieck J, Volesky J, Ortmann J (2007) Grassland management with prescribed fire. *Extension* **EC148**, 1–6. http://extensionpublications.unl.edu/assets/pdf/ec148.pdf.

Su WH, Shi Z, Zhou R, Zhao YJ, Zhang GF (2015) The role of fire in the Central Yunnan Plateau ecosystem, southwestern China. *Forest Ecology and Management* **356**, 22–30. doi:10.1016/j.foreco.2015.05.015.

Sugihara NG, Van Wagtendonk JW, Fites-Kaufman J, Shaffer KE, Thode AE (2006) 'Fire in California's ecosystems.' (University of California Press)

Summers WT, Coloff SG, Conard SG (2011) 'Synthesis of knowledge: fire history and climate change.' (Joint Fire Science Program Project 09-2-01-09, Ed.). (Boise, ID, USA)

Syphard AD, Keeley JE, Pfaff AH, Ferschweiler K (2017) Human presence diminishes the importance of climate in driving fire activity across the United States. *Proceedings of the National Academy of Sciences* **114**, 13750–13755. doi:10.1073/pnas.1713885114.

Tan B, Masek JG, Wolfe R, Gao F, Huang C, Vermote EF, Sexton JO, Ederer G (2013) Improved forest change detection with terrain illumination corrected Landsat images. *Remote Sensing of Environment* **136**, 469–483. doi:10.1016/j.rse.2013.05.013.

Tanase MA, Belenguer-Plomer MA, Roteta E, Bastarrika A, Wheeler J, Fernández-Carrillo Á, Tansey K, Wiedemann W, Navratil P, Lohberger S, Siegert F, Chuvieco E (2020) Burned area detection and mapping:

Intercomparison of Sentinel-1 and Sentinel-2 based algorithms over tropical Africa. *Remote Sensing* **12**, 334.

Tang CQ (2010) Subtropical montane evergreen broad-leaved forests of Yunnan, China: Diversity, succession dynamics, human influence. *Frontiers of Earth Science in China* **4**, 22–32. doi:10.1007/s11707-009-0057-x.

Tang CQ (2015) 'The subtropical vegetation of southwestern China: Plant distribution, diversity and ecology.' (Springer Netherlands: Dordrecht, Netherlands) doi:10.1007/978-94-017-9741-2.

Tang CQ, Ohsawa M (2009) Ecology of subtropical evergreen broad-leaved forests of Yunnan, southwestern China as compared to those of southwestern Japan. *Journal of Plant Research* **122**, 335–350. doi:10.1007/s10265-009-0221-0.

Tansey K (2004) Vegetation burning in the year 2000: Global burned area estimates from SPOT VEGETATION data. *Journal of Geophysical Research* **109**, D14S03. doi:10.1029/2003JD003598.

Tansey K, Grégoire J-M, Defourny P, Leigh R, Pekel J-F, van Bogaert E, Bartholomé E (2008) A new, global, multi-annual (2000–2007) burnt area product at 1 km resolution. *Geophysical Research Letters* **35**, 1–6. doi:10.1029/2007GL031567.

Tasser E, Leitinger G, Tappeiner U (2017) Climate change versus land-use change—What affects the mountain landscapes more? *Land Use Policy* **60**, 60–72. doi:10.1016/j.landusepol.2016.10.019.

Taylor AH, Beaty RM (2005) Climatic influences on fire regimes in the northern Sierra Nevada mountains, Lake Tahoe Basin, Nevada, USA. *Journal of Biogeography* **32**, 425–438. doi:10.1111/j.1365-2699.2004.01208.x.

Tehrany MS, Jones S, Shabani F, Martínez-álvarez F, Bui DT (2018) A novel ensemble modeling approach for the spatial prediction of tropical forest fire susceptibility using LogitBoost machine learning classifier and multi-source geospatial data. *Theoretical and Applied Climatology*.

Tian X, Mcrae DJ, Shu L, Wang M, Li H (2005) Satellite remote-sensing technologies used in forest fire management. *Journal of Forestry Research* **16**, 73–78. doi:10.1007/BF02856861.

Tian X, Shu L, Wang M, Zhao F, Chen L (2013) The fire danger and fire regime for the Daxing'anling region for 1987-2010. *Procedia Engineering* **62**, 1023–1031. doi:10.1016/j.proeng.2013.08.157.

Tian X, Zhao F, Shu L, Wang M (2014) Changes in forest fire danger for south-western China in the 21st century. *International Journal of Wildland Fire* **23**, 185–195. doi:10.1071/WF13014.

Trigg SN, Flasse SP (2001) An evaluation of different bi-spectral spaces for discriminating burned shrub-savannah. *International Journal of Remote Sensing* **22**, 2641–2647. doi:10.1080/01431160110053185.

Tsela P, Wessels K, Botai J, Archibald S, Swanepoel D, Steenkamp K, Frost P (2014) Validation of the two standard MODIS satellite burned-area products and an empirically-derived merged product in South Africa. *Remote Sensing* **6**, 1275–1293. doi:10.3390/rs6021275.

Turetsky MR, Benscoter B, Page S, Rein G, Van der Werf GR, Watts A (2015) Global vulnerability of peatlands to fire and carbon loss. *Nature Geoscience* **8**, 11–14. doi:10.1038/ngeo2325.

UN (1992) Agenda 21: programme of action for sustainable development, Rio Declaration on Environment and Development, statement of forest principles : the final text of agreements negotiated by Governments at the United Nations Conference on Environment and Develop. In 'UN Conf. Environ. Dev.', Rio de Janeiro, Brazil. 294 pp. (Rio de Janeiro, Brazil)

UN (1998) Proclamation of the International Year of the Mountains. Report on the 1998 UN General Assembly Meeting. (New York, USA)

UN (2012) The future we want: outcome documents of the United Nations Conference on Sustainable Development. In 'Int. Organ.', Rio de Janeiro, Brazil. 53 pp. (Rio de Janeiro, Brazil) doi:10.1017/S0020818300001806.

UNEP and GRID-Arendal (2019) Elevating Mountains in the post-2020 Global Biodiversity Framework. https://www.grida.no/publications/455.

Urbanski SP, Salmon JM, Nordgren BL, Hao WM (2009) A MODIS direct broadcast algorithm for mapping

wildfire burned area in the western United States. *Remote Sensing of Environment* **113**, 2511–2526. doi:10.1016/j.rse.2009.07.007.

Valdez MC, Chang K-T, Chen C-F, Chiang S-H, Santos JL (2017) Modelling the spatial variability of wildfire susceptibility in Honduras using remote sensing and geographical information systems. *Geomatics, Natural Hazards and Risk* **5705**, 1–17. doi:10.1080/19475705.2016.1278404.

Vanderhoof MK, Fairaux NM, Beal YJG, Hawbaker TJ (2017) Validation of the USGS Landsat Burned Area Essential Climate Variable (BAECV) across the conterminous United States. *Remote Sensing of Environment* **198**, 393–406. doi:10.1016/j.rse.2017.06.025.

Vannière B, Blarquez O, Rius D, Doyen E, Brücher T, Colombaroli D, Connor S, Feurdean A, Hickler T, Kaltenrieder P, Lemmen C, Leys B, Massa C, Olofsson J (2016) 7000-year human legacy of elevation-dependent European fire regimes. *Quaternary Science Reviews* **132**, 206–212. doi:10.1016/j.quascirev.2015.11.012.

Vázquez-Jiménez R, Ramos-Bernal RN, Romero-Calcerrada R, Arrogante-Funes P, Tizapa SS, Novillo CJ (2018) Thresholding Algorithm Optimization for Change Detection to Satellite Imagery. 'Color. Image Process.' (Ed C Travieso-Gonzalez) pp. 163–182. (IntechOpen: London) doi:10.5772/intechopen.71002.

Vázquez-Jiménez R, Romero-Calcerrada R, Novillo CJ, Ramos-Bernal RN, Arrogante-Funes P (2017) Applying the chi-square transformation and automatic secant thresholding to Landsat imagery as unsupervised change detection methods. *Journal of Applied Remote Sensing* **11**, 016016. doi:10.1117/1.JRS.11.016016.

Veraverbeke S, Lhermitte S, Verstraeten WW (2011) Evaluation of pre / post-fire differenced spectral indices for assessing burn severity in a Mediterranean environment with Landsat Thematic Mapper. *International Journal of Remote Sensing* **32**, 3521–3537. doi:10.1080/01431161003752430.

Veraverbeke S, Sedano F, Hook SJ, Randerson JT, Jin Y, Rogers BM (2014) Mapping the daily progression of large wildland fires using MODIS active fire data. *International Journal of Wildland Fire* **23**, 655–667. doi:10.1071/WF13015.

Veraverbeke S, Verstraeten WW, Lhermitte S, Goossens R (2010) Evaluating Landsat Thematic Mapper spectral indices for estimating burn severity of the 2007 Peloponnese wildfires in Greece. *International Journal of Wildland Fire* **19**, 558–569. doi:10.1071/WF09069.

Verbyla DL, Kasischke ES, Hoy EE (2008) Seasonal and topographic effects on estimating fire severity from Landsat TM/ETM+ data. *International Journal of Wildland Fire* **17**, 527. doi:10.1071/wf08038.

Vermote E, Justice C, Claverie M, Franch B (2016) Preliminary analysis of the performance of the Landsat 8/OLI land surface reflectance product. *Remote Sensing of Environment* **185**, 46–56. doi:10.1016/j.rse.2016.04.008.

Vermote EF, Tanr D, Deuz JL, Herman M, Morcrette J (1997) Second Simulation of the Satellite Signal in the Solar Spectrum, 6S : An Overview. *IEEE Transactions on Geoscience and Remote Sensing* **35**, 675–686.

Vetrita Y, Cochrane MA (2019) Annual Burned Area from Landsat, Mawas, Central Kalimantan, Indonesia, 1997-2015. doi:10.3334/ORNLDAAC/1708.

Vogelmann JE, Xian G, Homer C, Tolk B (2012) Monitoring gradual ecosystem change using Landsat time series analyses: Case studies in selected forest and rangeland ecosystems. *Remote Sensing of Environment* **122**, 92–105. doi:10.1016/j.rse.2011.06.027.

Wang X, He HS, Li X (2007) The long-term effects of fire suppression and reforestation on a forest landscape in Northeastern China after a catastrophic wildfire. *Landscape and Urban Planning* **79**, 84–95. doi:10.1016/j.landurbplan.2006.03.010.

Wang C, He Z, Zhu W (2001) Outline of vegetation in Dulongjiang river watershed, Yunnan. *Chinese Journal of Ecology* **20**, 26–33.

Ward E, Buytaert W, Peaver L, Wheater H (2011) Evaluation of precipitation products over complex mountainous terrain: A water resources perspective. *Advances in Water Resources* **34**, 1222–1231. doi:10.1016/j.advwatres.2011.05.007.

Weinstein DA, Woodbury PB (2010) Review of methods for developing probabilistic risk assessments. part 1: modeling fire. *Advances in threat assessment and their application to forest and rangeland management* **2**, 285–302. file:///C:/Users/jcronan.000/Documents/UW/JFSP_ASF/ASF_Info_LibraryPye_etal_2010_ThreatAssessment-1783596298/Pye_etal_2010_ThreatAssessment.pdf%5Cnhttp://084176486459010662 4clipping.bmp%5Cn%3CGo to ISI%3E://BCI:BCI201100057494.

Weiss DJ, Walsh SJ (2009) Remote Sensing of Mountain Environments. *Geography Compass* **3**, 1–21. doi:10.1111/j.1749-8198.2008.00200.x.

Van der Werf GR, Randerson JT, Giglio L, Collatz GJ, Kasibhatla PS, Arellano AF (2006) Interannual variability in global biomass burning emissions from 1997 to 2004. *Atmospheric Chemistry and Physics* **6**, 3423–3441. doi:10.5194/acp-6-3423-2006.

Van der Werf GR, Randerson JT, Giglio L, Collatz GJ, Mu M, Kasibhatla PS, Morton DC, Defries RS, Jin Y, Van Leeuwen TT (2010) Global fire emissions and the contribution of deforestation, savanna, forest, agricultural, and peat fires (1997-2009). *Atmospheric Chemistry and Physics* **10**, 11707–11735. doi:10.5194/acp-10-11707-2010.

Westerling AL, Hidalgo HG, Cayan DR, Swetnam TW (2006) Warming and earlier spring increase Western U.S. forest wildfire activity. *Science* **313**, 940–943. doi:10.1126/science.1128834.

White JC, Wulder MA, Hermosilla T, Coops NC, Hobart GW (2017) A nationwide annual characterization of 25 years of forest disturbance and recovery for Canada using Landsat time series. *Remote Sensing of Environment* **194**, 303–321. doi:10.1016/j.rse.2017.03.035.

White JC, Wulder MA, Hobart GW, Luther JE, Hermosilla T, Griffiths P, Coops NC, Hall RJ, Hostert P, Dyk A, Guindon L (2014) Pixel-based image compositing for large-area dense time series applications and science. *Canadian Journal of Remote Sensing* **40**, 192–212. doi:10.1080/07038992.2014.945827.

Willson A (2006) Forest conversion and land use change in rural Northwest Yunnan, China. *Mountain Research and Development* **26**, 227–236.

Wilson EH, Sader SA (2002) Detection of forest harvest type using multiple dates of Landsat TM imagery. *Remote Sensing of Environment* **80**, 385–396. doi:10.1016/S0034-4257(01)00318-2.

Winkler D (2000) Patterns of forest distribution and the impact of fire and pastoralism in the forest region of the Tibetan Plateau. 'Environ. Chang. High Asia'. (Eds G Miehe, Y Zhang) pp. 201–227. (Marburger Geographische Schriften)

Wondzell SM, King JG (2003) Postfire erosional processes in the Pacific Northwest and Rocky Mountain regions. *Forest Ecology and Management* **178**, 75–87. doi:10.1016/S0378-1127(03)00054-9.

Woźniak E, Aleksandrowicz S (2019) Self-adjusting thresholding for burnt area detection based on optical images. *Remote Sensing* **11**, 1–16. doi:10.3390/rs11222669.

Wu D, Li S, Yi S, Wang W (2009) 林火管理的调研报告 [Forest Fire Management Research Report]. '滇西北生物文化多样性保护与经济社会可持续协调发展研究'. (Eds S Duan, Y He) pp. 282–295. (Yunnan Publishing Group, Yunnan Science and Technology Press: Kunming, China)

Wulder MA, Loveland TR, Roy DP, Crawford CJ, Masek JG, Woodcock CE, Allen RG, Anderson MC, Belward AS, Cohen WB, Dwyer J, Erb A, Gao F, Griffiths P, Helder D, Hermosilla T, Hipple JD, Hostert P, Hughes MJ, Huntington J, Johnson DM, Kennedy R, Kilic A, Li Z, Lymburner L, McCorkel J, Pahlevan N, Scambos TA, Schaaf C, Schott JR, Sheng Y, Storey J, Vermote E, Vogelmann J, White JC, Wynne RH, Zhu Z (2019) Current status of Landsat program, science, and applications. *Remote Sensing of Environment* **225**, 127–147. doi:10.1016/j.rse.2019.02.015.

Wulder MA, Masek JG, Cohen WB, Loveland TR, Woodcock CE (2012) Opening the archive: How free data has enabled the science and monitoring promise of Landsat. *Remote Sensing of Environment* **122**, 2–10. doi:10.1016/j.rse.2012.01.010.

Xiao W, Ding W, Cui LW, Zhou RL, Zhao QK (2003) Habitat degradation of Rhinopithecus bieti in Yunnan,

China. *International Journal of Primatology* **24**, 389–398. doi:10.1023/A:1023009518806.

Xiao X, Haberle SG, Shen J, Xue B, Burrows M, Wang S (2017) Postglacial fire history and interactions with vegetation and climate in southwestern Yunnan Province of China. *Climate of the Past* **13**, 613–627. doi:10.5194/cp-13-613-2017.

Xiong Q, Luo X, Liang P, Xiao Y, Xiao Q, Sun H, Pan K, Wang L, Li L, Pang X (2020) Fire from policy, human interventions, or biophysical factors? Temporal–spatial patterns of forest fire in southwestern China. *Forest Ecology and Management* **474**. doi:10.1016/j.foreco.2020.118381.

Xu J, Wilkes A (2004) Biodiversity impact analysis in northwest Yunnan, southwest China. *Biodiversity and Conservation* **13**, 959–983. doi:10.1023/B:BIOC.0000014464.80847.02.

Xue J, Su B (2017) Significant remote sensing vegetation indices: a review of developments and applications. *Journal of sensors* **Vol.2017**, 17p.

Yan X, Ohara T, Akimoto H (2006) Bottom-up estimate of biomass burning in mainland China. *Atmospheric Environment* **40**, 5262–5273. doi:10.1016/j.atmosenv.2006.04.040.

Yang Y (2014) Discussion on existing problems and countermeasures of rural fire control - Take Yunnan province as an example. In 'Procedia Eng.', 519–522 doi:10.1016/j.proeng.2014.04.074.

Yang M, van Coillie F, Liu M, de Wulf R, Hens L, Ou X (2014) A GIS Approach to Estimating Tourists' Off-road Use in a Mountainous Protected Area of Northwest Yunnan, China. *Mountain Research and Development* **34**, 107–117. doi:10.1659/MRD-JOURNAL-D-13-00041.1.

Yang X, Skidmore AK, Melick D, Zhou Z, Xu J (2007) Towards an efficacious method of using Landsat TM imagery to map forest in complex mountain terrain in Northwest Yunnan, China. *Tropical Ecology* **48**, 227–239.

Yang Y, Tian K, Hao J, Pei S, Yang Y (2004) Biodiversity and biodiversity conservation in Yunnan, China. *Biodiversity and Conservation* **13**, 813–826.

Yang W, Zhang S, Tang J, Bu K, Yang J, Chang L (2013) A MODIS time series data based algorithm for mapping forest fire burned area. *Chinese Geographical Science* **23**, 344–352. doi:10.1007/s11769-013-0597-6.

Ye J, Wu M, Deng Z, Xu S, Zhou R, Clarke KC (2017) Modeling the spatial patterns of human wildfire ignition in Yunnan province, China. *Applied Geography* **89**, 150–162. doi:10.1016/j.apgeog.2017.09.012.

Young AM, Higuera PE, Duffy PA, Hu FS (2017) Climatic thresholds shape northern high-latitude fire regimes and imply vulnerability to future climate change. *Ecography* **40**, 606–617. doi:10.1111/ecog.02205.

Zhang Z, van Coillie F, Ou X, De Wulf R (2014) Integration of satellite imagery, topography and human disturbance factors based on canonical correspondence analysis ordination for mountain vegetation mapping: A case study in Yunnan, China. *Remote Sensing* **6**, 1026–1056. doi:10.3390/rs6021026.

Zhang J, Yao F, Liu C, Yang L, Boken VK (2011) Detection, emission estimation and risk prediction of forest fires in China using satellite sensors and simulation models in the past three decades - An overview. *International Journal of Environmental Research and Public Health* **8**, 3156–3178. doi:10.3390/ijerph8083156.

Zhao S, Liu X, Ding C, Liu S, Wu C, Wu L (2020) Mapping rice paddies in complex landscapes with Convolutional Neural Networks and phenological metrics. *GIScience and Remote Sensing* **57**, 37–48. doi:10.1080/15481603.2019.1658960.

Zhao F, Shu L, Tian X, Wang M (2009) Change trends of forest fire danger in Yunnan province in 1957-2007. *Chinese Journal of Ecology* **28**, 2333–2338.

Zhou M, Wang Y, Gao Y (2012) Effect of climatic factors on forest fires in Dali. *Journal of Sichuan Forestry Science and Technology* **33**. doi:10.16779/j.cnki.1003-5508.2012.06.022.

Zhu Z (2017) Change detection using Landsat time series: A review of frequencies, preprocessing, algorithms, and applications. *ISPRS J. Photogramm. Remote Sens.* **130**, 370–384. doi:10.1016/j.isprsjprs.2017.06.013.

Zhu Z, Woodcock CE (2012) Object-based cloud and cloud shadow detection in Landsat imagery. *Remote Sensing of Environment* **118**, 83–94. doi:10.1016/j.rse.2011.10.028.

Zhu Z, Woodcock CE (2014) Automated cloud, cloud shadow, and snow detection in multitemporal Landsat data: An algorithm designed specifically for monitoring land cover change. *Remote Sensing of Environment* **152**, 217–234. doi:10.1016/j.rse.2014.06.012.

Zhu Z, Wulder MA, Roy DP, Woodcock CE, Hansen MC, Radeloff VC, Healey SP, Schaaf C, Hostert P, Strobl P, Pekel JF, Lymburner L, Pahlevan N, Scambos TA (2019) Benefits of the free and open Landsat data policy. *Remote Sensing of Environment* **224**, 382–385. doi:10.1016/j.rse.2019.02.016.

Zimmermann P, Tasser E, Leitinger G, Tappeiner U (2010) Effects of land-use and land-cover pattern on landscape-scale biodiversity in the European Alps. *Agriculture, Ecosystems and Environment* **139**, 13–22. doi:10.1016/j.agee.2010.06.010.

Zumbrunnen T, Pezzatti GB, Menéndez P, Bugmann H, Bürgi M, Conedera M (2011) Weather and human impacts on forest fires: 100 years of fire history in two climatic regions of Switzerland. *Forest Ecology and Management* **261**, 2188–2199. doi:10.1016/j.foreco.2010.10.009.

Websites

All websites have been accessed and controlled on February 15, 2021.

ALOS World 3D – 30m (AW3D30): https://www.eorc.jaxa.jp/ALOS/en/aw3d30/index.htm

Canadian National Fire Database: http://cwfis.cfs.nrcan.gc.ca/ha/nfdb/

China Statistical Yearbooks: http://www.stats.gov.cn/english/Statisticaldata/AnnualData/

Chinese National Bureau of Statistics: https://www.stats.gov.cn/tjsj/.

Convention on Biological Diversity: https://www.cbd.int/mountain/

European Space Agency Climate Change Initiative (ESA-CCI): https://climate.esa.int/en/esa-climate/esa-cci/

European Space Agency Landcover product: https://climate.esa.int/en/projects/land-cover/

FAO Mountain Partnership: http://www.fao.org/mountain-partnership/

Fire_CCI Pixel BA version 4.1: https://catalogue.ceda.ac.uk/uuid/bcef9e87740e4cbabc743d295afbe849/

Global Administrative Boundaries project: https://gadm.org/

GlobeLand30 project: http://www.globallandcover.com/

Google Earth Engine: https://earthengine.google.com/

GRASS GIS software: https://grass.osgeo.org/

Harris Geospatial, ENVI software: https://www.harris.com/solution/envi/

MODIS Landcover yearly product (MCD12Q1): https://lpdaac.usgs.gov/products/mcd12q1v006/

Mountain Research Initiative: https://www.mountainresearchinitiative.org/

OpenCV project: https://docs.opencv.org/

Orfeo Toolbox: https://www.orfeo-toolbox.org/

QGIS software: http://www.qgis.org/

SAGA GIS software: http://www.saga-gis.org/

Switzerland's Swissfire database: http://www.wsl.ch/swissfire/index_EN

The Nature Conservancy: https://www.nature.org/

UNESCO World Heritage Sites: http://whc.unesco.org/en/list/

United Nations Sustainable Development Goals: https://sdgs.un.org/goals/

United States Geological Survey EarthExplorer: https://earthexplorer.usgs.gov/

University of Maryland MODIS Fire repository: http://modis-fire.umd.edu/

Appendices

Appendix A

Fig. 5 In a strict sense (*sensu stricto*) a fire regime is a description by means of parameters of when, where and which fires occur (**a**). Used less strictly, i.e. in *sensu lato*, a fire regime may also include parameters that refer to the conditions of fire occurrence (**b**) and to the immediate effects of fires (**c**). Combining and analyzing the data of these three categories may result in further derived parameters (**d**). All parameters are facultative and should be used in a well-defined context

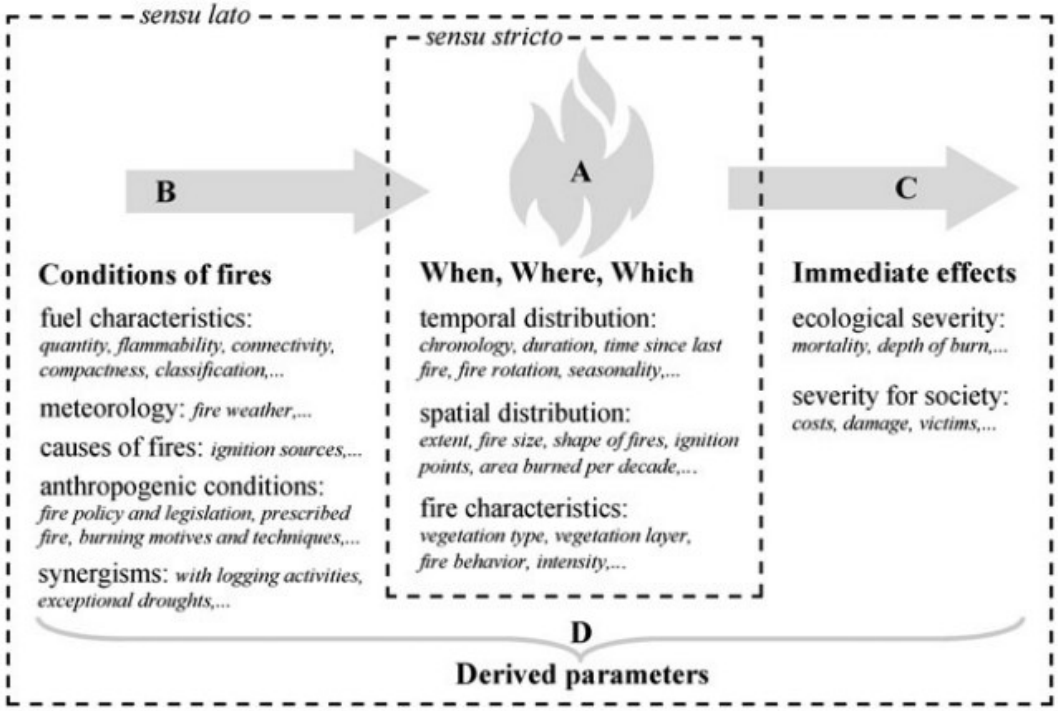

Figure A1. Proposal for a structuring of the most important categories and parameters describing fire regimes. Image courtesy from Krebs *et al.* (2010).

Appendix B

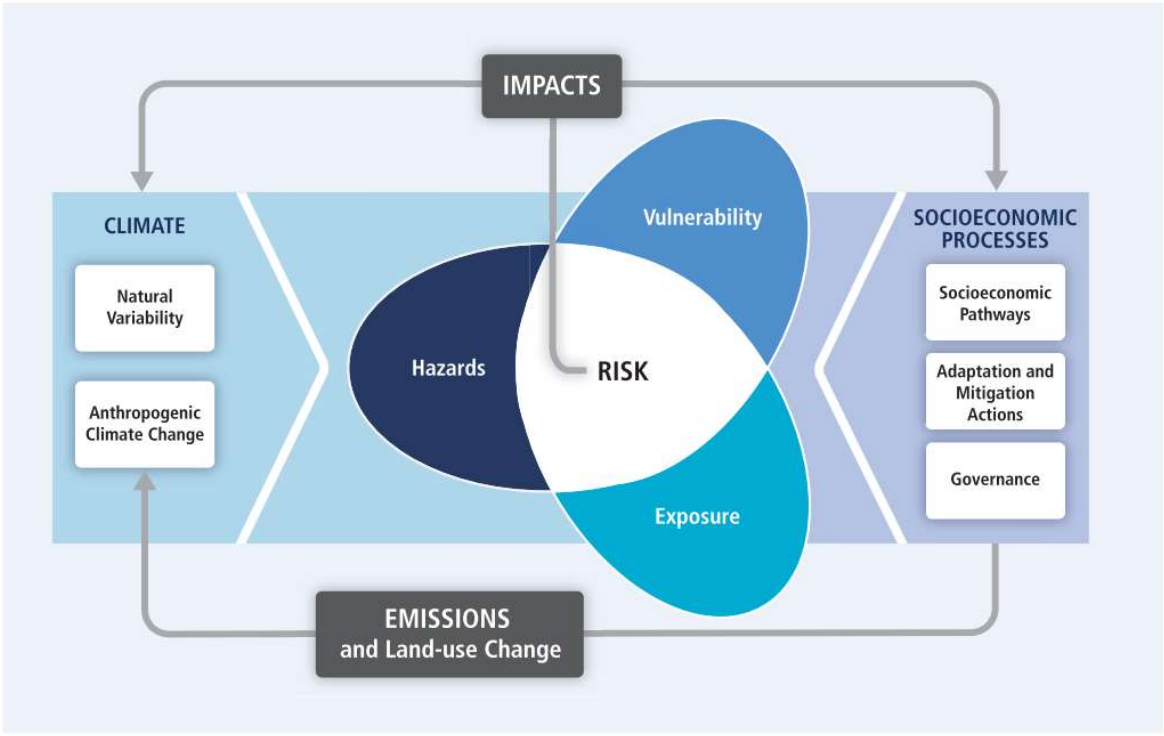

Figure B1. Illustration of the core concepts of the WGII AR5. Risk of climate-related impacts results from the interaction of climate-related hazards (including hazardous events and trends) with the vulnerability and exposure of human and natural systems. Changes in both the climate system (left) and socioeconomic processes including adaptation and mitigation (right) are drivers of hazards, exposure, and vulnerability. From IPCC (2014b)

Appendix C

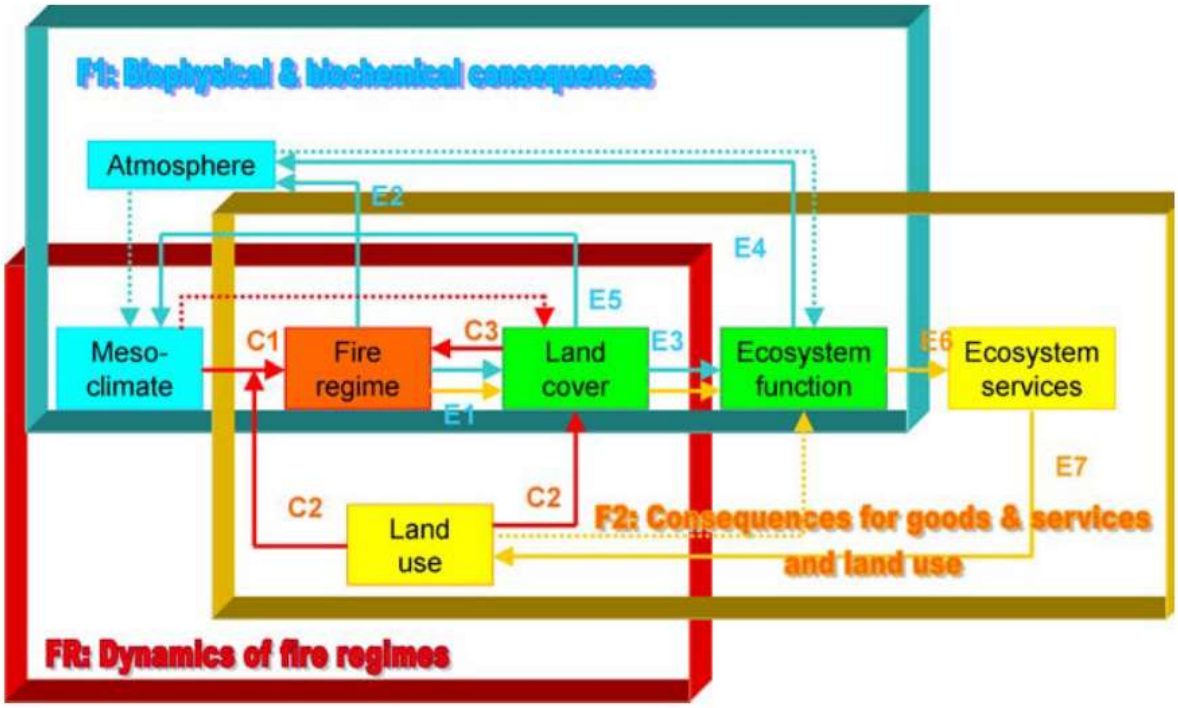

Figure C1. Integrated fire research framework employed in the study of Lavorel *et al.* (2007). The following caption is reported from the original publication. The framework presents relationships among different compartments of the human-environment system involved in fire causes and effects. These are organized into one control loop on fire regimes (FR, red box and arrows) and two feedback loops, the first one driving consequences of fire for biophysical and biochemical processes (F1, blue box and arrows), and the second one (F2, yellow box and arrows) driving consequences of fire for ecosystem services and land use. Full arrows indicate topics of direct concern to integrated fire research, while dotted arrows represent other important, often indirect effects. Arrows representing different causes (C) and effects (E) are numbered as referenced in the text.

Appendix D

Table D1. Dates of Landsat scenes used in the time-series.

	131041	131042	132040	132041	132042	133040	133041
1986	1987-01-21	1986-11-02	1986-11-25	1987-02-13	1986-12-11	1986-12-02	1986-12-02
1987	1988-02-09	1988-02-09	1987-11-28	1987-11-28	1987-11-28	1988-02-07	1987-12-21
1988	1988-12-25	1988-12-25	1988-11-14	1988-11-14	1989-03-06	1988-12-31	1988-12-31
1989	1989-11-26	1989-11-26	1990-01-04	1989-12-03	1990-01-04	1989-11-24	1989-11-24
1990	1990-12-31	1990-12-31	1990-11-20	1990-11-20	1990-11-20	1990-11-27	1990-12-13
1991	1991-12-18	1991-12-02	1991-11-07	1991-11-07	1991-11-23	1991-12-16	1991-12-16
1992	1992-11-18	1992-11-18	1992-12-27	1992-12-11	1992-12-11	1992-11-16	1992-11-16
1993	1994-01-08	1994-01-08	1993-11-28	1993-11-28	1993-12-30	1993-12-05	1993-12-05
1994	1994-12-26	1995-01-11	1994-11-15	1994-11-15	1995-02-03	1994-11-22	1994-12-24
1995	1996-02-15	1996-02-15	1996-02-06	1996-02-06	1996-02-06	1995-10-24	1995-11-09
1996	1996-12-31	1996-12-31	1996-12-22	1996-12-06	1996-11-20	1996-12-29	1996-12-29
1997	1998-01-03	1998-01-03	1997-11-07	1997-10-22	1998-01-10	1997-10-29	1997-10-29
1998	1999-02-07	1999-02-07	1998-12-28	1998-12-28	1998-12-28	1998-12-03	1998-12-19
1999	1999-11-22	1999-11-22	1999-10-28	1999-11-29	1999-11-29	2000-01-07	2000-01-07
2000	2001-02-12	2001-02-12	2001-01-18	2001-01-18	2001-01-18	2000-12-24	2000-12-24
2001	2002-02-15	2001-12-13	2001-12-04	2001-12-20	2001-12-20	2001-11-25	2001-12-11
2002	2003-01-17	2003-01-01	2002-12-07	2002-12-07	2003-01-08	2002-10-27	2002-12-14
2003	2003-12-03	2003-12-03	2003-11-24	2003-12-26	2004-02-12	2003-11-15	2003-12-01
2004	2005-01-06	2005-01-06	2004-12-12	2004-12-12	2004-12-28	2004-12-03	2004-12-19
2005	2006-01-25	2006-01-25	2005-11-13	2005-10-12	2006-02-01	2005-11-04	2005-11-04
2006	2006-12-11	2006-12-11	2006-12-02	2006-10-31	2006-10-31	2006-12-25	2007-01-26
2007	2008-02-16	2008-04-20	2008-02-23	2008-02-23	2008-03-10	2008-03-01	2008-03-01
2008	2009-02-18	2009-02-18	2009-01-24	2009-03-13	2009-01-08	2008-11-12	2008-11-12
2009	2010-02-05	2010-02-21	2010-02-12	2009-12-10	2009-12-10	2010-01-18	2010-01-18
2010	2011-01-07	2011-01-07	2010-12-29	2010-12-29	2010-12-29	2010-12-20	2010-12-20
2013	2013-11-12	2013-12-30	2013-12-05	2013-12-05	2014-01-22	2013-11-26	2013-11-26
2014	2015-01-02	2015-02-03	2014-12-24	2014-12-24	2014-12-24	2015-01-16	2015-01-16
2015	2016-01-05	2016-01-05	2015-11-09	2015-11-09	2015-12-27	2016-01-19	2016-01-03
2016	2017-01-23	2017-01-23	2016-12-13	2016-12-13	2017-01-14	2017-01-21	2017-01-21
2017	2017-12-25	2017-12-25	2017-12-16	2017-12-16	2018-01-17	2017-12-07	2017-12-07
2018	2019-01-13	2019-01-13	2019-01-20	2019-01-20	2019-01-04	2018-12-26	2018-12-26

Appendix E

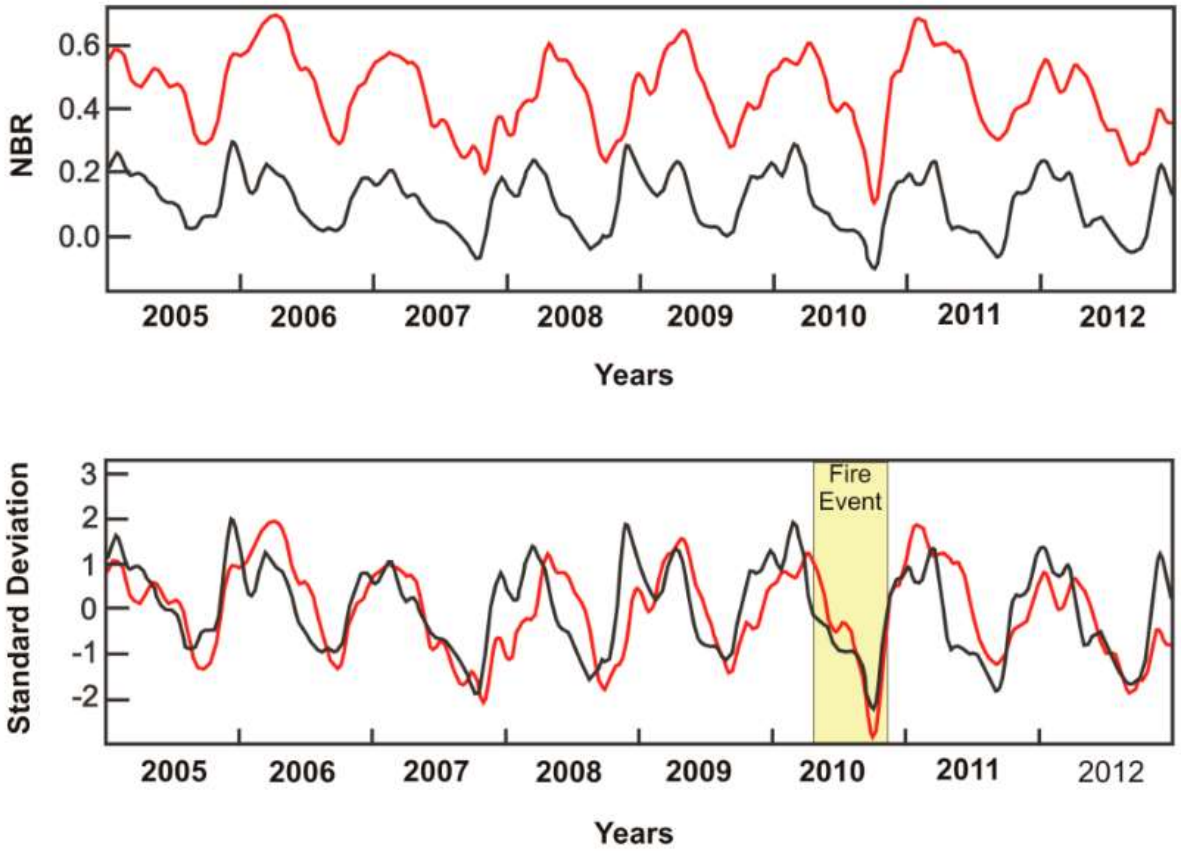

Figure E1. NBR-MODIS time-series of savanna (black curve) and Closed Savanna Woodland (red curve) before and after standardization. The standardized temporal curves homogenize and highlight the fire event, which reached different types of vegetation. Figure and caption from de Carvalho Júnior *et al.* (2015).

Appendix F

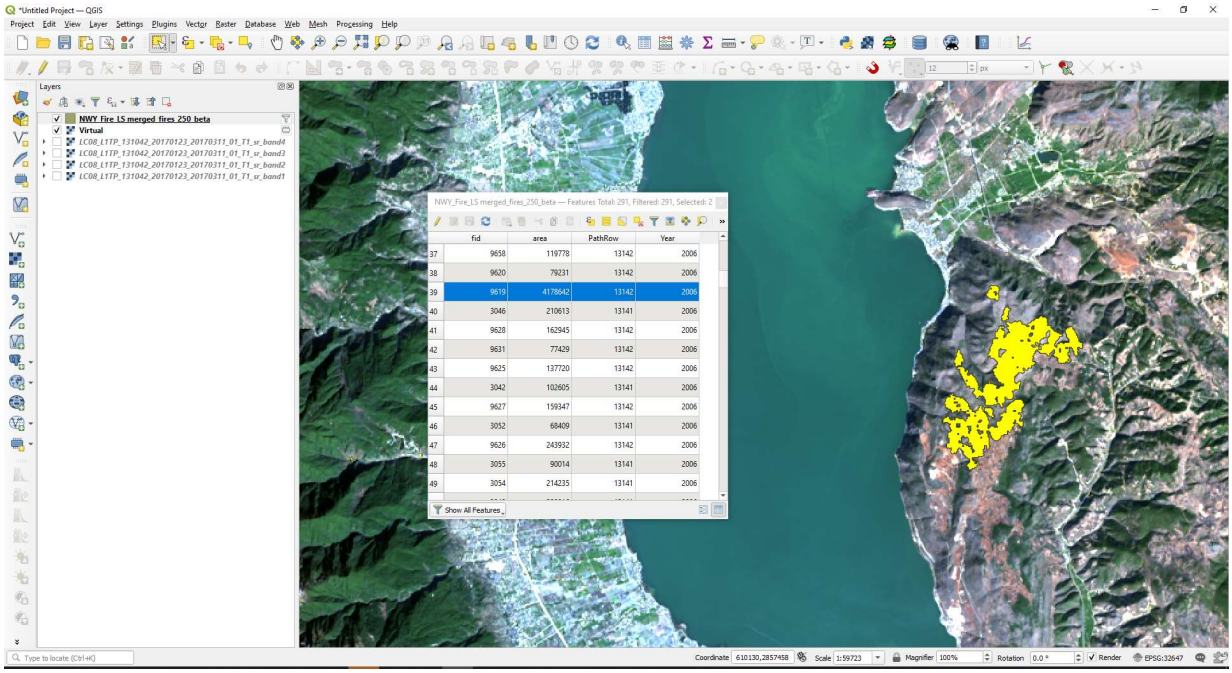

Figure F1. Visualization of a fire polygon and its attribute table the QGIS software, created with our methodology.

List of figures

List of tables